A Novel Methodology Assessing the Use of Semi-Transparent Photovoltaics Integrated onto Double Skin Facades and their Impact on the Energy Consumption of Buildings

Zisis Ioannidis

A Thesis
In the Department
of
Building, Civil and Environmental Engineering

Presented in Partial Fulfilment of the Requirements
For the Degree of
Doctor of Philosophy (Building Engineering) at
Concordia University
Montreal, Quebec, Canada

April 2023

CONCORDIA UNIVERSITY

SCHOOL OF GRADUATE STUDIES

This is to certify that the thesis prepared

By: Zisis Ioannidis

Entitled: A novel methodology assessing the use of Semi-Transparent Photovoltaics integrated onto Double

Skin Facades and their impact on the energy consumption of buildings

and submitted in partial fulfillment of the requirements for the degree of

Doctor Of Philosophy (Building Engineering)

complies with the regulations of the University and meets the accepted standards with respect to originality and quality.

Signed by the final examining committee:

Dr. Andrea Schiffauerova	Chair
Dr. Runming Yao	External Examiner
Dr. Marius Paraschivoiu	Examiner
Dr. Ali Nazemi	Examiner
Dr. Liangzhu Wang	Examiner
Dr. Andreas Athienitis	Thesis Co-Supervisor
Dr. Theodore Stathopoulos	Thesis Co-Supervisor

Approved by

Dr. Mazdak Nik-Bakht, Graduate Program Director

6/29/2023

Dr. Mourad Debbabi, Dean
Gina Cody School of Engineering and Computer Science

Abstract for PhD

A Novel Methodology Assessing the Use of Semi-Transparent Photovoltaics Integrated onto Double Skin Facades and their Impact on the Energy Consumption of Buildings

Zisis Ioannidis, Ph.D.

Concordia University, 2023

Building-integrated Photovoltaics (BIPV) can replace building elements in both facades and roofs improving at the same time the thermal, the electrical and the daylighting performance of the building. A novel approach in BIPV is the Double Skin Façade (DSF) that integrates Semi-Transparent Photovoltaics (STPV). In this approach, the air that passes within the cavity created between the layer of the STPV and the building, acts as a buffer zone and depending on the preferred strategy, it can be used for heating, cooling or ventilating the building. In addition, the STPV is the exterior layer of the envelope, controlling the solar gains but also allowing daylight into the interior space.

This thesis identifies the important parameters of a double skin façade integrating semi-transparent photovoltaics (DSF-STPV) as well as the gaps in the existing literature, namely the lack of experimental studies on mechanically-ventilated DSF-STPV buildings and the lack of investigation of heat transfer coefficients within the cavity in the presence of wind effects. In addition, it appears that there are neither tools to simulate such complex systems nor guidelines to assist architects and engineers to optimally design a DSF-STPV system.

A methodology was developed to assess the use of STPV integrated onto DSF and their impact on the energy consumption of buildings. The thermal model employed was verified in an outdoor experimental set-up of a mechanically-ventilated DSF-STPV and an insulating glazing unit (IGU) integrating STPV (IGU-STPV) built at Concordia University (Montreal, Canada). The forced convection within the cavity of the DSF-STPV has been investigated and three Nusselt number correlations were developed and validated. An experimental test-room was also used for a comparison between the DSF-STPV and the IGU-STPV under specific outdoor conditions. From the experimental analysis it has been found that a DSF-STPV can reduce the exterior heat losses due to wind, by more than 20%, whereas the total combined efficiency of the DSF-STPV, can reach the 75% level. The comparison between the DSF-STPV and the IGU-STPV presents increased electrical performance of the DSF-STPV up to 9% and lower average temperature difference that reaches up to 10°C.

The developed Nusselt number correlations were used for the development and validation of a parametric numerical model of a DSF-STPV. The model also allows the user to perform a parametric analysis changing the design parameters of the thermal zone and the DSF-STPV. This model can also simulate battery storage and its effect on peak demand. A parametric analysis was carried out for sixteen (16) different ASHRAE climate zones, two (2) insulation cases for every climate location (baseline and advanced), nine (9) different cavity widths, nine (9) different cavity

velocity set-points and twelve (12) different strategies, changing the operation of the DSF-STPV.

An analysis of the optimal operation for all sixteen (16) ASHRAE climate zones was presented, concluding that the climate locations can be separated into three main categories based on their behaviour, i.e. hot and mild, cold, and extreme cold locations, as they present similar patterns and strategies to achieve minimal energy consumption. In addition, the parametric analysis has shown that, for most cases, practical cavity widths under or over 0.50 m - 0.60 m show similar behaviour.

The mismatch between the electricity production by the STPV and the electricity needed for heating and lighting by the adjacent building perimeter zones was investigated, for Montreal, Canada. With the use of a predictive heating strategy, the peak demand of the building can coincide with the peak of the electricity production, resulting in more than 80% reduction in the electricity consumption by the grid during the peak hours.

Acknowledgements

Dedication

In the memory of my granmather Αvναμαρία and to my grandmother Αργυρούλα

Abbreviations

BAPV: *Building Applied Photovoltaics*
BIPV: *Building Integrated Photovoltaics*
BIPV/T: *Building Integrated Photovoltaics/ Thermal*
CFD: *Computational Fluid Dynamics*
CHTC: *convective heat transfer coefficient*
DSF: *Double skin façade*
DSF-STPV: *Double Skin Façade integrating Semi- Transparent Photovoltaics*
ESP-r: *Energy Simulation Program (software)*
HVAC: *Heating, Ventilation and Air Condition*
IGU: *Insulating glazing unit*
IGU-STPV: *Insulating Glazing Unit integrating Semi- Transparent Photovoltaics*
SC: *shading coefficient (-)*
SHGC: *Solar gain coefficient (-)*
STC: *Standard Testing Conditions*
STPV: *Semi-Transparent Photovoltaics*
TRNSYS: *Transient Systems (software)*

Nomenclature

a-Si:	*Amorphous Silicon*
A:	*Aspect ratio (-)*
A_i:	*Area of Surface i (m^2)*
c-Si:	*Crystalline Silicon*
eff:	*Efficiency (-)*
h:	*Heat transfer coefficient (W/m^2K)*
hc:	*convective heat transfer coefficient (W/m^2K)*
I:	*current (A)*
I/G	*Incident solar radiation (W/m^2)*
k:	*Thermal conductivity (W/mK)*
l:	*characteristic length (m)*
Nu:	*Nusselt number (-)*
P:	*Power (W)*
$\dot{Q}$:	*Energy flow (W)*
R:	*R-value (m^2K/W)*
Re:	*Reynolds number (-)*
SolAbs:	*Solar absorbance (%)*
SolTr:	*Solar transmittance (%)*
T:	*Temperature (°C or K)*
U:	*U-value (W/m^2K)*
V:	*Voltage (V)*
Vabs	*Visual absorbtance (%)*
Vtr:	*Visual transmittance (%)*
W_p:	*Watt peak*

Subscripts

a:	*exterior side of the DSF cavity*
abs:	*absorbtance*
b:	*interior side of the DSF cavity*
cv:	*control volume*
gl:	*glass/glazing*
gli:	*glass inside*
glo:	*glass outside*
p:	*peak*
rad:	*radiation*

Greek symbols

α:	*Absorbtance (-)*
τ:	*Transmittance (-)*

ρ: *Reflectance (-)*
η: *Electricity conversion factor (-)*

Table of Contents

Chapter 1

Introduction

Introduction

It is very common for both commercial and residential modern buildings to use curtain wall systems as part of their envelope design. A well-designed curtain wall system is able to seal the building, protect it from weather variations while providing for good aesthetics. The large transparent facades are often preferred due to their reduced cost and the great appreciation of daylighting, as the sun light can penetrate deeper into the building, as well as the higher demand for space with wide exterior views. This architectural tendency is likely to remain, due to the fact that many studies link daylight and view to the outdoors with increased worker productivity, well-being (Veitch and Galasiu 2011) and reduced lighting loads (Tzempelikos and Athienitis 2007). Highly glazed facades may maximize the daylight potential of the building, but they may require an oversized mechanical system, as excessive solar gains may lead to increased cooling loads during the day and low insulation may lead to increased heating loads during the night, adding to the thermal and visual discomfort of the occupants.

The energy performance of highly glazed facades can be significantly improved by either integrating photovoltaics (PV) on windows or by adding an additional exterior layer forming in this way a double skin façade (Miyazaki, Akisawa, and Kashiwagi 2005). Solar cells may be used instead of reflective coating or ceramic frits to reduce the solar gains, forming in this way semi-transparent photovoltaics (STPV) that could be integrated on parts of the façade of the building (James, Jentsch, and Bahaj 2009; Qiu et al. 2009; Baum and Grimshaw, n.d.). As a result, solar heat gains may be reduced, maintaining at the same time adequate levels of daylight, provide view to the outdoors (Vartiainen 2001) and generate electricity.

When PV cell overheating is of concern, instead of a window with a sealed cavity (IGU), a ventilated one can be utilized, turning the façade into a Double Skin Façade integrating photovoltaics (DSF-STPV). The possibility of recovering the heat from within the DSF-STPV, along with the electricity generation and the daylight transmission, gives the opportunity to the creation of an active façade (Gaillard, Giroux-Julien, et al. 2014). As the air circulates behind the PV cells, it cools down the cells through convection, reducing the temperature of the cells and increasing their electrical efficiency.

The stochastic nature of the wind is an important parameter to assess the natural airflow inside the cavity, because it might assist or oppose the buoyancy forces (Marques da Silva, Gomes, and Rodrigues 2015). In general, CFD simulations and wind-tunnel experiments are the most common ways to assess the wind effects on the performance of DSF. The findings of the available studies could be used as guidelines for future studies on DSF integrating STPV.

1.1. Building integrated photovoltaics (BIPV)

Building integrated photovoltaics (BIPV) is the latest trend in the PV industry. Because PV panels are mostly made from glass, their integration at the exterior layer of the envelope of a building can replace common building materials while protecting the building from weather phenomena. Building Integrated Photovoltaics can be part of the roof, the façade or even awnings of buildings. There is a distinct difference between the building integrated and building applied photovoltaics

(BAPV). The BAPV is the most common installed PV in buildings but usually do not replace envelope components but instead they are mounted on top of them. A big category of BIPV is the semi-transparent Photovoltaics (STPV) which could be integrated on roofs, canopies, atria, awnings etc. More about STPV will be described in paragraph 1.3.
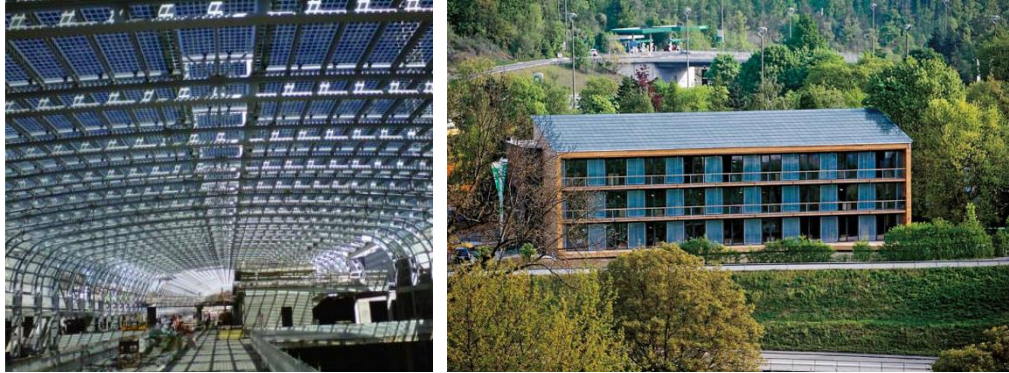
Figure 1-1 Stazione porta Susa Torino. Train Station in Turin.by EnergyGlass (left), Marché International Support Office © Willi Kracher (right)

1.2. BIPV/Thermal systems

Another sub-category of BIPV is the BIPV/Thermal or in short BIPV/T. Except from the electrical generation of the PV, a Building integrated system can be set-up in this way, that also allows for thermal generation by the same system. The principal of operation is seen in Figure 1-2.
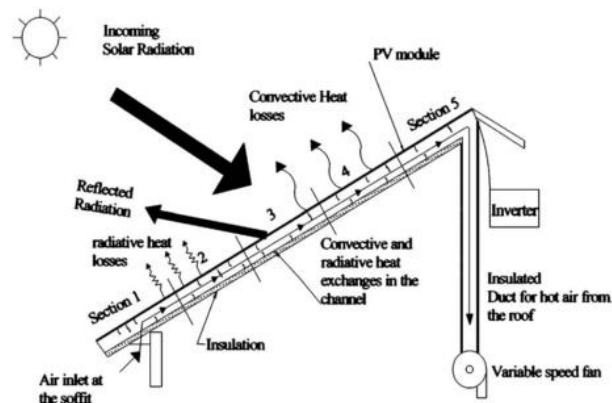
Figure 1-2 A schematic of a cross section of an air-based open loop BIPV/T system (Candanedo, Athienitis, and Park 2011)

The PV panels are mounted on the building envelope in this way that a cavity is created between the PV and the rest of the insulated envelope. This cavity is used as an air channel where the flowing air, captures the heat from the panels and later this preheated air can enter the building directly or assist the HVAC system of the building. In addition to the benefit of harvesting thermal energy, such systems increase the electrical production of the PV panels as the flowing air within the cavity, decreases the operating temperature of the PV. Building integrated photovoltaic/thermal systems can be integrated in roofs and facades (Figure 1-3) but also can be designed to integrate skylight systems similar to the one applied on the Solar Decathlon China 2018 house by team

Montreal (Figure 1-4).

Figure 1-3 Both Eco-Terra house (Left) and JMSB building, have BIPV/T (right)

Figure 1-4 The Varennes Library (left), the first institutional Net-Zero Energy Building in Canada and the Team Montreal Deep-Performance Dwelling from the Solar Decathlon Competition 2018 in China (right), with BIPV/T.

1.3. Building integrated STPV (BISTPV)

Semi-Transparent Photovoltaics (STPV) have started to become more common and are already getting installed in buildings, as they provide the flexibility of producing electricity and at the same time allow daylight to pass. There are many companies that use STPV for building applications (see paragraph A.2). The principle of operation of STPV can be seen in Figure 1-5 and can be described by the conservation of energy.

$$\alpha G_{tot} + \tau G_{tot} + \rho G_{tot} + \eta G_{tot} = G_{tot}$$

Where the G_{tot} is the total incident solar radiation, α is the absorbtance of the PV that is transformed into heat, τ is the transmittance of the STPV, ρ is the reflectance and η the fraction of the incident solar radiation that becomes electricity by the STPV. The absorbed solar radiation is then remitted inside $(\frac{\dot{Q}_i}{A_w})$ and outside $(\frac{\dot{Q}_o}{A_w})$. More about this energy balance will be described in the paragraph 1.5.1.3. where the Solar Heat Gain Coefficient will be explained.
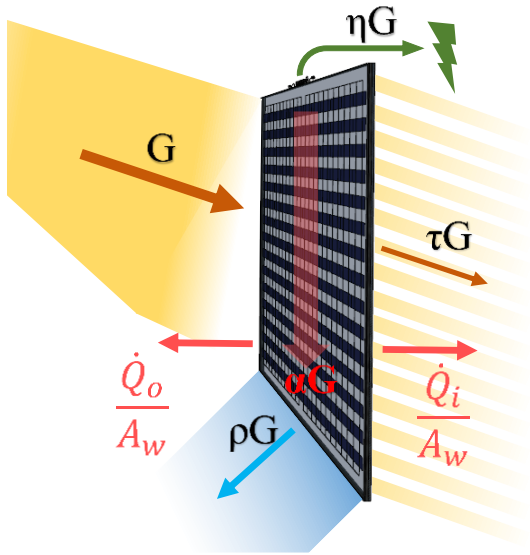
Figure 1-5 Energy balance of a semi-transparent Photovoltaic

1.4. Insulating glazing unit integrating STPV (IGU-STPV)

The integration of an STPV on the exterior glazing of a double or triple insulating glazing unit (IGU) is an IGU-STPV. The advanced thermal performance of double or triple glazing with low-e coatings has steered many companies to integrate STPV on IGU. The most common material used in IGU-STPV is the amorphous silicon (a-Si) and is also the most researched technology (see Table 2-1 and Table 2-2).
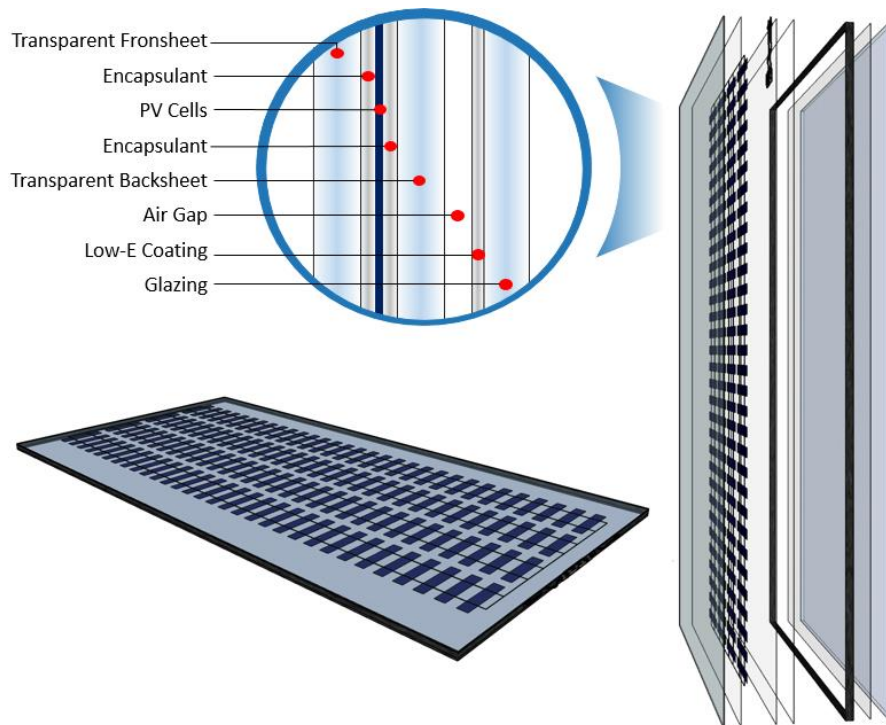
Figure 1-6 Cross section of an IGU-STPV, identifying the different layers

The cross section of a crystalline silicon (c-Si) STPV on an IGU can be seen in Figure 1-6, where the c-Si solar cells are encapsulated between the two panes of glass. This encapsulation is done usually with the use of ethylene vinyl acetate (EVA) film or more recently with polyvinyl butyral (PVB) film. The thickness of the two front glasses is usually between 4mm to 6mm and the gap thickness between the second STPV and the back glass ranges usually from approximately 15mm to 25 mm.

1.5. Double skin façade integrating STPV (DSF-STPV)

More recently, STPV have started to be integrated in double skin facades (DSF). In this way, the STPV can generate electricity and allow daylighting into the building but also allow the possibility to harvest heat from the cavity of the DSF or use the DSF as a buffer zone for the building. The cavity of a DSF can be naturally or mechanically ventilated and could also accommodate shading devices such as rollers, blinds and in some cases plants (Stec, Van Paassen, and Maziarz 2005). A schematic that shows the operation of a mechanically ventilated DSF-STPV is depicted in Figure 1-7.
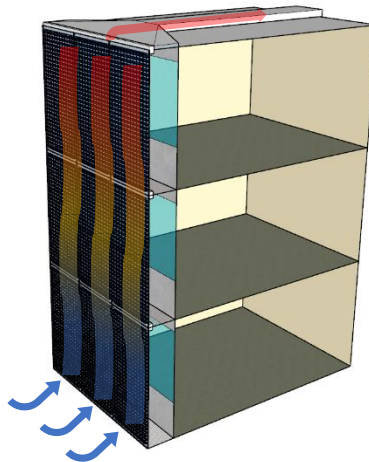
Figure 1-7 Operation of three story DSF integrating c-Si STPV.

1.5.1. Definitions and important parameters

1.5.1.1. Efficiency, W_p and W_p/m^2

The efficiency of a PV panels corresponds to the percentage of the incident solar radiation that is converted into electricity. The efficiency of the PV panel is different than the efficiency of a solar cell, as the solar cells don't cover the whole panel and in the case of STPV they are spread in the panel. The efficiency of a solar panel is characterized by the manufacturing companies and is measured with the use of a flash test under STC, meaning 21°C of ambient temperature and 1000W/m² of incident solar radiation. Under the same conditions, the production of the PV panel is measured and is called peak production or Watt peak (W_p). This depends on the manufacturing process but most importantly on the size of the panel. The more solar cells per panel there are, the greater the W_p will be. For building integrated solar panels, the value that is of interest is the peak production under the STC per square meters (W_p/m^2).

1.5.1.2. U-value

The thermal transmission, or else known as U-value/factor is the total heat transfer coefficient that signifies the rate in which heat is transferred through a building element caused by the temperature difference across the surfaces of the envelope where this building material is integrated. Being the inverse of the R-value, it has as units W/m^2K and is defined as the heat flux over the temperature difference across the surface of that material and that causes this heat flux.

$$U = \frac{\dot{Q}_{element\ area}}{\Delta T} = \frac{k_{element}}{l_{element}} \qquad (1\text{-}1)$$

Where $k_{element}$ is the thermal conductivity coefficient of the material of the element (W/mK) and $l_{element}$ is the thickness of the element (m).

It is common through for the U-value to be defined by using as additions the exterior and interior heat transfer coefficients along with the conductance of the IGU. Manufacturers thus provide two average U-values, one for winter and one for summer, depending on the region where this material is going to be integrated, as different heat transfer seasonal coefficient are used.

$$U = \frac{1}{\frac{1}{h_{out}} + \frac{1}{h_{in}} + R_{glazing}} \qquad (1\text{-}2)$$

Where h_{out} and h_{in} are the exterior and interior heat transfer coefficients and their values are suggested by ASHRAE depending on the location, angle of integration and more parameters. $R_{glazing}$ includes the thermal conductivity of each glazing layer and the total combined conductive, convective and radiative heat transfer coefficient of the glazing unit $\left(\frac{1}{h_t}\right)$.

$$R_{glazing} = \frac{l_1}{k_1} + \frac{1}{h_t} + \frac{l_2}{k_2} + \cdots \qquad (1\text{-}3)$$

A more simplified approach in which the resistance of each glazing is neglected as it can be sometimes even more than twenty (20) times smaller than a typical interior resistance can be adopted (Kreider, Curtiss, and Rabl 2002). This interior resistance can be approximated with a combined convective and radiative typical value of 0.12 m^2K/W

$$1/h_i \approx \frac{1}{8.29}\frac{W}{m^2K} = 0.12\frac{m^2K}{W} \gg \frac{l_{glass}}{k_{glass}} \approx \frac{0.006}{1} = 0.006\frac{m^2K}{W}$$

$$\frac{1}{U} = \frac{1}{h_i} + \sum_{j=1}^{M}\frac{1}{h_{s_j}} + \frac{1}{h_o} \qquad (1\text{-}4)$$

Where $\frac{1}{h_{s_j}}$ is the combined conductive, convective and radiative heat transfer coefficient within the air gap of an IGU and j signifies each air-gap out of M number of air-gaps.

1.5.1.3. Solar heat gain coefficient (SHGC)

The solar heat gains are defined as the total heat that flows towards an interior zone or a room because of the incident solar radiation and depends on the characteristics of the building envelope. For an opaque envelope component, the solar heat gain is the heat that flows towards the room and is caused by the absorbed solar radiation by the envelope. For transparent or semi-transparent envelope components, an additional term is added which is the transmitted solar radiation Figure 1-5.

$$SHG = \frac{\dot{Q}_i}{A_{component}} + \tau_{eff}G \tag{1-5}$$

The solar heat gain coefficient is defined as the solar heat gain over the incident solar radiation

$$SHGC = \frac{SHG}{G} = \frac{\dfrac{\dot{Q}_i}{A_{component}}}{G} + \tau_{eff} \tag{1-6}$$

The first term in equation (1-5), which represents the heat gain of the interior per unit component area, we will name it $q_{i_{sol}}$. Therefore, the SHGC, which also can be found in literature as F and in the Europe is commonly referred as g-Value is described as:

$$SHGC = \frac{q_{i_{sol}}}{G} + \tau_{eff} \tag{1-7}$$

The heat that flows towards the room or the outside respectively is defined with the use of the interior and the exterior heat transfer coefficients:

$$q_{i/o} = h_{i/o}(T_s - T_{i/o}) \tag{1-8}$$

The heat flow (eq. (1-8)) consist of two parameters; the solar heat gains that are caused by the absorbtance of the solar radiation ($q_{i_{sol}}$) and the conductive gains that are caused by the temperature difference between the interior and the exterior ($q_{i_{conv}}$). The latter is represented by the U-value as described in a previous paragraph 1.5.1.2. and we will show in equation (1-10).
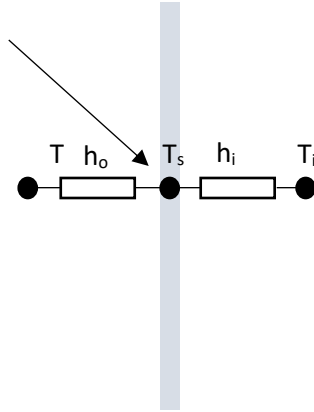
Figure 1-8 Simple nodal model of a single glazing

From the equation (1-8), considering the flow towards the room (q_i) and by using energy balance equation (1-9) we can derive:

$$aG = h_o(T_s - T_o) + h_i(T_s - T_i) \qquad \text{(1-9)}$$

$$T_s = \frac{aG + h_iT_i + h_oT_o}{h_i + h_o} \qquad \text{(1-10)}$$

And by substituting equation (1-10) to equation (1-8),

$$q_i = h_i(T_s - T_i) = aG\frac{h_i}{h_i + h_o} - \frac{1}{\frac{1}{h_i} + \frac{1}{h_o}}(T_i - T_o) \qquad \text{(1-11)}$$

$$\Leftrightarrow h_i(T_s - T_i) = aG\frac{h_i}{h_i + h_o} - U(T_i - T_o) \qquad \text{(1-12)}$$

$$\Leftrightarrow h_i(T_s - T_i) = q_{i_{sol}} - q_{i_{conv}} \qquad \text{(1-13)}$$

Therefore, the first term is the solar heat gains that are caused by the absorbtance of the solar radiation and the second term is the conductive term. We are interested in the solar heat gains term (eq. (1-13)).

$$q_{i_{sol}} = aG\frac{h_i}{h_i + h_o} \qquad \text{(1-14)}$$

It is also interesting to identify that if we are in a balance state, where there is not heat transfer between the inside and the outside, then $T_i = T_o$ and the conductive term $(q_{i_{conv}})$ will be equal to zero.

Equation (1-7) can therefore become:

$$SHGC = a\frac{h_i}{h_i + h_o} + \tau_{eff} \qquad \text{(1-15)}$$

Some typical values of solar heat gain coefficients are presented in Table 1-1. In General, the solar

heat gain coefficient depends on the incident angle and the surface heat transfer coefficients.

Table 1-1 Average typical values of SHGC for different types of glazing (Eicker 2014; McQuistin and Parker 2005)

Building Component	Thickness	SHGC
Uncoated Single glazing	3.2mm	0.86
Uncoated Double glazing	3.2mm	0.76
Uncoated Double glazing	6.4mm	0.70
Low-e Double glazing, e=0.1 on Surf 2	3.2mm	0.65
Low-e Double glazing, e=0.1 on Surf 3	3.2mm	0.60
Triple glazing	3.2mm	0.68
Triple glazing	6.4mm	0.61
Low-e Triple glazing e=0.2 on Surf 2	3.2mm	0.60
Low-e Triple glazing e=0.2 on Surf 2	3.2mm	0.62
Sun protective glazing	-	0.20-0.50
Transparent insulation	-	0.35-0.60

For a double glazing unit, Eicker proposes an equation that is derived by energy balance equations (Eicker 2014). For the solar heat gains that are caused by the absorbtance of the solar radiation,

$$\frac{q_{i_{sol}}}{G} = \frac{\left(\frac{\alpha_1 + \alpha_2}{h_o} + \frac{\alpha_2}{R_{glazing}}\right)}{\frac{1}{h_i} + \frac{1}{h_o} + R_{glazing}} \qquad (1\text{-}16)$$

Although, this equation seems to be problematic as this $\frac{q_{i_{sol}}}{G}$ should be dimensionless. When the same procedure is followed, a similar equation is developed.

$$\frac{q_{i_{sol}}}{G} = \frac{\left(\frac{\alpha_1 + \tau_1\alpha_2}{h_o} + \tau_1\alpha_2 R_{glazing}\right)}{\frac{1}{h_i} + \frac{1}{h_o} + R_{glazing}} \qquad (1\text{-}17)$$

It is important to note that the equation (1-17) also includes the transmittance of the first layer of the double glazing (τ_1) in comparison to the equation (1-16) where it is not included.

Following the Kreider, Curtis and Rabl approximation from equation (1-4) (Kreider, Curtiss, and Rabl 2002), where the resistance of each glazing is neglected, the equation (1-17) becomes:

$$\frac{q_{i_{sol}}}{G} = \frac{\left(\frac{\alpha_1 + \tau_1\alpha_2}{h_o} + \frac{\tau_1\alpha_2}{h_s}\right)}{\frac{1}{h_i} + \frac{1}{h_o} + \frac{1}{h_s}} \qquad (1\text{-}18)$$

Kreider, Curtis and Rabl present the SHGC of a Double Glazing unit with a very similar equation

to equation (1-18) (Kreider, Curtiss, and Rabl 2002).

$$SHGC = \tau_{eff} + \alpha_1 \frac{U}{h_o} + \alpha_2 U \left(\frac{1}{h_{s_1}} + \frac{1}{h_o} \right) \qquad (1\text{-}19)$$

It is also clear that if there is no air-gap then the $\frac{1}{h_{s_1}} \to 0$ and $\alpha_1 + \alpha_2 = \alpha$.

Therefore,

$$\lim_{\frac{1}{h_{s_1}} \to 0} SHCG = \tau_{eff} + \alpha_1 \frac{U}{h_o} + \alpha_2 U \left(\frac{1}{h_o} \right) = \tau_{eff} + (\alpha_1 + \alpha_2) \frac{U}{h_o} \qquad (1\text{-}20)$$

Which is equal to the equation of a single pane window (eq.(1-15))

Although the equation (1-20) is not exactly the same equation we derived earlier (eq.(1-18)) as it doesn't take into consideration that the incident solar radiation on the second layer is a fraction of the incident solar radiation on the first layer only a part of it is transmitted. So, by modifying equation (1-20):

$$SHGC = \tau_{eff} + \alpha_1 \frac{U}{h_o} + \tau_1 \alpha_2 U \left(\frac{1}{h_{s_1}} + \frac{1}{h_o} \right) \qquad (1\text{-}21)$$

Where U value follows the equation (1-4).

And therefore following this equation is easier for us to derive a more general equation for a *N*-layer glazing with *N-1* air-gaps, where $N > 1$.

$$SHGC_N = \tau_{eff} + U \frac{\alpha_1}{h_o} + U \sum_{i=2}^{N} a_i \left(\prod_{i=2}^{i} \tau_{i-1} \right) \left(\frac{1}{h_o} + \sum_{i=2}^{i} \frac{1}{h_{s_i}} \right) \qquad (1\text{-}22)$$

1.5.1.4. Shading coefficient (SC)

A more general way of characterizing the solar transmission and also compare different kinds of glazing and shading devices is the shading coefficient (SC). This is done by comparing the solar heat gain of a product to the solar heat gains of a reference glazing. This reference glazing is a 3 mm thick clear window glass with SHGC of 0.87.

$$SC = \frac{SHGC}{SHGC_{ref}} = \frac{SHGC}{0.87} = 1.15 \cdot SHGC$$

It is important to note that this numbers acts in a reverse analogous way, meaning that the largest the SC of a product is, the largest the solar heat gains are and the shading effect is smaller (Gengel 1985).

Another set of values that are important in the description of fenestration systems are the Solar Transmittance and the Visible Transmittance. Both refer to normal incident radiation and centre-glazing values. From the total solar spectrum, a glazing absorbs, reflects and transmits radiation based on their spectral properties. The percentage of the sun light that is transmitted through a glazing in the visual spectrum (380nm to 700nm) is the visual transmittance of the glazing (ASHRAE 2009), while the percentage of the sun light that is transmitted through a glazing in the total solar spectrum is the solar transmittance

1.5.1.6. Reynolds number (Re) and flows

Reynolds number is the dimensionless ratio of inertial forces to viscus forces. It is calculated as the product of the velocity (V) within a pipe or duct with its hydraulic diameter (D_h) over the kinematic viscosity (v).

$$Re_{D_h} = \frac{V D_h}{v} \qquad (1\text{-}23)$$

In laminar flow viscous forces are dominant and it is characterized by smooth, constant fluid motion. The layers of the fluid, flow in parallel without any mixing between them. Laminar flow usually occurs in lower velocities, but there are cases where turbulent flow can occur at lower velocities, this is why the Reynolds number is proposed to identify the type of the flow.

$$Re_{D_h} < 2300$$

In **transitional flow**, laminar flow exists near the edges of the pipe while at the middle of the pipe turbulent flow exists. It is a mix of laminar and turbulent flow.

$$2300 < Re_{D_h} < 10,000$$

Turbulent flow, is the most commonly observed flow in the nature. Vortices and eddies appear in the flow

$$Re_{D_h} > 10,000$$

1.5.1.7. Grashof number (Gr)

Another dimensionless number used in fluid mechanics and heat transfer is the Grashof number (Gr). The Grashof number describes the ratio of buoyant forces to viscous forces.

$$Gr_{D_h} = \frac{g\beta (T_{surf} - T_{bulk}) D_h{}^3}{v^2} \qquad (1\text{-}24)$$

It is a function of the coefficient of thermal expansion (β), the hydraulic diameter (D_h), the kinematic viscosity (v) and the temperature difference between the surface and the flowing air.

The Prandtl Number is the ratio of momentum diffusivity and thermal diffusivity.

$$Pr = \frac{v}{a}$$

(1-25)

The momentum diffusivity is also known as kinematic viscosity (v) and the thermal diffusivity (a) is function of the thermal conductivity (k), the specific heat (c_p) and the density of the fluid (ρ): $a = \frac{k}{c_p \rho}$.

The Prandtl number in many cases is assumed to be constant as it does not contain any length scale variable as it happens with Reynolds or Grashof numbers. For the cases of air in buildings, this value is typically 0.71 (Kreider, Curtiss, and Rabl 2002).

Rayleigh number (Ra)

The product of the Grashof number (Gr) and the Prandtl number (Pr) gives the Rayleigh number (Ra). Rayleigh number is associated with free convection. With the use of Grashof number, it can be identified the ratio of buoyant forces to viscous forces. With the use of Rayleigh number, it can be identified whether the free convection boundary layer is laminar or turbulent. For a vertical surface, the transition takes place at Ra~10^4.

$$Ra_{D_h} = \frac{g\beta \left(T_{surf} - T_{bulk}\right) D_h{}^3}{va}$$

(1-26)

This dimensionless number describes the natural convention, also known as free convection. Natural convection is a heat transfer mechanism that which is not generated by any external source like fun, pump etc. It is solely dependent on the pressure difference caused by temperature difference. It should be noted that for low Ra, convection is the primary form of heat transfer.

1.5.1.9. Nusselt number (Nu)

A dimensionless number that describes the ratio of convective to conductive heat transfer coefficient is defined by the Nusselt number. If the Nusselt number is close to one, then the convection and conduction are almost equal.

$$Nu_{D_h} = \frac{h_{conv} D_h}{k}$$

(1-27)

Nusselt number is a function of the convective heat transfer coefficient (h_{conv}) of the flow, the hydraulic diameter (D_h) and the thermal conductivity(k) of the fluid.

1.6. Objectives and methodology

The primary goal of this research is to develop a methodology for integrating STPV in building

envelopes for DSF.

The specific objectives are summed up as follows:

- Investigate the state of the art on double skin facades (DSF) and insulating glazing units integrating semi-transparent photovoltaics and identify the important design parameters and outputs; identify the research needs in double skin façade and insulating glazing unit related to DSF-STPV adoption.
- Design a STPV-DSF prototype and perform outdoor experiments for the DSF-STPV and assess the impact of weather variable on its performance, including wind effects, solar radiation, and ambient temperature.
- Develop a numerical model of the DSF-STPV validated through the experiments and implement it into a software tool.
- Identify the energy flexibility that such facades can provide in interacting with a smart grid.

1.7. Thesis overview

•   Chapter 1: The concept of BIPV, BIPV/T, DSF, IGU and STPV is introduced. The motivation behind this study is described along with definitions of important parameters and the objectives of this study.

•   Chapter 2: A literature review on DSF-STPV and IGU-STPV and the research needs are identified. This chapter along with the Appendix form a complete literature review, both from the state of the art and the technological point of view. At the end of this chapter, the identified missing research and the ways that this research will address them is presented.

•   Chapter 3: In this chapter, the outdoor and indoor experimental set-ups are described. Preliminary results of the analysis of these data are presented. These data are later used for the assessment of the wind effects, the incident solar radiation and the ambient temperature on the DSF-STPV. Also, these data are used for the validation of numerical models. Also in this chapter, parts of the published conference paper with tittle: "Experimental Comparison on the Energy Performance of Semi-Transparent PV Facades Under Continental Climate" is presented, showing a preliminary analysis of the experimental set-up.

•   Chapter 4: In this chapter, parts of the published paper with tittle: "Double Skin Façade Integrating Semi-Transparent Photovoltaics: Experimental Study on Forced Convection and Heat Recovery" are presented showing how three Nusselt number correlations were developed describing the convective heat transfer between the STPV surface and the air flowing in the DSF, the STPV cells and the flowing air and the inner layer of the DSF-STPV and the air flow.

•   Chapter 5: A description of numerical models development is presented along with preliminary simulation results. A validated numerical model is used to simulate STPV integrated on building facades on different climates. In addition, the interaction with the grid of a DSF-STPV is also investigated.

•   Chapter 6: In this chapter, parts of the under publication paper with tittle: "Design Methodology and Parametric Analysis for different climates on Double Skin Façades integrating Semi-Transparent Photovoltaics" is presented.

• Chapter 7: In this chapter, parts of the published conference paper with tittle: "Mechanically ventilated Double Skin Façade with Semi-Transparent Photovoltaics, implementing electrical storage and heat pumps to reduce peak demand" is presented. The validated numerical model of a double skin façade integrating semi-transparent photovoltaics has been utilized to assess the impact on the grid of the coupling of such system with battery storage and a HP.

• Chapter 8: Conclusions and Future work

• Appendix I: Heat Transfer coefficient and Nusselt number correlation presented used in Chapter 4

• Appendix II: Results of the analysis presented in Chapter 6, along with the tables generated (Table A1 and Table A2)

• Appendix III: technical literature review on companies developing STPV and their characteristics is presented.

Chapter 2

Literature Review

A series of experiments have been carried out to characterize the performance of windows and double skin facades integrating photovoltaic panels by a number of research teams. Single, double and ventilated windows have been investigated, while the majority of the studies used amorphous silicon (a-Si) photovoltaic panels. The experiments were mainly focused on the electrical performance of the integrated photovoltaics, but many studies focused as well on the thermal and daylight performance of such systems.

Table 2-1 Available literature on experimental research performed on windows and DSF integrating PVs

Study	PV				Window				DSF		Focus			Simulation				Location
	a-Si	Mono-Crystalline	Poly-Crystalline	Micromorph	Single	Double	Triple	Ventilated	Mechanically ventilated	Naturally Ventilated	Electrical	Thermal	Daylighting	Numerical model	Energy Plus	ESP-r	CFD	
J.J. Bloem (2012)	✓				✓						✓	✓		✓				Ispra, Lleida
J. Peng et al (2015)	✓										✓							Solar Simulator
L.Robinson and A.Athienitis (2009)			✓			✓					✓		✓	✓				Montreal
L. Olivieri et al (2014)	✓				✓						✓	✓	✓					Madrid
K. E. Park et al (2010)			✓			✓					✓	✓						Solar Simulator
W. Liao and S. Xu (2015)	✓					✓					✓	✓		✓	✓			
F. Chen et al. (2012)	✓			✓	✓	✓					✓	✓						Solar Simulator
W. He et al (2011)	✓				✓	✓		✓			✓	✓					✓	Hefei
T. T. Chow et al (2009)	✓							✓			✓	✓					✓	Hong Kong
S. Xu et al (2014)					✓						✓	✓	✓		✓			Wuhan
J. Peng et al (2013)	✓									✓		✓						Hong Kong
L. Gaillard et al (2014)			✓								✓		✓	✓				Toulouse
J. Peng et al (2015)	✓										✓	✓	✓					Hong Kong
M. Wang et al (2017)	✓					✓					✓	✓	✓	✓		✓		Hong Kong

In Table 2-1, the available work is summarized, presenting the experimental research performed on windows and double skin facades integrating semi-transparent photovoltaics. The available

literature is also analysed by presenting the different types of PV utilized, the types of windows used and whether the DSF is mechanically or naturally ventilated. In addition, the focus of the study is presented along with whether any simulation models are used. The last row states the location of the experimental facility, if it is an exterior one, or if the experiments are performed on a solar simulator. The majority of the research uses amorphous silicon PV (a-Si) as part of the STPV that are placed at the exterior side of double glazing windows. Triple glazing STPV windows have not been studied, while mechanically ventilated DSF integrating STPV have not also been experimentally investigated.

Many simulation studies have been published, which investigate the performance of semi-transparent photovoltaics integrated into buildings. The effect of the packing factor of the STPV on the performance of building integrated thermal system and an energetic and exergetic analysis of such a system has been performed by Vats and Tiwari (2012) and Vats et al. (2012). It was found that decreasing the packing factor from 83% to 42% leads to a PV module temperature drop by 10 $^\circ$C. Six different STPV modules were compared (m-Si, p-Si, a-Si, Cd Te, CIGS and HIT) and it was found that HIT technology demonstrated higher electrical production and maximum exergy while a-Si present maximum annual thermal energy.

Table 2-2 summarizes the state of the art of STPV, including the simulation research published on windows and double skin facades integrating semi-transparent photovoltaics. In the available literature the most common simulation parameters are the Packing Factor, the Transparency, the Window to Wall Ratio (WWR), the U-value and the Solar Heat Gain Coefficient (SHGC). In addition, the Orientation and the Inclination of the STVP are some of the parameters simulated. Energy Plus is mostly used for thermal and some daylighting simulation, TRNSYS is mostly used for electrical and thermal simulation, while WINDOW and Daysim are used for daylighting simulation. It can be seen that DSF integrating STPV is a field that needs further analysis, while a comparison between numerical models, Energy Plus and TRNSYS is worth investigating.

In addition, several case studies have been simulated. A building integrated with transparent thin film amorphous silicon photovoltaics in South Korea was monitored and then simulated using ESP-r (Yoon, Song, and Lee 2011). ESP-r uses a numerical algorithm of a finite volume approach. ESP-r presented relatively consistent results in comparison to the empirical data. The electrical efficiency a-Si thin film STPV windows of 10% visual transmittance was analysed under operating conditions to determine the factors that cause a decrease in the annual performance of such systems (Mun et al. 2017). A 5 storey in South Korea was monitored and the South façade was divided into four sections; the fan-coil, the vision, the daylighting and the spandrel section, with STPV to be integrated in the three sections except the viewing section. The importance of identifying the external parameters that may result into BIPV shading and its prevention from the design stage was underlined.

Table 2-2 Available literature on simulations performed on windows and DSF integrating PVs

Study	Parameters					DSF		Focus			Simulation						Building type
	Packing Factor	Transparencies	WWR	U-value / SHGC	Orientation / Inclination	Mechanically ventilated	Naturally Ventilated	Electrical	Thermal	Daylighting	Numerical model	Energy Plus	TRNSYS	WINDOW	Daysim	Other	
Chae et al, 2014		✓	✓					✓	✓			✓					Mid-sized Office
Chow et al., 2007	✓								✓	✓	✓						Office
de Boer and Van Helden, 2001		✓		✓	✓			✓	✓				✓	✓			Variable types
Didone and Wagner, 2013				✓				✓	✓	✓		✓			✓	✓	Office
Fung and Yang, 2008	✓										✓						
Ioannidis et al., 2017		✓				✓	✓	✓	✓	✓	✓						Office
Han et al, 2009				✓					✓		✓						
Kapsis and Athienitis, 2015		✓	✓	✓				✓	✓	✓	✓			✓	✓		Office
Li et al, 2009			✓	✓				✓	✓	✓	✓						Generic
Lu and Law, 2013				✓				✓	✓	✓	✓						Office
Miyazaki et al, 2005		✓	✓					✓	✓	✓		✓					Office
Olivieri, 2014		✓	✓					✓	✓	✓		✓		✓		✓	Mid-size Office
Song et al., 2008				✓				✓					✓				Mock-up Model
Vats, 2012	✓							✓	✓		✓						
Vats and Tiwari, 2012				✓				✓	✓		✓						
Wong et al., 2008		✓		✓				✓	✓	✓	✓	✓					Residential

2.1. Literature on IGU-STPV

Looking more into deep in the studies presented in Table 2-1 and Table 2-2, some of the most important parameters used to compare Semi-Transparent facades are analysed. The visual or the solar transmittance of facades with Insulating Glazing Units integrating STPV (IGU-STPV) is reported. Also the ways to measure and calculate the U-value (see 2.1.3.), the SHGC (see 2.1.4.)

and the Nusselt (see 2.1.5.) number of such systems is also presented.

2.1.1. Experimental work on IGU-STPV

Semi-Transparent Photovoltaics are integrated in an outdoor test facility to investigate simultaneously the thermal, electrical and daylight performance of four (4) a-Si STPV modules with visible transmittances between 0.1 and 0.4 (Olivieri, Caamaño-Martin, et al. 2014). Theses STPV have been experimentally compared to a reference glass and all four modules present higher SHGC (approximately 40% larger). The night-time heat loss through the STPV glazing (U-value) is measured to average at 5.7 W/m^{2}K for all the STPV indicating that the transparency of the glazing doesn't affect the U-value of the glazing. This value is high in comparison to typically installed double glazing insulating units, as they are single-glazing units of 3.2mm thickness. The findings on the electrical performance of the a-Si STPV glazing indicate that the transparency is not the most determining factor for the electrical performance of the glazing. The lower the transparency, the higher the temperature of the module is expected to be and that could result in lower cell efficiencies. Although, the authors indicate that this effect is smaller in comparison to other effects such as the manufacturing quality.

The modules that were experimentally investigated in the previous study are now simulated with a series of simulation software (Olivieri, Caamaño-Martín, et al. 2014). The integration of these STPV module on a double-glazing insulating unit increases their thermal resistance bringing the U-value down to 2.783 W/m^{2}K. EnergyPlus, PVsyst, and COMFEN are used to simulate the STPV integrated on a south facing façade of a building in Madrid with a 44% WWR, an 8 W/m^2 lighting power density. For the daylighting, a package of software from LBNL is used, including Optics, Window and Comfen tools. Using these software and having a target work-plane illuminance of 500lx, an energy balance index is presented adding the annual cooling energy demand the annual heating energy demand, the annual lighting energy demand and subtracting the annual photovoltaic energy generation. This energy balance index is then used for a parametric analysis, varying the WWR and the transparency, concluding that for WWR grater that 66%, the STPV with lower transmittances are preferred (10% transmittance).

The use of an interior calorimeter box is used by Chen et al. (2012) for the determination of the SHGC. Three (3) single glazing laminated STPV specimens and two (2) double glazing insulating units are tested under different incident angles. The nominal (0 deg) are reported in Table 2-3 while the SHGC for 45deg, 60deg and 70deg are also calculated in the paper. It provides information that can be useful for actual building integrated STPV, where the incident solar radiation will never be vertical to the façade. It is also reported that the SHGC reduces significantly for incident angles greater than 45º. Another parameter that is presented is the SHCG when the STPV are not connected to a load, and consequently their temperature is higher. This is the standard way of reporting SHGC and can also be a useful information as it is sets the limits for cases where there is an electrical failure at the system. For the use of the calorimeter, a correction factor should be applied as the calorimeter has losses towards the outside.

Kapsis (2016) performed experiments and simulations on IGU integrating STPV of four different solar transmittances. A 6mm thick STPV is integrated on a double glazing and then the SHGC is

measured with the use of a calorimeter box. Later, the same assembly is reconstructed with the use of the WINDOW software and the SHGC is calculated. The difference is that in this case, a correction factor is developed and proposed because the SHGC is not measured under NFRC standards conditions.

To assess the electrical performance of amorphous silicon STPV modules, the Sandia model was first validated experimentally by Peng et al, with indoors and outdoors experiments (Peng et al. 2015b). It is reported that Sandia model is able to predict the electrical output of the STPV modules on a sunny day but in order to predict the electricity production on an overcast day a spectral correction should be applied to correctly simulate the performance of the STPV windows. It is reported that a comprehensive spectral correction function is needed to be developed in the future.

An experiment was set-up by Robinson and Athienitis (2009), integrating STPV on a double glazing window in Montreal (Robinson and Athienitis 2009) focusing on its electrical and daylight performance. A design methodology for optimizing the electricity generation and the daylight utilization was validated showing the potentials of south facing STPV facades.

In addition to the electrical performance, the thermal performance of a double glazing STPV module was studied under standard test conditions and outdoor conditions (Park et al. 2010). For an increase of 1°C of the PV module, it is observed that the temperature coefficient (β) is 4.8% and 5.2% under STC and outdoor conditions respectively (irradiance of 500 W/m2). It is also reported that the type of glass used at the STPV window does not affect the electrical performance of the module but affects the thermal performance of the system.

In addition, a hot-box is used by He et al. (He et al. 2011) to compare an amorphous single-glazing PV window to a ventilated double-glazing PV window. With an electrical efficiency of less than 5% and with a packing factor of 0.8 the SHGC of the IGU integrating STPV is 46.5% in comparison to the single glazing STPV. A CFD analysis is held using ANSYS FLUENT and RNG k-epsilon turbulence model. The difference between the experiments and the model created, for the total heat gains, is 11.7% and 2.7% for the ventilated double-glazing PV window and the single-glazing respectively and the estimated temperature difference is less than a degree C for both cases.

A ventilated thin-film PV window is experimentally assessed and verified using a developed ESP-r simulation model that is then used to compare the STPV window with a simple absorptive glazing (Tin Tai Chow, Qiu, and Li 2009). For an electrical efficiency of less than 5%, the STPV window is compared to an a-Si STPV product available in the market and an to absorptive glazing. It is shown that the see-through PV installation can reduce the consumption of the HVAC by 28%.

2.1.2. Simulations on IGU-STPV

Amorphous silicon and organic STPV are simulated as part of a double-glazing unit (Didoné and Wagner 2013). The PV is therefore modelled as an applied film to the outer pane. The use of Optics 6 from LBNL is used for the generation of the characteristics of the two glazing that integrate STPV and then inserted to WINODW 7 software. Then the IGU-STPV is used to perform thermal, electrical and daylight simulation using the Energy Plus, Daysim and Radiance software for two cities in Brazil and one in Germany. The authors state that the use of IGU-STPV can reduce the

energy consumption for HVAC and lighting if the appropriate control strategy is followed and is generated by the STPV. For this simulating analysis, office buildings are used as the examined case and therefore an automatic dimming system for the lighting is used, aiming to provide 500lx at the work plane. In addition, two different building facades with WWR<50% and WWR>50% are used to represent typical cases of office buildings.

A model and a method was experimentally validated for the optimal cell coverage of STPV integrated on a single glazing unit (Xu et al. 2014). These techniques are later introduced to Energy Plus where different cell coverages are simulated along with different WWR, room geometries and orientations to identify the impact of different cell coverages into the energy consumption of the zone. It is concluded that the selection of the optimal configuration can reduce the energy consumption up to 13% in comparison to the least favourable configuration. The single glazing STPV modelled in this case consists of interior and exterior glazing of 6mm thick and the solar cells that are encapsulated between them with the use of EVA. Energy balance equations are used for a detailed thermal model for each of these four layers. The parameters that are of importance to calculate the heat and solar radiation that is transferred through the glazing is the U-factor and the SHGC.

A comparison is held between two a-Si STPV single glazing unit and common single and double glazing units in terms of their electrical and thermal performance (W. Liao and Xu 2015). Liao and Xu focused mainly on the room and façade dimensions to develop a model and later validate it with field experiments in order to simulate it with the use of Energy Plus. Amorphous silicon STPV windows are found to be better suited for tall rooms or small rooms with high WWR. It is also found that they perform better than single and double-glazing units, mainly because they reduce the cooling loads of the interior zone.

The electrical and thermal performance of semi-transparent PV was investigated as part of the envelope, including the façade the atrium and the awning (de Boer and van Helden 2001). Six different STPV modules integrated on double glazing window with transparencies from 10% to 50% corresponding to actual solar transmittances from 0.065 to 0.284. The WINDOW software is used for the generation of the thermal properties of these STPV glazing and later simulations with TRNSYS software were performed for an office room in Madrid. It is underline that changing the transparency of an awning with STPV window does not have a major impact on the energy consumption due to heating/cooling loads for the simulated building. Also, for façade applications, the STPV transparency does not have a major effect on the energy balance but the increase of the insulation values decreases the energy demand for both heating and cooling.

Optical and thermal PV characterization is performed by Skandalos and Karamanis (2016) along with micro-scale wind tunnel and room building experiments, on STPV that are intended for building integration. STPV, with a-Si and c-Si technology are simulated to be the exterior pane of a double glazing, with different cover ratios and orientations. Also, dynamic building energy simulations are performed with the use of WINDOW, Optics and later with TRNSYS for the calculation of SHGC, U-values and the heating and cooling loads of a building were calculated and is found that the STPV windows can drastically reduce the cooling loads of a zone but may also have an effect on the seasonal heating depending on the transparency.

An a-Si STPV glazing is compared to typically integrated energy efficient windows, like double glazing and low-e glazing (Zhang et al. 2016). With the use of WINDOW, the properties of the glazing are developed and then used in EnergyPlus simulation software. The Sandia Array Performance Model (SAPM) is used for the simulation of the electrical performance of the STPV. It is reported that the STPV can reduce the total electricity consumption of a typical office zone by 16% in comparison to double glazing window in a cooling dominated climate like Hong Kong. In addition, it is indicated that the overall energy performance of a low-e glazing and a single glazing STPV window is very close.

Fung and Yang developed a detailed thermal model to calculate the total heat gain of STPV with different cell coverages and different orientations (Fung and Yang 2008). This one-dimensional transient heat transfer model is experimentally validated by using a calorimeter box and then used for a parametric analysis and discussion. It is reported that cell coverage has a significant impact on the total heat gain as the cell coverage influences the solar heat gains. For four (4) different cell coverages (20%, 40%, 60% and 80%) the total heat gains are reported and for 60%, the solar heat gains are simulated for the different orientations for buildings in Hong Kong. By analysing the Solar heat gains for the south facing façade and the total incident solar radiation per month based on the figures generated by Fung and Yang (2008), the average SHGC for a 60% coverage STPV and solar cell efficiency of 16% is calculated 0.26 with a standard deviation of 0.02.

Except from the electrical effects, the optical parameters of Building Integrated STPV (BISTPV) on the overall performance is examined, for mid-sized commercial buildings under six different climate conditions (Chae et al. 2014). A three-floor office building with five thermal zones and 30% WWR was simulated in Energy Plus. Three different types of a-Si semi-transparent solar cells were simulated, and the results indicated that the thermo-optical characteristics of the STPV windows have a significant impact on the energy consumption of the simulated building zone. It was also reported that the BISTPV can result in to a 30% reduction of the HVAC energy consumption of low latitude sites.

Song et al. (2008) investigated the power output of a semi-transparent thin-film PV module of an IGU. The power performance for different surface inclination and azimuth angle was analysed with the use of TRNSYS. A mock-up model was used to validate the simulated performance with a relative error of 8.5%.

The thermal and power performance of single glazed STPV window for office buildings in Hong Kong was evaluated using a one-dimensional transient model, a power model and an indoor daylight model (Lu and Law 2013). The simulation assumed water and air-cooled air-conditioning systems. The STPV window resulted in a 65% reduction of the total heat gains in comparison to clear glass.

Miyazaki et al. (2005) compared a double to a single glazing STPV window showing that the former minimizes the electricity consumption for heating and cooling. Analysing the heating and cooling loads, the daylighting and the electricity production of a double and single glazing STPV window, for different solar cell transmittances and different window to wall ratios, it was observed that a 40% transmittance and 50% WWR, resulted in the minimum electricity consumption of the

building. Energy Plus simulations showed that this optimal configuration demonstrates a 55% reduction in electricity consumption to a single glazed STPV window configuration of 30% WWR and without an interior lighting control. (Didoné and Wagner 2013) carried out EnergyPlus, Daysim and Radiance simulations for four different STPV-IGUs with U-factors ranging from 2.73 to 1.67 W/m^{2}K, SHGC from 0.76 to 0.13 and one single 6mm STPV glass with a U-factor of 5.82 W/m^{2}K and SHGC of 0.82. It was noted that the low-E window presented the overall best performance among the different types of STPV windows simulated.

Wong et al. (2008) modelled and simulated the electrical, thermal and the daylighting performance of a poly-crystalline STPV panel. Energy Plus was used for the daylighting modelling, while a numerical model was used for the thermal simulation and a power generation equation was used to access the electrical performance of the STPV. It was concluded that a not-optimized STPV system might result in summer overeating, while being a favourable solution for cold climates.

Li et al. (2009a, 2009b) conducted a series of studies to compare STPV facades and skylights to a typical tinted glass. The case studies presented in both papers demonstrated a significant reduction in the energy consumption due to increased daylighting and lower cooling requirement (for the case of STPV. In addition, the STPV generates electricity and reduces the solar heat gain coefficient.

A methodology that integrates the assessment of electrical, thermal and daylighting performance of STPV windows was proposed by Kapsis and Athienitis (2015). Energy Plus was used for the assessment of the thermal and electrical performance of the STPV integrated into the model while Daysim was used for the daylighting. The optical properties of the STPV were found to have an impact on the daylighting and lighting controls of the building. It was suggested that for cold climates, STPV modules with higher than 10% visible transmittance should be selected.

Chow et al (2007b), evaluated the performance of a semi-transparent PV integrated in a ventilated window for an office building in Hong Kong. A combination of a 2D numerical model for the thermal analysis and Energy Plus for the daylight analysis was used. The optimal transmittance of the STPV in order to achieve electricity savings was reported to be between 45% and 55% for Hong Kong (T. T. Chow et al. 2007).

2.1.3. U-value on an IGU-STPV

Han et al (2010), when defining the U-value for an IGU integrating STPV, define the h_t as the total conductance of the glazing unit and is defined by the following equation modified for a more generic result.

$$\frac{1}{h_t} = \sum_{j=1}^{N} \frac{1}{h_{cavity_j}} + \sum_{j=1}^{N} \frac{l_{glass}}{k_{glass}} + \frac{l_{PVglass}}{k_{PVglass}} \qquad (2\text{-}1)$$

Where h_{cavity} is the heat transfer coefficient of the air within the cavity, and N is the number of cavities in the IGU. It can be broken down to the addition of the convection heat transfer coefficient

(h_c) and radiation heat transfer coefficient (h_r):

$$h_{cavity} = h_c + h_r \qquad (2\text{-}2)$$

For the convective heat transfer coefficient due to natural ventilation of the air within the air-gap of an IGU, the use of average Nusselt number coefficients are used.

$$h_c = \frac{\overline{Nu}k_{air}}{l_{air}} \qquad (2\text{-}3)$$

Different average Nusslet number correlation are used for this and will be described later in paragraph 2.1.5.

For the radiative heat transfer coefficient an approximation is commonly used:

$$h_r = 4\sigma \left(\frac{1}{\varepsilon_{PVglass}} + \frac{1}{\varepsilon_{glass}} - 1 \right)^{-1} T_m{}^3 \qquad (2\text{-}4)$$

Where σ is the Stefan-Bolrzmann constant, $\varepsilon_{PVglass}$ is the emittance of outer PV glass and the ε_{glass} is the emittance of the inner glass, T_m is the mean temperature of the PV pane and the glass pane. This could generate though a great error in calculations when STPV is integrated on the exterior pane as its temperature increases a lot and it doesn't contribute the same in the radiation exchange.

Han et al (2010), presented a numerical evaluation on the heat transfer that occurs within the double pane of a window that integrates a-Si STPV. By taking into consideration the combined convection and radiation effect along with air flow patterns, the Rayleigh number was investigated as well as the effect of low-e coatings on the U-value. The use of Navier-Stokes and energy equations are used to obtain numerical solutions. It is reported that the increase of Rayleigh number increases the convective flow strength and the heat transfer. Also Han et al. (2010, 2009) investigated the thermal behaviour and performed a numerical evaluation of the mixed convective heat transfer phenomena of an STPV. They reported that the Rayleigh numbers are in the range of 10^3 to $2\text{x}10^5$ and that the optimal thickness is found to be in between 60 mm and 80 mm. A numerical mathematical model based on momentum, stream function and energy non-dimensional equations is developed and later validated for a steady state buoyance induced natural convective airflow. In addition, the U-value of an STPV window was investigated, indicating that the radiative heat transfer could be significantly reduced by using low-e coating changing the emissivity from 0.88 to 0.05.

2.1.4. SHGC on an IGU-STPV

A calorimetric box that is developed by the Solar Energy Research Institute of Singapore (SERIS), is used for the SHGC measurement of STPV windows in a Solar Simulator (Shabunko 2018; Chen et al. 2012).

The Solar simulator used at SERIS is a single-lamp system located 10 m away from the specimen to achieve desired uniformity levels. It is presented that the solar simulator can provide 93.5% of the total solar energy in the spectrum of 300nm to 2500nm in comparison to the standard of the AM1.5 spectrum. In order to present data according to the AM1.5 standard, a method is broadly used (Harrison and Collins 1999; Collins 2016), which is based on simulations and uses correction factors.

$$c_1 = \frac{SHGC_{spectrum}}{SHGC_{AM1.5}} \qquad (2\text{-}5)$$

Where $SHGC_{AM1.5}$ is the SHGC obtained with simulation according to AM1.5 standard and the $SHGC_{spectrum}$ is the simulated SHGC for the spectrum and the condition of the solar simulator. The WINDOW software was used for the simulation of the solar heat gain coefficients.

Another correction term is used to avoid measuring on the SHGC the fraction of the solar radiation that is transmitted and then reflected at the back of the calorimeter. The correction factor proposed is:

$$c_2 = \tau^2 \rho_{box} \qquad (2\text{-}6)$$

Where τ is the solar transmittance of the specimen and ρ_{box} is the solar reflectance of the back of the plate. It is also reported that for a single glazing, 3.4% of the total incident solar radiation is transmitted again outside while for a double glazing it 0.5%.

The corrected SHGC is therefore given by the equation (2-7).

$$SHGC_{corrected} = \frac{SHGC_{spectrum}}{SHGC_{AM1.5}} \cdot SHGC_{Measured} + \tau^2 \rho_{box} \qquad (2\text{-}7)$$

$$SHGC_{corrected} = c_1 \cdot SHGC_{Measured} + c_2 \qquad (2\text{-}8)$$

The SHGC of each test specimen is calculated as the heat flow through the specimen over the total incident solar radiation.

$$SHGC_{Measured} = \frac{\dot{Q}_{SHG}}{A_s I_s} \qquad (2\text{-}9)$$

$$\dot{Q}_{SHG} = -\left(\dot{Q}_{flow} + \dot{Q}_{box\ losses} + \dot{Q}_{specimen\ losses}\right) \qquad (2\text{-}10)$$

$$\dot{Q}_{specimen\ losses} = U_{specime} A_{specimen}(T_{room} - T_{calorimeter}) \qquad (2\text{-}11)$$

Where $\dot{Q}_{flow}$ is the heat removed by the chilled water, $\dot{Q}_{box\ losses}$ is the heat losses from the calorimeter box and $\dot{Q}_{specimen\ losses}$ represents the losses through the specimen. This is given by equation (2-11) which corresponds to equation (1-8) described in the previous chapter.

A similar approach was followed by Kapsis (2016) to measure and estimate the SHGC using a calorimeter. The difference is this case is that Kapsis used a correction factor to identify the SHGC of STPV integrated in an IGU and working at its maximum power point. At this case, the SHGC is smaller, as part of the incident solar radiation is converted to electricity and not converted to thermal energy.

The methodology that is followed is that the optical properties of the STPV are imported to the WINDOW software that generates the SHGC under the NFRC 200 standard without being connected to a load. Then the SHGC of the IGU is experimentally determined and a correction factor is generated (c_3).

$$c_3 = \frac{SHGC_{simulated}}{SHGC_{measured\ without\ load}}$$ (2-12)

What follows is that the SHGC of the IGU under maximum power point is experimentally measured and the correction factor is used to identify the corrected SHGC of the STPV window.

$$SHGC_{corrected} = c_3 \cdot SHGC_{measured\ with\ load}$$ (2-13)

For a STPV on a window, the equations presented in paragraph 1.5.1.3. are used by (Fung and Yang 2008; Xu et al. 2014) for the SHGC measurement. More precisely, a similar form of the equation (1-15) is used for the SHGC where the cell coverage is used for the effective transparency of the panel, as well as the transparency of each layer of the STPV:

$$\tau_{eff} = \tau_1 \tau_2 \tau_3 (1 - cell\ coverage)$$ (2-14)

For an exterior experimental installation in Hong Kong, Wang et al, used conductive heat flux meters and radiant heat flux meters to measure the conductive and radiant heat gains respectively through the IGU integrating STPV and also DSF integrating STPV (Wang et al. 2017). The reported U-values are measured during the night when the solar gains are zero and the SHGC is measured when the incident solar radiation is higher than 200 W/m². The values measured are presented in Table 2-3.

2.1.5. Nusselt number correlation within the IGU-STPV

Nusselt number coefficients are used to calculate the convective heat transfer coefficient of the air within the air-gap of an IGU. Han et al (2009) presented a CFD analysis where the Nu correlation fits between the Nu correlations developed by Elsherbiny and Yin (1982; 1978). Although these equations are not present by the authors. Based on the data provided in the paper, these correlations are derived as:

$A = 8, Pr = 0.7$ $10^3 \leq Ra_{D_h} \leq 10^5$ (Han, Lu, and Yang 2009)	$*Nu_{D_h} = 0.1391 \cdot Ra_{D_h}{}^{0.278}$	(2-15)

$4.9 \leq A \leq 79.7, Pr = 0.7$ $10^3 \leq Ra_{D_h} \leq 5 \cdot 10^6$ (Han, Lu, and Yang 2009)	$*Nu_{D_h} = 0.23 A^{-0.131} Ra_{D_h}{}^{0.269}$	(2-16)

The presented equations in blue font color are derived based on data presented in the study

The EISherbiny equations are also presented:

	$Nu_{D_{h\,1}} = 0.0605 \cdot Ra_{D_h}{}^{1/3}$	(2-17)
$5 \leq A \leq 110,$ $A = (20/Ra_{D_h}) < 2 \cdot 10^6,$ $A = (40/Ra_{D_h}) < 2 \cdot 10^5,$ $A = (80/Ra_{D_h}) < 2 \cdot 10^5$ (EISherbiny, Raithby, and Hollands 1982)	$Nu_{D_{h\,2}} = \left\{ 1 + \left[\dfrac{0.104 \cdot Ra_{D_h}{}^{0.293}}{1 + (6310/Ra_{D_h})^{1.36}} \right]^3 \right\}^{1/3}$	(2-18)
	$Nu_{D_{h\,3}} = 0.242 \cdot \left(Ra_{D_h}/A \right)^{0.272}$	(2-19)
	$Nu_{D_h} = max\,[Nu_1, Nu_2, Nu_3]$	(2-20)

where A is the aspect ratio of the enclosure ($A = H/l$), where H is height and l is the thickness of the air gap of the glazing. Regarding the Elsherbiny correlations, the maximum of three proposed coreelation is each time used.

Frank, Manglik and Bohn in their book (2010) present Nu correlations for heated from one side enclosed spaces, similar to an IGU integrating STPV.

Heated from one side enclosed spaces. Free convection.		
$2 < A < 10, Pr < 10$ $Ra_{D_h} < 10^{10}$ (Frank, Manglik, and Bohn 2010)	$Nu_{D_h} = 0.22(A)^{-1/4} \left(\dfrac{Pr}{0.2 + Pr} Ra_{D_h} \right)^{0.28}$	(2-21)
$1 < A < 2, 10^{-3} < Pr < 10$ $10^3 < \dfrac{Ra_{D_h} Pr}{0.2 + Pr}$ (Frank, Manglik, and Bohn 2010)	$Nu_{D_h} = 0.18 \left(\dfrac{Pr}{0.2 + Pr} Ra_{D_h} \right)^{0.29}$	(2-22)

2.1.6. Complete table of important values for IGU-STPV

A series of studies that have focused on glazing STPV is analysed and is presented in Table 2-3. The studies are shorted based on the total solar transmittance (3rd row). The Visible Transmittance, the SHGC, the U-value, the Peak Production of the STPV, the technology of the STPV and the thickness of the glazing is presented. In addition, it is reported if the glazing is Single (SG) or Double (DG) along with, if these values are based on experiments (E) or simulations (S). For the thickness of the glazing, the front glazing thickness, the gap thickness, and the thickness of the back glazing is separated by a slash. In the majority of the studies, the STPV consists of two glasses, also known as glass on glass. If a glass on glass STPV is reported, the thicknesses of the

two glasses are presented as a summation. The values presented in the table with blue color, are values calculated based on the data provided by the authors. These calculations are based on the equations presented in paragraph 1.5.1.

Table 2-3 Table of important values, shorted based on the total solar transmittance Tsol.

Study	Tvis	Tsol	SHGC With load (w), Without load (w/o)	Glazing	U-value (W/m²K)	Wₚ/m²	Technology	Thickness in mm, front/gap/back (total)	Experimental/Simulation
(Olivieri, Caamaño-Martín, et al. 2014)	0.003	0.002	0.145(w)	DG	2.78	62.0	a-Si	21	S
(Kapsis 2016a)	0.058	0.046	0.096(w),0.125(w/o)	DG	2.01	153	c-Si	6/25.4/5.6	E
(Kapsis 2016a)	0.058	0.046	0.111(w),0.145(w/o)	DG	2.01	153	c-Si	6/25.4/5.6	S
(Xu et al. 2014)		0.057	0.311	SG	2.36		a-Si	6+1.8+6	S
(de Boer and van Helden 2001)	0.068	0.065	0.37	DG	1.93		c-Si	4.8/15/4	S
(Olivieri, Caamaño-Martín, et al. 2014)	0.101	0.077	0.216(w)	DG	2.78	44.3	a-Si	21	S
(Didoné and Wagner 2013)	0.09	0.08	0.13(w)	DG	1.67	50	a-Si	3/12/3	S
(Chae et al. 2014)	0.054	0.086	0.235	DG	2.75		a-Si	3/13/3	S
(Chen et al. 2012)		0.10	0.310(w), 0.289(w/o)	SG		45.1	a-Si	5+5	E
(Chen et al. 2012)		0.10	0.161(w), 0.154(w/o)	DG		35.7	a-Si	5+5/19/5	E
(Chen et al. 2012)		0.10	0.127(w), 0.123(w/o)	DG		47.3	a-Si	5+5/18/5	E
(Olivieri, Caamaño-Martin, et al. 2014)		0.10	0.655(w)	SG	5.7		a-Si	3.2	E
(Xu et al. 2014)		0.114	0.340	SG	2.36		a-Si	6+1.8+6	S
(Olivieri, Caamaño-Martín, et al. 2014)	0.158	0.120	0.253(w)	DG	2.78	38.0	a-Si	21	S
(de Boer and van Helden 2001)	0.135	0.120	0.38	DG	1.99		c-Si	4.8/15/4	S
(Skandalos and Karamanis 2016)		0.124	0.210(w),0.221(w/o)	DG	2.91		c-Si	4.6/12/4	S
(Kapsis 2016a)	0.172	0.135	0.203(w),0.225(w/o)	DG	2.01	125	c-Si	6/25.4/5.6	E
(Kapsis 2016a)	0.172	0.135	0.218(w),0.242(w/o)	DG	2.01	125	c-Si	6/25.4/5.6	S
(de Boer and van Helden 2001)	0.168	0.148	0.39	DG	2.21		c-Si	4.8/15/4	S
(Xu et al. 2014)		0.171	0.369	SG	2.36		a-Si	6+1.8+6	S
(de Boer and van Helden 2001)	0.203	0.175	0.39	DG	2.05		c-Si	4.8/15/4	S
(Olivieri, Caamaño-Martín, et al. 2014)	0.249	0.186	0.316(w)	DG	2.78	31.6	a-Si	21	S
(Olivieri, Caamaño-Martín, et al. 2014)		0.20	0.660(w)	SG	5.7		a-Si	3.2	E
(Wang et al. 2017)		0.2	0.238(w)	DG	2.28	61.5	a-Si	6.2/9/5	E
(W. Liao and Xu 2015)	0.20	0.22	0.26	SG	5.18	4.9	a-Si	6+0.15+6	S
(Chae et al. 2014)	0.128	0.221	0.326	DG	2.65		a-Si	3/13/3	S
(Kapsis 2016a)	0.285	0.223	0.314(w),0.331(w/o)	DG	2.01	97.4	c-Si	6/25.4/5.6	E
(Kapsis 2016a)	0.285	0.223	0.322(w),0.339(w/o)	DG	2.01	97.4	c-Si	6/25.4/5.6	S
(Xu et al. 2014)		0.228	0.397	SG	2.36		a-Si	6+1.8+6	S
(de Boer and van Helden 2001)	0.271	0.229	0.41	DG	2.10		c-Si	4.8/15/4	S
(Skandalos and Karamanis 2016)		0.235	0.327(w),0.335(w/o)	DG	2.63		a-Si	8/20/4	S
(Olivieri, Caamaño-Martín, et al. 2014)	0.324	0.242	0.367(w)	DG	2.78	25.3	a-Si	21	S
(Zhang et al. 2016)	0.153	0.268	0.471	SG	5.50	58.5	a-Si	9.7	S
(de Boer and van Helden 2001)	0.339	0.284	0.43	DG	2.15		c-Si	4.8/15/4	S
(Xu et al. 2014)		0.285	0.426	SG	2.36		a-Si	6+1.8+6	S
(Olivieri, Caamaño-Martin, et al. 2014)		0.30	0.679(w)	SG	5.7		a-Si	3.2	E
(Didoné and Wagner 2013)	0.23	0.30	0.22(w)	DG	1.67	30	Organic	3/12/3	S
(Chae et al. 2014)	0.277	0.307	0.401	DG	2.58		a-Si	3/13/3	S
(Kapsis 2016a)	0.398	0.312	0.428(w),0.438(w/o)	DG	2.01	69.4	c-Si	6/25.4/5.6	E
(Kapsis 2016a)	0.398	0.312	0.426(w),0.436(w/o)	DG	2.01	69.4	c-Si	6/25.4/5.6	S

(Xu et al. 2014)		0.342	0.455	SG	2.36		a-Si	6+1.8+6	S
(W. Liao and Xu 2015)	0.32	0.35	0.41	SG	5.18	4.1	a-Si	6+0.15+6	S
(Xu et al. 2014)		0.399	0.484	SG	2.36		a-Si	6+1.8+6	S
(Chen et al. 2012)		0.40	0.422(w), 0.413(w/o)	SG		56.0	m-morph	7	E
(Olivieri, Caamaño-Martin, et al. 2014)		0.40	0.734(w)	SG	5.7		a-Si	3.2	E
(Fung and Yang 2008)		0.40	0.26	SG		96	c-Si	6	S
(Xu et al. 2014)		0.456	0.512	SG	2.36		a-Si	6+1.8+6	S
(Xu et al. 2014)		0.513	0.541	SG	2.36		a-Si	6+1.8+6	S
(Chen et al. 2012)		0.60	0.304(w), 0.298(w/o)	SG		24.5	m-morph	7	E

The presented values in blue font color are derived based on data presented in each study

2.2. Literature on DSF-STPV

The integration of PV on DSF is an idea that has recently received the attention of the academic community. The majority of the research is focused on naturally ventilated DSF integrating STPV made out of amorphous silicon.

2.2.1. Experimental work on DSF-STPV

Peng et al, set-up an experimental facility in Hong Kong, that consists of a DSF integrating see-through a-Si PV (Peng, Lu, and Yang 2013a; Peng et al. 2015a). The DSF has a cavity width of 400 mm that is created between a double glazed see-through PV and the interior window and inlets at the top and the bottom, both at the exterior side. Four different operation modes of the dampers and the interior window were experimentally investigated showing that the temperature of the air at the outlet can be more than 2°C higher than the one at the inlet. It is also reported that the SHGC for the different operation modes are between 0.1 and 0.13.

The air inlet and outlet is at the top and bottom of the DSF respectively and can be controlled with the use of louvers. Two virtually identical DSF integrating PV, can operate under different ventilation modes by controlling the louvers. More specifically, the Mode 1 and 2 has as an objective to compare the thermal and electrical performance of the DSF-STPV under the non-ventilated and ventilated conditions and the buoyancy driven ventilated and ventilated conditions, respectively. By collecting local weather data; wind speed and direction, ambient temperature, humidity and diffused and horizontal incident solar radiation, the experiments have as an objective to calculate the SHGC and U-Value of the DSF-STPV. In addition, I–V and P–V curves for different ventilation modes were plotted to characterize and assess the STPV performance. It is indicated that the solar heat gains are reduced by 20% for the ventilated DSF-STPV in comparison to the non-ventilated, while the non-ventilated DSF-STPV presents lower and thus better U-values. A temperature difference of 10°C between the ambient and the air within the cavity is reported showing in this way the amount of wasted heat that can be recovered. This also highlights the importance of having different operation strategies in warmer climates. The SHGC is reported to be 0.1, 0.115 and 0.12 for the cases of naturally ventilated, buoyancy driven ventilated and non-ventilated, respectively. The corresponding U-values of the system are 3.4, 3.8 and 4.6 W/m²K.

The same experimental facility was later used to validate a developed simulation model, based Energy Plus (Peng et al. 2016). A sensitivity analysis is conducted to access the effect of the cavity depth on the overall performance of the DSF integrating PV. It is identified that the 0.2m gap is the worst thickness for the net-electricity use. Three different ventilation modes are investigated;

non-Ventilated, buoyancy driven ventilated and naturally ventilated. The buoyancy driven flow happens when there is only one opening at the top of the DSF-STPV from which the air is circulated through. For this experimental facility, which was placed in Berkley, California, the electricity consumption for cooling is on average 8 times higher than this for heating and for this reason the non-ventilated DSF-STPV results in poorer overall performance. It is also reported that the electricity production from the a-Si STPV integrated at the exterior of the DSF is not affected greatly by the different kind of ventilation mode (only by 3%). This happens for two reasons; one is because the STPV that is used is a-Si which has smaller power temperature coefficient and because the flow that occurs when it is naturally ventilated is not really high to increase the convection inside the cavity and drop the temperature of the PV. For a cool-summer Mediterranean climate zone, a thickness between 0.4m and 0.6m could be recommended as the optimal cavity width while the DSF-STPV, used 50% less net-electricity than other glazing systems. In addition, it is highlighted that the future of the DSF-STPV is promising because of the decrease of the prices and the increase of the efficiencies of the PVs.

A comparison of the energy performance of a STPV double skin façade and a conventional glass façade was made by Han et al. (2013). Two similar experimental test facilities were built in Hong Kong, one with the DSF and one with the conventional glass façade. The DSF facility has openings at the top and bottom to allow natural ventilation within the cavity. A 2D numerical model was developed to assess the thermal performance of the two façade types, showing that the solar heat gains during the cooling season can be reduced, resulting in a better thermal comfort for the occupants.

Gaillard et al (2014) focused on monitoring and evaluating a DSF integrating PV. The prototype is not an optimized system but is rather used as an innovative design that can improve the electrical, thermal and daylighting performance of the building. From the energetic approach, the main objective is to increase the efficiency of the PV by cooling them down and removing the excessive heat from the cavity via natural ventilation. This cavity has an air gap of 60cm to 80cm and the DSF is facing West-North-West with openings at the upper and lower ends of the DSF. Typical days were retrieved from a database and then classified into 'sunny', 'windy and sunny' etc. to assess the effect of the weather phenomena on the performance of the DSF. The thermal performance of the DSF is defined as the heat recovered over the incident solar radiation. It is particularly noted that the PV façade is not the only nor the dominant source of heat to the air within the cavity. The heat recovered from the building is significant and thus creates problems in the calculation of the thermal efficiency of the system. It is reported that on sunny summer days, the temperature difference between the inlet and the outlet of the DSF can be more than 10ºC, while the Reynolds number is of the order of 10^4. It is also reported that there is no clear correlation between the wind speed and the air velocity within the cavity. To define the effect of the wind and stuck effect on the flow of the air, the Archimedes number is used. The square of the Reynolds is higher than the Grashof number and thus the stack effect is dominant against the forced convection of the wind effects, for all days during periods of incident solar radiation. The stack effect does not seem to be affected by the fluctuations of the wind and the natural convection flow is not disrupted. On the other hand, the wind effects seem to increase the cooling of the PV by increasing

the exterior heat transfer coefficient and for this reason, the authors indicate that further analysis should be done to the reveal relationships between wind effects and the airflow.

Three prototype DSFs integrating semi-transparent photovoltaics are tested and a comparison between the thermal response of the semi-transparent photovoltaics and the air inside the cavity is presented (Gaillard, Ménézo, et al. 2014). The two-storey West North-West DSF of the building is designed to increase the electrical performance of the semi-transparent photovoltaics installed by utilizing the stack effect (Gaillard, Giroux-Julien, et al. 2014). As reported by the experimental data collected under real conditions, in a span of a year, the behaviour of the system can be predicted by using simple relationships.

Based on the Mataro Library in Barcelona, Mei et al, developed a dynamic thermal model on TRNSYS for a DSF integrating STPV (Mei et al. 2003). For a 15% transparency and an assumed as constant transmittance-absorptance of 0.8 STPV panel a thermal model was developed. It is reported that the air at the outlet of the DSF-STPV can reach 50°C in summer and 40°C in winter and this preheated air can be introduced into the HVAC system to reduce the heating load by 12%. Based on the same building the potential to use a desiccant cooling machine in combination with the DSF-PV is investigated (Mei et al. 2006). The 70°C heated air within the DSF can be fed into the desiccant cooling machine and regenerate the sorption wheel, resulting into an average COP of 0.518 during the summer season. The approach of four different terms describing the ventilation gains, the transmission losses and the temperature components are used in a steady state analysis to simulate the Mataro Library DSF-PV (Infield, Mei, and Eicker 2004; Infield et al. 2006). In this way, monthly U and g values have been derived and the energy thermal gains have been calculated.

An integral (electrical, thermal and daylight) simulation model is used to conduct an annual performance study for an architype office building located at Toronto, Canada. The model is experimentally verified. The analysis demonstrates that the use of STPV façades have the ability to generate enough electricity to cover the annual electricity demand of the building on electric lighting and plug loads. In case of STPV/T or double skin façade, a significant amount of heat (in the form of preheated outdoor air) could be also generated. The heated air could be used to a solar assisted air-source heat pump that could be used to partially cover the heating and cooling demands of the building. Moreover, the use of STPV/T or double skin façade reduces the heat losses through the building skin during the heating season.

2.2.2. Simulations on DSF-STPV

Simulating models have been used to assess the performance of Double Skin Façade (DSF) integrating Semi-transparent Photovoltaics. The concept of DSF emerged from the need for improved heat, noise, and pollutant transfer control, while maintaining superior aesthetics. Their primary function is to regulate the indoor environment and passively reduce the energy consumption of the building (Poirazis 2007). However, recently, DSF have further been implemented to actively contribute towards the creation of energy positive facades with the integration of STPV. DSF have been extensively reviewed in the past and are mainly separated into two categories; naturally ventilated and mechanically ventilated DSF (Quesada et al. 2012a). The academic community has focused on the different types of shading devices implemented

within naturally ventilated DSF, mainly because of the complexity of the mechanically ventilated DSF but also because of the noise that shading devices within a mechanically ventilated DSF would create (Gratia and De Herde 2004). Additionally, the modelling and the experimental validation for different typologies of DSF has been performed, indicating that a whole building analysis including the DSF is imperative in order to analyse the effect that the flowing air within the DSF has on the building (Saelens, Carmeliet, and Hens 2003). On the other hand, the integration of PVs on DSF made the idea of mechanically ventilated DSF more relevant. Agathokleous and Kalogirou (2015) suggested the use of mechanically ventilated facades given the fact that such systems can operate under different conditions and applications, as well as the potential for PV cooling and heat recovery (Agathokleous and Kalogirou 2016). The author (Z. Ioannidis et al. 2017; Zissis Ioannidis 2016; Z Ioannidis et al. 2016) presented a novel mechanically ventilated DSF integrating opaque and semi-transparent PV reporting that integrated PV can supply with electricity an adjacent zone of the building up to 27m^2 (290 ft^2).

A DSF and an IGU, both integrating STPV are compared (Wang et al. 2017) and their applicability is investigated for the energy savings potentials in five different climates of China. The electrical, thermal and daylighting performance of the DSF and IGU are investigated experimentally and then simulation models are developed and validated. After the models are validated, they are used to investigate their performance at the five different climates of China. The SHGC and the U-values of the presented technologies are experimentally calculated and then simulations are conducted with the use of EnergyPlus simulation software. For these simulations, a typical sized office room of 18m^2 with a WWR of 40% is used. Comparing the IGU-STPV to a typical IGU, it is found that the IGU-STPV performs better because it present lower SHGC and thus has reduced cooling loads. The DSF-STPV reduces the cooling energy consumptions and increases the performance of the STPV, while the IGU-STPV reduces the energy consumption for heating and daylighting. In general, it is reported that the IGU-STPV performs better than the DSF-STPV for the five investigated climates in China. In addition, three different ventilation modes of the cavity of the DSF-STPV are simulated indicating the importance of the selection of the appropriate ventilation mode for cold climates.

2.2.3. U-value on DSF-STPV

To calculate the U-value of a DSF integrating STPV, the total heat loss transferring from the inside to the outside should be measured. This includes the conductive heat loss and the radiation exchange of the STPV with the surrounding (Peng, Lu, and Yang 2013a; Peng et al. 2015a; Wang et al. 2017).

$$U \approx \frac{Q_{conv,o} + Q_{rad,o}}{(T_i - T_o)} \qquad (2\text{-}23)$$

With $Q_{rad,o}$ is the radiation exchange with of the STPV with the sky and the surrounding.

The authors present that for the U-value, the conductive heat loss transferring from the inside window to the outside should be measured. The following equation could describe the previous

statement.

$$Q_{conv,o} = \frac{T_{s2} - T_o}{\frac{1}{h_{c_o}} + R_{pv} + \frac{1}{h_{c_{cavity}}} + R_g + \frac{1}{h_{c_i}}} \qquad (2\text{-}24)$$

Although another definition is proposed that should be used in a definition of the U-value of a DSF. The exterior skin of the DSF-STPV, which is the STPV, does not affect the heat losses of the building, as this heat loss is recovered in the air within the DSF. For this reason, the U-value should not be calculated between the inside and outside temperature, but it would rather be calculated as the conductive heat transfer between the inside temperature and the temperature within the cavity and the radiant heat exchange between the glazing and the STPV.

2.2.4. SHGC on DSF-STPV

The SHGC of an STPV on a DSF follows the definition of the SHGC as it is described in paragraph 1.5.1.3. (Peng, Lu, and Yang 2013a; Peng et al. 2015a; Wang et al. 2017).

$$SHGC \approx \frac{G_{trnas} + Q_{rad,i} + Q_{conv,i}}{G_{solar}} \approx \tau + \frac{Q_{rad,i} + Q_{conv,i}}{G_{solar}} \qquad (2\text{-}25)$$

$$Q_{conv,i} = h_{c_i}(T_g - T_i) \qquad (2\text{-}26)$$

The $Q_{rad,i}$ is not described how it is calculated but in general it given by:

$$Q_{rad,i} = \frac{A_{window}(\sigma T_{window}^4 - \sigma T_{wall}^4)}{\frac{\rho_{window}}{\epsilon_{window}} + \frac{1}{F_{window \to wall}} + \frac{\rho_{wall}A_{window}}{\epsilon_{wall}A_{wall}}} \qquad (2\text{-}27)$$

Sometimes, a radiation heat transfer coefficient is used as a shortcut in the calculation of the radiation heat exchange.

$$h_{rad} = \frac{4\sigma \bar{T}^3}{\frac{1}{\epsilon_{window}} - \frac{1}{\epsilon_{wall}} - 1} \qquad (2\text{-}28)$$

Where,

$$\bar{T} = \frac{\bar{T}_{window} + \bar{T}_{wall}}{2} \qquad (2\text{-}29)$$

2.2.5. Nusselt number correlation within the DSF-STPV

There are not many studies that have focused on the Nusselt number correlation for a DSF integrating STPV. For forced convection, the Nusselt number correlation developed by Petukov and Tan and Charters are presented by Eicker (2014). Although these numbers are not generated based on experiments done on DSF integrating STPV, Eicker suggest that these numbers can be

used.

Petukov equation $Re_{D_h} > 3100$ (Eicker 2014)	$$Nu_{D_h} = \frac{(Re_{D_h} - 1000)Pr\frac{f}{8}}{1 + 112.7\sqrt{\frac{f}{8}}(Pr^{2/3} - 1)}\left(1 + \left(\frac{D_h}{l}\right)^{2/3}\right)$$	*(2-30)*
Tan and Charters $Re_{D_h} > 3100$ (Eicker 2014)	$$Nu_{D_h} = 0.0158Re_{D_h}^{0.8} + \left(0.00181Re_{D_h} + 2.92\right)e^{-0.03795\frac{l}{D_h}}$$	*(2-31)*

Where $f = \left(0.791Re_{D_h}^{0.8} - 1.64\right)^{-2}$

While the last term in both equations is a correction term for short channels.

2.2.6. Complete table of important values for DSF-STPV

Similarly, to the Table 2-3, another table is created for the DSF that integrate STPV. It is clear that the number of studies in this field and the data provided by each study are limited. In addition to Table 2-3, the dimensions of the DSF-STPV are presented along with the flow characteristics. These characteristics consists of the Reynolds number, the min max and average air velocities of the air within the cavity, the volumetric flow rates, and the air changes per hour. Based on graphs with experimental data some of these values are calculated and presented for comparison.

Table 2-4 Table of important values for DSF integrating STPV

Study	Tvis	Tsol	SHGC	Glazing	U-value (W/m²K)	W_p/m²	Technology	Reynolds	DSF-dimension	Average velocities (m/s)	Min, Max Velocities (m/s)	Flow rates (m3/s)	ACH	Mechanically/Naturally ventilated DSF	Thickness of PV	Thickness of glass	Experimental/Simulation
(Peng et al. 2015a)	NA	NA	0.1	SG	3.4	59.4	a-Si	104<Re<11210	0.4	0.09	0,0.29	0.12	0.088	Nvent	8	3	E
(Peng et al. 2015a)	NA	NA	0.115	SG	3.8	59.4	a-Si	104<Re<4662	0.4	0.06	0,0.12	0.07	0.057	Buoy	8	3	E
(Peng et al. 2016)	NA	0.07	-	SG	-	59.4	CdTe	NA	0.4-0.6	NA	NA	NA	NA	NA	NA	NA	S
(Wang et al. 2017)	NA	0.2	0.152	SG	2.54	62.8	a-Si	NA	0.4	NA	NA	NA	NA	NA	6.2	5	E
(Gaillard, Giroux-Julien, et al. 2014)	NA	NA	NA	NA	NA	NA	c-Si	6·10⁴<Re<13·10⁴	0.55	0.73	0.50,1.00	0.48	0.065	Nvent	NA	NA	E

The presented values in blue font color are derived based on data presented in each study

2.3. Exterior and interior heat transfer coefficient and the impact of wind

The heat transfer between the exterior skin of a building and ambient air is described by the exterior heat transfer coefficient $(h_{c,o})$. It can be either free convection or forced convection. The majority of the cases, where wind is present, forced convection is identified.

Free convection can be either laminar or turbulent. In most of the flows around buildings, in which forced convection is dominant, the flow will be turbulent.

For free convection, the exterior heat transfer coefficient for laminar and turbulent flows over a tilted surface is given by equation (2-32) and (2-33).

Free convection		
Laminar ($H^3 \Delta T < 1$) Tilted (Kreider, Curtiss, and Rabl 2002)	$h_{c,o} = 1.42 \left(\dfrac{\Delta T \sin \beta}{H}\right)^{1/4} (W/m^2 K)$	(2-32)
Turbulent Tilted (Kreider, Curtiss, and Rabl 2002)	$h_{c,o} = 1.31(\Delta T \sin \beta)^{1/3} (W/m^2 K)$	(2-33)
(Assumed turbulent) (Eicker 2014)	$h_{c,o} = 1.78(\Delta T)^{1/3} (W/m^2 K)$	(2-34)

For the majority of the cases where wind is present, exterior heat transfer coefficients have been generated and are used broadly in the literature:

Forced convection		
Laminar ($vH < 1.4\ m^2/s$) (Kreider, Curtiss, and Rabl 2002)	$h_{c,o} = 2 \left(\dfrac{v}{H}\right)^{1/2} (W/m^2 K)$	(2-35)
Turbulent (Kreider, Curtiss, and Rabl 2002)	$h_{c,o} = 6.2 \left(\dfrac{v^4}{H}\right)^{1/5} (W/m^2 K)$	(2-36)
Turbulent (Eicker 2014)	$Nu_{c,o} = \dfrac{0.037 Re^{0.8} Pr}{1 + 2.443 Re^{-0.1}(Pr^{2/3} - 1)} \Longrightarrow h_{c,o_{wind}} = \dfrac{Nu_{c,o} k}{D_h}$ $h_{c,o} = \sqrt[3]{h_{c,o_{wind}}{}^3 + h_{c,o_{free}}{}^3} (W/m^2 K)$	(2-37)

Where ΔT is the temperature difference between the surface and the air that flows and H is the length of the plate in the direction of the flow. In the case if a building, the length is in the vertical

direction, this is why it is given by *H*.

More general equations are presented by Fung and Yang (Fung and Yang 2008) who used the correlations developed by Loveday and Taki (Loveday and Taki 1996) for the exterior and interior heat transfer coefficients, based on the wind velocity around buildings.

Windward (Loveday and Taki 1996)	$h_{c,o} = 2v + 8.91 \ (W/m^2K)$	(2-38)
Leeward (Loveday and Taki 1996)	$h_{c,o} = 1.77v + 4.93 \ (W/m^2K)$	(2-39)
(Candanedo, Athienitis, and Park 2011)	$h_{c,o} = 2.56v + 8.55 \ (W/m^2K)$	(2-40)
	$h_{c,o} = 2.2v + 11.9 \ (W/m^2K)$	(2-41)
	$h_{c,o} = 3.8v + 5.7 \ (W/m^2K)$	(2-42)

While there are many cases where the exterior heat transfer coefficient is assumed to be constant and is function of the climate of the region, the prevailing wind direction, and the average wind velocities for the region.

(Eicker 2014)	$h_{c,o} = 25 \ (W/m^2K)$
(Han, Lu, and Yang 2010)	$h_{c,o} = 16.7 \ (W/m^2K)$
(W. Liao and Xu 2015)	$h_{c,o} = 20.2 \ (W/m^2K)$

For the interior heat transfer coefficient Fung and Yang (Fung and Yang 2008) used the equation:

(Fung and Yang 2008)	$h_{c,i} = 1.46 \left(\dfrac{\Delta T}{H}\right)^{0.25} \ (W/m^2K)$	(2-43)

*where ΔT is the temperature difference between the interior glazing surface and temperature of the room and **H** is the height of the glazing.*

It is very common though to assume this value to be constant.

(Eicker 2014)	$h_{c,i} = 7.7 \ (W/m^2K)$
(Han, Lu, and Yang 2010)	$h_{c,i} = 8.3 \ (W/m^2K)$
(W. Liao and Xu 2015)	$h_{c,i} = 8.3 \ (W/m^2K)$

From experimental results and in order to characterize the DSF behaviour, the discharge coefficients were estimated for different angles of the venetian blind implemented within the cavity. A numerical and a CFD model are compared with experimental data to assess the wind and buoyancy driven natural ventilation in double skin façades (Dama and Angeli 2016). The models take into consideration the effects that the wind has on the cavity velocity by assessing the pressure

coefficients at the top and bottom of the DSF. A maximum of 15% deviation is reported between the numerical and the CFD model with the experimental data. It is also reported that the case specific pressure coefficients should be defined with CFD analysis, as the wind effects have a significant impact on their values. An airflow zonal model for DSFs is developed and validated with wind-tunnel experiments (Lou et al. 2012). For different DSF widths and lengths, the wind pressure distribution has been investigated. It was concluded that the zonal approach is an accurate tool and a good alternative of wind tunnel experiments and CFD analysis, in order to investigate the performance of corridor-type DSF in tall buildings. CFD simulations are also used to assess the possibility of harvesting wind energy with the use of corridor-type DSF (Hu et al. 2017; Hassanli et al. 2017). With the proper design of the DSF, the wind-driven velocity within the cavity can be used to power wind turbines to generate electricity.

2.4. Conclusion and research needs

Building-integrated photovoltaics have become a key new technology of seamlessly integrating photovoltaics into buildings. Double Skin Façades (DSF) and Insulating Glazing Units (IGU) integrating Semi-Transparent photovoltaics (STPV) are some of the options of BIPV that can combine the electricity generation and the daylighting control of the building.

The available literature on DSF and IGU integrating STPV is presented. It can be concluded that the electrical and thermal performance of both the DSF and IGU integrating STPV is investigated the most, while most of the simulations are done with numerical models, since the available simulating software have not yet incorporated these innovative technologies into their libraries.

To conclude, for the IGU-STPV:

- There are no studies presenting the effect of cut-in fraction solar cells, on the SHGC and the performance of the STPV

- There are no studies on the temperature that the STPV cells reach when they are integrated on an IGU. This is important for durability of the windows and for electricity generation.

- There appear to be no studies that have experimentally investigated the performance of IGU-STPV both indoors and outdoors. This is necessary to study wind effects.

To conclude, for the DSF-STPV:

- There are limited studies (seen in Table 2-4) on DSF integrating STPV.

- There is only one study of DSF integrating c-Si STPV (Gaillard, Ménézo, et al. 2014).

- DSF-STPV and IGU-STPV are only compared once (Wang et al. 2017), where the STPV is made from a-Si.

- There are no experimental studies that include the electrical and thermal performance for mechanically ventilated DSFs integrating STPV.

- Heat transfer coefficients within the cavity of DSF-STPV have not been investigated.

- The impact of the wind effects on the velocity of the air within the cavity has not been

reported in any of the previous studies.

This research aims to address some of the previously presented points. Mechanically ventilated DSF-STPV is going to be tested in an outdoor facility monitoring its thermal and electrical performance. Also, the heat transfer coefficients within the cavity of a DSF-STPV will be investigated and the impact of the weather conditions, such as temperature, incident solar radiation and wind velocity on the performance of such systems is going to be investigated.

The objective of this study is to promote the implementation of the DSF-STPV in order to make it easier for professionals to choose the appropriate DSF-STPV configuration and provide design solutions and guidelines for the optimal operation of a DSF-STPV. Another objective is to address the DSF-STPV in its totality and not as an add-on system to the building, addressing in this way a complex system, from every angle, and lastly, if needed, to develop new dimensionless numbers.

To do so, a DSF-STPV prototype was developed and tested in outdoor experiments, under real weather condition. The convective heat transfer coefficients within the cavity of a DSF-STPV were investigated and a numerical model of the DSF-STPV was developed that was able to perform parametric analyses for different climates and generate general trends and tables. Lastly, the energy flexibility that DSF-STPV can provide in interacting with a smart grid is identified.

Chapter 3
Experimental set-up and preliminary results

Parts of this chapter are presented in the papers:

Z. Ioannidis et al. 2017. Study on the Energy Performance of the Semi-Transparent PV Facades under Continental Climate. ISES.2017 Abu Dhabi. UAE.

Z. Ioannidis et al. 2018. Comparison of the Electrical and Thermal Performance of Double Skin Façade and Insulating. PVSEC.2018 Brussels, Belgium.

Rounis et al. 2019. Thermal Performance of Semi-transparent PV for Curtain Wall Applications. 14th Conference on Advanced Building Skins. 2019. Kursaal Bern. Switzerland

For this research, three prototype STPV are developed and tested. Being part of the ReMAP (Refined Manufacturing Acceleration Program) Network, Concordia University has the advantage of collaborating with Canadian leading companies to bridge the commercialization gap between applied research and industry for the development of STPV windows. These companies are the Canadian Solar, one of the top worldwide manufacturers of solar panels, Unicel Architectural, a very experienced company in the field of glass in buildings and Internat Energy Solutions, a consultancy company that is assigned for the marketing of the final product. In Figure 3-1, the three prototypes (1st to 3rd generation) are presented. The 1st generation consists of eight rows of typical solar cells (156mm x 156mm). Two of these 1st generation STPV window are integrated on a DSF and an IGU at the exterior experimental research facility (see paragraph 3.2.). The second and third generation are also shown in Figure 3-1. Their main difference is the layout; portrait in 2nd generation and landscape in the 3rd and their cell coverage. Also, the thickness of solar cells different, 31x156 for the 2nd generation and 22x156 for the 3rd generation. Experiments are held at the solar simulator of Concordia university for the 2nd and the 3rd generation STPV (see paragraph 3.1.).
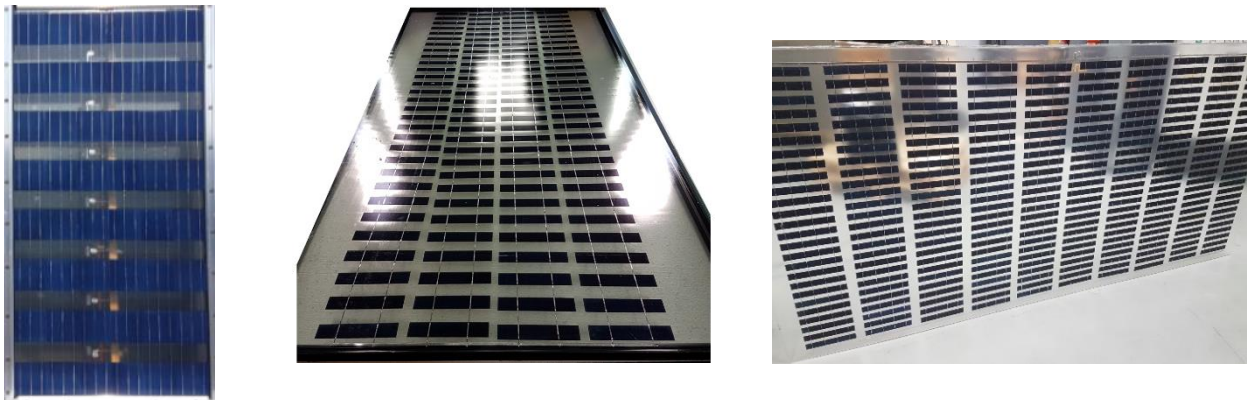
Figure 3-1 First, second and third generation of the developed STPV prototypes.

An exterior experiment is set-up at the roof of the old BE building. At this experimental set-up, a DSF-STPV and an IGU-STPV are placed one next to each other and their performance is monitored (see paragraph 3.1.).

Two virtually identical semi-transparent photovoltaics (STPV) are used for this experimental set-up, located in Montreal, Canada (45° 30' N / 73° 35' W). The first STPV is used as the exterior layer of a DSF forming in this way a DSF-STPV and the second one is used as the exterior layer of an Insulating Glazing Unit (IGU-STPV).

The custom-built double skin façade integrating a semi-transparent has custom made monocrystalline STPV module that was integrated at the exterior skin of the DSF using mullions and pressure plates that are mainly used in curtain-wall applications. The STPV has a packing (or covering factor – ratio of area covered by solar cells – i.e. opaque) of 63.4%.

In Figure 3-2 the south façade of the experimental test-room is shown. An insulating glazing unit integrating STPV is installed on the left side. On the right side of the façade of the test-room, the DSF-STPV is installed. In the same figure, the thermal imaging of the experimental test-room is

depicted and the PV cell strips are distinguished by the glass strips as they present higher temperatures. All the surfaces investigated in this experimental set-up are made out of glass and the emissivity taken into consideration for the thermal photography was set to 0.9.

The test cell faces towards the south, while the south view of the façade is shown on the panoramic picture of Figure 3-3. It can be seen that during most of the days of the year, a high-rise building on the east, south-east shades the test-room, in the early morning. Also, for a couple hours after the solar noon the test-room is shaded by a building that is located between south and south-west. In Figure 3-3 the sun-path diagram is shown, depicting the 20th of September at 8 am when the test room is shaded by the high-rise building.
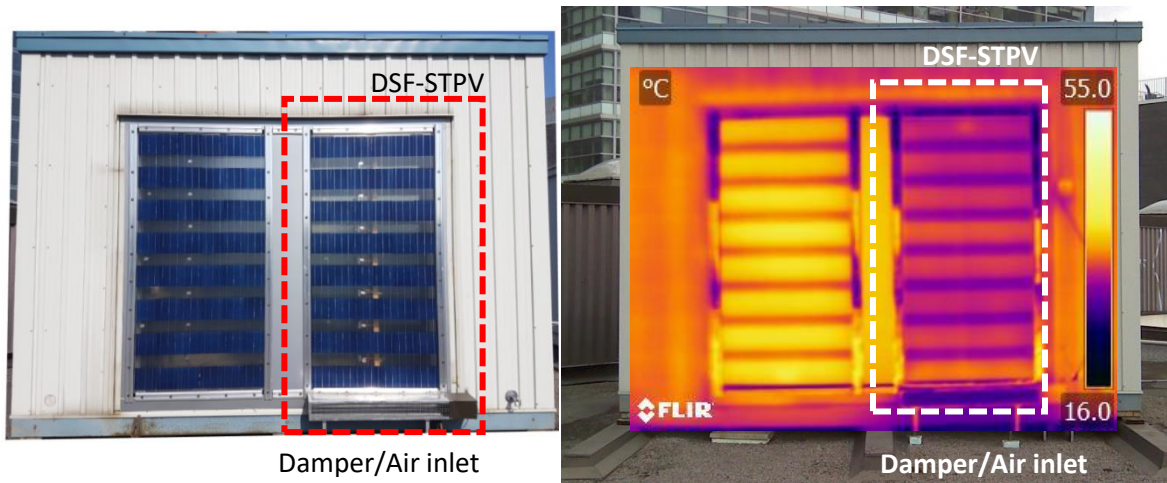
Figure 3-2 The view of the south façade of the experimental test-room. The DSF-STPV is marked and the damper (that is the air inlet) of the DSF-STPV is specified. A thermal image of the experimental test-room is shown on the righthand side.
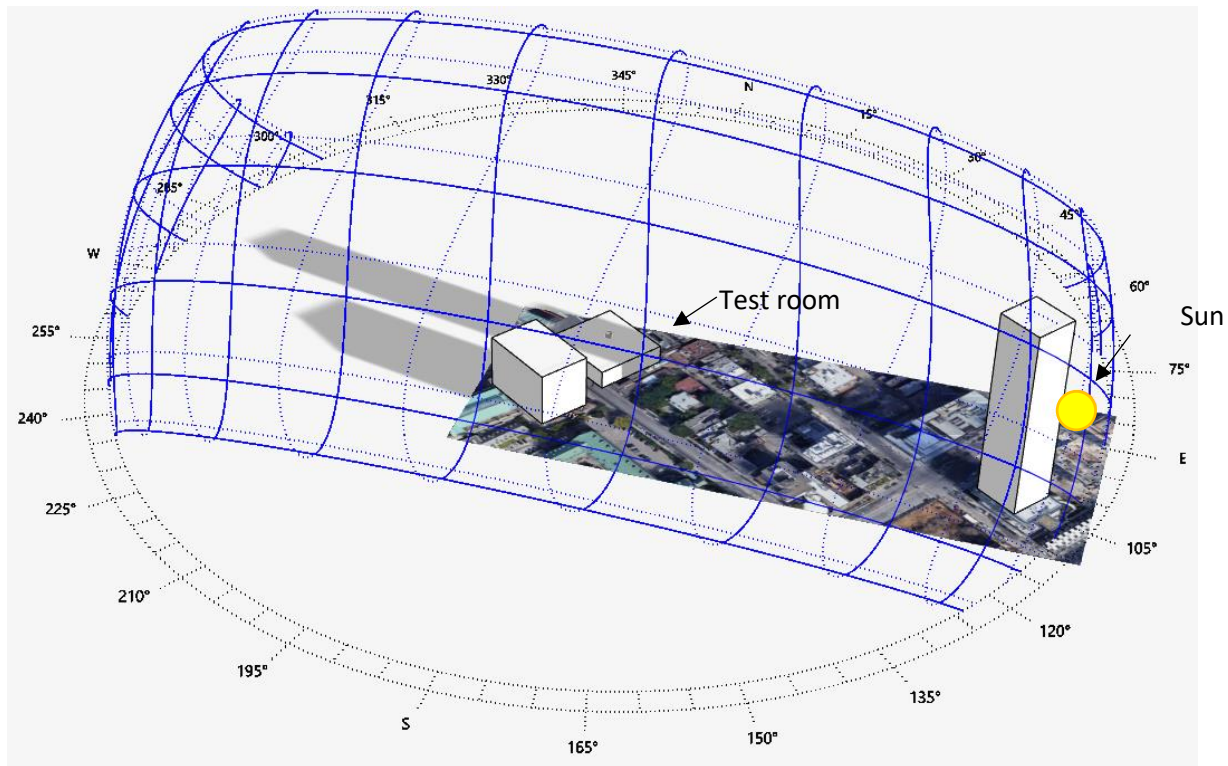
Figure 3-3 A sun-path diagram at the location of the experimental test-room. The instance depicted is for 20th of September at 8 am when the high-rise building is shading the test-room.

3.1. Experimental set-up

The cavity of the DSF-STPV is 17.5cm wide and the back layer of the DSF-STPV extends from the bottom of the test-room to a height of 1.95m. The insulating glazing unit that comprises the interior surface of the DSF is assembled with a hard low-emissivity coating on surface three (#3). The 13 mm wide air-gap of the double glazing is filled with Argon. It has a SHGC of 0.624 and its U-value ranges between 1.64 W/m^{2}K and 1.56 W/m^{2}K between winter and summer conditions.

3.1.1. Mechanically ventilated double skin façade

An automated damper with a 0-5 VDC (control signal) actuator was integrated in the inlet underneath the DSF-STPV and is used to control the flow rate of the DSF-STPV. It is programmed to fully open at 7.00 and fully close at 16.00. This time period was selected as it coincides with a

typical schedule on commercial or institutional buildings, that most commonly adopt DSF. In addition, during this time period, the test room is exposed the most to sun-light as it is shaded after 16.00 for the majority of the Winter (Figure 3-3). The dampers are not controlled depending on the relation of the outdoor or indoor conditions as goal of the experiment is to develop convective heat transfer coefficients for different boundary conditions and not to assess the performance of the system under different operating strategies.

The top of the DSF-STPV is sealed and a plenum is used to collect the air and drive it through a manifold (Figure 3-4). A rectangular flange FLST 25.4 cm by 25.4 cm (10 in by 10 in) flow meter is installed at the middle of this manifold and its location is selected to be at an appropriate distance from flow changes/fittings. At the end of the duct, a variable-speed fan is located that follows the same schedule with the damper. The control input of the fan is 2-10VDC (control signal) with velocity corresponding starting at 0.2 m/s. The fan was never operated at its maximum as with approximately 6 VDC an average velocity of 2 m/s was achieved in the cavity.
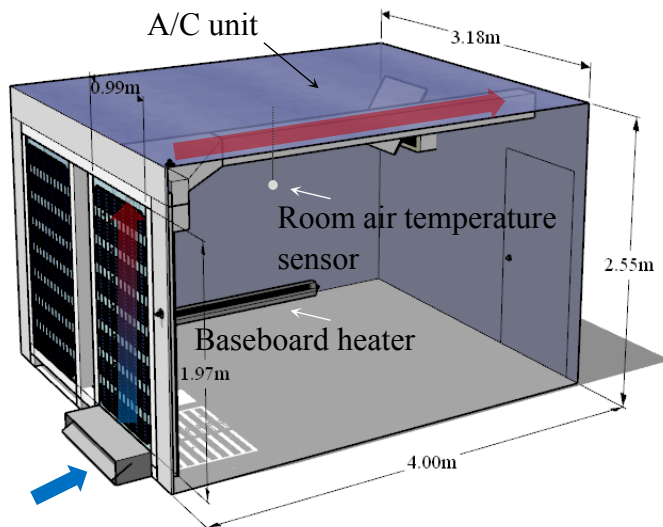
Figure 3-4 Schematic of the experimental facility showing the airflow in the cavity of the DSF-STPV, the collection of the air by the plenum and the shading pattern of the STPV.

3.1.2. Instrumentation

A data acquisition system was used to collect experimental data and control the test conditions. A shunt resistor with a high voltage analog input module (NI 9229, ±60 V max, 24-bit) was used to measure current while the voltage of the STPV modules were measured directly.

Temperature was measured with thermocouples (type T, 30 AWG), on different DSF surfaces and in the air space along the vertical direction at 15 equally distributed heights, as shown in Figure 3-5. The analog modules used were the NI 9214, ±78.125 mV, ±0.3°C, 24-bit. The locations of the thermocouples are depicted with different colour depending on the layer on which the thermocouples are placed. At each height, these thermocouples were placed on the interior surface of the STPV, on both sides of the clear IGU, and in the middle of the air cavity. The thermocouples were not installed on lowest height of the STPV and at the top height of the IGU because the inlet damper and the air exhaust manifold were installed at these locations, respectively. On the same

figure, the location of the pyranometers is shown.

Five pyranometers (Li-Cor, LI-200R: ±5%) were used to measure the incident horizontal and vertical radiation, the vertical irradiance transmitted through the STPV and the total vertical transmitted irradiance through the DSF-STPV. The STPV consists of opaque and transparent strips that block or allow respectively the direct solar radiation, having an effect on the total transmitted solar radiation. Thus, to measure more effectively the total vertical transmitted radiation, two pyranometers were used.
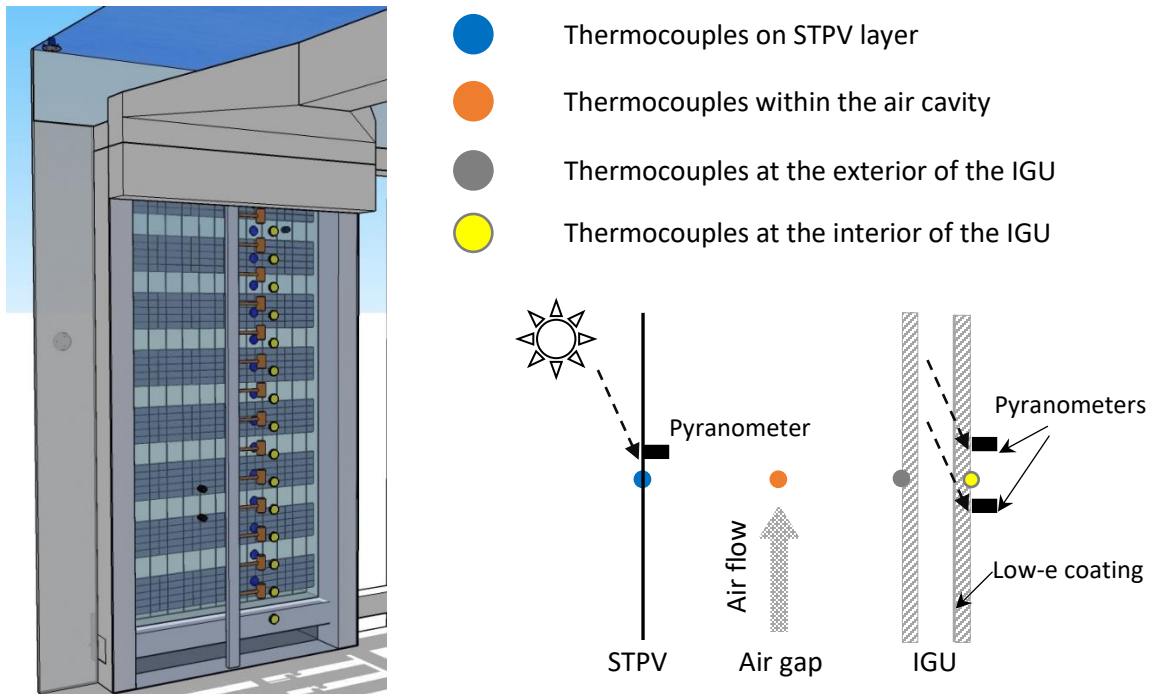
Figure 3-5 The thermocouples are depicted with different colour depending on the layer on which are placed. The location of the pyranometers and the low-e coating is shown.

A heater and an air-conditioning unit were installed to regulate the room temperature between 18ºC and 25 ºC. The ambient temperature was measured at two locations, one at the air inlet of the DSF damper and the other behind the test-room. Wind velocity and direction were measured at the weather station close to the test location.

3.1.3. STPV and electricity storage properties.

The STPV is the exterior layer of the DSF and integrates 48 monocrystalline cells with a nominal efficiency of 17.80%. The cells are distributed in 8 rows with 6 cells each. The manufacturer specifications of the STPV modules are shown in Table 3-1. The STPV consists of the following layers: glass, EVA (ethylene-vinyl acetate), PV cells, EVA and PET (polyethylene terephalate). The dimensions of the STPV panel is 1.968 m by 0.992 m and the PV cells used are square and have sides of 15.6 cm, while the seven transparent strips have a width of approximately 9.6 cm. With this configuration, 63.4% or 1.24 m^2 of the area is covered by the opaque cells and the remaining 36.6% is transparent.

Table 3-1 Properties of the STPV and the IGU, which are the outer and inner skin of the DSF-STPV respectively

STPV (DSF-STPV)				IGU			
I_{sc}	8.55 A	Transmittance	33.9%	Uvalue Winter	1.64 W/m²·K	VTr	72.9%
V_{oc}	29.90 V	Packing factor	66.1%	Uvalue Summer	1.56 W/m²·K	VAbs	11.8%
P_{max}	186.39 W	Cell size	156mm x 156mm	SHGC	0.624	SolTr	54.1%
eff	10.6 %	Dimensions	1984mm x 996mm	SC	0.72	SolAbs	32.6%
*under Standard Test Conditions							

For the accurate measurement of the power output of the DSF-STPV and the IGU-STPV, an identical electric assembly was set up for each PV module. This assembly consist of a charge controller with maximum power point tracker (MPPT) a battery of 12 V and 110 Ah and a dump load (TE Connectivity 2005). The multi-stage MPPT solar charge controllers used are the Solar Boost SB3024i (Blue Sky Energy Inc. 2009) and the battery is the 8A31DT AGM sealed (MK Battery 2015). The voltage of each PV module is measured with a NI 9223 module (National Instruments 2016) and a shunt resistor (Riedon Inc. 2018) is used to measure the current flowing from the PV. The electrical configuration and connections are shown in Figure 3-6. The selection of shut resistor was based on the range and precision of the voltmeter. In our case a NI 9213 was used to measure the voltage difference (range of ± 78 mV) and using a safety factor of two (2) over the short circuit current from the PV (~ 16 A), the value of the shunt resistor was calculated to be 5 mΩ. For the selection of the battery, an empirical rule was used to calculate the battery capacity (Ah), which is equal to the watt peak of the STPV multiplied by the daily solar exposure and the days of battery autonomy of the system, divided by the battery loss factor, the depth of discharge and the battery voltage. In order the MPPT to supply the battery with the maximum current possible, the battery should not be full and this is why a single day of battery autonomy was preferred. Assuming that the PV average daily solar exposure is three hours, the battery loss is 0.85 and the depth of discharge is 0.5 the battery capacity is calculated to be approximately 110 Ah. A resistor is used as dump load to release, in the form of heat, the total electricity generated by the STPV and stored at the battery, during the night, when the heating loads from the resistors will not interact with the STPV experiments. For a 1 Ω resistor and a 12 V battery supply, a 144 W resistor should be used, instead a 300 W resistor was selected to avoid the overheating of the resistor.
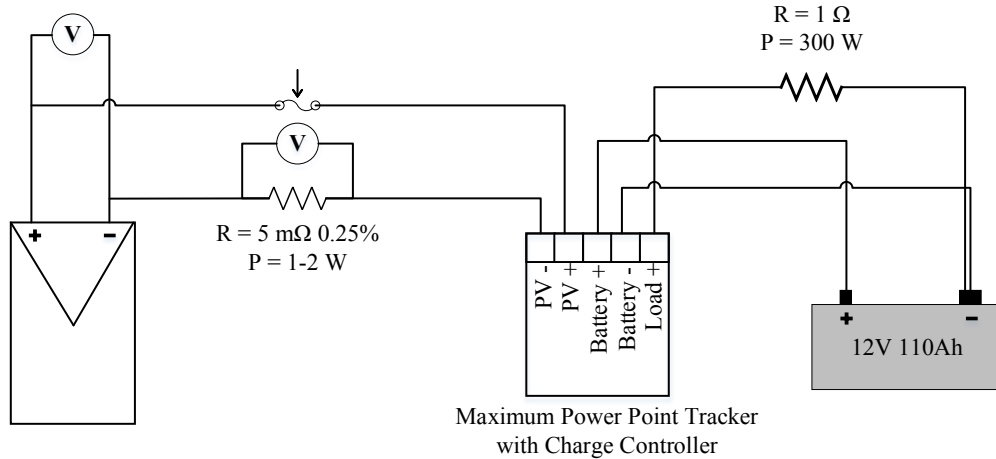
Figure 3-6 Schematic showing the electrical connection between the STPV, the MPPT and the batteries. The location of the shunt resistors used for the current measurement and the resistors used as a dump load is shown.

3.2. Exterior data, preliminary analysis

The preliminary analysis expands from April to July. The Ambient Temperature, the Incident Solar Radiation and the Average velocity within the cavity are presented. July is month with the higher mean values. The DSF-STPV was not ventilated in the greatest part of April, presenting a high distribution. The data were collected from 7.00 to 16.00.
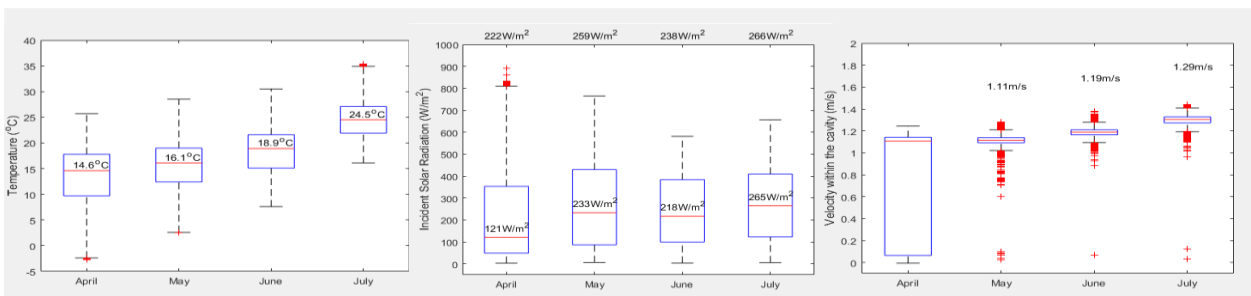
Figure 3-7 Experimental conditions from April to July 2018, presenting Ambient Temperature, Incident Solar Radiation and Velocity measurements within the cavity.

For the electrical comparison of the DSF-STPV and the IGU-STPV, the Power production of the STPV is plotted over the incident normal radiation. The efficiency of each technology is then calculated. Under STC, the DSF-STPV and the IGU-STPV had efficiencies of 10.6% and 10.7% and the calculated efficiencies are 9.02% and 8.50% respectively.
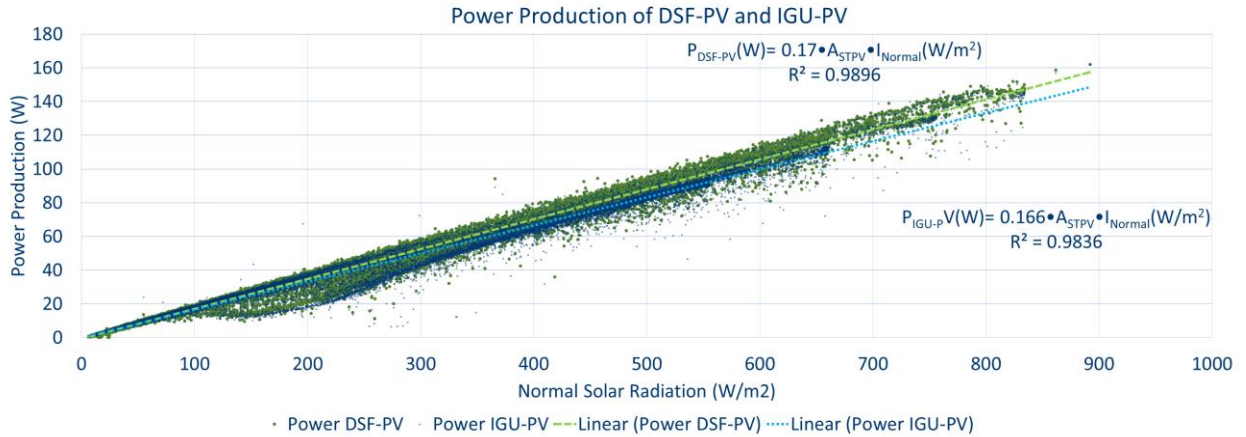
Figure 3-8 Power production of DSF-STPV and IGU-STPV as a function of the incident normal solar radiation.

For the presented months, the DSF-STPV outperformed the IGU-STPV, presenting a maximum difference of 9.77%. July was the month with the highest average velocity within the cavity and the highest incident solar radiation.

Table 3-2 Electricity production per month and the difference between the DSF-STPV and IGU-STPV

Months	DSF-STPV (kWh)	IGU-STPV (kWh)	Difference (%)
April	2.335	2.290	2.00
May	2.617	2.455	6.60
June	2.330	2.178	6.96
July	2.594	2.363	9.77

A FLIR thermal camera is also used to compare the temperature of the PV cells of the IGU-STPV and the DSF-STPV. A series of thermal photos were taken and analysed. The average ΔT is more than 10ºC and around 5ºC for days with higher and lower incident solar radiation, respectively. This has an effect on the measured Power production of the STPV integrated on DSF-STPV and IGU-STPV as it can be seen in Figure 3-10.
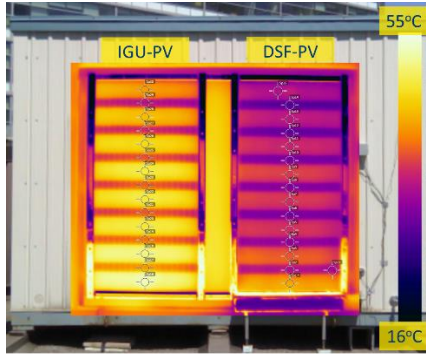
Figure 3-9 Infrared camera picture of the Test facility showing the difference between DSF-STPV and IGU-STPV
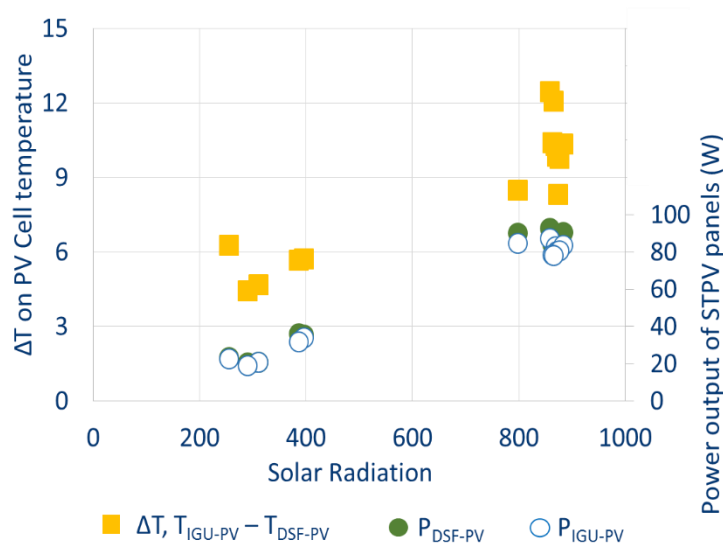
Figure 3-10 Temperature difference between the cells of the STPV on DSF-STPV and IGU-STPV and the equivalent power production

3.3. Multiple day preliminary analysis

This study focuses on offices in a continental climate region (North-eastern United States and South-eastern Canada) and it is part of a bigger effort to provide input to the design guidelines for the utilization of advance fenestration technologies that will help to achieve net-zero energy building performance targets and beyond, through energy conservation and renewable energy generation.

The test-cell and the experimental set-up described earlier, is used to characterize the electrical performance of the DSF-STPV and the IGU-STPV. In addition, a comparison is held between their performance under the same exterior and interior condition.

Experiments that are presented in this chapter are for a series of eight (8) consecutive days, under different weather conditions and under different ventilation strategies for the cavity of the DSF-STPV. The average velocity within the cavity and the incident solar radiation for these days are

presented in Table 3-3. From Table 3-3, it can be extracted that for all the monitored days, the DSF-STPV out-performs the IGU-STPV by a 3% to 10% difference, depending on the strategy selected for the ventilation of the cavity of the DSF-STPV.

From the same table, it can be seen that clear sky days are Day 1,4,6,7 and 8 and the overcast days are Day 2, 3, 5. If the cavity is ventilated, the electricity production of the STPV integrated on the DSF is greater than this of the IGU-STPV by 7.27% to 9.20%. The days that the cavity is ventilated but the sky is overcast (Day 2 and 3), the electrical performance of the DSF-STPV is approximately 4.5% greater than the IGU-STPV. Lastly, when the cavity is closed, the difference between the electricity generated by both the STPV, is the smallest encountered but is still between 3.6% and 4.1%. On the last column of Table 3-3, the percentage of the time that the power of the DSF-STPV is greater than the Power of the IGU-STPV is presented showing that more than 87% of the time, the DSF-STPV performs better than IGU-STPV

In Figure 3-11, a comparison of the power produced and the current generated by the DSF-STPV and the IGU-STPV is depicted for Day 1 between 7:00 AM and 2:40 PM. The shaded with different colours zones, represent time-periods where different average velocities within the cavity were measured, due to different fan operation.

As it can be seen, the power generation between 7:30AM and 8:00AM drops and this is because of the shading that is provided to the test-cell by the sky-scraper presented in Figure 3-3. For the same reason, the power drops after 2:15PM, where the building located at the south-west shades the test-cell. The power of the IGU-STPV drops first, as it is located on the west side of the test-cell.

When the cavity of the DSF-STPV starts to be ventilated, the power generated by the DSF-STPV starts to be greater that this of the IGU-STPV. The current generated by both the STPVs is almost identical, and this is because the STPV are similar and under the same incident solar radiation. On the other hand, the difference of the power generated by the integrated STPVs should be correlated to the voltage difference created by each system and thus the temperature their cells, as the operating voltage of the STPV panels is dependent on the temperature of the cells.

For the same day (Day 1), the power generated by the DSF-STPV and IGU-STPV and the voltage at which this power is generated is shown in Figure 3-11. It can be seen that the DSF-STPV operated at a higher voltage of about 2 V than the IGU-STPV. Consequently, the power generated by the DSF-STPV is approximately 10 W higher than this of the IGU-STPV, for the majority of the time, resulting in the average 9.20% difference presented in Table 3-3.

Table 3-3 Experimental data for eight (8) consecutive days in Montreal.

	Average Velocity within the Cavity	Average Incident Solar Radiation (W/m²/day)	Average diffuse Solar Radiation (W/m²/day)	Electricity generated by the DSF-STPV (Wh/day)	Electricity generated by the IGU-STPV (Wh/day)	Daily Difference	Percentage of time $P_{DSF} > P_{IGU}$
Day 1	1.25 m/s	194	44	704.01	644.67	9.20%	96.49
Day 2	0.65 m/s	156	70	561.06	537.31	4.42%	93.81
Day 3	1.10 m/s	156	77	462.91	442.40	4.64%	89.27
Day 4	closed	201	46	637.04	611.58	4.16%	91.24
Day 5	1.20 m/s	170	61	637.62	594.39	7.27%	95.72
Day 6	closed	203	29	754.09	725.23	3.98%	89.85
Day 7	closed	201	25	768.62	741.85	3.61%	87.58
Day 8	1.20 m/s	192	31	742.65	683.23	8.70%	97.72
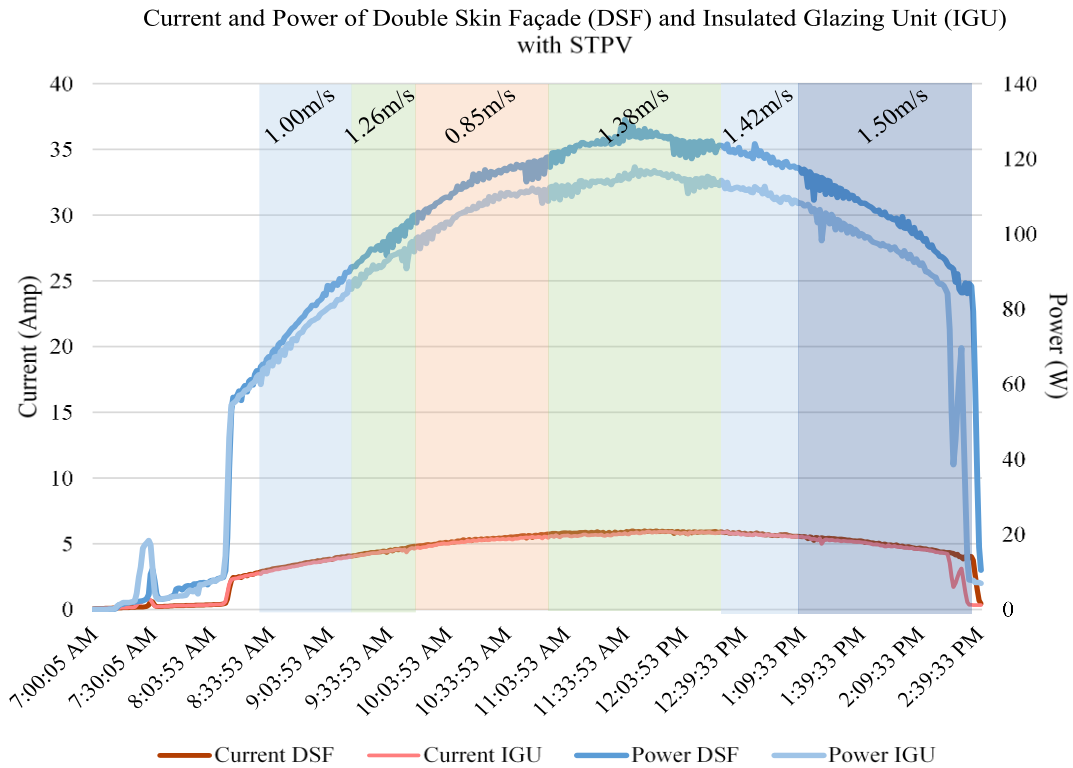
Figure 3-11 Power production and current of the STPV panels integrated on the DSF and the IGU on Day 1, with an average velocity within the cavity of approximately 1.25m/s.
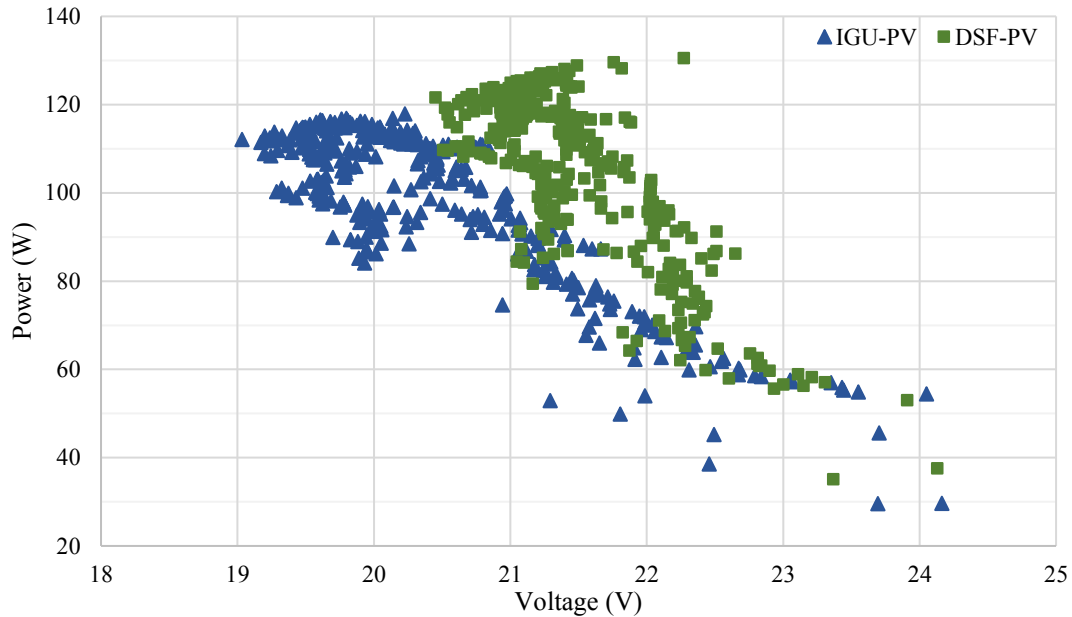
Figure 3-12 Power production of the STPV panels integrated on the DSF and the IGU in comparison to their voltage output on Day1, with an average velocity within the cavity of approximately 1.25m/s.

During the monitored days, the STPV integrated on the DSF out-performs the one integrated on the IGU. For all the eight (8) monitored days that the experiment lasted, the electrical performance of the DSF-STPV presented increased values between 3% and 9% depending on the ventilation strategy of the cavity of the DSF-STPV and the incident solar radiation. Even when the DSF-STPV is not ventilated and acts as a buffer zone, the electrical performance of the STPV panels is 3% to 4.5% greater than this of the IGU-STPV.

3.4. Interior data preliminary analysis

The Solar Simulator at Concordia University is used to characterize the SHGC and the temperature of the cells of STPV and IGU-STPV. The 2nd and 3rd generation prototypes developed under ReMAP network (Figure 3-1) are tested at the solar simulator of Concordia University. In this way their performance can be characterized, and their operation can be compared with the outdoor experiments.

A calorimeter is used to measure the SHGC, and thermocouples are placed to measure the temperature of the PV cells. In addition, measurements are recorded for the STPV when it is connected to a load, under MPPT and when the STPV is in an open circuit mode. These values will be used to develop a numerical model both the thermal performance and the electrical performance of an IGU integrating STPV.
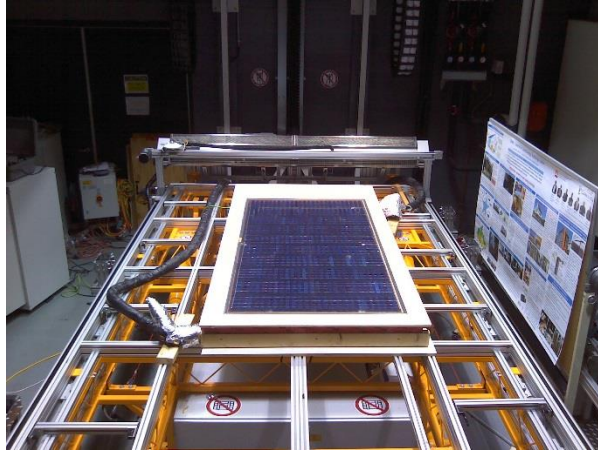
Figure 3-13 STPV with cut-cells is tested on the calorimeter at the Solar Simulator

A series of IV curves are collected for two semi-transparent PV with different cell coverages and consequently different solar transmittances. The IV curves depict the operational range of each PV under certain conditions. The point that the PV generates the greatest amount of electricity is called "maximum power point" or MPP. In Figures Figure 3-14 and Figure 3-15 the IV curves for the STPV under different incident solar radiation and airflow on top of the STPV is shown for cell coverages of 31.7% and 47.4% respectively. Also, the maximum power is presented with a callout for each case.

IV curves for Portrait mode (31.7% cell coverage)
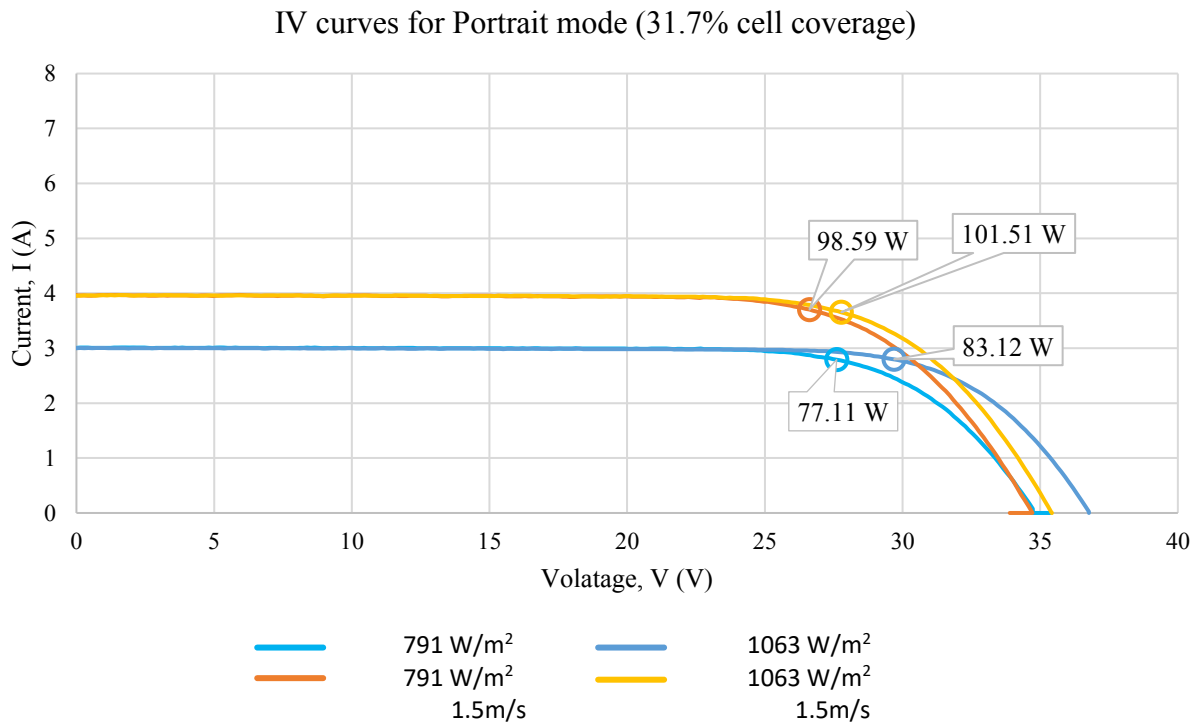
Figure 3-14 I-V curves for the same STPV module of 31.7% cell coverage under 791 W/m² and 1063W/m² with and without air flow on top of the STPV.

IV curves for Portrait mode (47.4% cell coverage)
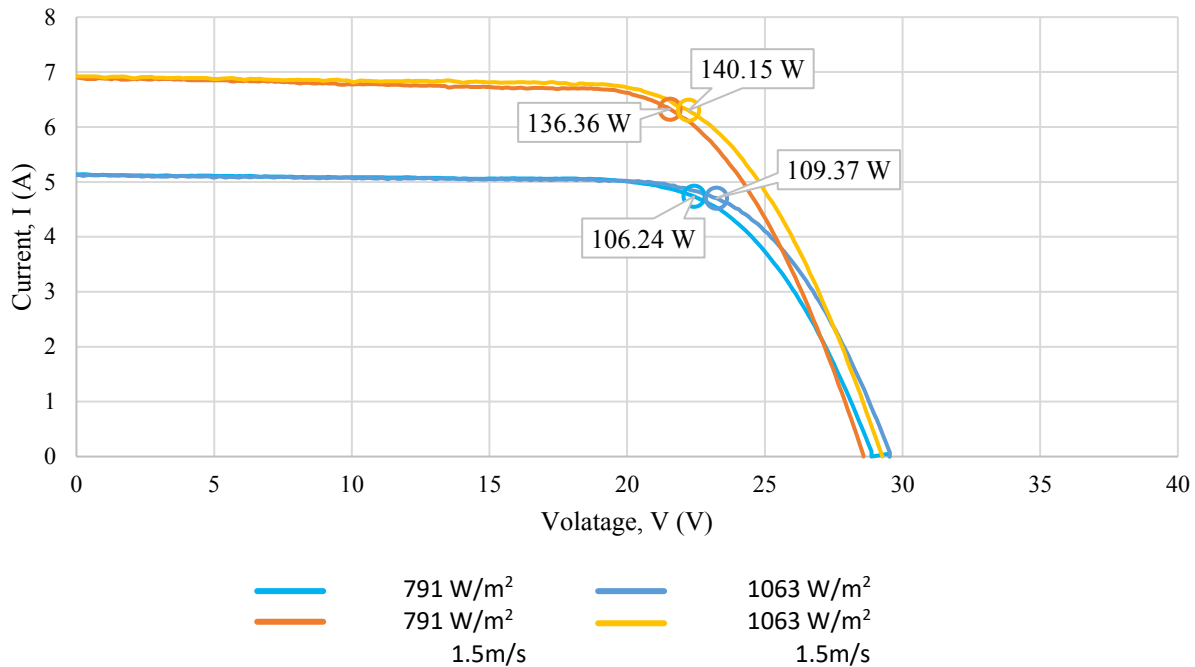
Figure 3-15 I-V curves for the same STPV module of 47.4% cell coverage under 791 W/m² and 1063W/m² with and without air flow on top of the STPV.

The data from the graphs are summed in Table 3-4 along with the effect that each change of the conditions has on the maximum power. It can be seen that the existence of air-flow on top of the STPV results in approximately 3% increase in the maximum power output of the STPV except of the case that the transmittance of the STPV is high and the power output is lower where the difference reaches 7.2%. At the same time, the increase of the incident solar radiation by 25.6% lead to an approximate increase of 20% in the power output of the STPV.

Table 3-4 Maximum power generation of the STPV under different conditions and a comparison between each case.

Cell Coverage	Radiation	Air velocity	Maximum Power	ΔPower flow	ΔPower solar
31.7%	791 W/m²	-	77.11 W		
31.7%	791 W/m²	1.5 m/s	83.12 W	7.2%	
31.7%	1063 W/m²	-	98.59 W		21.2%
31.7%	1063 W/m²	1.5 m/s	101.51 W	2.8%	18.1%
47.4%	791 W/m²	-	106.24 W		
47.4%	791 W/m²	1.5 m/s	109.37 W	3.1%	
47.4%	1063 W/m²	-	136.36 W		22.1%
47.4%	1063 W/m²	1.5 m/s	140.15 W	2.7%	22.0%

For three different airflows on top of the STPV (0.6m/s, 1.2m/s and 1.8m/s) the IV curves are presented in Figure 3-16. In the same graph the MPP is depicted showing the maximum power output of the STPV for the different air-flows on top of the STPV.

IV curve for 47.4% cell coverage for different air-flows
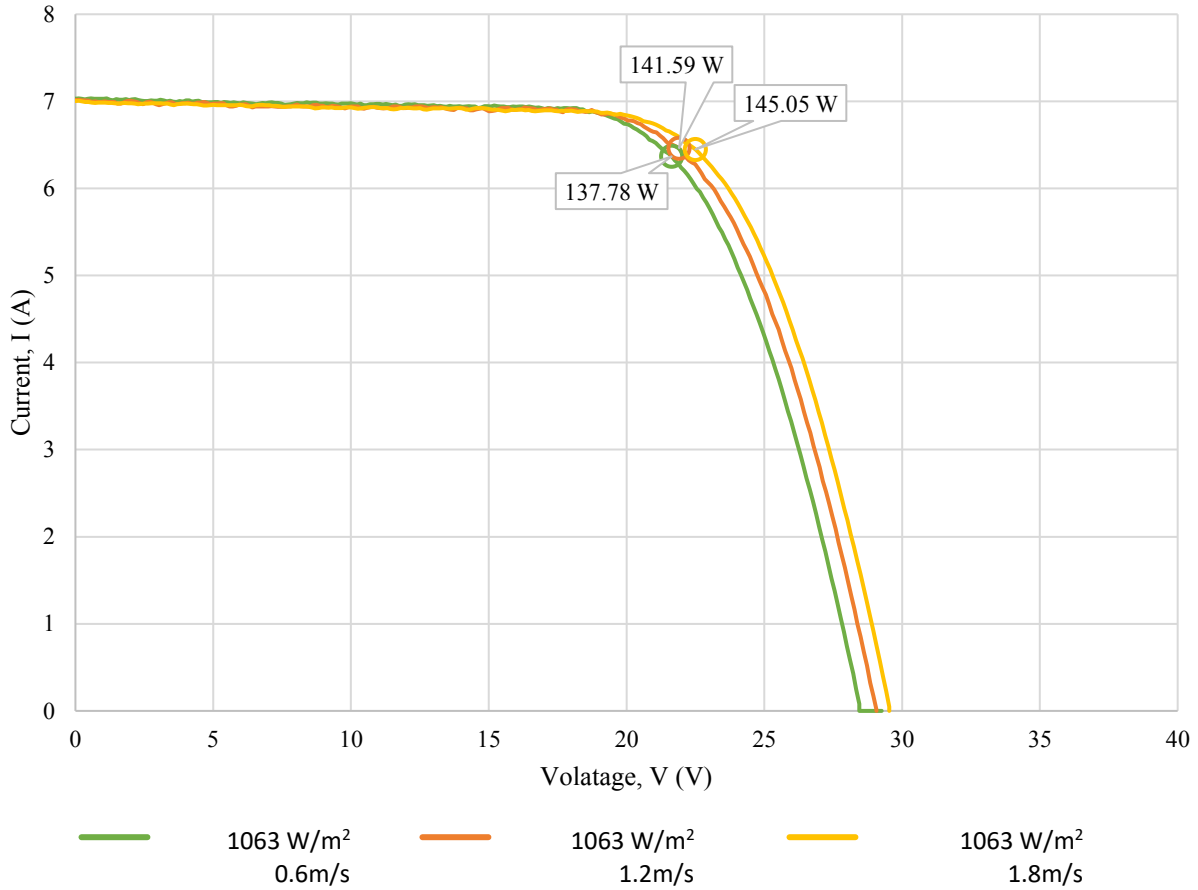
Figure 3-16 IV curves of the STPV window with 47.4% cell coverage for three different air-flows on top of the STPV.

In Table 3-5 the maximum power output is presented for three different air velocities under the same incident solar radiation. In the same table, the difference in the power output is presented showing that if the air velocity increases from 0.6 m/s to 1.8 m/s the power output increases to 7.3%.

Table 3-5 Maximum power output for three different air velocities under the same incident solar radiation

Transparency	Radiation	Air velocity	Maximum Power	ΔPower flow	
47.4%	1063 W/m^2	0.6 m/s	137.78 W		
				2.7%	
47.4%	1063 W/m^2	1.2 m/s	141.59 W		7.3%
				2.4%	
47.4%	1063 W/m^2	1.8 m/s	145.05		

3.5. Conclusion

An experimental set-up with a DSF and an IGU integrating STPV was built at Concordia University. The custom-built STPV have a packing (or covering factor – ratio of area covered by solar cells – i.e. opaque) of 63.4%.. The equipment of the experimental set-up and the measurements instrumentation was presented, and a preliminary analysis was conducted. It was shown that when the cavity was ventilated, the electricity production of the STPV integrated on the DSF was greater than this of the IGU-STPV by up to 9.20%. The days that the cavity was ventilated but the sky was overcast, the electrical performance of the DSF-STPV was approximately 4.5% greater than the IGU-STPV. Lastly, when the cavity was closed, the difference between the electricity generated by both the STPV, was the smallest encountered but was still up by 4.1%. The experiment is easy to be replicated in other regions as the set-up does not present any specific instrumentation or geometric restrictions. The experimental results can be considered inconsistent for incident solar radiation that is lower than 300W/m^2 as the low incident solar would result in lower power output by the PV, and the temperature difference between the different layers of the DSF would be minimal. In addition, during the period of the experiment the ambient temperature ranged between -5ºC and 30ºC, the Reynolds number between 10,000 and 26,000 and the incident solar radiation between 250 W/m^2 and 1200 W/m^2 indicating that the results are limited for these conditions.

Chapter 4

Experimental Study on Forced Convection and Heat Recovery.

Parts of this chapter are presented in the paper:

Z. Ioannidis, et al. 2020. "Double Skin Façade Integrating Semi-Transparent Photovoltaics: Experimental Study on Forced Convection and Heat Recovery." Applied Energy 278 (March): 115647

4.1. Introduction

Building Integrated Photovoltaics (BIPV) have become a widely known technology to replace common building materials with PV that can be seamlessly integrated onto building envelope. BIPV can be applied on both the roof or the façade of a building, the former being the most common application type. Semi-transparent Photovoltaics (STPV) provide the option of replacing building elements that are made from glass, such as windows, skylights and the exterior layer of double skin facades that can be integrated in new buildings or as retrofit layer in existing buildings.

4.1.1. Double Skin façades

A Double Skin Façade (DSF) is a multi-layer building envelope system, the outermost layer of which is separated by the innermost layer by an air cavity that creates a buffer space around the building (Z. Ioannidis et al. 2017). There is much research performed on DSF, a building envelope configuration that has been employed and investigated for many years (Oesterle 2001).

Noise reduction, water shedding and improved aesthetics are some of the advantages of a common DSF, while the cavity of a DSF can be used to integrate shading devices or even as a space for plants (Stec, Van Paassen, and Maziarz 2005).

A DSF system in many applications often utilized the buoyancy effect for the passive ventilation of the cavity, with the heated air usually being exhausted to the outside. With the utilization of fan-driven flow, the preheated air from the cavity can be introduced into the building as fresh air or into its HVAC system for heat recovery and/or ventilation. The integration of DSF onto buildings allows architects and engineers to create a shell around buildings and thus enhance the protection from weather phenomena. This system is also very useful for renovation purposes as the building can be sealed externally, updating its look while maintaining its functionality during the renovation period without making major costly changes to the existing envelope. A further advantage is that during renovation the building indoor functions and operation may still continue.

The radiative heat exchange between the occupants and the envelope of the building can result in great levels of discomfort, especially in the case of buildings with facades that consist primarily of glass elements. A DSF can help regulate the temperature of the envelope components that exchange radiation with the occupants, thus allowing the occupants to operate closer to the window area while maintaining their thermal comfort.

Although, it is consistently reported that a naturally ventilated DSF tends to overheat during the summer period and this could affect the cooling energy consumption (Andelkovic et al. 2015; Gratia and De Herde 2007).

4.1.2. Double Skin façade integrating STPV

The use of glass as a protective layer for the PV cells, has allowed the industry to develop products that can safely replace glazing sections of the building envelope by integrating Semi-Transparent PV (STPV) (Miyazaki, Akisawa, and Kashiwagi 2005). Quesada et al and Biyik et al (Quesada et al. 2012b; Biyik et al. 2017) reviews different possible configurations of transparent solar façades, naturally or mechanically ventilated, integrating or not photovoltaic panels.

The safety of such a system is ensured if all the requirements of building code are followed, while a possible way of reducing the cost of a DSF is to take advantage of the area of the building to generate electricity by integrating STPV on the exterior layer of the DSF (DSF-STPV) that can enhance the energy performance of the building in multiple ways. A DSF-STPV, in which the fans assist the flow will result in more heat extracted by the flowing air than in a conventional DSF adding furthermore that the flow is more predictable as it is controlled. The coupling of an active DSF-STPV with a heat pump of the building HVAC system, if optimally controlled, will increase the coefficient of performance (COP) of the heat pump and the system.

A DSF-STPV can also contribute towards shifting the peak demand of the building outside the peak periods of the grid with the simultaneous generation of electrical and thermal energy. The electricity generated by the STPV can drive the fans and the mechanical system. Also, the performance of the HVAC system is boosted as it is supplied with warmer air intake (fresh air for ventilation or as a source for a heat pump). However, a necessary condition for shifting the peak demand of the building is the combination of an active DSF-STPV system with thermal and optionally with electrical storage.

Amorphous-Silicon (a-Si) STPV have been integrated in a DSF experimental facility in different natural ventilation modes (Peng, Lu, and Yang 2013b; Peng et al. 2015a). The solar heat gain coefficient (SHGC) and the thermal transmission (U-value) for each mode was calculated and presented, in order to assess the thermal performance of the system. In addition, the electrical output characteristics for the a-Si STPV were studied for each mode. It was reported that a naturally ventilated DSF-STPV results in reduced SHGC and slightly better electrical performance than a non-ventilated one but has lower thermal insulation values. The reported results were limited to a-Si technology, which has lower power temperature coefficient than the c-Si. The same experimental set-up was also used for the validation of a simulation model based on the building simulation software "Energy Plus" (Peng et al. 2016). It was reported that the optimal cavity thickness of a DSF-STPV is between 0.4m to 0.6m for a Mediterranean climate zone. A similar experimental facility, comparing a DSF and an IGU integrating semi-transparent a-Si PV was described by (Wang et al. 2017). The thermal and the electrical performance was investigated, and a simulation model was developed to compare such system to a conventional IGU.

Regarding crystalline Silicon (c-Si) technology used in DSF-STPV, three DSFs integrating STPV with different packing factors were investigated by Gaillard *et al.* (Gaillard, Ménézo, et al. 2014). In this study, prototype naturally ventilated DSFs are investigated under real operating conditions, while the authors encountered limitations such as a geometrically complicated DSF with limited available data on the thermal, electrical and optical aspect of the study.

A DSF that is not optimally designed or is not optimally operated may result in overheating. For a DSF-STPV this results in lower electrical efficiencies and can affect the occupant's comfort due to the overheating of the inner layer of the DSF. Another possible issue is the accumulation of dust in the cavity that affects the aesthetics of such system. This requires access to the cavity of the DSF for maintenance or the implementation of filters that will have an impact on the pressure drop of the airflow in the cavity. A common issue that appears generally in BIPV/T applications, and thus in the DSF-STPV is the wiring of the PV and the return of investment. Although, the cost of

the integration of STPVs on DSF is not significantly greater in comparison to a common DSF from glass.

4.1.3. Cavity convective heat transfer coefficients

None of the studies on DSF-STPV previously reviewed, report correlations for the convective heat transfer coefficients (CHTC) in the cavity. Mei et al. (Mei et al. 2003) stated that the convective heat transfer coefficients in the cavity are very difficult to evaluate due to the fact that heat transfer can be natural, mixed or forced, and the flow may vary from laminar to fully turbulent (usually within the transitional region). In addition, the geometric features of the DSF itself (usually presented as the ratio of its length to its hydraulic diameter) add further complexity as entrance effects may be dominant and the flow can be developing along the height of the cavity. Regardless, a sufficiently accurate correlation of the cavity CHTC is crucial both for the evaluation of the thermal performance, as well as the optimal control of a DSF-STPV façade in the expected range of operating conditions.

Convective heat transfer in the air cavity is usually represented in the form of the Nusselt number, which is a dimensionless number indicating the ratio of convective over conductive heat transfer and is defined as follows:

$$Nu = \frac{h_c L}{k} \qquad\qquad (4\text{-}1)$$

Where L is the characteristic length of the flow, which for the case of convective heat transfer in pipe/duct flow, is the hydraulic diameter of the duct (DSF cavity in this case) and k is the thermal conductivity of the air.

The majority of studies on DSF focus on buoyancy-driven ventilation and to our knowledge there is a lack of studies that develop Nusselt correlations for the case of fan driven (forced) flow in a DSF-STPV.

For the case of fan-driven flow in hybrid photovoltaic-thermal systems, Nusselt number correlations developed for heat transfer in pipe flow are usually employed, usually presented as functions of the Reynolds and the Prandtl number. The most commonly used Nu expressions are those developed by:

- Dittus-Boelter (Dittus and Boelter 1930), as seen in Zogou & Stapountzis (Zogou and Stapountzis 2011), Sohel et al (Sohel et al. 2014), also used in the commercial building physics simulation software TRNSYS,
- Petukhov (Petukhov 1970), used by Eicker (Eicker 2003), Pantic et al (Pantic, Candanedo, and Athienitis 2010) and Teo et al (Teo, Lee, and Hawlader 2012)
- Gnielinski (Gnielinki 1983), used by Charon & Athienitis (Charron and Athienitis 2006) and Candanedo et al (Candanedo, Athienitis, and Park 2011),
- Tan & Charters (Tan and Charters 1969; 1970) used by Shahsavar et al (Shahsavar and Ameri 2010), Tonui & Tripanagnostopoulos (Tonui and Tripanagnostopoulos 2006; 2008), Rajoria et al (Rajoria et al. 2016), Eicker (Eicker 2003) and Hegazy (Hegazy 2000), and

- Kays and Crawford (Kays and Crawford 1966), used by Kumar & Rosen (Kumar and Rosen 2011) and Kamel & Fung (Kamel and Fung 2014).

The expressions by Dittus-Boelter (Dittus and Boelter 1930) and Gnielinski (Gnielinki 1983) are average Nu correlations, developed for smooth ducts with fully developed flow and symmetrical heating. The expressions by Kays (Kays and Crawford 1966), Petukhov (Petukhov 1970) and Tan & Charters (Tan and Charters 1969; 1970) further take into consideration the effect of the entrance length, while the latter also consider asymmetric heating.

Several researchers developed local and average Nusselt numbers specifically for air-based PV/T, taking into account the non-smooth interior of the air-channel, as well as the heating asymmetry of the PV and the insulation surface (Yang and Athienitis 2014; Candanedo, Athienitis, and Park 2011). The Nusselt numbers in said studies are again given as functions of the Reynolds, Prandtl and aspect ratio of the air channel, while the insulated back surface opposite the PV layer is assumed adiabatic.

There are several issues with the use of the Nusselt number correlations presented previously in PV/T and DSF-STPV systems' modelling and these have primarily to do with the assumptions under which these correlations have been developed. One other consideration is the different conditions under which these have been developed (i.e. boundary conditions, geometric features of the system) and as a result, even the correlations developed for air-based thermal systems are applicable for very similar test conditions.

Figure 4-1 depicts Nusselt number plotted against Reynolds number, including the correlations developed for pipes or ducts, for PV/T and natural ventilation for DSF, as well as the ones evaluated from the experimental data of the present study. It can be seen from the graph that the correlations for pipes or ducts underpredict the convective heat transfer for PV/T thermal systems. Most importantly, the experimental data used in this study, do not fall within any of the marked zones and present a significant variance from a linear or exponential function.

In the authors' opinion, a main explanation for the behaviour of the measured Nusselt number is that of varying boundary conditions of the system, especially on the PV side, which are determined by the combination of incident radiation, impinging wind and ambient temperature. Furthermore, the electrical efficiency of the PV is also very important, as it determines the amount of incident radiation that is available as heat after a part of the incident solar radiation is converted to electricity. For the interior side (insulating glazing unit), the U-value has an effect on the energy balance but also, the net-transmittance is of importance as it deducts part of the energy of the DSF-STPV that is accounted as transmitted to the building zone.
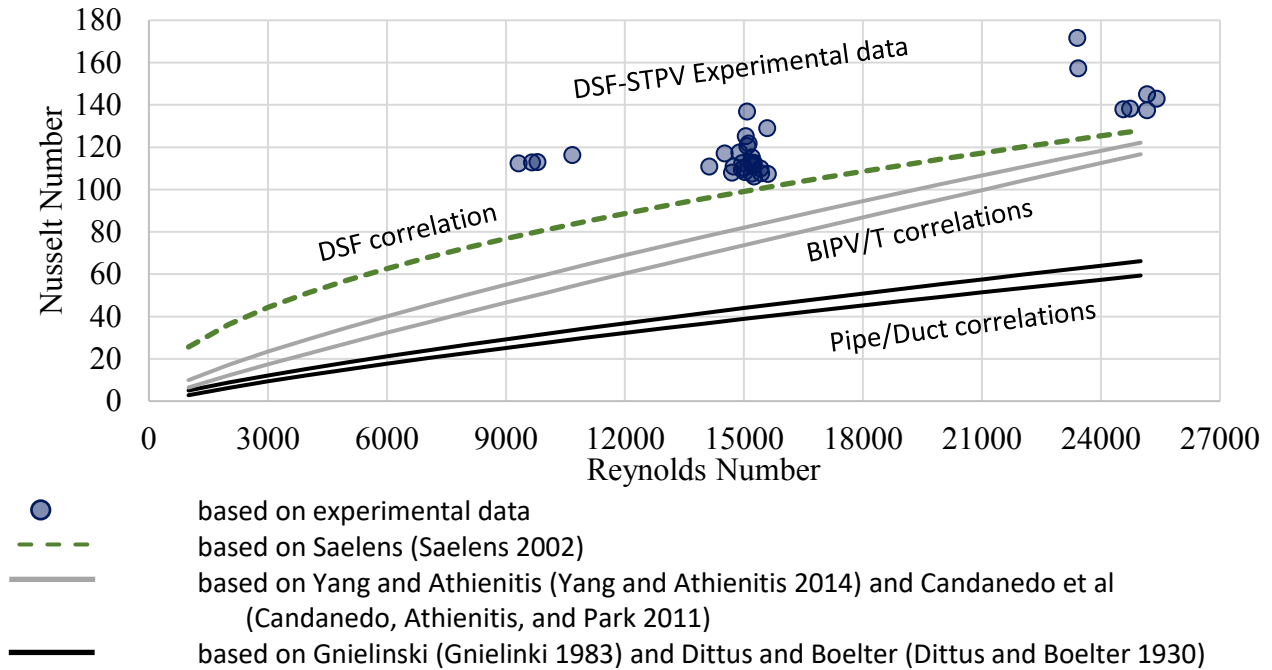
Figure 4-1 Average Nusselt number correlations as a function of Reynolds number, showing correlations that were developed for pipes or ducts, for BIPV/T applications and DSF and presenting the DSF-STPV experimental data.

4.1.4. Wind effect on external convective heat transfer coefficients

Arguably, the most important aspect of the DSF-STPV system and of solar-thermal and PV/T systems in general, is wind-driven exterior convection. Depending on the conditions (wind velocity, direction, neighbouring obstacles) the heat transferred to the ambient environment via wind-driven convection may account for more than 50-60% of the energy balance. This is due to the fact, that contrary to glazed solar-thermal collectors, in DSF-STPV systems the PV layer is in direct contact with the environment. On the other hand, the DSF system acts as a buffer zone, significantly reducing the impact of wind on the building itself and thus reducing the thermal losses of the zone to the environment.

Contrary to the cavity heat transfer coefficients, the external convective heat transfer coefficient $(h_{c,o})$ has been extensively studied. Several heat transfer coefficient correlations refer to free convection and are developed taking into consideration the temperature difference between the exterior surface and the flowing air (Kreider, Curtiss, and Rabl 2002; Eicker 2014).

In most wind-driven flows around buildings, turbulent forced convection is observed and the CHTC correlations are function of the wind velocity, the wind direction and the surroundings of the concerned area (Vasan and Stathopoulos 2014).

Power functions are proposed by Kreider *et al.* (Kreider, Curtiss, and Rabl 2002) for the exterior heat transfer coefficient, while Emmel *et al.* (Emmel, Abadie, and Mendes 2007) presented five (5) different exterior heat transfer coefficient correlations depending on the wind direction. There are also several studies which discretize the wind CHTC correlations for the windward and leeward

building sides (Loveday and Taki 1996; Palyvos 2008; Sharples 1984). In most of the cases, more general equations are presented as a linear function of the wind velocity (McAdams 1954; Test, Lessmann, and Johary 1981; Sharples 1984; Hagishima and Tanimoto 2003; Duffie and Beckman 2006; Shao et al. 2009). One of the most commonly used correlations is the one developed by Sharples and Charlesworth (Sharples and Charlesworth 1998) $h_{c,out} = 11.9 + 2.2 \cdot V_{wind}$, which is also used in the present study.

There are many cases where the exterior heat transfer coefficient is often assumed to be constant and is a function of the climate of the region, the prevailing wind direction and the average wind velocities for the region (Han, Lu, and Yang 2010; Eicker 2014; W. Liao and Xu 2015). These values range between 15 to 25 W/m²K.

The effect the exterior convective heat transfer coefficient has on the boundaries of the DSF-STPV system and consequently to the Nusselt number correlation has not been investigated and the effect that the weather conditions have on the convection in the cavity are discussed, as strong wind effects result in higher exterior convection losses that affect significantly the energy balance of such systems. In addition, lower incident solar radiation levels result in lower electricity production by the STPV and less absorbed solar radiation, affecting in this way the energy balance of a DSF-STPV.

4.2. Overview

In this study, the boundary conditions have been taken into account for the development of Nusselt number correlations based on the measured data. The electrical efficiency and solar transmittance are dimensionless numbers and the climatic conditions (irradiance, wind velocity and ambient temperature) have been re-arranged in a new dimensionless number as will be described in section 4.3.6.

In this study, the gap in the literature in the Nusselt number correlations for DSF-STPV is addressed. Most specifically, the Nusselt number correlations for DSF-STPV for forced convection in the turbulent region, for both sides of the cavity are developed, as well as the Nusselt number correlation for the average solar cell region of the STPV. In this approach, the authors consider the varying boundary conditions and the primary factors that affect them.

In order to assess the total solar efficiency of such a system, the electrical, thermal and daylight efficiency should be evaluated since solar energy is converted to electricity and heat or transmitted as daylight that is also useful. The fact that the air flows in the cavity and is in contact with both the STPV and the inner building layer, adds a complexity to the definition of the thermal efficiency as the interface between the DSF-STPV and the building inner layer cannot be considered as adiabatic. The determination of the convective heat transfer coefficient in the cavity and the heat transfer from each skin is critical for the calculation of the temperature at the outlet of the DSF-STPV.

In addition, the heat extracted from a DSF-STPV under forced convection is quantified and modelled and a new index that can quantify the heat recovery of such systems is introduced.

4.3. Methodology

STPVs integrated onto DSFs generate electricity but also absorb more incident solar radiation than a typical glass integrated on a DSF. Therefore, a more detailed analysis is required to evaluate the effect of the DSF-STPV on the energy balance of the air cavity and the transmitted solar radiation to the interior pane.

4.3.1. STPV transmittance and shading effect

The shading that the opaque PV cells provide to the interior layer of the DSF-STPV has an effect on the energy balance of the cavity and consequently has to be taken into consideration. The shading effect of the cells is expected to vary considerably both diurnally and seasonally due to the sun position. Two pyranometers are placed at the interior side of the IGU as shown in Figure 3-5 and Figure 4-2. These two pyranometers are placed directly behind the centre lines of the opaque PV strip and the transparent strip, in an effort to capture this shading effect. Although, the height of the PV cell is greater than the height of the glass strip and for this reason, there are times where both pyranometers are shaded by the STPV cells (see Figure 4-2b). These specific times are identified and excluded in the analysis. In Figure 4-2 (a), an instant of the day when the values of the pyranometers mounted on the side #4 of the IGU are different is depicted. For this instant, the experimental data can be reliable. In Figure 4-2 (b), an instant of the day on which the experimental data cannot be reliable is depicted as the values of the pyranometers mounted on the side #4 of the IGU are similar, an assumption that could falsely conclude that the IGU is completely shaded, instead of having stripes of shadow and lighting affecting the energy balance calculations (emissivity 0.9).

The PV cell and glass strips are 15.6 cm and 9.6 cm high respectively. The greatest common divisor (1.2 cm) is used to discretize the façade into sections. Each PV cell strip is represented by 13 sections and each glass strip by 8 sections. In total, the façade is discretized into 160 sections, 104 of which represent the cell strips and 56 the glass strips. This discretization is helpful for the more accurate assessment of the shading effect and of the radiative heat exchange within the cavity of the DSF-STPV.

4.3.2. Assumption about temperature distribution

As shown in Figure 3-5 the temperature profile of the air in the cavity is measured with 15 sensors along the height of the DSF-STPV. The temperature rise between the sensors is assumed to be linear.

It is also assumed that the temperature along each strip on the STPV remains constant and does not vary along the height of the strip. The validity of this assumption can be verified by infrared thermography (Figure 3-2), where the location of the PV cell strips and the glass strips is clearly identified, as the temperatures of the PV cells are higher than the glass temperatures. It can be seen in Figure 3-2 that the first cell row from the bottom is warmer than other rows on the STPV panel. There are two explanations for this overheating; this is due to the entrance (recirculation) effect because of the tunnel that is created between the air inlet and the DSF cavity, and the reflected solar radiation by the surface of the damper casing. For this reason, the two bottom and one top-

most PV strips were excluded from this analysis. This image supports the assumption that each medium (PV or glass) presents constant temperatures for each strip, along both x and z-axis.
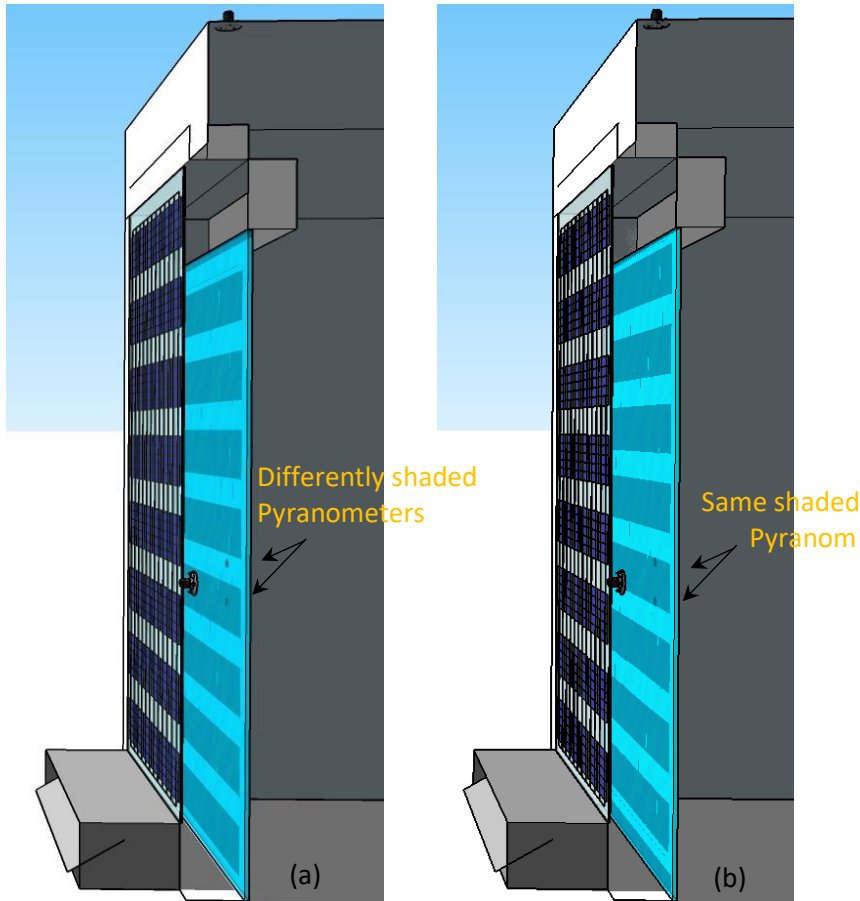
Figure 4-2 (a) An instant of the day on which the values of the pyranometers mounted on the side #4 of the IGU are different. (b) An instant of the day on which the pyranometers mounted on the side #4 of the IGU are similar.

4.3.3. Radiative heat exchange in a DSF

The radiative heat exchange in the DSF is calculated with the use of view factors (Z. Ioannidis et al. 2017). Both layers of the DSF; the STPV and the IGU are discretized into 160 control volumes and the view factors between them are calculated. The four remaining sides of the DSF are assumed to be at the average temperature of the air in the cavity.

4.3.4. Energy balance and convective heat transfer coefficients calculation

To calculate the convective heat transfer coefficients in the cavity, a system of two energy balance equations was solved based on (Figure 4-3a). First, the convective heat transfer coefficient towards the side of the IGU (hc_b) is calculated

$$hc_b = \frac{U_{gl}\left(T_{gli} - T_{glo}\right) + I_{abs_{glo}}/A_{cv} + Q_{rad_{glo}}/A_{cv}}{T_{glo} - T_{airflow}} \tag{4-2}$$

where U_{gl} is the thermal transmission of the IGU provided by the manufacturer, $Q_{rad_{glo}}$ is the radiative heat exchange calculated as described in section (4.3.3.), while the remaining parameters are measured as described in section 4.3.6. The convective heat transfer coefficient towards the side of the IGU, hc_b, is then used to calculate the convective heat transfer coefficient towards the side of the STPV (hc_a) in:

$$hc_a = \frac{\dot{m}c_p \Delta T / A_{cv} - hc_b\left(T_{glo} - T_{airflow}\right)}{T_{STPV} - T_{airflow}} \qquad (4\text{-}3)$$

These convective heat transfer coefficients are later used for the calculation of the Nusselt number. In the next sections (4.4.1.), the calculated Nusselt numbers will be used for the development of average Nusselt number correlations.

4.3.5. Calculation of a heat recovery index

The complexity of such system creates the need to introduce a new index which corresponds to the availability of heat to be recovered. The conventional way of calculating the thermal efficiency as the ratio of the heat recovered over the incident solar radiation may not be the index that indicate the heat recovery of BIPV/T systems as it may result in an over or under estimation of the heat recovery. This new index is different from the thermal efficiency as it differs from the ratio of the useful output over the input of energy. In building integrated photovoltaics, the system exchanges heat with the building that has an impact on the total heat recovered. The new index is the ratio of the total recovered energy over the input energy. The input energy to the system is the summation of the incident solar radiation and the heat exchanged with the building. The heat exchange with the building is positive or negative, depending on the direction of the heat exchange. Positive direction, is defined as the direction from the building or from the exterior skin towards the cavity of the DSF, as it is seen in Figure 4-3b and c.

$$Q_{recovered_{DSF-STPV}} = Q_{exchanged_{STPV}} + Q_{exchanged_{building}} \qquad (4\text{-}4)$$

$$\mathcal{H}_{heat\ recovery\ index} = \frac{Q_{recovered_{DSF-STPV}}}{I_{incident} \cdot A_{STPV} + Q_{exchanged_{building}}} = \frac{\dot{m}c_p \Delta T}{I_{incident} \cdot A_{STPV} + hc_b\left(T_{glo} - T_{airflow}\right) \cdot A_{STPV}} \qquad (4\text{-}5)$$

It should be noted that during the winter, the heat exchanged with the building will most likely be positive ($T_{glo} > T_{airflow}$) and during the summer, the heat exchanged with the building will most likely be negative ($T_{glo} < T_{airflow}$). The heat recovered by the DSF-STPV ($Q_{recovered_{DSF-STPV}}$) consists of the heat exchange with both the STPV and the building. During the heating season, this heat recovered by the DSF-STPV ($Q_{recovered_{DSF-STPV}}$) will be greater than that of cooling season, as the heat exchange with both the STPV and the building will be positive, whilst during the cooling season, the heat exchange with the STPV can be positive and the heat exchange with the building can be negative.

To accurately calculate the heat recovered by the system, the convective heat transfer coefficient between the air-flow in the cavity and the inner layer (hc_b) of the DSF-STPV (in this case the

IGU), must be identified.
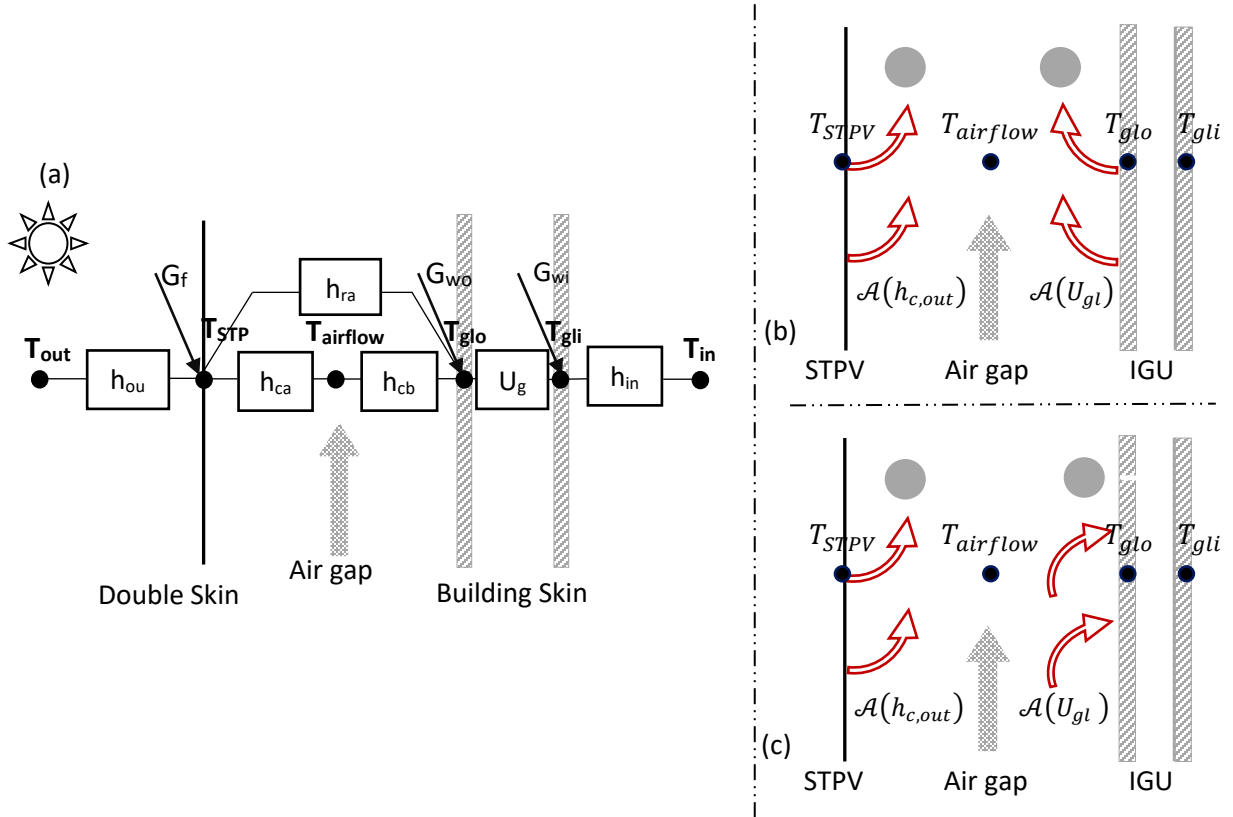
Figure 4-3 (a) Schematic of the thermal network of a DSF-STPV, (b) typical winter case, with heat being extracted from both the STPV and the building, (c) typical summer case, when air is warmer than the building zone.

4.3.6. Dimensionless numbers

The importance of the varying boundary conditions, as well as of the electrical efficiency and transparency of the system, especially for the of a DSF-STPV system was discussed in section 4.1.3.

These factors have been considered in the investigation of the convective phenomena in the air channel and the development of the respective Nusselt number correlations in the present study. As mentioned earlier, the electrical efficiency and the transparency are already dimensionless numbers. In this study, a new dimensionless number has been developed to account for the incident solar radiation, the wind velocity and the temperature difference between the interior and exterior that form the boundaries of the DSF-STPV system. In order to achieve non-dimensionality, the wind velocity was used implicitly by replacing it with an empirical linear correlation for wind-driven convection employed by Sharples and Charlesworth (Sharples and Charlesworth 1998).

It should be mentioned that the choice of the proper wind-driven CHTC correlation is very important and highly dependent on the local climate, the surroundings and system geometry. Palyvos (Palyvos 2008) suggests that the engineers/researchers can choose among the various correlations provided in literature based on the common conditions to the study in which the

correlations were developed. Regardless, as shown later on, the correlation between the newly implemented dimensionless number and the Nusselt number is clear and independent of the chosen wind-driven CHTC formula, the only change being in the actual numerical correlation.

The new dimensionless number is defined as: $\frac{U \cdot |T_{ambient} - T_{room}|}{I_{incident}}$

For low incident solar radiation values, this new number would tend to be infinity. To avoid that, an additional factor of 300W/m² was added to the denominator. Values less than 300 W/m² were also neglected from the experimental analysis as they would present greater error since the ΔT would be lower but also, they are less important in calculating the energy generation. In addition, the heat transfer coefficient (U) is either the exterior heat transfer coefficient ($h_{c,out}$) or the overall heat transfer coefficient of the inner and transparent layer of the DSF (U_{gl}). The selection of the $h_{c,out}$ or the U_{gl} depends on which side of the DSF-STPV the Nusselt number needs to be calculated for. For the calculation of the Nusselt number towards the side of the STPV (exterior layer of the DSF-STPV), the exterior convective heat transfer coefficient is used ($h_{c,out}$). For the calculation of the Nusselt number towards the interior side of the DSF-STPV (IGU side), the U-value of the glazing is used (U_{gl}). For clarification, this distinction is shown in Figure 4-3 (b) and Figure 4-3(c). This new dimensionless number has its final form as:

$$\mathcal{A} = \frac{(h_{c,out} \; or \; U_{gl}) \cdot |T_{ambient} - T_{room}|}{I_{incident} + 300(W/m^2)} \qquad (4\text{-}6)$$

Commonly used Nusselt number correlations are often developed having Reynolds number and Prandtl number dependencies for the heat transfer in pipes or ducts. As it is shown in Figure 4-1, there is no correlation that can be derived between the existing in the literature Nusselt number correlations and this new dimensionless number ($\mathcal{A}$). The advantages of using this new dimensionless number ($\mathcal{A}$), is that it can be used for the development of Nusselt number correlation taking into consideration the boundary conditions and the material properties of more complex systems.

4.4. Results and Discussion

Based on the methodology presented in section 3.1. and the experimental data collected as described in section 4.3. , an analysis followed for the generation of average Nusselt numbers as a function of a combination of dimensionless numbers. In this analysis, the exterior convective heat transfer coefficient, which is a function of the wind, the Reynolds number of the flow in the cavity, the measured efficiency of the PV cell, the incident solar radiation and the transmittance of the STPV are to form the dimensionless numbers as described in section 4.3.6.

4.4.1. Average Nusselt number

The crystalline Silicon STPV panels used in this experiment consist of eight (8) rows of PV cells and seven (7) transparent strips made from glass (Figure 3-2). For the region of the PV cell strips, the average Nusselt number correlation is generated as a function of the wind heat transfer coefficient ($h_{c,out}$), the Reynolds number, the efficiency of the PV cell and the incident solar radiation. An additional factor of 300W/m² is added to the incident solar radiation to avoid having

small values in the denominator. It should also be noted that values less that 300W/m^2 were not included in the generation of the Nusselt number correlations to avoid using data with large measurement errors due to small temperature differences. In addition, the heat gains are expected to be low, below this irradiance level.
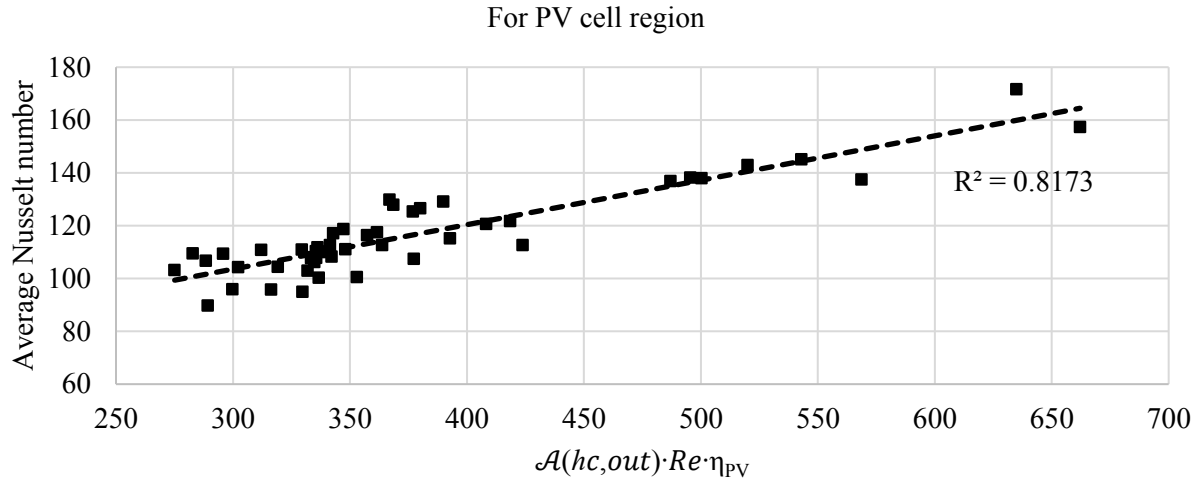
Figure 4-4 Average Nusselt number correlation for the region of the STPV that is covered by PV cells, as a function of a dimensionless number.

The average Nusselt number for the cell regions is:

$$Nu_{Average\ cell} = 0.1682 \cdot \mathcal{A}(hc, out) \cdot Re \cdot \eta_{PV} + 53.10 \qquad (4\text{-}7)$$

For the whole STPV layer, including the PV cell region, the developed Nusselt number correlation is presented in Figure 4-5. This average Nusselt number can be used for the calculation of the convective heat transfer coefficient between the air flowing in the cavity and the STPV layer (h_{ca}). Similarly with the average Nusselt number correlation for the PV cell region, the correlation for the STPV layer takes into consideration the wind effects, the Reynolds number, the efficiency of the STPV and the incident solar radiation. What is added in this case, is a factor that corresponds to the absorbed solar radiation by the glass section of the STPV ($1 - \tau_{glass}$).
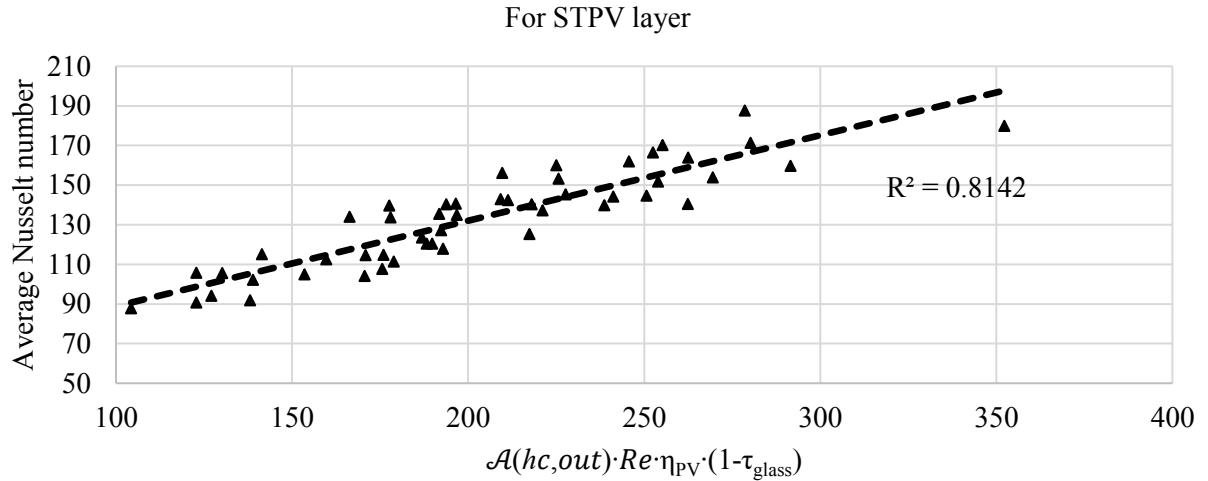
For STPV layer

Figure 4-5 Average Nusselt number correlation for the region of the STPV, as a function of a dimensionless number.

The average Nusselt number correlations for the STPV layer is presented in equations (4-8) and (4-9). In equation (4-9) the average Nusselt number is presented as a function of the overall efficiency and overall transmittance of the STPV and not as a function of the efficiency of the PV cell and the transmittance of the glass, generalizing in this way the result to other STPV technologies.

$$Nu_{Average\ STPV} = 0.4316 \cdot \mathcal{A}(hc, out) \cdot Re \cdot \eta_{cell} \cdot \left(1 - \tau_{glass}\right) + 47.71 \tag{4-8}$$

$$Nu_{STPV} = 0.2852 \cdot \mathcal{A}(hc, out) \cdot Re \cdot \eta_{STPV} \cdot (1 - 0.339\ \tau_{STPV}) + 47.71 \tag{4-9}$$

For IGU layer
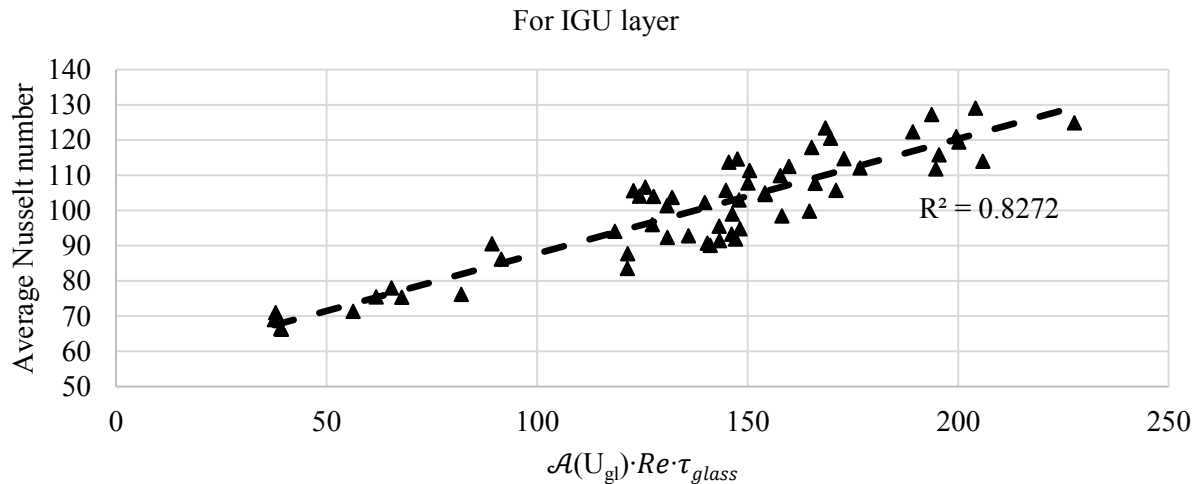
Figure 4-6 Average Nusselt number correlation for the interior layer of the DSF-STPV (in the case the IGU side), as a function of a dimensionless number

Following the same methodology, the dimensionless number in this case includes the thermal

transmittance of the IGU (U_{gl}), and the solar transmittance of the glass strip of the STPV (Figure 4-6). The overall solar transmittance of the STPV is used in equation (4-11) for a general Nusselt number correlation. In this way, the losses from the building to the DSF-STPV over the gains from incident solar radiation are multiplied by the transmittance of the STPV.

$$Nu_{Average\ IGU} = 0.3259 \cdot \mathcal{A}(U_{gl}) \cdot Re \cdot \tau_{glass} + 55.19 \qquad \qquad (4\text{-}10)$$

$$Nu_{IGU} = 0.1105 \cdot \mathcal{A}(U_{gl}) \cdot Re \cdot \tau_{STPV} + 55.19 \qquad \qquad (4\text{-}11)$$

It should be noted here that each dimensionless number has a physical meaning as it includes the system losses to the outside due to wind induced convection over the incident solar radiation to the DSF-STPV system. Depending on the layer of the STPV that is analysed, this fraction is multiplied by the electrical efficiency of the STPV, or the absorbtance or the transmittance of it respectively.

4.4.2. Sensitivity analysis for wind speeds

The importance of the wind effects on the Nusselt number is investigated through a sensitivity analysis shown in Figure 4-7. For the PV cell region (also presented in Figure 4-4), the new dimensionless number is calculated for three cases, namely for the measured wind speed and for low and high wind speeds. These values correspond to a Nusselt number calculated as presented in section 4.3.4. It should be noted that for low wind speeds the wind speed is assumed to be close to zero (0.1 m/s) and the $h_{c,out}$ is calculated to be close to 12 W/m^{2}K and for high wind speeds, the value of 5 m/s is selected resulting in an exterior convective heat transfer coefficient of around 23 W/m^{2}K. For both adjusted wind speeds, the coefficient of determination (R^2) is the same as the wind speed has a linear dependency to the exterior heat transfer coefficient.
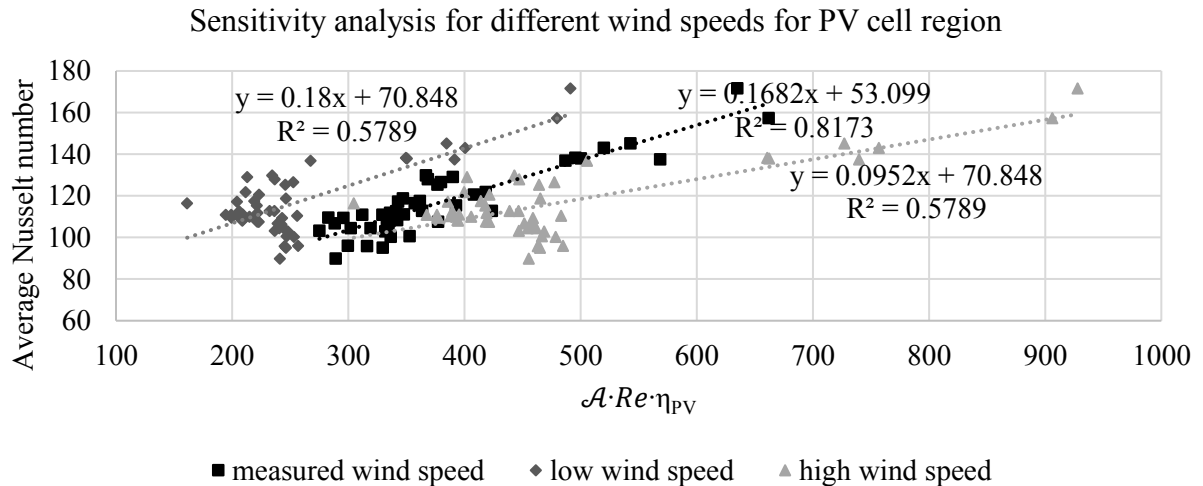
Figure 4-7 The average Nusselt number coefficient is presented for the measured wind speed but also for two cases of adjusted wind speeds (high wind and low winds).

4.4.3. Thermal analysis

The addition of an external layer on the DSF, creates a cavity between this exterior layer and the interior layer of the building envelope. This cavity creates a buffer zone around the building which can isolate the building from the ambient weather phenomena. In this way, the effect of the wind on the thermal losses of building decreases as the wind flow is not in direct contact with a building envelope layer that interacts with a thermal zone. In Table 4-1, the building losses for a case of a building with and without a DSF-STPV are calculated. The per-cent difference between the two cases is shown, as well as the net difference, presented as "Net gains". For different Reynolds numbers, incident solar radiation and wind velocities, the thermal losses for a building without a DSF ("Typical Building") and a building with a DSF-STPV are compared. For the "Typical building", the same IGU used as the interior layer of the DSF-STPV is assumed for both cases, the same correlation calculating the exterior heat transfer coefficient is also used. Representative cases, for flows in the cavity, incident solar radiation and wind velocity, covering the whole range of the experiment are presented in Table 4-1. The "Net-gains" represent the heat extracted from the building that would be lost to the outside if the DSF was not implemented.

For high incident solar radiation ($\sim 1000 W/m^2$) and high wind velocities ($V_{wind} > 7.0$ m/s) the building losses for both cases present their highest values (around 41 W/m^2 and 33 W/m^2 respectively). For similar Reynolds numbers and incident solar radiation but with relatively low wind velocity (~ 2 m/s) the thermal losses present a decrease by 16%. For the same case, the net gains present its highest value ($8.35 W/m^2$), indicating that increased solar radiation and low-velocity flows in the cavity of the DSF-STPV can minimize the building losses. It should be noted that the per-cent difference of the losses between both cases is greater than 15%, while for low incident solar radiation, the building losses are minimal.

The calculated thermal efficiency of such a system is presented in

Table 4-2, along with the measured electrical efficiency and the visual transmittance. In the same table, the difference between the conventional thermal efficiency definition and the equation suggested in section 4.3.5. is also presented. Also, the total solar efficiency of such a system is presented, as it consists of the summation of the new heat recovery index, the electrical and the visual efficiency of the system.

The concept of the equivalent thermal efficiency, as introduced by Athienitis et al (2011), is also used but is also updated in this study as equivalent heat recovery index. The coefficient of performance of a heat pump, which represents the conversion of electricity to heat, is multiplied with the electrical efficiency and then is added to the heat recovery index of the system. The values of the COP presented in

Table 4-2, are typical market values of an air to water heat pump and are based on the ambient temperature. The equivalent heat recovery index ranges from 34% to 72% depending on the incident solar radiation and the Reynolds number. It is noteworthy that for lower incident solar radiations (670.2 W/m^2) the equivalent heat recovery index can reach up to 34%, even when the ambient temperature is below zero.

For lower Reynolds numbers the heat recovery index increases and can reach more than 35%. As the heat recovery index of the system represents the heat extracted by both the interior and the exterior layer of the DSF-STPV, the absorbed by these layers solar radiation has a major effect on this new index. The measured electrical efficiencies shown in

Table 4-2, present discrepancies between its values because during the experiment the dumping load failed which resulted in less power drawn out of the STPV. This unexpected equipment failure actually generalized the data collected in this experiment as it made it possible to draw less electricity by the STPV that could correspond to PV technologies with lower efficiencies.

In

Table 4-2, the total solar efficiency is presented in the last column. Starting from almost 30% it can reach up to 77.3% for different experimental conditions. The visual transmission depends on the incident angle as the reflected solar radiation increases with the increase of the incident angle. Consequently, the measured transmitted solar radiation ranges between 5% to almost 40%, depending on the time of the day and the period of the year.

Table 4-1 Thermal building losses for a typical building (glazed façade consisted of IGU) and a building with DSF-STPV with the same IGU as the interior layer.

Reynolds number	Incident solar radiation (W/m^2)	Wind velocity (m/s)	Typical Building losses (W/m^2)	Building losses DSF-STPV (W/m^2)	Difference (%)	Net gains (W/m^2)
9500	1031.0	2.1	34.74	26.39	24.0	8.35
10400	1003.3	7.8	41.38	33.20	19.8	8.18
15200	994.8	2.9	29.04	22.55	22.4	6.50
15300	712.2	2.5	33.28	28.01	15.8	5.26
26100	347.4	3.6	0.16	0.10	36.4	0.06
26600	500.4	2.7	4.98	3.81	23.4	1.16

Table 4-2 Thermal, electrical and visual efficiency are presented along with their summation named "combined efficiency". The thermal efficiency calculated with the conventional definition and the definition of section 4.3.5. are presented and compared as their per-cent difference is also given.

Reynolds	Incident Solar radiation (W/m^2)	Temperature at the outlet (°C)	Coefficient of Performance (-)	Wind Velocity (m/s)	Conventional thermal efficiency (%)	Heat recovery index (%)	Difference (%)	Electrical efficiency (%)	Visual transmission (%)	Equivalent heat recovery index (%)	Total solar efficiency (%)
8900	929.2	-2.6	2.9	4.5	27.8	31.4	13.2	4.1	31.3	43.29	66.8
9500	1118.4	-2.2	2.9	5.6	30.5	34.5	13.2	3.9	37.5	45.81	76.0
10100	958.8	-2.2	2.9	6.3	28.3	31.5	11.3	4.0	28.3	43.1	63.8
10300	1070.3	-0.3	3.1	6.7	31.4	35.7	13.5	3.7	37.9	47.17	77.3
15100	981.6	6.8	3.7	4.7	24.3	26.3	8.3	4.6	8.6	43.32	39.5
15200	994.8	6.0	3.7	2.9	23.5	25.6	9.2	4.5	14.2	42.25	44.3
15200	991.4	6.6	3.7	2.9	24.2	26.2	8.4	4.5	10.3	42.85	41.1
15800	670.2	-0.1	3.1	1.1	14.4	16.2	12.8	6.0	33.6	34.8	55.8
24800	589.5	28.6	5.6	1.1	16.7	17.3	3.6	9.8	6.2	72.18	33.3
25300	632.2	21.9	5.0	3.6	12.7	13.1	3.5	10.0	5.8	63.1	28.9

4.4.4. Validated temperature profiles

In Figure 4-8, the experimental conditions, under which the newly developed correlations were validated are presented. The validation was performed for different Reynolds numbers, ambient temperatures and incident solar radiations with time intervals of 15 minutes. In Figure 4-8, the ambient temperature and the Reynolds number divided by 1000 are presented in the left y-axis, while the incident solar radiation is in the right y-axis. The ambient temperature ranges between -5°C and 30°C, the Reynolds number between 10,000 and 26,000 and the incident solar radiation between 250 W/m^2 and 1200 W/m^2. For the validation, the same methodology and assumptions followed for filtering the experimental data, were used. At the top of Figure 4-8, the first of the days used for the validation are presented, depicting one summer day. At the bottom of Figure 4-8 four summer, two autumn and four winter days are presented. They are presented in the same figure in order to minimize the figures needed for presentation, although they refer to different time periods.
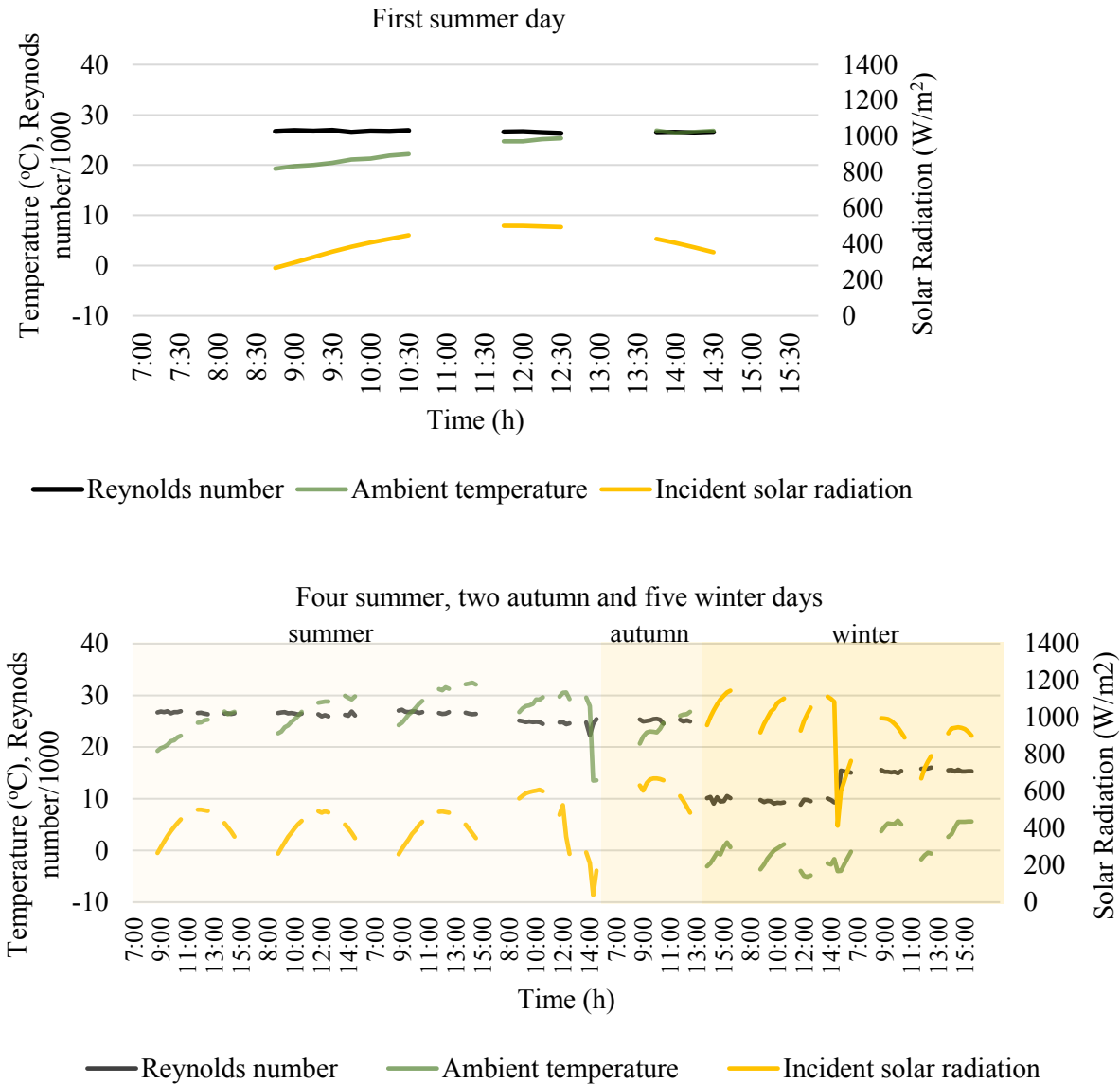
Figure 4-8 Experimental conditions used as boundary conditions for the validation of the developed Nusselt number correlations for four summer, two autumn and five winter days. At the top, the first summer day is depicted.

Using the Nusselt number correlations developed in section 4.4.1. and the energy balance equations that were used to develop equations (4-2) and (4-3), a validation followed for the temperatures of the air at the outlet of the DSF-STPV (Figure 4-9) and for the temperatures of the cells of the PV (Figure 4-10).

In Figure 4-9, the measured temperature of the air at the outlet of the DSF-STPV is depicted and compared with the predicted outlet temperature of the DSF-STPV. For the prediction of the outlet temperature, the measured temperatures of the STPV and the IGU are used as boundary conditions and the measured airflow is used as the mass flow rate in the cavity. The difference between the

predicted and the measured outlet temperature of the DSF-STPV is shown in the same graph and it does not exceed 1°C. This difference appears negligible for warmer ambient temperature conditions and lower incident solar radiation.
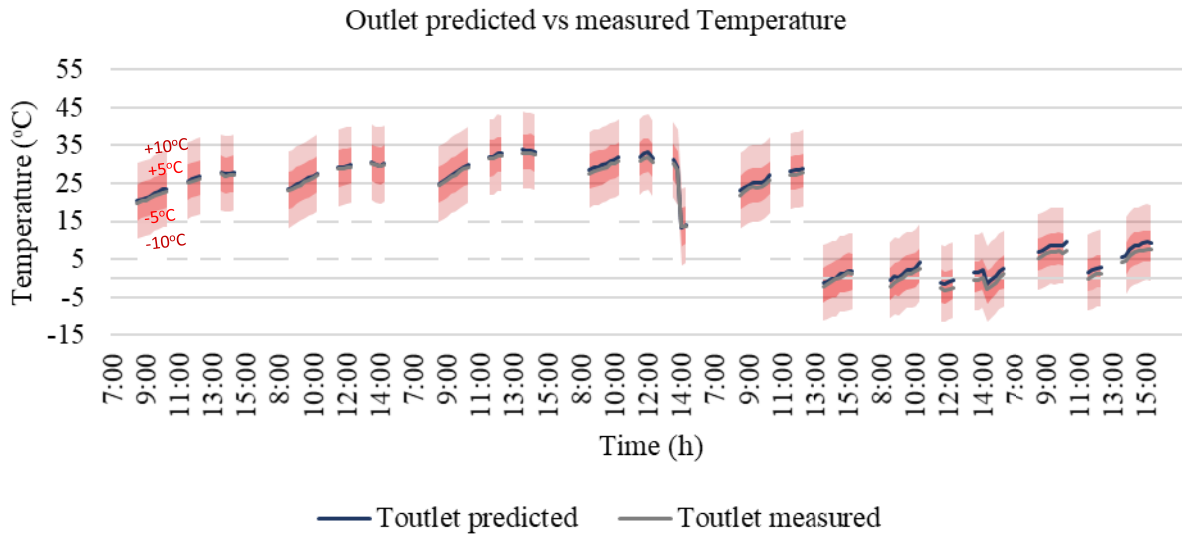
Figure 4-9 Temperatures at the outlet of the DSF-STPV as measured and predicted using the Nusselt number correlation developed in section 4.4.1.
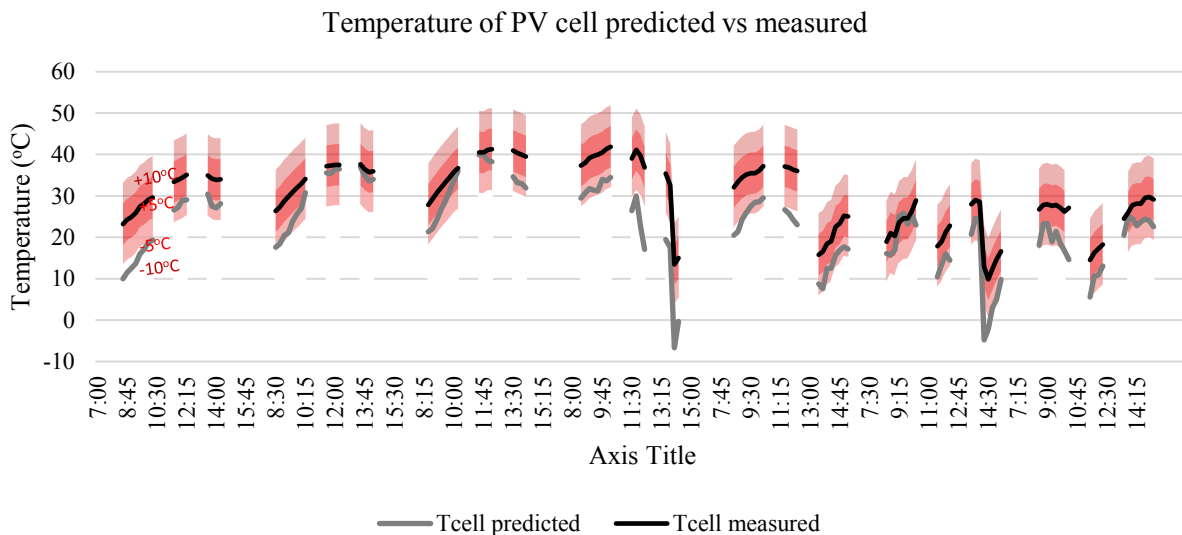
Figure 4-10 Temperatures of the cells of the STPV as measured and predicted using the Nusselt number correlation developed in section 4.4.1.

In Figure 4-10, the predicted and the measured temperature of the PV cell are shown. The temperatures of the PV cell depicted in this figure, represent the average temperature of the PV cells that are spaced into strips to form in this way the STPV. It should be noted that for most of the PV technologies, the temperature of the cell affects its electrical performance, and the accurate prediction of this temperature is important for the identification of the electrical output of such

system. In addition, for c-Si, which is the most commonly used PV technology, this dependence of the electrical power performance to the temperature is in the range of 0.5%/°C. This means that for a typical 300Wp panel, a 10°C increase in the cell temperature will result in a 15Wp decrease in the power output and vice-versa.

The difference between the predicted and the measured temperatures of the PV cells is mostly within a 5°C temperature difference range. As it can be seen in Figure 4-10, the only moments where this difference is higher, is for the cases of lower incident solar radiation, which are cases that would also result in lower power outputs by the PV and are thus less important.

4.5. Limitations and future work

This specific experimental work was performed in the span of a year in Montreal Canada. This study is limited by the STPV technology used (c-Si) and the flow within the cavity of the DSF that present Reynold numbers between 10,000 and 26,000 and velocities from 0.3 m/s to 1.2 m/s. These limitations in combination to the boundary condition, the specific materials used, and the location of the test-room make the experiment case specific, but the results are expected to be quite general for similar air speeds in the cavity that represent the main practical region of airflows of interest.

A following study will present in more detail the dimensional analysis generalized for BIPV/T applications including the expansion of the presented methodology for BIPV/T in roofs and facades. In addition, future work must include the expansion of the same methodology to test-rooms in different locations and different climatic regions. Lastly, the performance of the system under different operation strategies needs to be investigated.

4.6. Conclusions

In this study, an outdoor experimental test-room based in Montreal, Canada, implementing DSF-STPV was used for the development of Nusselt number correlations for the convective heat transfer of the flowing air in the cavity of a DSF-STPV. In this process, the effect of the incident solar radiation, the wind driven convection and the ambient temperature have been taken into consideration.

Three Nusselt number correlations were developed describing the convective heat transfer between the STPV surface and the air flowing in the DSF, the STPV cells and the flowing air and the inner layer of the DSF-STPV and the air flow. In this case, the inner layer of the DSF-STPV was a clear insulating glazing unit thus, the inner surface of the DSF-STPV contribute to the heat recovered by the system. It should be noted that the range of the Reynolds numbers in this study was between 10,000 and 26,000 representing air velocities from 0.3 m/s to 1.2 m/s. The experimental results can be considered inconsistent for incident solar radiation that is lower than 300W/m^2 as the low incident solar would result in lower power output by the PV, and ambient temperature that ranges outside of the -5°C and 30°C range that the experiment was conducted.

The importance that the wind effects have on the energy balance of a building was highlighted in this study. The thermal losses due to wind effects are calculated for a typical office building and a building integrating DSF-STPV. It is noteworthy that the DSF-STPV can reduce the exterior heat losses of the building by more than 20%.

The heat recovery index ($\mathcal{H}$) of such system was defined and was differentiated from the typical definition of thermal efficiency of such systems, as the heat recovered by the building is an energy source to the system. This difference in definitions can lead up to 13% difference in the calculation of the heat recovery of such system. The total combined efficiency of the DSF-STPV, as calculated based on the conducted experiments can vary between 25% to 75%.

Finally, a validation of the developed Nusselt number correlations was performed, using the experimental data for the boundary conditions. The temperature of the outlet of the DSF-STPV and the temperature of the PV cells was compared to the measured experimental data. It was shown that the difference between the predicted and the measured temperature at the outlet of the DSF-STPV does not exceed 2°C. Similarly, for the temperature of the PV cells, the difference between the predicted and the measured values was within a 5°C range, with the exception of the cases with lower incident solar radiation, when this difference was increasing.

Chapter 5

Model Development and preliminary results

Parts of this chapter are presented in the paper:

Z. Ioannidis et al. 2017. Double skin façades integrating photovoltaics and active shadings: a case study for different climates. BIRES.2017 Dublin. Ireland

5.1. Modelling of DSF-STPV

A numerical model of a Double Skin Façade integrating Photovoltaic panels (DSF-STPV) was developed based on energy balance equations. This model is validated with the outdoor experimental data collected and are described in Chapter 3.

The model can simulate opaque or semi-transparent photovoltaics integrated on the exterior layer of the double skin façade as well as shading devices inside the cavity including the shading that they provide to the building (Figure 5-1). It is also capable to assess the active and passive effects of the generic DSF-STPV on the thermal and visual comfort and energy performance of the building in which the system is integrated.

The model also allows the user to perform a parametric analysis changing the design parameters of the building and the DSF-STPV that he wants to simulate. Specifically, the user can select the location of the building, loading the relevant weather file, and the orientation in which the DSF-STPV will be placed. The user may also select the dimensions of the adjacent to the DSF-STPV room and the distance between the two skins of the DSF-STPV. What can also be adjusted be the user is the existence or not of opaque and semi-transparent photovoltaics, their location on the exterior skin and their dimensions. This also applies for the glazing and the insulation of the interior wall.

The characteristics of the skins can also be determined, defining the height and the insulating values of the spandrel and the upper spandrel, their absorbtance and emissivity. The efficiency of the photovoltaics integrated on the exterior skin defined under standard test conditions can be determined by the use as well as their height and transmittance. The model is also able to determine the appropriate position of the photovoltaics on the exterior skin, in order to provide shading to the interior of the building.

Although the integrated photovoltaics provide shading to the building, the model is ready to consider the existence of a roller blind implemented within the cavity. The height of the blind, and its thermal and optical properties can be defined by the user. The existence of a roller blind is affecting the flow of the air inside the cavity, the thermal balance and the shading to the interior skin.

Taking into consideration the temperature distribution of the air inside the cavity, as well as the wind velocities and directions imported from the weather file, the airflow inside the cavity can be determined by the model. It is also possible to manually set a desired airflow rate inside the cavity, enabling in this way a mechanical ventilation which assists the stack and wind effects. The model parameters can be determined by the user are summarized in Table 5-1.

The interactive nature of the model and the flexibility that it provides to the user gives the opportunity to be used for pre-feasibility studies. Engineers, architects and builders can take advantage of this model in the early stages of the design of a building or in the decision-making process of retrofit projects, allowing the integration of BIPV/T technologies in new or retrofitted building facades.
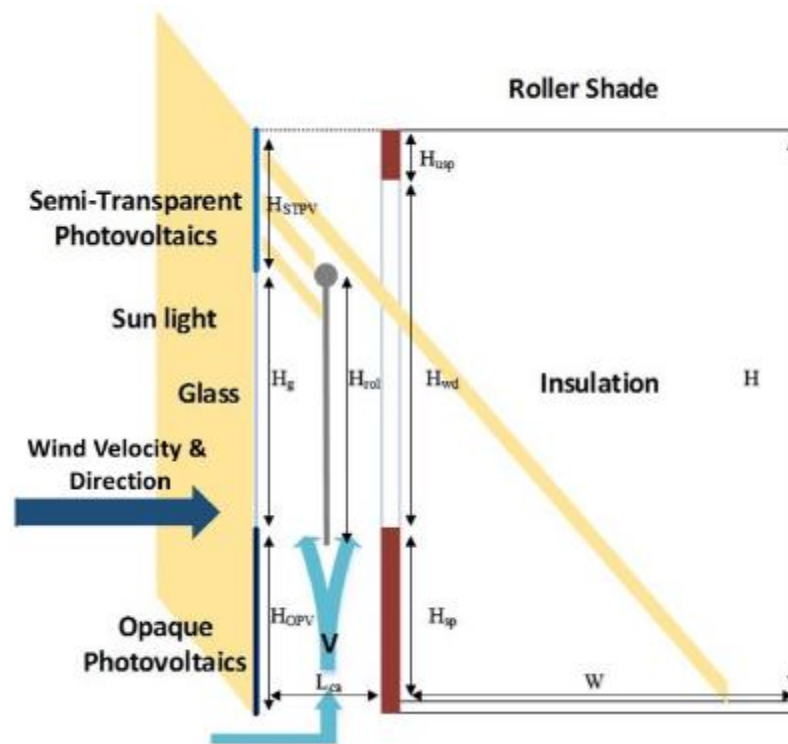
Figure 5-1 Sketch of the double façade section (one floor)

Table 5-1 Input parameters for the numerical model

Design parameters	Number of floors		**Optical properties**	STPV transmittance
	Position of PV			Roller shade transmittance
	Position of roller blind			Glazing transmittance
	Interior skin design			PV efficiencies
Geometric parameters	H_{OPV}/H	H_{sp}/H	**Thermal properties**	Roller emissivity
	H_g/H	H_{wd}/H		Glazing emissivity
	H_{STPV}/H	H_{usp}/H		SHCG
	L_{ca}/H	H_{rol}/H_g		Insulation of the room
	W	H		COP of the heat pump
Site properties	Location of the building		**Flow properties**	Reynolds number
	Orientation of the DSF-PV			Velocity

The integrated with photovoltaics DSF takes full advantage of the cavity and especially of the air flow inside the cavity, which serves the system in three ways:

- The cavity during the winter months acts as a thermal buffer zone for the building.

- The air flow absorbs the heat from the integrated photovoltaics through convection and thus increases their electrical efficiency.

- Utilizes the preheated air as a source for natural or hybrid ventilation (heating or cooling) for the building.

In addition, the warmer than the outdoors air at the top of the cavity, can be introduced to the HVAC system. In this way the energy consumption to heat the air used into the HVAC system is decreased.

Also, the air inside the cavity can be introduced directly to the interior of the building if the temperature of the air does not exceed the comfort levels of the occupants. Energy conservation can also be achieved by providing natural ventilation to the building or naturally heating or cooling the interior zone.

The modelled cavity could also include automated roller shades, which help to reduce the space cooling and heating loads and control the daylight levels in the indoor space.

Air can flow on both sides of the shading devices placed within the cavity, extracting more heat from and increasing the thermal efficiency of the system (Figure 5-2).

In this study an interactive numerical model for the assessment of the energy performance of a multi-storey Double Skin Façade integrating photovoltaics (DSF-STPV) has been implemented in MatLab (Mathworks). The whole exterior, and, similarly, the interior skin of a multi-storey building is designed as multiple strips made of semi-transparent photovoltaics, glazing, and opaque photovoltaic elements. Control volumes are formed between the strips on the exterior skin and those on the interior.
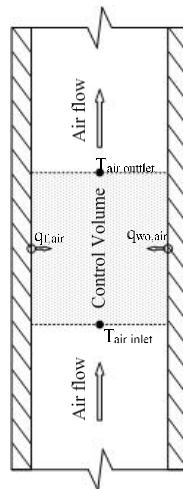
Figure 5-2 Schematic of a control volume in the DSF-STPV

The mass entering the control volume is equal to the mass leaving the control volume and in the case of steady state and in the absence of work and heat transfer, the energy within the control volume remains constant.

5.2. Grid interaction of DSF-STPV and IGU-STPV

The mismatch between the electricity production from the PV and the electricity needed used for heating is of great interest to the utility companies. In addition, the peak demand that occurs in early mornings and early evenings in cold climates is a concern to the utility companies as a greater number of factories should be ready to operate only for certain hours per day or even for certain days per year.

The previously mentioned model is used to investigate the grid interaction of DSF-STPV. In this paragraph, some preliminary results are presented for a DSF-STPV for two cold and sunny days in January in Montreal. In Figure 5-3, the weather conditions for the simulations performed is presented, along with the average temperature of the cavity of the DSF-STPV and the room temperature set-point. It can be seen that the incident solar radiation for these days can almost reach the 800W/m^2 and the ambient temperature fluctuates between -25°C and -15°C. The temperature of the air within the cavity can be five to ten degrees higher than the ambient temperature and the temperature of the room is set to be at 18°C and 21°C depending on the time of the day. More precisely, at 7am, the temperature set point will change to 21°C and this leads to peak demand explained earlier.
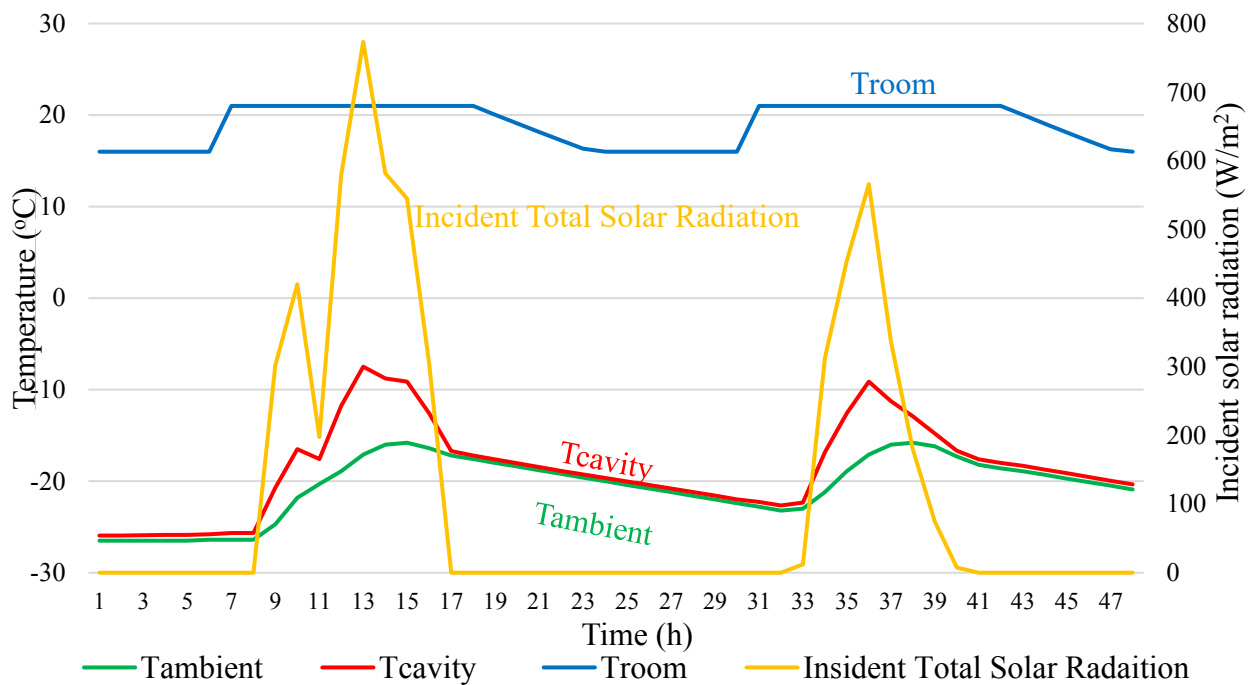
Figure 5-3 Weather conditions for the simulations performed the temperature set-point for the interior zone and the average cavity of the temperature.

What contributes to this peak demand can be seen in Figure 5-3, where the electricity consumption for heating and lighting per sq. meter is presented along with the electricity production from the photovoltaics integrated per sq. meter of the façade. In Figure 5-4, two different transmittances of the STPV are simulated presenting an increase in the electricity production that reaches 30%. Because STPV are integrated in the DSF, the heating demand during the day decreases as the

building receives solar heat gains and at the same time it produces electricity.
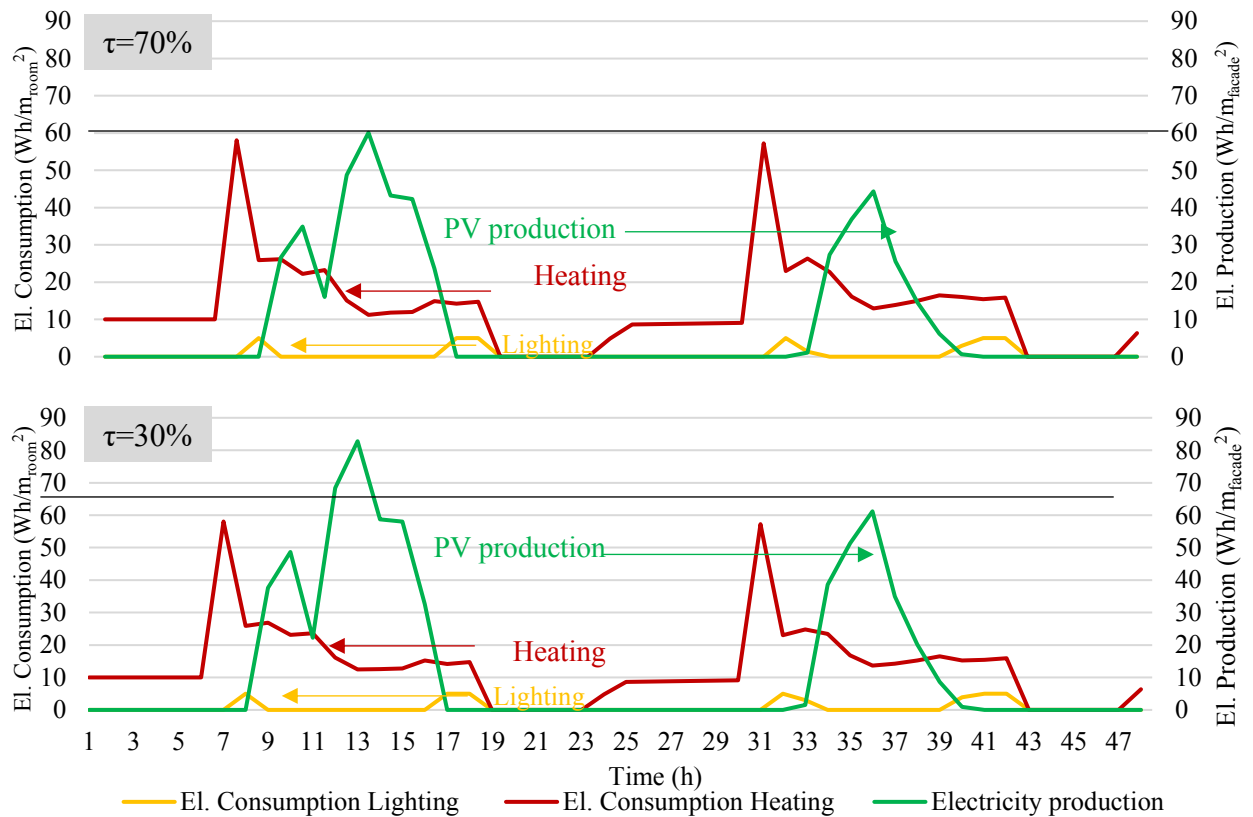
Figure 5-4 Electricity consumption for heating and lighting and the electricity production from the PV. The consumption per sq. meter follows the primary axis and the electricity generation the secondary axis.

For the same weather conditions shown in Figure 5-3, a comparison is held for a different heating schedule and different temperature set-points. The potentially available heating calculated by the Coefficient of Performance (COP) multiplied by the electricity produced by the PV is presented along with the electricity consumed for heating in

Figure 5-5. These values cannot be compared as of their magnitude but as of their time off occurrence. If the set-point is increased to 26°C but is shifted to 12pm to 20pm instead of 7am to 18pm and the set-back is set to 21°C from 18°C to avoid thermal uncomfortableness. It can be seen that the peak for the heating occurs when the peak of the electricity production happens, in the case of the 26°C set-point. In Table 5-2 the electricity consumption for heating is presented between 7am and 2pm for the two heating strategies. The electricity consumed for heating between 7am and 8am is five times greater in the first case where the temperature is set to 18 °C during the night and reaches 21 °C when people are expected to arrive in the building than in the second case. In the second case, the temperature is set to 21°C during the night, so when people arrive will not feel uncomfortable and the building is heated to 26°C at 12pm when the electricity produced by the solar panels can be utilized. In addition, the COP of the heat pump used for heating is higher during that time as it is assisted by the preheated air within the DSF cavity.
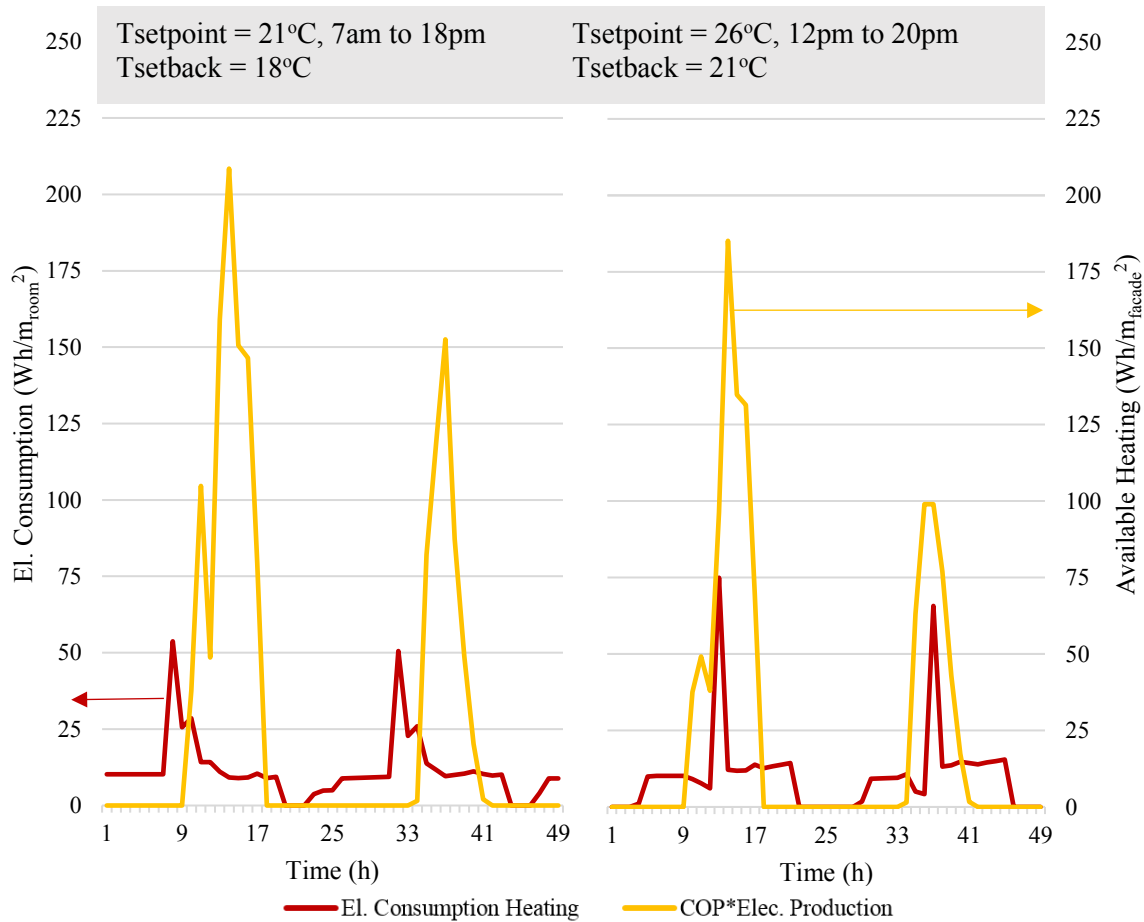
Figure 5-5 Electricity consumption for heating and potentially available heating from the electricity produced by the PV.

Table 5-2 Electricity consumption for Heating for the two days of the simulation. The hours of the peak demand are highlighted with pink.

	Hours of the day	Day 1								Day 2							
		7	8	9	10	11	12	13	14	7	8	9	10	11	12	13	14
Electricity for heating (Wh)	21ºC, 7am to 18pm Tsetback = 18ºC	53.7	25.6	28.6	14.3	14.2	11.1	9.1	9.0	50.5	22.8	25.9	13.7	11.7	9.6	10.0	10.4
	26ºC, 12pm to 20pm Tsetback = 21ºC	10.9	10.9	10.0	4.8	5.5	45.4	11.4	11.2	10.1	10.2	11.5	4.6	4.2	41.0	12.3	12.7

5.3. Different climate simulations

Simulation can also be performed, identifying the optimal characteristics of DSF-STPV and strategies of operation for different climates. For a conventional high-rise office building, the modelled DSF-STPV is installed on the South facing façade and its energy consumptions are compared to a Reference System (RS) configuration obtained by simulating the same building without DSF-STPV, but with the same shading strategy. The cavity width is set to be 0.5m and the

minimum air velocity is set at 0.25 m/s; if natural convection allows higher flow rates the fan is switched off. A roller shading is placed at the middle of the cavity (0.25m from both ends) and the transmittance of the STPV is set equal to 30%. The South interior skin façade consists of: i) a window (4-16-4 air filled double-glazed low-e system) with U-value = 1.28W/m2K; ii) an insulated wall with U-value = 0.24W/ m^2K or 0.48W/m ^2K, iii) floor/ceiling with U-value = 1.10W/m ^2K. Finally, artificial lighting energy use, depending on daylighting illuminance, is calculated in order to provide 300lux on office desk level. The DSF cavity, operated in hybrid ventilation mode, is closed when the ambient air temperature is lower than the heating set point Tsp,heat + 3°C.

Both the DSF-STPV and traditional (RS) buildings are simulated by taking into account a week-day schedule from 8.00 to 18:00 (week days only). The heating and cooling set points are 20°C and 26°C, maintained by an air-to-air electric heat pump/chiller. Two weather zones are considered: Naples (Italy, Mediterranean temperate climate) and Montreal (Canada, humid continental climate with very cold and snowy winter). Simulations are carried out with one hour time step and starts on 0:00 of January 1st and ends at 24:00 of December 31st. The heating and cooling periods are shown in Table 5-3 along with the heating and cooling degree days (HDD and CDD) and the incident solar radiation (ISR) indexes.

Table 5-3 Climatic zones, climatic indexes and system scheduling

Weather zone	HDD [Kd]	CDD [Kd]	ISR [kWh/m²y]	Heating [hours]	Cooling [hours]
Montreal	4567	297	1350	15/Sep.-31/Mar.	1/Jun.-15/Sep.
Naples	1479	499	1470	15/Nov.-31/Mar.	1/Jun.-30/Sep.

Figure 5-6 shows the average monthly electricity production and maximum power output of a single thermal zone of the South-facing DSF-STPV, for both the investigated locations. In this figure it is possible to observe that the monthly energy output obtained during winter is much higher than that observed during summer. Specifically, the maximum monthly PV output is about 120kWh in March in Montreal and 115kWh in October in Naples; the minimum production is obtained in November in Montreal (47kWh) and in January in Naples (67kWh).
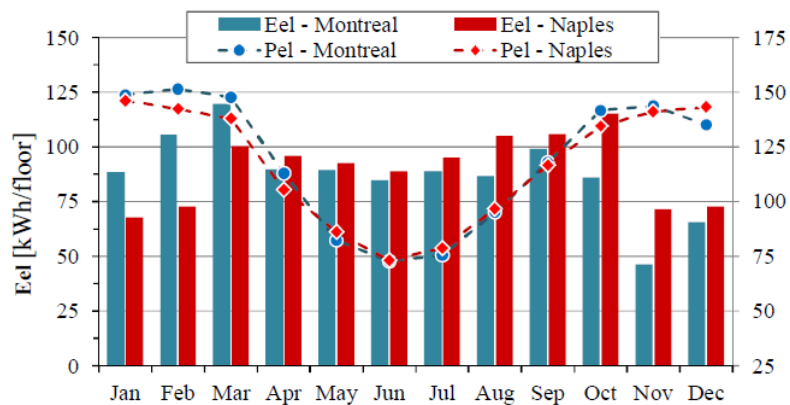
Figure 5-6 Monthly average electricity production and maximum power output

Finally, in Table 5-4, the electricity demands due to heating, cooling, lighting, fans and equipment are reported, together with the produced PV panels' electricity and the net electricity demands for both the RS (E_{RS}) and the DSF-STPV ($E_{DSF-STPV}$) configurations. The table also includes the percentage energy difference (ΔE) for each energy use. By comparing E_{RS} with $E_{DSF-STPV}$, it is worth noting that although the solar radiation is greatly exploited in both weather zones, i.e. Montreal and Naples, in Naples, the investigated system allows reaching the NZEB goal (related to the adjacent thermal zones only), showing a surplus of electricity (about 357kWh/y, net demand). Differently, in Montreal due to the severe winter conditions (i.e. very high heating demands), the DSF-STPV is not able to completely balance the overall electricity demands of the adjacent zones; however, the overall electricity final demand, $E_{el,TOT}$, is reduced up to 79%.

Table 5-4Electrical performance of RS and DSF-STPV configurations

	Naples			Montreal		
	E_{RS} (kWh/y)	$E_{DSF-STPV}$ (kWh/y)	ΔE (%)	E_{RS} (kWh/y)	$E_{DSF-STPV}$ (kWh/y)	ΔE (%)
Heating	88.0	66.1	28.5	703.6	694.1	1.4
Cooling	158.8	137.7	13.3	95.0	90.0	5.2
Lighting	104.8	105.4	-0.5	111.3	111.6	-0.3
Fan_{DSF}(x100)	-	7.9	-	-	6.3	-
Equipment	420.8	420.8	0.0	420.8	420.8	0.0
Total Demand	774.8	760.9	1.8	1326.1	1316.1	0.8
PV production	-	1118.1	-	-	1094.0	-
Net demand	774.8	-357.2	146.1	1096.3	222.1	79.7

5.4. Conclusions

A numerical model of a Double Skin Façade integrating Photovoltaic (DSF-STPV) was developed based on energy balance equations. This model is validated with the outdoor experimental data collected and are described in Chapter 3.

The model can simulate opaque or semi-transparent photovoltaics and perform a parametric analysis changing the design parameters of the building and the DSF-STPV: the location of the building, the orientation of the DSF-STPV, the dimensions of the adjacent to the DSF-STPV room, the cavity width, and the physical characteristics of the skins. It is seen that if an appropriate study

is implemented, the DSF-STPV can utilize the energy production by the STPV to preheat the building, using solar energy and minimize the energy consumption during peak hours.

A preliminary analysis was held comparing the climates of Naples (Italy, Mediterranean temperate climate) and Montreal (Canada, humid continental climate with very cold and snowy winter). Although the solar radiation is greatly exploited in both weather zones, for Naples, the investigated system allows reaching the NZEB goal, while for Montreal, due to the severe winter conditions, the overall electricity final demand is reduced up to 79%.

Chapter 6

Parametric Analysis for different climates

Parts of this chapter are presented in the paper "Design Methodology and Parametric Analysis for different climates on Double Skin Façades integrating Semi-Transparent Photovoltaics" that is submitted at the Journal Science and Technology for the Built Environment.

A design methodology is presented for different configurations and operation of a ventilated Double Skin Façade integrating Semi-Transparent Photovoltaics (DSF-STPV). A simulation model is utilized to assess the air temperature within the DSF-STPV and the adjacent zone to the DSF-STPV, along with the energy production by the STPV and the building energy consumption. A parametric analysis is carried out to determine the strategies that increase the net-balance of a DSF-STPV system. The ventilated DSF can supply warmer air to the heat pump based mechanical system of the building and increase its Coefficient of Performance (COP), during the winter months or release it to the exterior in the summer months. A comprehensive analysis for a three-story office building in sixteen different climate zones is performed. The simulations are carried out for two insulation cases, nine different DSF-STPV cavity widths, five different velocity set-points and eleven operating strategies. The numerical results show that, for most cases, cavity widths between 0.50m (1.63ft) or 0.60m (1.90ft) width have similar behaviour. In addition, the impact that the incident solar radiation and wind velocity have on the operation of the cavity and the choice to mechanical ventilation, natural ventilation or closed cavity operation, is highlighted.

6.1. Introduction

Energy-related CO_2 emissions from buildings are rising continuously. Buildings account for 39 % of the total energy-related CO_2 emissions, while the construction materials industry , particularly for steel, cement and glass, accounts for another 11 % of the energy-related CO_2 emissions (Figure 6-1) (IEA 2019). The building sector has the highest electricity consumption (Argonne et al., 2017; European Comission 2019), forcing an increase in the energy efficiency investment in buildings, appliances and the increased demand for heating and cooling results in an increased demand for HVAC applications (IEA 2020). The additional expenditure on products and services that deliver energy efficiency in a building has increased, for both residential and non-residential buildings, and the incremental energy efficiency investment is devoted mainly in improving building envelopes and HVAC, aiming at reducing space heating and cooling (Figure 6-1) (IEA 2018).

A technology that could play a role in improving building envelopes and assisting the HVAC system in buildings is the Double Skin Façade (DSF) integrating Semi-Transparent Photovoltaics (STPV). The DSF-STPV consists of STPC glass and an interior skin that is usually made from an Insulating Glazing Unit (IGU). These two layers are separated by an air cavity that acts as a buffer zone around the building (Poirazis 2005). The vertically building integrated PV panels (BIPV) can significantly increase the total area of the building which can generate electricity, especially in the case of high rise buildings, controlling at the same time the amount of the solar gains that can be introduced into the building (Z. Ioannidis et al. 2017; Kapsis and Athienitis 2015b). In Figure 6-2, a schematic of a DSF-STPV and a basic thermal network of a DSF-STPV is shown.

A DSF integrating STPV can generate electricity through the STPV but can also recover heat both from the STPV and from the building itself via the flowing air, which would otherwise be dissipated to the exterior environment. The recovered, preheated air from the cavity can then be either introduced directly into the building or into the HVAC system to enhance its energy performance. The temperature of the preheated air depends on many variables such as the weather conditions (incident solar radiation, wind speed, ambient temperature), the type of ventilation

(natural or mechanical ventilation), the strategies following the operation of the DSF (i.e. closed during the night etc.), the velocity of the mechanically ventilated cavity, the transmittance of the STPV, the width of the cavity and the total building height (number of floors) that the DSF runs along.

Figure 6-1 (Left) Global share of buildings and construction final emissions for 2018, showing 39% of process-related emissions to be accounted for buildings and construction (IEA 2019). (Right) Buildings incremental investment by sector and end-use for 2015-2017 (IEA 2018).

Figure 6-2 (Left) A schematic of a DSF-STPV and (Right) A thermal network representation of a DSF, showing the temperature nodes, the flow, and the incident and transmitted solar radiation.

The complexity of system increases considering the fact that the active ventilation of the DSF can increase the heat extraction rate from the building and thus affect the heat exchange with the zone adjacent to the DSF-STPV. A DSF, can help regulate the temperature of the envelope components that exchange radiation with the occupants, if optimally designed and operated in terms of geometry, airflow within the cavity, STPV transparency etc. This may allow the occupants to operate closer to the window area while maintaining their thermal comfort, increasing the production area of the building.

6.2. Modelling

In this thesis, a DSF integrating STPV (DSF-STPV) is modelled based on a transient, finite difference mathematical thermal network (Figure 7-1). The numerical model for the assessment of the energy performance of a multi-story DSF-STPV has been implemented in MatLab (Mathworks) and is capable of performing parametric analyses for different variable parameters such as: site properties (location orientation), design parameters (number of floors, interior skin design), geometric parameters (floor height, DSF dimensions, room dimensions), optical properties (STPV transmittance, PV efficiency, etc), thermal properties (emissivity, SHGC insulation, etc), flow properties (Reynolds number, velocity set point) and operating strategies of the DSF-STPV (Ioannidis 2016; Ioannidis et al. 2017). In addition, the model evaluates the COP of air source heat-pumps (HP) as a function of the source air temperature.

The simulation model is based on a lumped parameter thermal network approach and takes into consideration all of the heat transfer mechanisms that happen within the cavity of the DSF-STPV. A set of explicit finite difference equations is obtained for each node of the thermal network. The multi-story building on which the DSF-STPV is integrated on is also divided in thermal zones, equal to the number of the floors. A more detailed description of the model is provided in previous publications of the authors (Ioannidis 2016; Ioannidis et al. 2017).

6.2.1. Modelling assumptions

In the presented DSF-STPV model a series of assumption have been taken into consideration. The efficiency of the integrated STPV is assumed to be 20 % under standard testing conditions and varies linearly with the temperature of the PV cells (Florschuetz 1976). In addition, in order to simulate the transparency of the STPV, the outermost skin of the DSF is simulated as having opaque and transparent strips (Z. Ioannidis et al. 2017). The PV cells are represented by the opaque strips, and glass by the transparent. The transparent strips have a transmittance of (0.9) under normal incident radiation. The total transparency of the STPV layer is set to be 50 %. The shading of the opaque PV cells to the interior layer of the DSF-STPV affects the energy balance of the cavity and must be taken into consideration while modelling a DSF-STPV system and the shading effect is expected to vary considerably both diurnally and seasonally due to the sun position.

A simple daylight modelling is used to assess the illuminance levels on the work-plane and when daylight is not enough to meet 300 lx, dimmable LED lighting is assumed that will provides additional light to reach the required illuminance on the work-plane. Blinds are assumed to be manually operated by the owners to avoid glare.

A reference office, as described in (Reinhart, Jakubiec, and Ibarra, n.d.), was taken into account; with dimensions 3.2 m height (10.5 ft), 3.6 m width (11.8 ft) and 8.2 m length (26.9 ft), while the plug load factor is assumed 3.55 W/m^2 for a 12.5 m^2 (134.5 ft^2) workstation with all occupants assumed to use (laptops?) and one printer assigned every ten occupants (Wilkins and Hosni, 2011). The schedule for heating or cooling of the zone is presented in Figure 6-3 starting to heat or cool the building at 7.00 am till 6.00 pm keeping the temperature between 20 °C (69.8 F) and 24 °C (75.2 F). Prior to or after this time, a heating or cooling set-back is applied at 18 °C (64.4 F) or 28 °C (82.4 F) for heating and cooling respectively.
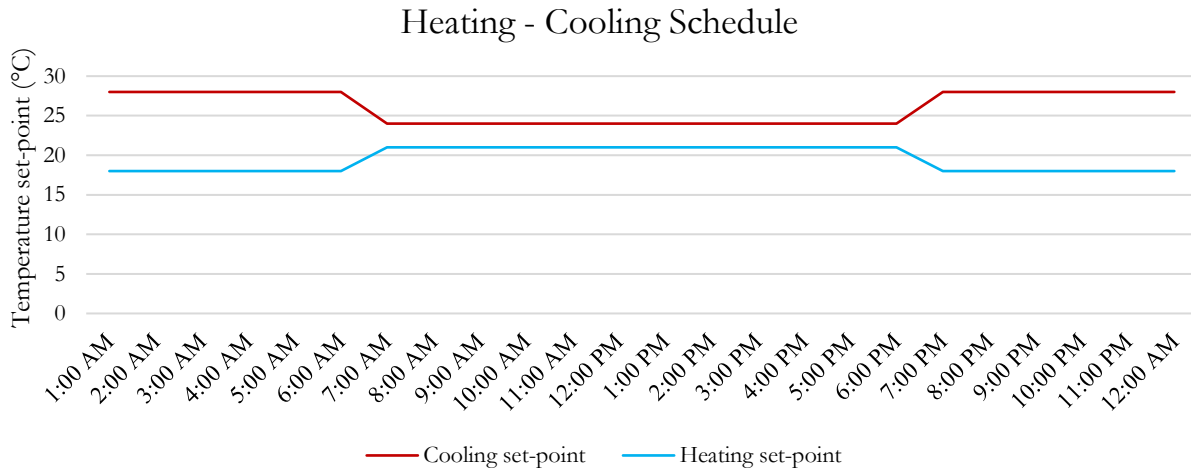
Figure 6-3 Schedule for heating or cooling of the zone, starting to heat or cool the building at 7.00 am till 6.00 pm

Wind-driven turbulent forced convection is assumed around the building and the convective heat transfer coefficient correlations are function of the wind velocity, the wind direction and the surroundings of the concerned area (Vasan and Stathopoulos 2014). The exterior convective heat transfer coefficients (h_{out}) are calculated based on the correlation developed by Sharples and Charlesworth (1998) $h_{c,out}= 11.9 + 2.2 \cdot V_{wind}$, where V_{wind} is the wind velocity in S.I..

The orifice equation is used for the cavity air flow. employing a discharge coefficient of $C_d = 0.62$ while the pressure coefficients for the wind-induced flow were determined experimentally by Lou et al. (2012) and are used to calculate the difference between the pressure coefficients at the exterior and the interior skin of the DSF-STPV. Because of the DSF-STPV cavity size and smoothness (glass walls), the pressure drop along the cavity was found to be small (less than 5 Pa)

For the calculation of the radiative heat exchange in the DSF view factors are used (Z. Ioannidis et al. 2017). The discretization of the cavity into 10 control volumes, creates 10 surfaces on each side of the DSF and the view factors between them are calculated. The four remaining sides of the DSF are assumed to be at the average temperature of the air within the cavity. More details of how this is modelled can be found (Z. Ioannidis et al. 2017).

6.2.2. Energy balance and convective heat transfer coefficients calculation

The Nu correlations used in this study are presented in detail in (Zisis Ioannidis et al. 2020) and

are developed by the authors with different Nusselt number correlations for the STPV side (Nu_{STPV}) and for the IGU side (Nu_{IGU}), as a function of the weather conditions ($I_{incident}$, $T_{ambient}$, $h_{c,out}$) the STPV parameters (η_{STPV}, τ_{STPV}) and the the flow within the cavity (Re) in S.I..

$$Nu_{STPV} = 0.2852 \cdot \frac{h_{c,out} \cdot |T_{ambient} - T_{room}|}{I_{incident} + 300(W/m^2)} \cdot Re \cdot \eta_{STPV} \cdot (1 - 0.339\,\tau_{STPV}) + 47.71 \qquad (6\text{-}1)$$

$$Nu_{IGU} = 0.1105 \cdot \frac{U_{gl} \cdot |T_{ambient} - T_{room}|}{I_{incident} + 300(W/m^2)} \cdot Re \cdot \tau_{STPV} + 55.19 \qquad (6\text{-}2)$$

6.2.3. Model validation

For the validation of the model an outdoor test-room with a custom-built DSF-STPV module was created in Montreal, Canada (45° 30' N / 73° 35' W). The details of the model validation can be found in a previous study published by the authors (Zisis Ioannidis et al. 2020). For the experimental validation, the ambient temperature ranges between -5 °C (23 F) and 30 °C (86 F), while the Reynolds number ranges between 10,000 and 26,000 and the incident solar radiation between 250 W/m² and 1200 W/m², values that are similar to the values used in this study. The validation step has intervals of 15 minutes, while the interval in this study is 1 hour.

6.3. Case Studies

A double skin façade integrating semi-transparent photovoltaics (DSF-STPV), is simulated for a 3-story south-facing DSF system located in sixteen different locations. The locations selected represent ASHRAE climate zones as shown in Table 6-1. The eight climate regions are based on the climate designations used by the IECC and ASHRAE and depend on heating degree days, average temperatures, and precipitation. The map depicted in Figure 6-4 provides a simplified and consistent approach to define climate for implementation of building codes. The United States are divided into climate zones based on their temperatures, and if applicable, further divided into sub-categories based on their moisture regimes (A to C), forming in this way a combination of five sub-categories: Hot-humid, hot-dry/mixed dry, mixed humid, marine, cold/very cold, and subarctic (Baechler et al. 2015).

Table 6-1 Cities simulated representing the climate zones by ASHRAE

1A	Miami, Florida (hot, humid)	4B	Albuquerque, New Mexico (mild, dry)
2A	Houston, Texas (hot, humid)	4C	Seattle, Washington (marine)
2B	Phoenix, Arizona (hot, dry)	5A	Chicago, Illinois (cold, humid)
3A	Atlanta, Georgia (hot, humid)	5B	Denver, Colorado (cold, dry)
3B-CA	Los Angeles, California (hot dry)	6A	Minneapolis, Minnesota (cold, humid)
3B-other	Las Vegas, Nevada (hot, dry)	6B	Helena, Montana (cold, dry)
3C	San Francisco, California (marine)	7	Duluth, Minnesota (very cold)
4A	Baltimore, Maryland (mild, humid)	8	Fairbanks, Alaska (extreme cold)
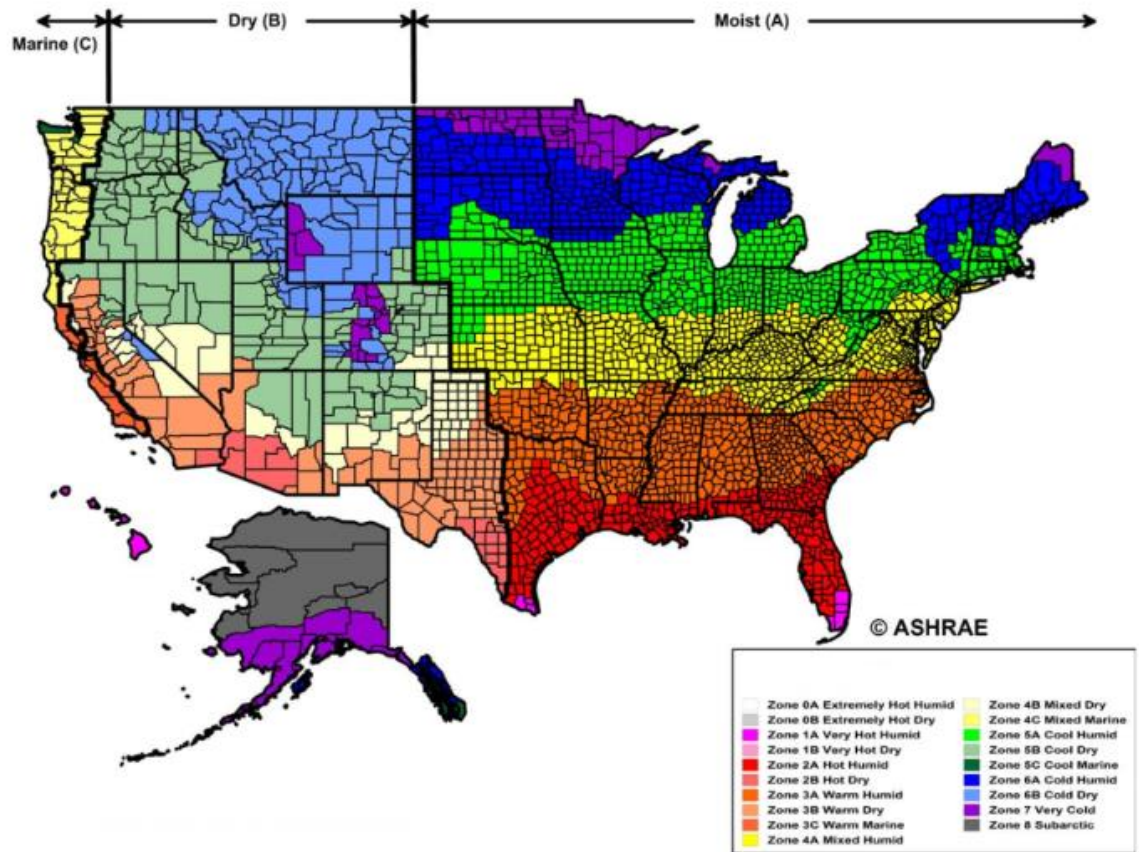
Figure 6-4 Climate Zones for the United States as presented in ASHRAE standard 169-2013 (Crawley et al. 2020)

For the sixteen locations presented in Table 6-1 (ASHRAE 2019) a DSF-STPV is simulated having a height of 3.2 m (10.5 ft) per floor and consisting of 5 rows of PV cells (0.32 m height each / 1.05 ft) and 5 rows of glass. For the insulation of adjacent to the DSF zone, two cases are simulated for every city: the baseline simulation and the advanced simulation according to the values in Table 6-2 (Thornton et al. 2010). The basic insulation case represents a behaviour of a DSF-STPV applied on an old building that is retrofitted without upgrading its insulation, and the advanced insulation case represents the insulation of a newly built building that is constructed with a DSF.

Table 6-2 Insulation requirements for above grade Steel framed walls Fenestrations U-factor Btu/hft²F (W/m²K)

	Steel Framed Wall		Fenestration	
	Baseline	Advanced	Baseline	Advanced
1	0.124 (0.705)	0.064 (0.365)	1.08 (6.13)	0.51 (2.89)
2	0.124 (0.705)	0.064 (0.365)	1.08 (6.13)	0.51 (2.89)
3A, 3B	0.124 (0.705)	0.064 (0.365)	0.51 (2.89)	0.51 (2.89)
3C	0.124 (0.705)	0.064 (0.365)	0.94 (5.33)	0.51 (2.89)
4	0.124 (0.705)	0.064 (0.365)	0.55 (3.12)	0.44 (2.50)
5	0.084 (0.479)	0.042 (0.240)	0.55 (3.12)	0.44 (2.50)
6	0.084 (0.479)	0.037 (0.212)	0.55 (3.12)	0.42 (2.38)
7	0.064 (0.365)	0.037 (0.212)	0.55 (3.12)	0.31 (1.76)
8	0.064 (0.365)	0.037 (0.212)	0.48 (2.72)	0.31 (1.76)

6.3.1. Simulated strategies

Twelve different strategies are simulated changing the operation of the DSF-STPV. This consists of the operation of the fans and whether the DSF-STPV is ventilated or not, in conjunction with temperature differences between the cavity temperature, the ambient temperature and the zone temperature. For strategies 1 to 3 the DSF-STPV keeps the same mode all day and night; Mechanical Ventilation, Natural Ventilation and Closed cavity respectively. Strategies 4, 5 and 6 change the ventilation mode depending on whether there is incident solar radiation on the façade (greater or lower than 200W/m²), while for the rest of the strategies, a temperature difference is used to decide which is the appropriate operation of the DSF. In strategies 7 and 8 the temperature difference between the cavity of the DSF (Tca) and the adjacent room (Troom) is used to determine whether the DSF will be ventilated or will be closed. In strategy 9 the cavity is closed if the ambient temperature is lower than the minimum temperature set-point of the building zone (18 °C / 64.4 F). Additionally, if the ambient temperature is higher than the maximum temperature set-point (26°C / 78.8 F) then the fans turn on, at the velocity set-point of the zone. Strategy 10 works similarly, but in this case the temperature at the middle of the set-points is used (22 °C / 71.6 F) to decide if the DSF-STPV will be mechanically ventilated or closed. In strategy 11 the cavity is closed when the average temperature of the cavity is lower than the middle of the occupants' comfort level (22 °C/ 71.6 F), and mechanically ventilated otherwise or naturally ventilated if it is day and the average temperature of the cavity is greater than the middle of the occupants' comfort level (22 °C / 71.6 F). In strategy 12 the cavity is closed when the incident solar radiation is lower than 200 W/m² and the ambient temperature is lower than the room heating set-point (18 °C / 64.4 F) and is mechanically ventilated otherwise. A list of the strategies is shown in Table 6-3. In Figure 6-5 a schematic of the three story DSF-STPV with the adjacent zones is shown. The temperature nodes taken into consideration for the strategies are also shown along with the discretization of the cavity into control volumes and the operation and the potential operation of the DSF. The strategies are selected in this way, to avoid overheating within the cavity, minimize the energy consumption by the fans, maximize the energy production by the STPV and consequently minimize the total energy consumption by the system.

Table 6-3 Simulated strategies for the operation of fan on the DSF-STPV

Strategy	Description
1	Always mechanically ventilated (no conditions)
2	Always naturally ventilated (no conditions)
3	Always closed (no conditions)
4	Mechanically ventilated when the incident solar radiation is greater than 200 W/m^2 and naturally ventilated otherwise
5	Mechanically ventilated when the incident solar radiation is greater than 200 W/m^2 and closed otherwise
6	Naturally ventilated when the incident solar radiation is greater than 200 W/m^2 and closed otherwise
7	Closed when the average temperature of the cavity is lower than the room temperature and mechanically ventilated otherwise
8	Closed when the average temperature of the cavity is lower than the room temperature and naturally ventilated otherwise
9	Closed when the average temperature of the cavity is lower than the room heating set-point (18 °C / 64.4 F), mechanically ventilated when it is greater than the room heating set-point (18 °C / 64.4 F)
10	Closed when the average temperature of the cavity is lower than the middle of the occupants' comfort level (22 °C / 71.6 F), and mechanically ventilated otherwise
11	Closed when the average temperature of the cavity is lower than the middle of the occupants' comfort level (22 °C / 71.6 F), and mechanically ventilated otherwise or naturally ventilated if it is day and the average temperature of the cavity is greater than the middle of the occupants' comfort level (22 °C / 71.6 F).
12	Closed when the incident solar radiation is lower than 200 W/m^2 and the ambient temperature is lower than the room heating set-point (18 °C / 64.4 F) and mechanically ventilated otherwise
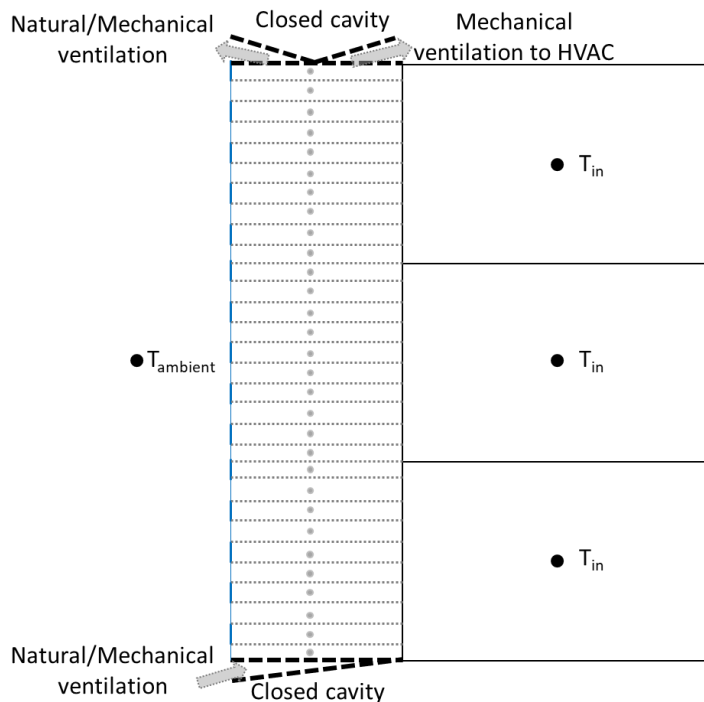
Figure 6-5 Schematic of the three story DSF-STPV with the adjacent zones, showing the discretization of the cavity into control volumes, the temperature nodes taken into consideration and the potential operation of the DSF.

6.4. Results and application of methodology

In

Appendix Table A 1, all the simulated cities can be found along with the respective heating degree days (HDD) and cooling degree days (CDD), and the mean values per month of the climate parameters used in the simulations: Total incident solar radiation (Itotal), incident direct solar radiation (Idir), incident diffuse solar radiation (Idif), average ambient dry bulb temperature (Tamb) and average wind velocity (Vwind). All values presented in this table are in S.I.

The Appendix Table A 2 is the most important table of this research. For each simulated location, all the simulated cavity widths are found on the left-hand side (0.15 m to 1.00 m / 0.50 ft to 3.28 ft). The top of the table indicates the simulated months (January -J- to December -D-) and for each month the two simulated insulation cases (basic -B1- and advanced -B2- insulation). This way, the information given in the cells of this table represent one location, one cavity width, one month and one insulation configuration. Starting from the top, each cell presents three values: the velocity set-point within the cavity, the simulated strategy and the energy net-balance of the DSF-STPV and adjacent zone system. The energy net-balance presented at the bottom of each cell, represents the greatest value of the above configurations and the corresponding velocity set-point and the strategy for which it was observed. An example is shown in Figure 6-6, for the first cell in Appendix Table A 2, for the month of January in Miami, for the basic insulation configuration (B1) and for the smallest cavity width simulated in this study (0.15 m / 0.50 ft), out of all strategies and air velocity set-points within the cavity simulated, the greatest energy balance of the system was found to be 0.89 W/m^2/month, achieved with strategy #9 with a 0.20m/s (0.66 ft/s) air cavity velocity set-point. At the right-hand side of Appendix Table A 2, the yearly summation of the months is presented. Positive net-balance means that the integrated STPV generate more electricity than it is consumed in the adjacent zone, while negative means the opposite.

The way Appendix Table A 2 is set-up can assist engineers and architects in the designing phase as well as the operation of a DSF-STPV. Frequent limitation on the selected cavity width, can be addressed by choosing the optimal configuration of such system (mechanical operation), while the cases of the addition of a DSF-STPV on an old envelope or the addition to a newly built envelope is covered by the basic or advanced insulation cases (B1 or B2).
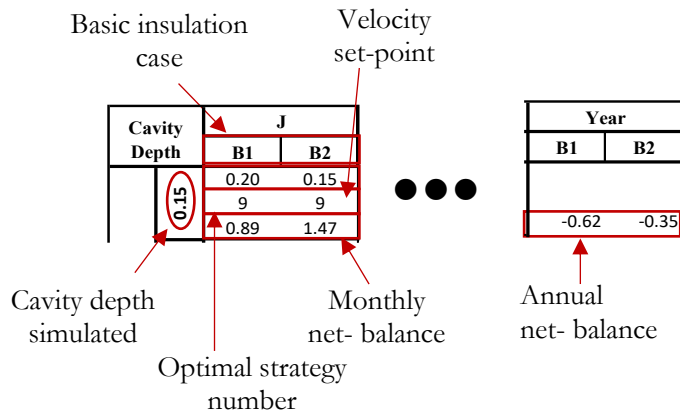
Figure 6-6 Explanation of the values presented in Appendix Table A 2

1A, Miami, Florida (hot, humid)

Miami (Florida) represents the 1A ASHRAE climate zone, with a hot and humid climate, 200 heating degree days and 4198 cooling degree days. A differentiation in the preferred strategies appears at a cavity depth of 0.60 m (1.97 ft). From 0.15 m to 0.50 m depth (0.5ft to 1.64 ft), the preferred strategy suggests that the cavity should be mechanically ventilated almost all year round. Most prevalent is the strategy where the cavity is mechanically ventilated if the cavity temperature is greater than 18 °C (64.4 F) and closed otherwise (strategy #9). From November till January, the DSF-STPV follows the same pattern, with lower velocity set-points, while for the rest of the months, higher velocity set-points are preferred. Due to the mild winter of Miami, with average ambient temperatures around 20 °C (68 F) and average total incident solar radiation greater than 140 W/m², the heating load of the zone is minimal and the preheated air within the DSF doesn't need to be introduced into the HVAC. The cavity though, needs to be ventilated to cool down the integrated STPV and increase their efficiency. Similarly, during the summer months, the cavity needs to be cooled down and higher cavity velocities are preferred but, when the average temperature of the cavity falls below 18 °C (64.4 F) then the fan does not need to operate and consume electricity. For wider cavities (0.80 m and 1.00 m / 2.62 ft and 3.28 ft), the DSF-STPV operates better if the cavity is closed throughout the year, as the electricity needed to drive air in such big cavity would increaser the consumption of electricity by the DSF-STPV system. The operation of the DSF-STPV is optimal in this way as the total solar gains are lower during the summer, as the sun angle is high, and the building zone is shaded by the STPV. A small differentiation appears in the months of February and March between the basic and the advanced insulation, as the basic insulation case requires higher velocity set points than the advanced insulation case. This difference is due to the increased need for preheated air resulting from the greater heat loss of the building. Similarly, for the month of May, the opposite phenomenon appears as the zone is better insulated and the cavity can be ventilated with greater velocities without extracting coolth from the zone.

Looking at the annual performance of such system, it seems that for the basic insulation case, wider

and closed cavities throughout the year are preferred, or mechanically ventilated cavities of 0.40 m (1.3 ft) wide, if the cavity temperature is greater than 18 °C (64.4 F) and closed otherwise (strategy #9), presenting different velocity set-points, depending on the season. On the other hand, there are not significant differences in the net energy balance between the cases with advanced insulation. It is seen that the DSF-STPV system is not net zero for this configuration. The difference in the energy consumption between the basic and the advanced insulation case can be more than 40%. This difference is minimized for wider cavities which perform better when it is closed.

6.5. General results and trends

Certain general trends and results can be identified from this analysis. It is seen that for the specific archetype of DSF-STPV analysed in this study, the DSF cavity can be separated into two main cavity-width regions: narrower and wider than 0.50 (1.64 ft) or 0.60 m (1.97 ft). The DSF is always in balance with the weather conditions and the indoor zone, and for this reason, different strategies are optimal for different months and different cavity widths. In addition, it is seen that as the incident solar radiation decreases the need for mechanical ventilation decreases, for both winter and summer.

For hot climates, DSF-STPV with narrower cavities need to be mechanically ventilated to operate optimally, with higher velocity set-points during the summer and lower during the winter. For hot climates, DSF-STPV with wider cavities perform better when either closed or naturally ventilated, depending also on the wind velocity of the area. Different strategies that include mechanical ventilation are preferred, showing that the temperature difference between the average cavity temperature and the occupants' comfort level (22 °C / 71.6 F), is a better indicator for the selection of the operation of the DSF (Strategy #10). Similarly, great indicator about the optimal operation of the DSF is the incident solar radiation (Strategy #5).

For mild and cold climates, DSF-STPV with narrower cavities still need to be mechanically ventilated to operate optimally, with different strategies being selected. The temperature difference between the average cavity temperature and the occupants' comfort level (22 °C / 71.6 F), Strategy #10, or the difference between the average cavity temperature and the adjacent zone temperature (Strategy #7) are the most common strategies. For wider cavities, mechanical ventilation (strategy #1) is preferred during the winter months, with velocity set-points that depend on weather conditions, while during the summer months, natural ventilation is preferred, either when there is incident solar radiation or all the time (Strategy #6 or Strategy #2).

For colder and extreme cold climates, the DSF operates optimally primarily when closed. For wider cavities, natural ventilation may be preferred, especially during the summer months (strategy #2 and strategy #6), while there are few cases where mechanical ventilation is preferred with low-velocity set-points.

In this analysis there are some limitations such as the assumed south orientation of the building and the three-story height of the façade. Another limitation is the semi-transparent PV technology simulated, that is based on crystalline silicon, while there are other newly developed technologies of STPV. Lastly, as a future work an analysis on different transparencies of both the STPV and

the shading blinds, as well as automated blinds operation could provide an added value to this research.

6.6. Conclusion

A design tool has been developed that is able to perform parametric analyses on DSF integrating semi-transparent PV for different locations and parameters that are listed below. In this study, a design methodology of a DSF integrating semi-transparent PV is presented (DSF-STPV). A parametric analysis is held for:

- Sixteen (16) different ASHRAE climate zones,
- Two (2) insulation cases for every climate location: the baseline and the advanced,
- Nine (9) different cavity widths,
- Nine (9) different cavity velocity set-points and
- Twelve (12) different strategies, changing the operation of the DSF-STPV.

The complexity of such system is addressed, as the DSF interact both with the ambient conditions and the building zone, can generate electricity from the STPV, heat from the cavity and at the same time introduce heat into the HVAC system. In addition, flow within the cavity might extract heat from the building that would be lost to the outside, but it can also warm up the building, if the exterior temperature is higher than the one of the building zone.

For each ASHRAE climate zone an analysis is presented, and a table is generated showing the simulated months (January to December) and for each month the two simulated insulation cases (basic and advanced insulation) along with all the values of different cavity widths. In addition, the energy net-balance value of the above configurations is presented. The table is set-up to assists engineers and architects in the designing phase as well as the operation of a DSF-STPV.

The numerical results show that, for most cases, cavity widths less or greater than 0.50 m (1.63 ft) 0.60 m (1.97 ft) width have similar behaviour. In addition, it is seen that as the incident solar radiation decreases the need for mechanical ventilation decreases, for both winter and summer.

As it is presented earlier, the climate locations are separated into three main categorize based on their behaviour, the hot and mild, the cold, and the colder and extreme cold locations. The locations under each category present similar patterns and strategies to achieve minimal energy consumption by the zone and increased energy production by the DSF-STPV.

Chapter 7

Electrical storage and heat pumps to reduce peak demand

Parts of this chapter are presented in the paper:

Z. Ioannidis, et al. 2020. Mechanically Ventilated Double Skin Façade Integrating Semi-Transparent Photovoltaics, Implementing Thermal Storage for Grid Interaction. 2020 ASHRAE Virtual Conference.

Semi-Transparent Photovoltaics (STPV) can be integrated on Double Skin Facades (DSF) to enhance the electrical and thermal performance of a building. In a mechanically ventilated DSF, the heat extracted from the DSF can be used to increase the Coefficient of Performance (COP) of a heat pump based mechanical system, or it can be introduced directly to the building. In addition, the STPV integrated on the outermost layer of the DSF, can control the solar gains, may allow controlled levels of the daylight into the zone and creates a microclimate around the building. In the present study we investigate the mismatch between the electricity production by the STPV and the electricity needed for heating and lighting by the adjacent building zones and develop ways of reducing this mismatch. A DSF-STPV combination, coupled with battery storage within the building, is considered in order to shift the peak demand of the building and provide better matching of generation and loads. Because STPV is integrated in the DSF, the heating demand during the day decreases as the building receives solar heat gains and at the same time produces electricity. This electricity produced by the STPV can be stored in a battery and later be used at the grid peak hours to reduce the peak demand by operating the heat pump. The preheated air, that is flowing within the cavity of the DSF-STPV, assists an air sourced heat pump to increase its COP and the heat produced is used to keep the building warm during the grid peak hours when the set point is reduced. With the use of such a predictive heating strategy, the peak demand of the building can coincide with the peak of the solar electricity production resulting in more than 80% reduction in the electricity consumption during the peak demand hours of the grid.

7.1. Introduction

In both the US and the European Union, the building sector has the highest electricity consumption among all the other sectors (Argonne et al., 2017; European Comission 2019). Buildings consume more than 55% of the total electricity consumption in Canada, while Quebec is the province with the highest electricity consumption among other provinces, being responsible for 35% of the total electrical consumption (NRCAN 2019). To reduce the power demand during winter peak times, Hydro-Quebec has initiated a demand response program and a dynamic electricity pricing (Hydro Quebec 2019).

The double skin façade (DSF) consists of an exterior and an interior skin that are separated by an air cavity that creates a buffer space around the building (Poirazis 2005). Photovoltaic panels can be integrated in the exterior skin of the DSF, and increase the area of the building which can generate electricity (Ioannidis et al. 2017). Figure 7-1 depicts a schematic of a DSF integrating STPV (DSF-STPV) and its thermal network. The STPV is integrated in the exterior layer of the DSF, while the interior layer consists of an insulating glazing unit (IGU). STPV, allow light to pass through and generate electricity at the same time, increasing the energy performance of the building (Kapsis and Athienitis 2015b).

A mechanically ventilated DSF, can take advantage of the preheated air from the cavity and introduce it into the building or into the HVAC system to enhance its energy performance. A DSF can help regulate the temperature of the envelope components that exchange radiation with the occupants, allowing in this way the occupants to operate closer to the window area while maintaining their thermal comfort.
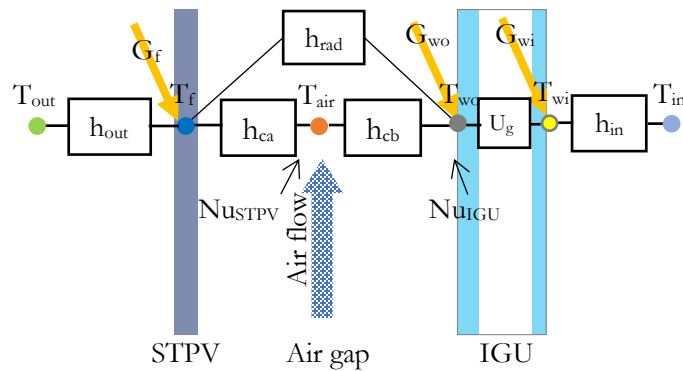
Figure 7-1 Schematic of the thermal network of a DSF showing the temperature nodes, the flow and the incident and transmitted solar radiation. For the calculation of the h_{ca} the Nu_{STPV} and for the h_{cb}, the Nu_{IGU} is used.

Electric utilities are considering the adoption of battery storage to shift the peak demand and avoid the upgrade of the electrical grid in order to accommodate the peak demand. In cold climates, such as the location considered in this study (Montreal, latitude 45 N), during the winter months, the peak demand hours are between 7am and 10am and 4pm and 8pm. For a typical winter day in the US, there is an increase of 20% and 10% in the electricity demand is the morning and the evening peak respectively (U.S. Energy Information Administration 2019).

The objective of this study is to shift the peak demand of the building out of the grid peak hours by utilizing electric storage and different heating strategies and reduce the electricity demand during the grid peak periods.

7.2. Modelling

In this study, a DSF integrating STPV (DSF-STPV) is modelled based on a transient finite difference mathematical thermal network (Figure 7-1). The model also implements an electric battery that gives the possibility to offset the peak demand and model the grid interaction with the building. The fan driven flow inside the cavity of the DSF-STPV is modelled and the wind and buoyancy effects that assist the flow are taken into consideration. The numerical model for the assessment of the energy performance of a multi-story DSF-STPV has been implemented in MatLab (Mathworks) and models the heat-pump (HP) based on available in the market models (Ioannidis 2016; Ioannidis et al. 2017).

7.2.1. DSF-STPV thermal and flow network

The simulation model is based on a lumped parameter thermal network approach and takes into consideration all of the heat transfer mechanisms that happen within the cavity of the DSF-STPV. A set of explicit finite difference equations are obtained for each node of the thermal network. The cavity of the DSF-STPV is discretized into 46 control volumes. The multi-story building on which the DSF-STPV is integrated on is also divided in thermal zones, equal to the number of the floors. A more detailed description of the model is provided in previous publications of the authors (Ioannidis 2016; Ioannidis et al. 2017). The flow of the air within the cavity is mechanically

assisted and the pressure drop due to the mechanical system is calculated by equation (7-1) where the used orifice equation employs a discharge coefficient of Cd = 0.62. The pressure drop due to natural effects (ΔPnat) is the summation of the stack and wind effects. The pressure difference due to stack effect is given by equation (7-2), while the pressure drop due to wind effect is given by equation (7-3). The pressure coefficients, determined experimentally by Lou et al. (2012) are used to calculate the difference between the pressure coefficients at the exterior and the interior skin of the DSF-STPV (ΔC_p).

$$\Delta P_{mech} = \left(\frac{V_{ca}A_{ca}}{C_d}\right)^2 - \Delta P_{nat} \qquad (7\text{-}1)$$

$$\Delta P_{th} = 0.5\rho_{air}gH_{ca}\left[\frac{T_{ca}-T_{out}}{T_{ca}}\right], \ T_{ca} - T_{out} \geq 0, \ \Delta P_{th} = 0.5\rho_{air}gH_{ca}\left[\frac{T_{ca}-T_{out}}{T_{out}}\right], T_{ca} - \\ T_{out} < 0 \qquad (7\text{-}2)$$

$$\Delta P_w = \Delta C_p 0.5\rho_{air}V_w^2 \qquad (7\text{-}3)$$

7.2.2. DSF-STPV flow coefficients

Local Nusselt number coefficients (Nu) are used in order to represent the convective heat transfer coefficients along the channel height. The Nu correlations developed by the authors are used and for the brevity of this study, the procedure followed for the development of the Nu correlations is briefly presented here and is presented in more details in another study. A set of energy balance equation is solved to calculate the convective heat transfer coefficient towards the side of the IGU (h$_{cb}$). Then, this calculated convective heat transfer coefficient towards the side of the IGU (h$_{cb}$) is used to calculate the convective heat transfer coefficient towards the side of the STPV (h$_{ca}$). These convective heat transfer coefficients are later used to calculate the Nu correlations. The authors developed different Nu correlations for the two boundary sides of the flow, the side towards the STPV (Nu$_{STPV}$) and the side towards the interior layer, which in most of the DSF cases are insulating glazing units (Nu$_{IGU}$), as it can be seen in Figure 7-1.

For the side of the cavity towards the STPV, the average Nu correlation was developed as a function of the wind heat transfer coefficient (hc,out), the Reynolds number, the efficiency of the STPV, the incident solar radiation and a factor that depends on the absorbed solar radiation by the glass section of the STPV (1 – 0.339 τ$_{STPV}$). Similarly, the Nu correlation for the interior side of the DSF-STPV, includes the thermal transmittance of the IGU (Uglazing), the Reynolds number and the overall solar transmittance of the STPV. In this way, the losses from the building to the DSF-STPV over the gains from incident solar radiation are multiplied by the transmittance of the STPV. Later, by using the definitions of Nusselt and Reynolds number, the local convective heat transfer coefficients were calculated.

In most wind-driven flows around buildings, turbulent forced convection is observed and the convective heat transfer coefficient correlations are function of the wind velocity, the wind direction and the surroundings of the concerned area (Vasan and Stathopoulos 2014). The exterior convective heat transfer coefficients (h$_{out}$) are calculated based on the correlation developed by

Sharples and Charlesworth (1998), where V_{wind} is the wind velocity.

$$Nu_{STPV} = 0.2852 \cdot \frac{h_{c,out} \cdot |T_{ambient} - T_{room}|}{I_{incident} + 300(W/m^2)} \cdot Re \cdot \eta_{STPV} \cdot (1 - 0.339\, \tau_{STPV}) + 47.71 \qquad (7\text{-}4)$$

$$Nu_{IGU} = 0.1105 \cdot \frac{U_{gl} \cdot |T_{ambient} - T_{room}|}{I_{incident} + 300(W/m^2)} \cdot Re \cdot \tau_{STPV} + 55.19 \qquad (7\text{-}5)$$

$$h_{c,out} = 11.9 + 2.2 \cdot V_{wind} \qquad (7\text{-}6)$$

7.2.3. STPV and battery modelling

To model the STPV integrated on a DSF, it is assumed that the PVs operate at the maximum power point condition in each moment and the STPV efficiency is assumed to be linearly dependent on the operating temperature of the PV cells, on the PV cell efficiency at standard test conditions (nSTC), on the PV temperature coefficient (βPV) and the PV cell temperature under standard test conditions (TSTC).

$$n_{PV} = n_{STC} \cdot [1 - \beta_{PV} \cdot (T_{PV} - T_{STC})] \qquad (7\text{-}7)$$

The STPV is modelled under the assumption that it consists of two different components: the opaque and the transparent one, with the opaque being the PV cells and the transparent being the glass between the PV cells of the STPV. In addition, the PV cells are arranged in strips thus, opaque and transparent strips are modelled.

The electric battery charging and discharging modes are modelled by implementing their characteristic curves of a Li-ion battery (Andwari et al. 2017). Its charging and discharging behaviour is modelled by means of an equivalent circuit by considering a scaled model associating the battery internal charge curve with the operating power(Tremblay et al 2007). Specifically, the behaviour of a battery cell is modelled with respect to the discharge/charge power and state of charge (by considering a constant current for both the charging and discharging modes).

7.2.4. Model validation

An outdoor test-room with a custom-built DSF-STPV module is installed in Montreal, Canada (45° 30' N / 73° 35' W). The STPV module has a packing factor (or covering factor – ratio of area covered by solar cells – i.e., opaque) of 63.4%. The cavity of the DSF-STPV is 17.5cm wide and 1.95m high. The insulating glazing unit that comprises the interior surface of the DSF has a hard low-emissivity coating and has a 13 mm wide air-gap that is filled with Argon. It has a SHGC of 0.624 and its U-value ranges between 1.64 W/m²K and 1.56 W/m²K for winter and summer conditions.

The STPV is the exterior layer of the DSF and integrates 48 monocrystalline cells with a nominal efficiency of 17.80% and the temperature is measured with thermocouples, mounted on the different layers of the DSF and in the air space along the z-axis direction at 15 equally distributed heights. The wind velocity and direction are measured at the weather station close to the test location and the data are averaged per 15 minutes. The experimental facility that is used for the

development of the Nu correlations, is also used for the validation of the model. For the experimental validation, the ambient temperature ranges between -5°C and 30°C. The Reynolds number ranges between 10,000 and 26,000 and the incident solar radiation between 250 W/m² and 1200 W/m². A validation is performed for different Reynolds numbers, ambient temperatures and incident solar radiation with time intervals of 15 minutes.

Using the Nu correlations presented in a previous section, a model validation is conducted for the temperatures of the air at the outlet of the DSF-STPV. The measured temperatures of the STPV and the IGU are used as boundary conditions and the measured airflow is used as the mass flow rate within the cavity to predict the outlet temperature of the DSF-STPV. The measured temperature of the air at the outlet of the DSF-STPV when compared with the predicted outlet temperature of the DSF-STPV presents a difference that does not exceed 1°C. This difference appears negligible for warmer ambient temperature conditions and lower incident solar radiation.

7.3. Case Studies

A double skin façade integrating semi-transparent photovoltaics (DSF-STPV), is simulated for a 3-story south facing DSF system located in Montreal, Canada. This case study falls under the 6th climate zone of ASHRAE (ASHRAE 2019). The DSF-STPV has a height of 3.28 m per floor and consists of 14 rows of PV cells (0.16 m height each) and 13 rows of glass (0.08 m height each). This results in a packing factor of 68% and an effective transparency of around 29%. The PV cell efficiency is assumed to be 20%. The DSF-STPV has a width of 3.6 m sideways, and the cavity gap is 0.4 m. Because of the size of the cavity of the DSF-STPV and the smoothness of the materials of the layers, which are glasses, the pressure drop inside the cavity is small. With less than 5 Pa pressure drop along the cavity, the impact on the total fan power will not be significant but is taken into consideration in the simulations. Each thermal zone has the same width with the DSF-STPV (3.6 m) and is 8.2 m deep, following the dimensions of a typical reference office (Reinhart et al. 2013). The interior side of the façade is a curtainwall and consists of an IGU with U-value equal to 2 W/m²K.

The DSF-STPV is coupled with an electrical storage and the battery that is selected for this case study has a capacity of 9.9 kWh (3.3 kWh per floor). The maximum charging power is 5 kW while the maximum and the minimum total capacity is set to 95% and 10% respectively. The DSF-STPV is also coupled with a heat pump that has a maximum capacity of 2.5 kW for each zone, meaning 7.5 kW for three floors. The heat pump performance data are provided by manufactures and are in accordance with the standard EN14511 and it includes defrost cycles losses. Each indoor space is assumed to have a plug load factor of 3.55 W/m², and each office/workstation is 12.5 m², while all the occupants use notebooks and one printer is assigned for every ten occupants (Sarfraz 2018).

7.3.1. Strategies

A series of strategies are adopted to reduce the electricity consumption for heating and to achieve the shift in the peak demand from the grid. The dampers that allow air to enter the DSF-STPV are set to open when the incident solar radiation is greater than 200 W/m². This threshold is selected to minimize the losses from the building and to enhance the heat recovery from the STPV. For the supply of the heat pump with preheated air by the DSF-STPV and not mix it with the colder

ambient air, the velocity set-point of the air flowing within the cavity of the DSF-STPV must be selected appropriately. The velocity set-point for the air flowing within the cavity was selected at 0.4 m/s.

To reduce the electricity consumption for heating, during the grid peak hours, the setpoint of the temperature of the thermal zone varies depending on the time. A new adjusted temperature schedule is introduced where the temperature set-point is at 22°C from 5 am to 7 am and at 26°C from 11 am to 5 pm with a temperature set-back at 18°C. The typical schedule for heating a commercial building has a set-point at 22°C from 7 am to 7 pm with a temperature set-back at 18°C. The aim of the new schedule is to consume electricity and preheat the building prior the peak in the grid and use the stored electricity in the battery for the grid peak hours. At the same time, the temperature set-point of the adjusted schedule is selected so that it does not create discomfort to the occupants.

7.4. Results and discussions

Figure 7-2 depicts, the ambient temperature, the incident solar radiation, the average temperature of the air within the cavity of the DSF-STPV and the temperature of the air at the outlet of the DSF-STPV. The time period investigated in this study (January 12th to 15th), presents a series of sunny and semi-overcast days, followed by an overcast day. The ambient temperature fluctuates between -30°C and -15°C. The temperature rise between the ambient temperature and the temperature at the outlet of the DSF-STPV reaches more than 10°C for the colder days and during the peak of the incident solar radiation, while the average temperature of the cavity is always 2.5°C warmer than the ambient air, creating in this way a buffer zone and decreasing the heating losses of the building. The incident solar radiation on the DSF-STPV reaches 800 W/m², for the sunny days, while for the overcast days, it barely reaches 200 W/m². The mechanical system that assists the flow within the DSF-STPV operates when the incident solar radiation is greater than 200 W/m².

In Figure 7-3 the interaction of the system with the grid is shown. The STPV electricity production, the total building consumption and the consumption of the electricity from the grid is depicted for the days chosen for this study. For the hours prior to the morning peak and after the evening peak period (before 7 am and after 8 pm) the consumption of the building coincides with the consumption of electricity by the grid. During the peak periods, the consumption of electricity by the grid is decreased and the battery is used to drive the heat pump. The heating demand during the grid peak hours is also decreased as the strategy to heat up the building prior the peak demand hours is followed. The battery is mostly discharged on the overcast day, while a full discharge cycle takes around three days. The temperature of the thermal zone increases before the grid peak demand hours and is let free to float during them. This pre-heating prior the grid peak hours can maintain the temperature of the zone above the set point for two to three hours. For the remaining grid peak hours, the stored electricity can run the heat pump to keep the zone over the set-back.
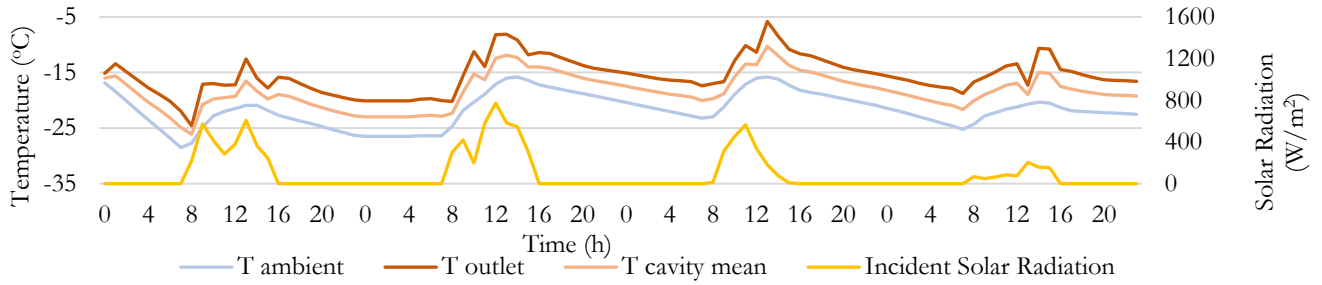
Figure 7-2 Three sunny and semi-overcast days are followed by an overcast day from January 12th to 15th. Ambient temperature (Tamb), incident solar radiation, average temperature of the air in the cavity (Tcavity mean) of the DSF-STPV and the temperature of the air at the outlet of the DSF-STPV (Toutlet) are presented.
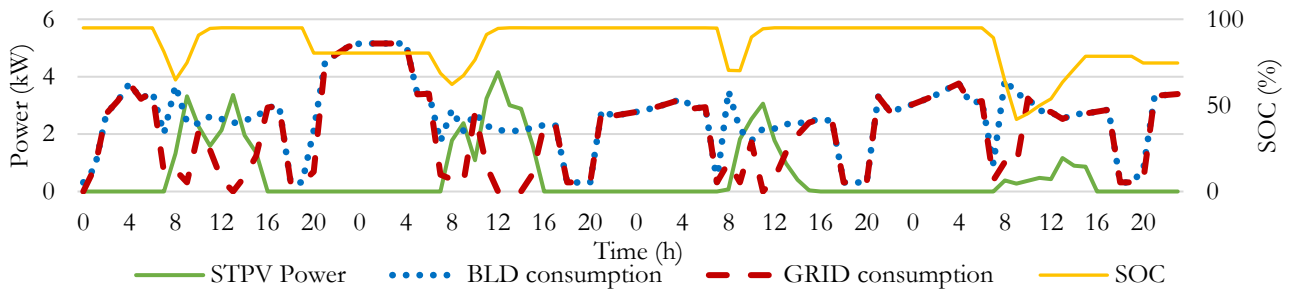
Figure 7-3 The power production by the STPV, the building electricity consumption (BLD consumption), the grid consumption (GRID consumption) and the state of charge of the battery (SOC) are depicted.
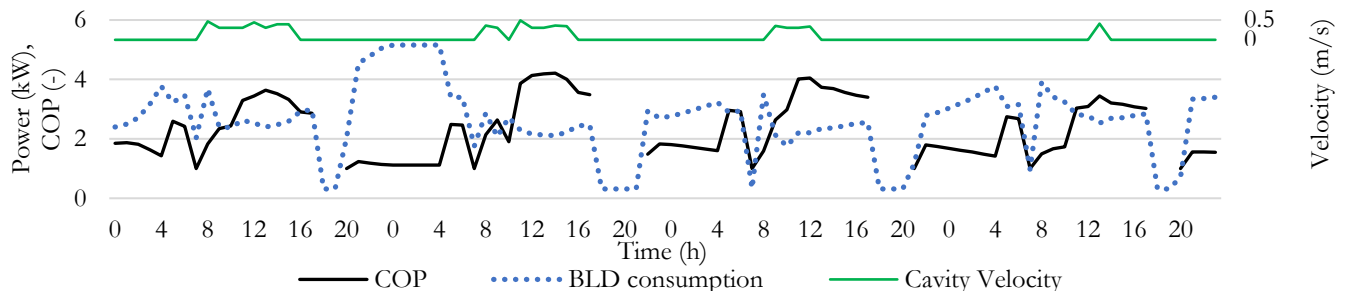
Figure 7-4 The coefficient of performance (COP) of the heat pump and the building consumption (BLD consumption) are depicted. The velocity of the air within the cavity of the DSF-STPV (Cavity Velocity) indicates the times when the heat pump is supplied with the pre-heated air from the cavity of the DSF.
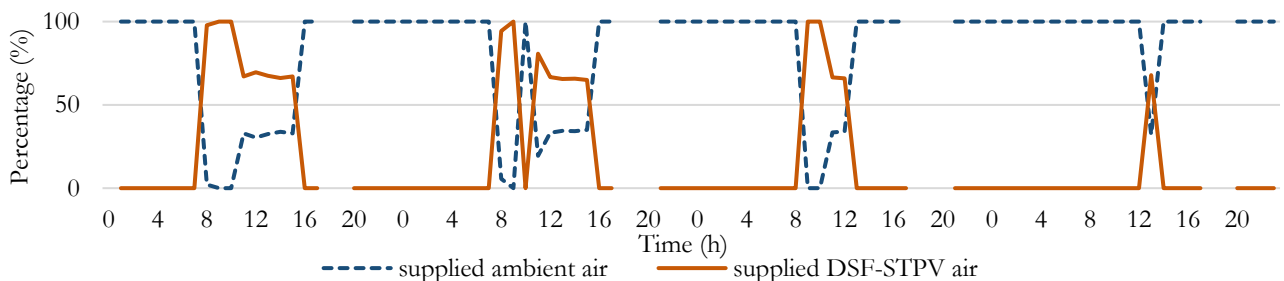
Figure 7-5 The percentage of the mixing of the supplied air with ambient and air from the DSF-STPV is depicted in the graph.

In Figure 7-4 the electricity consumption of the building and the coefficient of performance (COP)

113

of the heat pump is shown. The advantage that the DSF-STPV provides to the system by preheating the air that passes through the cavity can be seen in this figure as the increase of the COP at the time around noon is significant. The COP can reach values more the 3, thus the electricity consumption for heating decreases a lot, allowing at the same time the electricity produced by the STPV to recharge the battery. In Figure 7-4, the velocity of the air within the cavity is also plotted and signifies the moment of the time that the preheated air from the DSF-STPV is used to increase the COP of the HP.

This increase in the COP is due to the higher ambient temperature and to the increased temperature at the outlet of the DSF-STPV. The temperature of the air at the outlet of the DSF-STPV is mixed with ambient air prior supplying the heat pump. The selection of the velocity set-point within the cavity of the DSF-STPV is selected to decrease the mixing with the colder ambient air and therefore increase the COP. The percentage of the air supplied to the heat pump by the ambient air and the DSF-STPV is shown in Figure 7-5.The DSF-STPV can fully supply the heat pump for certain periods, while depending on the need and the available heat, the DSF-STPV can supply the heat pump with preheated air at percentages that exceed 65%. There is an increase that ranges from 4ºC to 10ºC between the ambient air, which would normally be used, and the supplied air that is preheated by the DSF-STPV depending on the incident solar radiation. During the night-time, the heat pump is supplied solely by the ambient air, because the DSF-STPV is closed and acts as a buffer zone.

7.4.1. Grid interaction

A comparison between a sunny day and the overcast day is shown in Table 7-1. In this table, the difference between these two schedules is presented with respect to the reduction of the peak demand, for the specific geometry simulated but also as a percentage difference between the two schedules. The savings in the electricity consumption during the grid peak demand hours ranges from 10% to 90%, with saving of more than 80% for many hours.

Table 7-1 Difference Between the Typical and the Adjusted Schedule for a Sunny and an Overcast Day.

	Morning Peak				Evening Peak				
Hour	7	8	9	10	16	17	18	19	20
Sunny day	-5.4kW	-2.5kW	-2.4kW	-0.5kW	-0.4kW	-0.5kW	-3.3kW	-3.4kW	-1.9kW
Overcast day	-4.1kW	-2.1kW	-2.0kW	0.4kW	-0.2kW	-0.3kW	-2.8kW	-2.9kW	-2.5kW
	Morning Peak				Evening Peak				
Hour	7	8	9	10	16	17	18	19	20
Sunny day	-89.1%	-76.9%	-88.5%	-20.6%	-12.2%	-13.4%	-91.3%	-91.6%	-47.6%
Overcast day	-91.2%	-66.8%	-68.2%	12.1%	-6.4%	-8.6%	-90.0%	-90.1%	-76.8%

7.5. Conclusion

A validated numerical model of a double skin façade integrating semi-transparent photovoltaics has been utilized to assess the impact on the grid of the coupling of such system with battery storage and a HP. A set of consecutive winter days, for the month of January have been

investigated. The set of days is simulated for a three-story commercial building located in Montreal, Canada which is in the 6th zone of the ASHRAE climatic zones.

The mismatch between the electricity production by the STPV and the electricity needed for heating and lighting by the building zones is investigated and an adjusted heating schedule has been proposed in order to reduce the heating demand of the building. To take full advantage of the pre-heated air that flows within the cavity of the DSF-STPV, the heating set-point during the solar peak hours is increased. At this time, the temperature of the air flowing within the cavity, which later is introduced to the heat pump, is highest and thus the COP of the heat pump is increased.

With the use of such a predictive heating strategy, the peak demand of the building can coincide with the peak of the electricity production resulting in substantial reduction in the electricity consumption by the grid during the peak hours of the grid. This reduction can reach more than 80% even for cold and overcast winter days.

Chapter 8
Conclusions and Future work

In this thesis, the novel technology of concept of the application of semi-transparent photovoltaics on Double Skin Facades is investigated (DSF-STPV). Double Skin Façades integrating Semi-Transparent photovoltaics (DSF-STPV) are some of the options of Building integrated (BIPV) that can combine the electricity and heat generation along with daylighting control for the building.

The objectives of this thesis is to investigate the state of the art on double skin facades (DSF) and insulating glazing units integrating semi-transparent photovoltaics and identify the important design parameters and outputs; identify the research needs in double skin façade and insulating glazing unit related to DSF-STPV adoption. Another objective is to design a STPV-DSF prototype and perform outdoor experiments for the DSF-STPV and assess the impact of weather variable on its performance, including wind effects, solar radiation, and ambient temperature. In addition, this thesis aims at the development of a numerical model of the DSF-STPV validated through the experiments and implement it into a software tool. The last objective is to identify the energy flexibility that such facades can provide in interacting with a smart grid.

The available literature on double skin facade (DSF) and insulating glazing unit (IGU) integrating semi-transparent photovoltaics was presented concluding that the concept of DSF-STPV needs further analysis as there are limited studies on this field. From the literature it was also shown that there are no experimental studies that include the electrical and thermal performance for mechanically ventilated DSFs integrating STPV. In addition, there is no literature on heat transfer coefficients within the cavity of DSF-STPV as well as the impact of the wind effects on the velocity of the air within the cavity.

To address these points a prototype exterior experiment was set-up at Concordia University (Montreal, Canada) with two virtually identical semi-transparent photovoltaics with a packing factor of 63.4%. The first STPV was used as the exterior layer of a DSF forming in this way a DSF-STPV and the second one is used as the exterior layer of an Insulating Glazing Unit forming an IGU-STPV.

This outdoor experimental test-room was used for the development of three Nusselt number correlations for the convective heat transfer of the flowing air in the cavity of a DSF-STPV, covering in this way the gap in the literature. The Nusselt number correlations were developed describing the convective heat transfer between the STPV surface and the air flowing in the DSF, the STPV cells and the flowing air and the inner layer of the DSF-STPV and the air flow. In addition, a new term of "heat recovery index (H)" that describes such systems was introduced in this thesis, presenting at the same time its differences with the typical term of "thermal efficiency", as the heat recovered by the building is an energy source to the system.

A validation of the developed Nusselt number correlations was performed, using the experimental data for the boundary conditions. It was shown that the difference between the predicted and the measured temperature at the outlet of the DSF-STPV does not exceed 2°C. In addition, the importance that the wind effects have on the energy balance of a building was highlighted. The thermal losses due to wind effects are calculated and it is reported that a DSF-STPV can reduce the exterior heat losses of the building by more than 20%. The difference between the new introduced term of "heat recovery index (H)" and the typical term of "thermal efficiency", can lead

up to 13% difference in the calculation of the heat recovery of such system. The total combined efficiency of the DSF-STPV, as calculated based on the conducted experiments can vary between 25% to 75%.

This outdoor experimental test-room was also used to perform a preliminary comparison between the DSF-STPV and the IGU-STPV. The electrical performance of the DSF-STPV, presented increased values between 3% and 9% depending on the ventilation strategy of the cavity of the DSF-STPV and the incident solar radiation. Even when the DSF-STPV is not ventilated and acts as a buffer zone, the electrical performance of the STPV panels is 3% to 4.5% greater than this of the IGU-STPV. Also, the average ΔT is more than 10°C and around 5°C for days with higher and lower incident solar radiation, respectively.

Following the experimental analysis and the experimental data collected, a numerical model of a DSF-STPV was developed and validated. The model can simulate opaque or semi-transparent photovoltaics integrated on the exterior layer of the double skin façade, their location on the exterior skin and their dimensions, as well as shading devices inside the cavity including the shading that they provide to the building. The model also allows the user to perform a parametric analysis changing the design parameters of the building and the DSF-STPV that he wants to simulate. The characteristics of the skins can also be determined, defining the height and the insulating values of the spandrel and the upper spandrel, their absorbtance and emissivity. The efficiency of the photovoltaics integrated on the exterior skin defined under standard test conditions can be determined by the use as well as their height and transmittance. The model is also able to determine the appropriate position of the photovoltaics on the exterior skin, in order to provide shading to the interior of the building. Also, this model can simulate battery storage and its effect on peak demand.

After its development, this design tool is used to perform a parametric analysis for sixteen (16) different ASHRAE climate zones, two (2) insulation cases for every climate location: the baseline and the advanced, nine (9) different cavity widths, nine (9) different cavity velocity set-points and twelve (12) different control strategies, changing the operation of the DSF-STPV.

For each of the sixteen (16) different ASHRAE climate zones an analysis was presented, and a table was generated showing the simulated months (January to December) and for each month the two simulated insulation cases (basic and advanced insulation) along with all the values of different cavity widths. In addition, the energy net-balance value of the above configurations is presented.

The numerical results show that, for most cases, cavity widths less or greater than 0.50 m - 0.60 m width have similar behaviour. In addition, it has been that as the incident solar radiation decreases the need for mechanical ventilation decreases, for both winter and summer. The climate locations are separated into three main categorise and the locations under each category present similar patterns and strategies to achieve minimal energy consumption by the zone and increased energy production by the DSF-STPV.

Also, this validated numerical model was used to assess the impact on the grid of the coupling of such system with battery storage and a heat-pump. A set of consecutive winter days, for the month

of January have been investigated. The mismatch between the electricity production by the STPV and the electricity needed for heating and lighting by the building zones was investigated and an adjusted heating schedule has been proposed in order to reduce the heating demand of the building. With the use of a predictive heating strategy, the peak demand of the building can coincide with the peak of the electricity production resulting in substantial reduction in the electricity consumption by the grid during the peak hours of the grid. This reduction can reach more than 80% even for cold and overcast winter days.

To summarize, this thesis identifies the gaps in the literature on studies for DSF-STPV and addresses them. An experimental facility was built to study heat transfer phenomena in such system and to validate a numerical model. This model was used to generate multi-parametric tables representing the optimal operation of a DSF-STPV for different location and climate zone and was also used to present the energy flexibility potential of such system.

8.1. List of published work

- Ioannidis, Z, ED Rounis, A Athienitis, T Stathopoulos. 2022. "Double Skin Façade Integrating Semi-Transparent Photovoltaics: An Analysis for Different Climates", ASHRAE Transactions, Vol. 128, pp., Pt. 2.

- Ioannidis, Z, ED Rounis, A Athienitis, T Stathopoulos. 2020. "Double Skin Façade Integrating Semi-Transparent Photovoltaics: Experimental Study on Forced Convection and Heat Recovery." Applied Energy 278 (March): 115647.

- Ioannidis, Z, ED Rounis, A Athienitis, T Stathopoulos. 2020. Mechanically Ventilated Double Skin Façade Integrating Semi-Transparent Photovoltaics, Implementing Thermal Storage for Grid Interaction. 2020 ASHRAE Virtual Conference.

- Ioannidis, Z, A Buonomano, ED Rounis, A Athienitis, T Stathopoulos. 2017. Comparison of the Electrical and Thermal Performance of Double Skin Façade and Insulating. PVSEC.2018 Brussels, Belgium. (award winning poster)

- Ioannidis, Z, A Buonomano, ED Rounis, A Athienitis, T Stathopoulos. 2017. Study on the Energy Performance of the Semi-Transparent PV Facades under Continental Climate. ISES.2017 Abu Dhabi. UAE.

- Ioannidis, Z, A Buonomano, A Athienitis, T Stathopoulos. 2017, "Modeling of double skin façades integrating photovoltaic panels and automated roller shades: Analysis of the thermal and electrical performance," Energy and Buildings, 154, 618–632.

  Contribution:
- Rounis, ED, Z Ioannidis, AM Sigounis, A Athienitis, T Stathopoulos. 2022. "A novel approach for the modelling of convective phenomena for building integrated photovoltaic thermal (BIPV/T) systems", Solar Energy, Volume 232, Pages 328-343.
  On the development of the methodology analyzing the convective heat transfer coefficient within the cavity of the BIPV/T

- Rounis, ED, Z Ioannidis, R Dumoulin, O. Kruglov, A. Athienitis, T. Stathopoulos. 2018. Design, development and simulation on performance of a building integrated

photovoltaic/thermal (BIPV/T) roof system. EuroSun 2018. Rapperswil, Switzerland. (award winning poster).
On the development of the BIPV/T design and its operation

- Rounis, ED, Z Ioannidis, R Dumoulin, O. Kruglov, A. Athienitis, T. Stathopoulos. 2017. Experimental investigation of thermal enhancements for a Building Integrated Photovoltaic/Thermal curtain wall ISES.2017 Abu Dhabi. UAE.
On the development of the BIPV/T design and its operation

- Rounis, ED, Z Ioannidis, O. Kruglov, A. Athienitis, T. Stathopoulos.. 2017. Experimental investigation and characterization of Building Integrated Photovoltaic/Thermal envelope system with thermal enhancements, for roof and curtain wall applications. PVSEC.2017 Amsterdam.
On the development of the BIPV/T design and its operation

<u>Submitted</u>
Z. Ioannidis et al. 2023. Design Methodology and Parametric Analysis for different climates on Double Skin Façades integrating Semi-Transparent Photovoltaics, Science and Technology for the Built Environment

8.2. Limitations and Future work

This study is limited by the STPV technology used (c-Si), that is the most common PV technology nowadays, and the flow within the cavity of the DSF that present Reynold numbers between 10,000 and 26,000 and velocities from 0.3 m/s to 1.2 m/s, that represent a typical flow within the cavity of a DSF. The experimental study presented in this study was performed in the span of a year in Montreal Canada and the location of the test-room make the experiment case specific, but the results are expected to be quite general for similar air speeds in the cavity that represent the main practical region of airflows of interest. The experimental results can be considered inconsistent for incident solar radiation that is lower than 300W/m^2 as the low incident solar would result in lower power output by the PV, and ambient temperature that ranges outside of the -5ºC and 30ºC range that the experiment was conducted.

In this analysis there are some limitations such as the assumed south orientation of the building and the three-story height of the façade.

In order to achieve wider adoption of DSF-STPV in newly or renovated buildings, further research is needed, on design, testing and modelling.

The need for a standardized solutions is identified, that will make the installation of DSF-STPV easy for application and building integration. This standardized solution will incorporate modularity of such system, that is ready to install, and easy to replace. This prefabricated solution can also include a built-in micro-inverter and easy cable connection for each STPV.

Further investigation is needed in the heat recovery mechanism and how the preheated air can be optimally introduced into the HVAC system. The investigation can be focused on manifold designs that will minimize the energy consumption by the fans and optimally direct it to the HVAC system.

Another area that needs to be researched is operating the inlets of the DSF-STPV and the flow within the cavity with the use of AI. This could also work for optimizing the energy production by the STPV and the energy consumption of the adjacent zone to minimize the energy consumption during the grid peak hours.

In addition, the area of viewing comfort needs to be explored, as the STPV can be placed onto the DSF in a way that could minimize glare effects along with an analysis on different transparencies of both the STPV and the shading blinds, as well as automated blinds operation could provide an added value to this research.

Future work could be extended to more in-depth comparison of an IGU integrating STPV and DSF-STPV, especially for the climate zone where the DSF-STPV operates optimally if it closed most of the times. In addition, a full comparison of a typical building envelope, an envelope with an IGU-STPV and an envelope with DSF-STPV would be of great interest.

References

Agathokleous, RA, and SA Kalogirou. 2016. "Double Skin Facades (DSF) and Building Integrated Photovoltaics (BIPV): A Review of Configurations and Heat Transfer Characteristics." *Renewable Energy* 89: 743–56. https://doi.org/10.1016/j.renene.2015.12.043.

Andelkovic, A, B Gvozdenac-Urosevic, M Kljajic, and M Ignjatovic. 2015. "Experimental Research of the Thermal Characteristics of a Multi-Storey Naturally Ventilated Double Skin Facade" 86: 766–81.

Andwari, AM, A Pesiridis, S Rajoo, and R Martinez-. 2017. "A Review of Battery Electric Vehicle Technology and Readiness Levels." *Renewable and Sustainable Energy Reviews*. Vol. 78. Elsevier Ltd.

ASHRAE. 2009. *ASHRAE HANDBOOK Fundamentals*. ASHRAE.

ASHRAE. 2019. "ANSI/ASHRAE/IES Standard 90.1-2019 -- Energy Standard for Buildings Except Low-Rise Residential Buildings."

Athienitis, AK, J Bambara, B O'Neill, and J Faille. 2011. "A Prototype Photovoltaic/Thermal System Integrated with Transpired Collector." *Solar Energy* 85 (1): 139–53.

Baechler, MC, TL Gilbride, PC Cole, MG Hefty, and K Ruiz. 2015. "High-Performance Home Technologies: Guide to Determining Climate Regions by County." *Pacific Northwest National Laboratory & Oak Ridge National Laboratory*. Vol. 7.3. https://www.energy.gov/sites/prod/files/2015/10/f27/ba_climate_region_guide_7.3.pdf.

Baum, R, and N Grimshaw. n.d. "Architectural Integration of Light-Transmissive Photovoltaic Systems An Analysis at the Cell and Laminate Level Abstract This Paper Is a Study of Light-Transmissive Photovoltaic Systems (LTPV) and the State of the Art of Their Architectural Integration ."

Biyik, E, M Araz, A Hepbasli, M Shahrestani, R Yao, L Shao, E Essah, et al. 2017. "A Key Review of Building Integrated Photovoltaic (BIPV) Systems." *Engineering Science and Technology, an International Journal* 20 (3): 833–58. https://doi.org/10.1016/j.jestch.2017.01.009.

Blue Sky Energy Inc. 2009. "SB3024i Datasheet." 2009. http://www.blueskyenergyinc.com/uploads/pdf/SB3024(D)iL_Datasheet_(2017)_1.pdf.

Boer, J de, and WGJ van Helden. 2001. "PV Mobi - PV Modules Optimsed for Building Integration." *9th International Conference on Solar Energy in High Latitudes*, no. May: 13.

Candanedo, LM, A Athienitis, and K-W Park. 2011. "Convective Heat Transfer Coefficients in a Building-Integrated Photovoltaic/Thermal System." *Journal of Solar Energy Engineering* 133 (2): 021002.

Chae, YT, J Kim, H Park, and B Shin. 2014. "Building Energy Performance Evaluation of Building Integrated Photovoltaic (BIPV) Window with Semi-Transparent Solar Cells." *Applied Energy* 129: 217–27. https://doi.org/10.1016/j.apenergy.2014.04.106.

Charron, R, and AK Athienitis. 2006. "Optimization of the Performance of Double-Façades with Integrated Photovoltaic Panels and Motorized Blinds." *Solar Energy* 80 (5): 482–91.

Chen, F, SK Wittkopf, P Khai Ng, and H Du. 2012. "Solar Heat Gain Coefficient Measurement of Semi-Transparent Photovoltaic Modules with Indoor Calorimetric Hot Box and Solar Simulator." *Energy and Buildings* 53: 74–84. https://doi.org/10.1016/j.enbuild.2012.06.005.

Chow, T. T., W He, J Ji, and ALS Chan. 2007. "Performance Evaluation of Photovoltaic-

Thermosyphon System for Subtropical Climate Application." *Solar Energy* 81 (1): 123–30. https://doi.org/10.1016/j.solener.2006.05.005.

Chow, Tin Tai, Z Qiu, and C Li. 2009. "Potential Application of 'See-through' Solar Cells in Ventilated Glazing in Hong Kong." *Solar Energy Materials and Solar Cells* 93 (2): 230–38. https://doi.org/10.1016/j.solmat.2008.10.002.

Collins, MR. 2016. "Queen ' S University Solar Calorimeter – Design , Calibration , and Operating," no. December.

Connectivity, TE. 2005. "HSC100 METAL HOUSED POWER RESISTOR." 2005. http://www.te.com/commerce/DocumentDelivery/DDEController?Action=srchrtrv&DocN m=1625999&DocType=Customer+Drawing&DocLang=English.

Crawley, DB, J New, JN Lott, RJ Morris, M Roth, R Vose, CS Barnaby, RB Burkhead, and SS Hanson. 2020. "Climatic Data for Building Design Standards" 8400.

Dama, A, and D Angeli. 2016. "Wind and Buoyancy Driven Natural Ventilation in Double Skin Facades." *International Journal of Ventilation* 15 (3–4): 288–301.

Didoné, EL, and A Wagner. 2013. "Semi-Transparent PV Windows : A Study for Office Buildings in Brazil." *Energy & Buildings* 67: 136–42. https://doi.org/10.1016/j.enbuild.2013.08.002.

Dittus, FW, and LMK Boelter. 1930. *Heat Transfer in Automobile Radiators of the Tubular Type*. University of California, Berkeley: Publications in Engineering.

Duffie, J, and W Beckman. 2006. *Solar Engineering of Thermal Processes*.

Eicker, U. 2003. *Solar Technologies for Buildings*. 1st ed. Wiley & Sons.Ltd.

Eicker, U. 2014. *Energy Efficient Buildings with Solar and Geothermal Resources*. Wiley.

EISherbiny, SM, GD Raithby, and KGT Hollands. 1982. "Heat Transfer by Natural Convection Across Vertical and Inclined Sir Layers." *Journal of Heat Transfer - Transactions of Asme* 104 (1): 96–102.

Emmel, MG, MO Abadie, and N Mendes. 2007. "New External Convective Heat Transfer Coefficient Correlations for Isolated Low-Rise Buildings." *Energy and Buildings* 39 (3): 335–42.

Energy, D o. 2017. "Department of Energy, Buildings Energy Databook, Office of Energy, Efficiency & Renewable Energy."

European Comission. 2019. "The Energy Performance of Buildings Directive."

Florschuetz, LW. 1976. "Extension of the Hottel-Whillier-Bliss Model To the Analysis of Combined Photovoltaic/Thermal Flat Plate Collectors." 22: 361–66.

Frank, K, RM Manglik, and MS Bohn. 2010. *Principles of Heat Transfer*. Edited by Brooks/Cole.

Fung, TYY, and H Yang. 2008. "Study on Thermal Performance of Semi-Transparent Building-Integrated Photovoltaic Glazings." *Energy and Buildings* 40 (3): 341–50. https://doi.org/10.1016/j.enbuild.2007.03.002.

Gaillard, L, S Giroux-Julien, C Ménézo, and H Pabiou. 2014. "Experimental Evaluation of a Naturally Ventilated PV Double-Skin Building Envelope in Real Operating Conditions." *Solar Energy* 103: 223–41.

Gaillard, L, C Ménézo, S Giroux, H Pabiou, and R Le-Berre. 2014. "Experimental Study of Thermal Response of PV Modules Integrated into Naturally-Ventilated Double Skin Facades." *Energy Procedia* 48: 1254–61.

Gengel, YA. 1985. *HEAT TRANSFER A Practical Approach*. *DM Glover*. 2nd ed.

Gnielinki, V. 1983. *Forced Convection in Ducts, Heat Exchanger Design Handbook*. New York,

NY: Hemisphere.

Gratia, E, and A De Herde. 2004. "Natural Ventilation in a Double-Skin Facade." *Energy and Buildings* 36 (2): 137–46.

Gratia, E, and A De Herde. 2007. "Are Energy Consumptions Decreased with the Addition of a Double-Skin?" *Energy and Buildings* 39 (5): 605–19.

Hagishima, A, and J Tanimoto. 2003. "Field Measurements for Estimating the Convective Heat Transfer Coefficient at Building Surfaces." *Building and Environment* 38 (7): 873–81.

Han, J, L Lu, J Peng, and H Yang. 2013. "Performance of Ventilated Double-Sided PV Facade Compared with Conventional Clear Glass Facade." *Energy and Buildings* 56: 204–9. https://doi.org/10.1016/j.enbuild.2012.08.017.

Han, J, L Lu, and H Yang. 2009. "Thermal Behavior of a Novel Type See-through Glazing System with Integrated PV Cells." *Building and Environment* 44 (10): 2129–36. http://dx.doi.org/10.1016/j.buildenv.2009.03.003.

Han, J, L Lu, and H Yang. 2010. "Numerical Evaluation of the Mixed Convective Heat Transfer in a Double-Pane Window Integrated with See-through a-Si PV Cells with Low-e Coatings." *Applied Energy* 87 (11): 3431–37.

Harrison, SJ, and MR Collins. 1999. "Queen's University Solar Calorimeter--Design, Calibration, and Operating Procedure." *Solar Energy Society of Canada Conference*, no. August.

Hassanli, S, G Hu, KCS Kwok, and DF Fletcher. 2017. "Utilizing Cavity Flow within Double Skin Façade for Wind Energy Harvesting in Buildings." *Journal of Wind Engineering and Industrial Aerodynamics* 167 (December 2016): 114–27.

He, W, YX Zhang, W Sun, JX Hou, QY Jiang, and J Ji. 2011. "Experimental and Numerical Investigation on the Performance of Amorphous Silicon Photovoltaics Window in East China." *Building and Environment* 46 (2): 363–69.

Hegazy, AA. 2000. "Comparative Study of the Performances of Four Photovoltaic/Thermal Solar Air Collectors." *Energy Conversion and Management* 41 (8): 861–81.

Hu, G, S Hassanli, KCS Kwok, and KT Tse. 2017. "Wind-Induced Responses of a Tall Building with a Double-Skin Façade System." *Journal of Wind Engineering and Industrial Aerodynamics* 168 (November 2016): 91–100.

Hydro Quebec. 2019. "GUIDE DU PARTICIPANT HIVER 2019-2020 Marchés Commercial et Institutionnel Ainsi Que Petites et Moyennes Entreprises Industrielles."

IEA. 2018. "Energy Efficiency 2018." Paris.

IEA. 2019. "Global Status Report for Buildings and Construction 2019." *Global Status Report*. Paris.

IEA. 2020. "Tracking Buildings 2020." Paris. https://www.iea.org/reports/tracking-buildings-2020.

Incropera, FP, DP DeWitt, TL Bergman, and AS Lavine. 2007. *Fundamentals of Heat and Mass Transfer*. Edited by FP Incropera and FPFOHAMT Incropera. *Water*. Vol. 6th. Dekker Mechanical Engineering. John Wiley & Sons.

Infield, D, U Eicker, V Fux, L Mei, and J Schumacher. 2006. "A Simplified Approach to Thermal Performance Calculation for Building Integrated Mechanically Ventilated PV Facades." *Building and Environment* 41 (7): 893–901. https://doi.org/10.1016/j.buildenv.2005.04.010.

Infield, D, L Mei, and U Eicker. 2004. "Thermal Performance Estimation for Ventilated PV Facades." *Solar Energy* 76 (1–3): 93–98.

Ioannidis, Z, A Buonomano, AK Athienitis, and T Stathopoulos. 2017. "Modeling of Double Skin Façades Integrating Photovoltaic Panels and Automated Roller Shades: Analysis of the Thermal and Electrical Performance." *Energy and Buildings* 154: 618–32.

Ioannidis, Z, A Buonomano, AK Athienitis, and T Stathopoulos. 2016. "A Detailed Dynamic Model of Multi-Story Double Skin Facades with Integrated Photovoltaic Panels." In . Hamilton, Ontario, Canada.

Ioannidis, Z. 2016. "Double Skin Facades Integrating Photovoltaic Panels , Motorized Shades and Controlled Air Flow." Concordia University.

Ioannidis, Z, ED Rounis, A Athienitis, and T Stathopoulos. 2020. "Double Skin Façade Integrating Semi-Transparent Photovoltaics: Experimental Study on Forced Convection and Heat Recovery." *Applied Energy* 278 (March): 115647. https://doi.org/10.1016/j.apenergy.2020.115647.

Ioannidis, Z. 2016. "Double Skin Facades Integrating Photovoltaic Panels , Motorized Shades and Controlled Air Flow." Concordia University.

James, PAB, MF Jentsch, and AS Bahaj. 2009. "Quantifying the Added Value of BiPV as a Shading Solution in Atria." *Solar Energy* 83 (2): 220–31. https://doi.org/10.1016/j.solener.2008.07.016.

Kamel, RS, and AS Fung. 2014. "Modeling, Simulation and Feasibility Analysis of Residential BIPV/T+ASHP System in Cold Climate - Canada." *Energy and Buildings* 82: 758–70.

Kapsis, K. 2016a. "Modelling, Design and Experimental Study of Semi-Transparent Photovoltaic Windows for Commercial Building Applications."

Kapsis, K. 2016b. "Modelling , Design and Experimental Study of Semi-Transparent Photovoltaic Windows for Commercial Building Applications Konstantinos Kapsis A Thesis In the Department of Building , Civil and Environmental Engineering Presented in Partial Fulfilment of The," no. April.

Kapsis, K, and AK Athienitis. 2015a. "A Study of the Potential Benefits of Semi-Transparent Photovoltaics in Commercial Buildings." *Solar Energy* 115: 120–32.

Kapsis, K, and AK Athienitis. 2015b. "A Study of the Potential Benefits of Semi-Transparent Photovoltaics in Commercial Buildings." *Solar Energy* 115: 120–32.

Kays, W, and M Crawford. 1966. *Convective Heat and Mass Transfer*. Edited by JP Holman. McGraw-Hill.

Kreider, JF, PS Curtiss, and A Rabl. 2002. *Heating and Cooling of Buildings: Design for Efficiency*. Second. NewYork: McGraw-Hill.

Kumar, R, and M Rosen. 2011. "Rosen, M.A.: Performance Evaluation of a Double Pass PV/T Solar Air Heater with and without Fins. Applied Thermal Engineering 31(8), 1402-1410." *Applied Thermal Engineering - APPL THERM ENG* 31 (June): 1402–10.

Li, DHW, TNT Lam, WWH Chan, and AHL Mak. 2009. "Energy and Cost Analysis of Semi-Transparent Photovoltaic in Office Buildings." *Applied Energy* 86 (5): 722–29. https://doi.org/10.1016/j.apenergy.2008.08.009.

Li, DHW, TNT Lam, and KL Cheung. 2009. "Energy and Cost Studies of Semi-Transparent Photovoltaic Skylight." *Energy Conversion and Management* 50 (8): 1981–90. https://doi.org/10.1016/j.enconman.2009.04.011.

Liao, L, AK Athienitis, L Candanedo, K-W Park, Y Poissant, and M Collins. 2007. "Numerical and Experimental Study of Heat Transfer in a BIPV-Thermal System." *Journal of Solar Energy Engineering* 129 (4): 423.

Liao, W, and S Xu. 2015. "Energy Performance Comparison among See-through Amorphous-

Silicon PV (Photovoltaic) Glazings and Traditional Glazings under Different Architectural Conditions in China." *Energy* 83: 267–75.

Lou, W, M Huang, M Zhang, and N Lin. 2012. "Experimental and Zonal Modeling for Wind Pressures on Double-Skin Facades of a Tall Building." *Energy and Buildings* 54: 179–91.

Loveday, DL, and AH Taki. 1996. "Convective Heat Transfer Coefficients at a Plane Surface on a Full-Scale Building Facade." *International Journal of Heat and Mass Transfer* 39 (8): 1729–42.

Lu, L, and KM Law. 2013. "Overall Energy Performance of Semi-Transparent Single-Glazed Photovoltaic (PV) Window for a Typical Office in Hong Kong." *Renewable Energy* 49: 250–54. https://doi.org/10.1016/j.renene.2012.01.021.

Marques da Silva, F, MG Gomes, and AM Rodrigues. 2015. "Measuring and Estimating Airflow in Naturally Ventilated Double Skin Facades." *Building and Environment* 87: 292–301.

Matlab. n.d. "Matworks." 2016.

McAdams, WH. 1954. *Heat Transmission*. R.E. Krieger Publishing Company, 1954.

McQuistin, FC, and JD Parker. 2005. *Heating, Ventilating, and Air Conditioning: Analysis and Design*. Wiley.

Mei, L, D Infield, U Eicker, and V Fux. 2003. "Thermal Modelling of a Building with an Integrated Ventilated PV Facade." *Energy and Buildings* 35 (6): 605–17.

Mei, L, D Infield, U Eicker, and D Loveday. 2006. "Cooling Potential of Ventilated PV Facade and Solar Air Heaters Combined with a Desiccant Cooling Machine" 31: 1265–78.

Miyazaki, T, A Akisawa, and T Kashiwagi. 2005. "Energy Savings of Office Buildings by the Use of Semi-Transparent Solar Cells for Windows." *Renewable Energy* 30: 281–304.

MK Battery. 2015. "8A31DT AGM Battery." 2015. http://www.mkbattery.com/images/8A31DT.pdf.

Mun, H, J Ho, S Chul, and UC Shin. 2017. "Operational Power Performance of South-Facing Vertical BIPV Window System Applied in Office Building." *Solar Energy* 145: 66–77. https://doi.org/10.1016/j.solener.2016.07.056.

National Instruments. 2016. "NI 9223 Datasheet." 2016. http://www.ni.com/pdf/manuals/374223a_02.pdf.

NRCAN. 2019. "Electricity Facts | Natural Resources Canada." 2019. https://www.nrcan.gc.ca/science-data/data-analysis/energy-data-analysis/energy-facts/electricity-facts/20068.

Oesterle, E. 2001. *Double-Skin Facades: Integrated Planning (Architecture)*. Munich, Germany: Prestel.

Olivieri, L, E Caamaño-Martín, FJ Moralejo-Vázquez, N Martín-Chivelet, F Olivieri, and FJ Neila-Gonzalez. 2014. "Energy Saving Potential of Semi-Transparent Photovoltaic Elements for Building Integration." *Energy* 76: 572–83. https://doi.org/10.1016/j.energy.2014.08.054.

Olivieri, L, E Caamaño-Martin, F Olivieri, and J Neila. 2014. "Integral Energy Performance Characterization of Semi-Transparent Photovoltaic Elements for Building Integration under Real Operation Conditions." *Energy and Buildings* 68: 280–91. https://doi.org/10.1016/j.enbuild.2013.09.035.

Palyvos, JA. 2008. "A Survey of Wind Convection Coefficient Correlations for Building Envelope Energy Systems' Modeling." *Applied Thermal Engineering* 28 (8–9): 801–8.

Pantic, S, L Candanedo, and AK Athienitis. 2010. "Modeling of Energy Performance of a House with Three Configurations of Building-Integrated Photovoltaic/Thermal Systems." *Energy*

and Buildings 42 (10): 1779–89. https://doi.org/10.1016/j.enbuild.2010.05.014.

Park, KE, GH Kang, HI Kim, GJ Yu, and JT Kim. 2010. "Analysis of Thermal and Electrical Performance of Semi-Transparent Photovoltaic (PV) Module." *Energy* 35 (6): 2681–87.

Peng, J, DC Curcija, L Lu, SE Selkowitz, H Yang, and W Zhang. 2016. "Numerical Investigation of the Energy Saving Potential of a Semi-Transparent Photovoltaic Double-Skin Facade in a Cool-Summer Mediterranean Climate." *Applied Energy* 165: 345–56.

Peng, J, L Lu, and H Yang. 2013a. "An Experimental Study of the Thermal Performance of a Novel Photovoltaic Double-Skin Facade in Hong Kong." *Solar Energy* 97: 293–304. http://dx.doi.org/10.1016/j.solener.2013.08.031.

Peng, J, L Lu, and H Yang. 2013b. "An Experimental Study of the Thermal Performance of a Novel Photovoltaic Double-Skin Facade in Hong Kong." *Solar Energy* 97: 293–304.

Peng, J, L Lu, H Yang, and T Ma. 2015a. "Comparative Study of the Thermal and Power Performances of a Semi-Transparent Photovoltaic Façade under Different Ventilation Modes." *Applied Energy* 138: 572–83.

Peng, J, L Lu, H Yang, and T Ma. 2015b. "Validation of the Sandia Model with Indoor and Outdoor Measurements for Semi-Transparent Amorphous Silicon PV Modules." *Renewable Energy* 80.

Petukhov, BS. 1970. "Heat Transfer and Friction in Turbulent Pipe Flow with Variable Physical Properties." In , edited by JP Hartnett and TFBT-A in HT Irvine, 6:503–64. Elsevier. https://doi.org/https://doi.org/10.1016/S0065-2717(08)70153-9.

Poirazis, H. 2005. *Single Skin Glazed Office Buildings Energy Use and Indoor Climate Simulations*.

Poirazis, H. 2007. "Double-Skin Façades." *ASHRAE Journal* 49 (10): 70–73.

Qiu, Z, TT Chow, P Li, C Li, J Ren, and W Wang. 2009. "Performance Evaluation of the Photovoltaic Double Skin Facade." *11th International IBPSA*, 2251–57.

Quesada, G, D Rousse, Y Dutil, M Badache, and S Hallé. 2012a. "A Comprehensive Review of Solar Facades. Transparent and Translucent Solar Facades." *Renewable and Sustainable Energy Reviews* 16 (5): 2820–32. https://doi.org/10.1016/j.rser.2012.01.078.

Quesada, G, D Rousse, Y Dutil, M Badache, and S Hallé. 2012b. "A Comprehensive Review of Solar Facades. Transparent and Translucent Solar Facades." *Renewable and Sustainable Energy Reviews* 16 (5): 2643–51.

Rajoria, CS, S Agrawal, S Chandra, GN Tiwari, and DS Chauhan. 2016. "A Novel Investigation of Building Integrated Photovoltaic Thermal (BiPVT) System: A Comparative Study." *Solar Energy* 131 (June): 107–18.

Reinhart, CF, JA Jakubiec, and D Ibarra. n.d. *Definition of the Reference Office for Standarized Evaluations of Dynamica Facade and Lighting Technologies 1 Massachusetts Institute of Technology , Cambridge , MA 02139 , USA 2 Harvard University , Graduate School of Design , Cambridge , MA 02138 , USA*. Cambridge.

Reinhart, CF, JA Jakubiec, and D Ibarra. 2013. "Definition Of A Reference Office For Standardized Evaluations Of Dynamic Façade And Lighting Technologies." *13th Conference of International Building Performance Simulation Association*, 3645–52.

Riedon Inc. 2018. "Precision Current Resistor / DC Current Shunts." 2018. https://riedon.com/media/pdf/RS.pdf.

Robinson, L, and A Athienitis. 2009. "Design Methodology For Optimization Of Electricity Generation And Daylight Utilization For Façade With Semi-Transparent Photovoltaics." *11th International IBPSA Conference, Building Simulation 2009*, 811–18.

Saelens, D. 2002. *Energy Performance Assessment of Single Storey Multiple-Skin Facades*. https://doi.org/Ph. D. thesis.

Saelens, D, J Carmeliet, and H Hens. 2003. "Energy Performance Assessment of Multiple-Skin Facades." *HVAC and R Research* 9 (2): 167–85. https://doi.org/10.1080/10789669.2003.10391063.

Sarfraz, O, CK Bach, and CK Wilkins. 2018. "Plug Load Design Factors." *ASHRAE Journal* 60 (1): 14–19.

Shabunko, V. 2018. "Measurment of Solar Heat Gain Coefficient for Semi-Transparent Building-Integrated Photovoltaics in the Tropics." In *35th European Photovoltaic Solar Energy Conference and Exhibition MEASUREMENT*, 5–9.

Shahsavar, A, and M Ameri. 2010. "Experimental Investigation and Modeling of a Direct-Coupled PV/T Air Collector." *Solar Energy* 84: 1938–58.

Shao, J, J Liu, J Zhao, W Zhang, D Sun, and Z Fu. 2009. "A Novel Method for Full-Scale Measurement of the External Convective Heat Transfer Coefficient for Building Horizontal Roof." *Energy and Buildings* 41 (8): 840–47.

Sharples, S. 1984. "Full-Scale Measurements of Convective Energy Losses from Exterior Building Surfaces." *Building and Environment* 19 (1): 31–39.

Sharples, S, and PS Charlesworth. 1998. *Full-Scale Measurements of Wind-Induced: Convective Heat Transfer from a Roof Mounted Flat Plate Solar Collector*. *Solar Energy*. Vol. 62.

Skandalos, N, and D Karamanis. 2016. "Investigation of Thermal Performance of Semi-Transparent PV Technologies." *Energy and Buildings* 124: 19–34. https://doi.org/10.1016/j.enbuild.2016.04.072.

Sohel, MI, Z Ma, P Cooper, J Adams, and R Scott. 2014. "A Dynamic Model for Air-Based Photovoltaic Thermal Systems Working under Real Operating Conditions." *Applied Energy* 132: 216–25. https://doi.org/10.1016/j.apenergy.2014.07.010.

Song, JH, YS An, SG Kim, SJ Lee, JH Yoon, and YK Choung. 2008. "Power Output Analysis of Transparent Thin-Film Module in Building Integrated Photovoltaic System (BIPV)." *Energy and Buildings* 40 (11): 2067–75. https://doi.org/10.1016/j.enbuild.2008.05.013.

Stec, WJ, AHC Van Paassen, and A Maziarz. 2005. "Modelling the Double Skin Façade with Plants." *Energy and Buildings* 37 (5): 419–27. https://doi.org/10.1016/j.enbuild.2004.08.008.

Tan, HM, and WWS Charters. 1969. "Effect of Thermal Entrance Region on Turbulent Forced-Convective Heat Transfer for an Asymmetrically Heated Rectangular Duct with Uniform Heat Flux." *Solar Energy* 12 (4): 513–16.

Tan, HM, and WWS Charters. 1970. "An Experimental Investigation of Forced-Convective Heat Transfer for Fully-Developed Turbulent Flow in a Rectangular Duct with Asymmetric Heating." *Solar Energy* 13 (1): 121–25.

Teo, HG, PS Lee, and M Hawlader. 2012. "An Active Cooling System for Photovoltaic Modules." *Applied Energy* 90 (February): 309–15.

Test, FL, RC Lessmann, and A Johary. 1981. "Heat Transfer During Wind Flow over Rectangular Bodies in the Natural Environment." *Journal of Heat Transfer* 103 (2): 262–67.

Thornton, B, W Wang, Y Huang, M Lane, and B Liu. 2010. "Technical Support Document: 50% Energy Savings for Small Office Buildings." Richland, Washington 99352. http://www.pnl.gov/main/publications/external/technical_reports/PNNL-19341.pdf.

Tonui, JK, and Y Tripanagnostopoulos. 2006. "Improved PV/T Solar Collectors with Heat Extraction by Forced or Natural Air Circulation." *International Journal of Hydrogen*

Energy 31 (15): 2137–46.

Tonui, JK, and Y Tripanagnostopoulos. 2008. "Performance Improvement of PV/T Solar Collectors with Natural Air Flow Operation." *Solar Energy* 82 (1): 1–12.

Tremblay, O, L Dessaint, and A Dekkiche. 2007. "A Generic Battery Model for the Dynamic Simulation of Hybrid Electric Vehicles." In *2007 IEEE Vehicle Power and Propulsion Conference*, 284–89.

Tzempelikos, A, and AK Athienitis. 2007. "The Impact of Shading Design and Control on Building Cooling and Lighting Demand." *Solar Energy* 81 (3): 369–82. https://doi.org/10.1016/j.solener.2006.06.015.

U.S. Energy Information Administration. 2019. "Real-Time Operating Grid." 2019. https://www.eia.gov/beta/electricity/gridmonitor/dashboard/electric_overview/US48/US48.

Vartiainen, E. 2001. "Electricity Benefits of Daylighting and Photovoltaics for Various Solar Facade Layouts in Office Buildings." *Energy and Buildings* 33: 113–20. https://doi.org/10.1016/S0378-7788(00)00073-6.

Vasan, N, and T Stathopoulos. 2014. "Experimental Study of Wind Effects on Unglazed Transpired Collectors." *Solar Energy* 101: 138–49.

Vats, K, and GN Tiwari. 2012. "Energy and Exergy Analysis of a Building Integrated Semitransparent Photovoltaic Thermal (BISPVT) System." *Applied Energy* 96: 409–16. https://doi.org/10.1016/j.apenergy.2012.02.079.

Vats, K, V Tomar, and GN Tiwari. 2012. "Effect of Packing Factor on the Performance of a Building Integrated Semitransparent Photovoltaic Thermal (BISPVT) System with Air Duct." *Energy and Buildings* 53: 159–65. https://doi.org/10.1016/j.enbuild.2012.07.004.

Veitch, JA, and AD Galasiu. 2011. "The Physiological and Psychological Effects of Windows, Daylight and View at Home." *National Research Council of Canada*, 60. https://doi.org/10.1037/e554552013-001.

Wang, M, J Peng, N Li, H Yang, C Wang, X Li, and T Lu. 2017. "Comparison of Energy Performance between PV Double Skin Facades and PV Insulating Glass Units." *Applied Energy* 194: 148–60.

Wong, PW, Y Shimoda, M Nonaka, M Inoue, and M Mizuno. 2008. "Semi-Transparent PV: Thermal Performance, Power Generation, Daylight Modelling and Energy Saving Potential in a Residential Application." *Renewable Energy* 33 (5): 1024–36. https://doi.org/10.1016/j.renene.2007.06.016.

Xu, S, W Liao, J Huang, and J Kang. 2014. "Optimal PV Cell Coverage Ratio for Semi-Transparent Photovoltaics on Office Building Façades in Central China." *Energy and Buildings* 77: 130–38.

Yang, T, and AK Athienitis. 2014. "A Study of Design Options for a Building Integrated Photovoltaic/Thermal (BIPV/T) System with Glazed Air Collector and Multiple Inlets." *Solar Energy* 104: 82–92.

Yin, SH, TY Wung, and K Chen. 1978. "Natural Convection in an Air Layer Enclosed within Rectangular Cavities." *International Journal of Heat and Mass Transfer* 21 (3): 307–15. https://doi.org/10.1016/0017-9310(78)90123-0.

Yoon, JH, J Song, and SJ Lee. 2011. "Practical Application of Building Integrated Photovoltaic (BIPV) System Using Transparent Amorphous Silicon Thin-Film PV Module." *Solar Energy* 85 (5): 723–33. https://doi.org/10.1016/j.solener.2010.12.026.

Zhang, W, L Lu, J Peng, and A Song. 2016. "Comparison of the Overall Energy Performance of Semi-Transparent Photovoltaic Windows and Common Energy-Efficient Windows in Hong

Kong." *Energy and Buildings* 128.

Zogou, O, and H Stapountzis. 2011. "Experimental Validation of an Improved Concept of Building Integrated Photovoltaic Panels." *Renewable Energy* 36 (12): 3488–98.

Appendix I: Heat transfer coefficient and Nusselt number correlations

Different correlations have been used for the calculation of the heat transfer coefficient and the Nusselt number. In the case of forced convection, where the flow is driven by a fan, very few convective heat transfer or Nusselt number correlations are presented. Most of the correlations developed are based on tube structures and few are based on BIPV/T applications. Some of the most commonly used correlations are presented.

Laminar flow, low incident solar radiation, Incropera and De Witt (Incropera et al. 2007):

$$h_c = \frac{k_{air}}{H} \cdot 0.664 \cdot Re_H^{0.5} Pr^{1/3} \tag{1}$$

Laminar flow, high incident solar radiation on a DSF, Saelens (Saelens 2002):

$$h_c = \frac{k_{air}}{H} \cdot 0.906 \cdot Re_H^{0.5} Pr^{1/3} \tag{2}$$

Combined laminar and turbulent flow on a DS,F Saelens (Saelens 2002):

$$h_c = \frac{k_{air}}{H} \cdot 0.664 \cdot Re_{x,tr}^{0.5} Pr^{1/3} + 0.0296\left(Re_H^{4/5} - Re_{x,tr}^{4/5}\right) Pr^{1/3} \tag{3}$$

Taking into consideration the friction factor for fully developed flow Gnielinski (Gnielinki 1983).

$$h_c = \frac{k_{air}}{D_h} \cdot \left(\frac{\frac{f}{8} \cdot (Re_{D_h} - 1000)Pr}{1 + 12.7\sqrt{\frac{f}{8}}\left(Pr^{1/3} - 1\right)}\right)\left(1 + \left(\frac{D_h}{H}\right)^{2/3}\right) \tag{4}$$

Where f is friction factor and is given by the equation $f = 0.046 \cdot Re^{-1/5}$ for $2 \cdot 10^4 < Re < 10^5$
Gnielinski (Gnielinki 1983) developed a simpler alternative Nusselt number correlation:

$$Nu = 0.0214 \cdot (Re^{0.80} - 100)Pr^{0.40} \text{ for } 10^4 < Re < 5 \cdot 10^4 \text{ and } 0.5 < Pr < 1.5 \tag{5}$$

The Petukov equation for the Nusselt number is presented by Eicker (Eicker 2014).

$$Nu_{D_h} = \frac{\left(Re_{D_h} - 1000\right)Pr\frac{f}{8}}{1 + 112.7\sqrt{\frac{f}{8}}(Pr^{2/3} - 1)}\left(1 + \left(\frac{D_h}{l}\right)^{2/3}\right) \text{ for } Re_{D_h} > 3100 \tag{6}$$

Where $f = \left(0.791Re_{D_h}^{0.8} - 1.64\right)^{-2}$
Fully developed flow and forced convection (Dittus and Boelter 1930):

$$Nu = 0.023 \cdot Re^{0.80} Pr^{0.40} \text{ for heating the fluid} \tag{7}$$

$$Nu = 0.023 \cdot Re^{0.80} Pr^{0.30} \text{ for cooling the fluid} \tag{8}$$

Fully developed flow and forced convection, with asymmetrical heating but for a horizontal duct and for Re>9500, (Tan and Charters 1970):

$$Nu(x) = 0.0158 \cdot Re^{0.80} + (0.00181 \cdot Re + 2.92) \cdot e^{-0.03795x/D_h} \tag{9}$$

For laminar and turbulent region, for forced convection, for BIPV/T, (Yang and Athienitis 2014):

$$Nu_{front}(x) = 8.188 \cdot Re^{0.77} \cdot Pr^{3.85} \cdot e^{-\frac{x^{0.2}}{2.8D_h}} + 0.061 \cdot Re^{0.77} \cdot Pr^{3.85} \text{ for } 2300 < Re < 9500 \tag{10}$$

$$Nu_{back}(x) = 4.02 \cdot Re^{1.09} \cdot Pr^{19.3} \cdot e^{-\frac{x^{0.2}}{14D_h}} + 0.005 \cdot Re^{1.09} \cdot Pr^{19.3} \text{ for } 2300 < Re < 9500 \tag{11}$$

And for laminar flows:

$$Nu_{front}(x) = 0.6883 \cdot Re^{0.7} \cdot Pr^{0.80} \cdot e^{-\frac{x^{0.3}}{6.45D_h}} + 0.0124 \cdot Re^{0.7} \cdot Pr^{0.80} \text{ for } 1190 < Re < 2300 \tag{12}$$

$$Nu_{back}(x) = 50 \cdot Re^{0.5} \cdot Pr^{0.2} \cdot e^{-\frac{x^{0.3}}{1.37D_h}} + 0.428 \cdot Re^{0.5} \cdot Pr^{0.2} \text{ for } 1190 < Re < 2300 \tag{13}$$

For non-developed flow (L. Liao et al. 2007):

$$Nu_{front}(x) = (0.011 \cdot Re + 62.856) \cdot e^{-0.475x} + (2.766 \cdot 10^{-3}) \cdot Re + 5.58 \qquad (14)$$

$$Nu_{back}(x) = (0.109 \cdot Re - 124.344) \cdot e^{(-0.475 \cdot 10^{-5}Re - 0.593)x} + (4.098 \cdot 10^{-3}) \cdot Re + 3.896 \qquad (15)$$

Error analysis: For the error analysis, the propagation of error methodology is used to calculate the error of the measurements.

For the ΔT between the outlet and the inlet of the DSF-STPV and the ΔT between each surface and the flowing air around it, the uncertainty is calculated by using the uncertainty of the T-thermocouples that are used in the experimental set-up (0.3°C). The $\delta T = \sqrt{0.3^2 + 0.3^2} = 0.424\ °C \rightarrow 0.4\ °C$.

For the measurement of the velocity in the cavity, which is the prevalent error in the propagation, when calculating the error of Reynolds number or the mass flow rate, the error of the measuring equipment was used. The flow-meter has a 2% error and the pressure transducer has a 0.5% error. For the range of velocities in this experiment 0.300-1.20m/s the error ranges from 0.008 m/s to 0.03m/s. The equivalent Reynolds values range from $85.0 \cdot 10^2 \pm 2.00 \cdot 10^2$ to $26.0 \cdot 10^3 \pm 7.00 \cdot 10^2$.

For the PV voltage measurements through the NI 9229, a gain error and an offset error of ±0.04% and ±7.66 mV respectively is assumed

Appendix II Detailed parametric analysis for each climate zone

2A Houston, Texas (hot, humid)

Houston (Texas) that represents 2A ASHRAE zone, has differences from 1A climate zone (Miami), although both present better performance when higher velocity set-points are preferred. The DSF-STPV behaves differently for widths smaller and greater than 0.50 m (1.64 ft). For smaller cavities, strategy #10 is preferred throughout the year, meaning that the DSF-STPV is closed when the average temperature of the cavity is lower than the middle of the occupants' comfort level (22 °C / 71.6 F), and it is mechanically ventilated otherwise. From October to March, higher velocity set-points are optimal for basic insulation case and lower velocities are optimal for advanced insulation case, as the heating loads needed for the advanced insulation case is less. For the rest of the months, higher velocity set-points are preferred for both insulation cases, with the exception of July and August when the DSF-STPV is ventilated with lower velocities. During the winter months, the preheated air from the DSF-STPV is introduced into the HVAC, while when the average air cavity temperature is lower than (22 °C / 71.6 F) then the cavity is closed to build up heat and then extract it. For the advanced thermal insulation case of the building, lower velocities are preferred, as less heat is needed to be extracted and then introduced into the HVAC. For wider cavities, (0.60 m to 1.00 m / 1.97 ft to 3.28 ft) and for advanced thermal insulation, the cavity is either naturally ventilated or closed, strategy #2 and #3 respectively. Similarly, to narrower cavities, strategy #10 is preferred with high velocity set-points, for basic insulated zones as more heat needs to be extracted from the system. In addition, Houston does not present a high variance in the average wind velocity throughout the year, but the low wind speeds presented in the summer in combination with the warmer air that appears in the cavity favours natural ventilation (strategy #2) or natural ventilation during the night (strategy #6).

Similarly, to Miami, a combination of a closed and a mechanically ventilated cavity is preferred. The most commonly preferred strategy was the mechanical ventilation of the DSF cavity if the temperature of the zone is greater than 22 °C (71.6 F) and closed otherwise (Strategy #10), followed by the strategy where the cavity is closed if the incident solar radiation is lower than 200W/m^2 and the ambient temperature is lower than 18 °C (64.4 F) and mechanically ventilated otherwise (strategy #12). The difference between the basic and the advanced insulation case, in the energy balance of the DSF-STPV is generally greater than 50% and wider cavities with higher airflow rates operate optimally.

2B Phoenix, Arizona (hot, dry)

Phoenix (Arizona) presents similar degree days count with Houston, Phoenix and presents the same behaviour for all cavity widths with the exception of very narrow and very wide cavities (0.15 m, 0.2 m and 1.00 m respectively / 0.50 ft, 0.66 ft. and 3.28 ft). This can be attributed to the higher incident solar radiation and to the lower average wind speed that Phoenix presents through the year. For the basic insulation cases, the DSF prefers to be closed at night or when it is very

overcast (total incident solar radiation on the façade is less than 200 W/m^2) and at the same time the ambient temperature is less than the zone temperature, and to be mechanically ventilated otherwise (strategy #12). For the advanced insulation case, a similar strategy is preferred, as it is closed when the incident solar radiation is lower than 200 W/m^2 and mechanically assisted otherwise. The difference between these two cases, indicate the impact that the insulation of the zone has on the operation of the DSF-STPV. For the basic insulation case, the ambient temperature needs to be considered as it interacts greatly with the building zone, as with the advanced insulation case, the ambient temperature is not taken into consideration. For June, July and August, the DSF-STPV is preferred to be closed as the average ambient temperature for these months is higher than 30 °C (86 F) and a mechanically ventilated DSF would encourage the extraction of coolth from the zone. For the wider cavity, natural ventilation or closed cavity is preferred for the advanced insulation case. The same pattern as Houston is observed, where the cavity is naturally ventilated at nights during the summer months as the exhausted heat from the building that is captured in the cavity drives the air upwards in combination with the low average wind speeds.

For the basic insulation case (B1), there are preferred either smaller ventilated cavities (0.15 m, 0.20m / 0.50 ft, 0.66 ft) with strategy #5 or 10, or wider cavities (0.80 m, 1.00 m / 2.62 ft, 3.28 ft) that are either closed or naturally ventilated (strategy #3 or #2). In contrary, for the basic insulation case (B2), increased cavity widths present increased energy balance with exception of the wider cavity where the mechanical ventilation of the DSF-STPV would result in increased fan consumption.

3A Atlanta, Georgia (hot, humid)

The behaviour of the DSF-STPV for Atlanta, Georgia, that represents 3A ASHRAE zone, alters at 0.40 m (1.31 ft) cavity width. The ASHRAE zones 3A and 3B don't have a different insulation minimum for a basic and an advanced fenestration insulation and the values of the basic and the advanced insulation cases are the same. For narrower cavities, the DSF-STPV system consumes less electricity when it is closed when the average temperature of the cavity is lower than 22 °C (71.6 F) (the middle of the occupants' comfort level) and is mechanically ventilated otherwise (strategy #10), while for the wider cavities (0.50 m to 1.00 m / 1.64 ft to 3.28 ft) the cavity is naturally ventilated (strategy #2). For January and February, that the ambient temperature is low (4.7 °C /40.5 F and 6.6°C / 43.9 F respectively) and the needs for heating in the zone are greater, the velocity set-point is lower (0.20 m/s, 0.66 ft/s) in comparison to the rest of the months as the preheated air is used to meet the needs of the HVAC. For the rest of the months, the velocity set-point is high for different reasons. For the cooler months (March April, November and December), the cavity is closed most of the time, as the average temperature in the cavity is lower than 22 °C (71.6 F) but when it is higher the extracted heat is needed for the HVAC and used to heat-up the zone through convection, and thus high velocity set-point is used. For the warmer months (June, July and August) the velocity set-point is high due to the need to cool down the STPV. For September and October, lower velocity set-points are preferred as the incident solar radiation is high, and the ambient temperatures are lower, resulting in high STPV efficiency and higher velocity set points would result in higher convection within the cavity and an over cooling of the building.

Smaller cavities (0.15 m or 0.20 m / 0.50 ft or 0.66 ft) that are closed when the average temperature of the cavity is lower than 22 °C (71.6 F) and is mechanically ventilated otherwise (strategy #10), with different velocity set-points, depending on the time of the year.

3B-CA Los Angeles, California (hot dry)

Los Angeles (3B of ASHRAE climate zone) has a balanced weather profile. For almost all year round, the average incident solar radiation on the façade is greater than 100W/m^2 and the cavity operates optimally if it is mechanically ventilated when the average temperature of the cavity is higher than the middle of the occupants' comfort level (22 °C / 71.6 F) and closed otherwise (strategy #12). More specifically, from October to February, the incident solar radiation is greater than 150W/m^2, the average wind velocity is lower, and this period coincides with the differentiation on the velocity set-point of the airflow within the cavity. Although these months are the winter months, the heating load needed is not significant as the average ambient temperature ranges from 13°C (55.4 F) to 18 °C (64.4 F). Low velocity set-points are preferred as the need for preheated air is not significant, the ambient temperatures are lower and the STPV can be cooled down easier and the lower air-flow rates within the cavity result in less heat extracted by the building, keeping it warm. In contrary, for the rest of the months, that the incident solar radiation is lower, and the average ambient temperatures are slightly higher, the cavity is ventilated with higher flow rates. The need to cool down the STPV and extract heat from the building leads to these higher flow rates, while during the summer nights, when the average temperature within the cavity drops below 22 °C (71.6 F) the cavity closes to keep the building cool, as the building does not need to be precooled. It is evident that for wide cavities (1.00 m / 3.28 ft) the strategy preferred is for the cavity to be closed. The ventilation of a wide cavity would result in greater energy consumption than reduction for both winter and summer periods.

In general, there are not significant differences in the net-energy balance between smaller or wider cavities, with a small increase in the balance as the cavities get wider. Los Angeles presents a positive energy balance with the worst months being the summer months, where even then, the net balance is zero.

3B-other Las Vegas, Nevada (hot, dry)

The DSF-STPV system in Las Vegas (3B ASHRAE climate zone) is preferred to be ventilated at all times, with the exception of wide cavities during the summer. For cavity widths from 0.15 m to 0.6 m (0.50 ft to 1.97 ft) the DSF-STPV operates optimally when the cavity is mechanically ventilated if the incident solar radiation is greater than 200 W/m^2 and closed otherwise (strategy #5). For the months of June, July and August, when ambient temperature is warmer (average temperature greater than 30 °C (86 F)) and the average incident solar radiation is greater than 100 W/m^2, the cavity is ventilated with lower velocities if the incident solar radiation is greater than 200 W/m^2 and closed otherwise or it is naturally ventilated during the day and closed during the night (strategy #6). Due to the higher incident solar radiation, the STPV needs to be ventilated but the preheated air does not need to be introduced into the HVAC. In addition, high flow rates would result in an increased consumption by the fans and an increased convection with the building that would result in removing the coolth from the building. Another parameter that should be taken into consideration is the high wind velocity during these months that would enhance the natural

ventilation of the cavity. The behaviour of the DSF-STPV change for wider cavities (0.80 m to 1.00 m / 2.62 ft to 3.28 ft) where the cavity is closed when the average temperature of the cavity is lower than the room heating set-point (18 °C / 64.4 F) and mechanically ventilated when it is greater (strategy #9). In this way the warm air from the DSF-STPV is either introduced into the HVAC system or it is exhausted to the environment. On the other hand, because the incident solar radiation on the STPV is not great during the summer months, as the STPVs are mounted vertically, the STPV do not need to be cooled down that much, the cavity does not need to be ventilated and the energy consumption by the fans is avoided.

Las Vegas presents increased net-energy balance as the cavity gets wider till the width of 0.80 m (2.62 ft). Strategy #5 is preferred as the cavity is mechanically ventilated if the incident solar radiation is greater than 200 W/m^2 and closed otherwise, with different cavity ventilation set-points depending on the time of the year. The net-balance for Las Vegas is positive with winter months generating more, while the increased consumption is during the summer, where the need for HVAC consumption is greater.

3C San Francisco, California (marine)

San Francisco (3C ASHRAE climate zone) is a heating dominated climate with more heating degree days than cooling degree days. The complexity of such system is shown here where the DSF-STPV behaves differently for three different cavity width regions. Narrow cavities widths (0.15 m to 0.20 m / 0.50 ft to 0.66 ft), medium cavity widths (0.25 m to 0.60 m / 0.82 ft to 1.97 ft) and wide cavity widths (0.80 m to 1.00 m / 2.62 ft to 3.28 ft). The average ambient temperatures between winter and summer does not differ significantly (9.3 °C / 48.7 F in January to 17.6 °C / 63.7 in August), and mechanical ventilation is in general preferred with small differentiations. For narrow and wider cavities and for the wintertime, the cavity is mechanically ventilated when the air temperature within the cavity is greater than 22 °C (71.6 F) and closed otherwise. For December and January and for the basic insulation case, the DSF-STPV needs to be ventilated with higher flow rates than the advanced insulation. For February and November both insulation cases (B1 and B2) need the maximum flow rates and for March and April, the basic insulation case needs less ventilation than the advanced case. For December and January, the DSF is rarely mechanically ventilated, as the mean air temperature within the cavity is rarely greater than 22 °C (71.6 F). In the basic insulation case, and because of the greater losses from the building to the DSF, the cavity reaches easier the 22 °C (71.6 F) mark and uses this preheated air to introduce it to the HVAC and compensate for the losses, something that doesn't happen for the advanced insulation case and less flow rate is needed. For February and November that the average incident solar radiation are comparable and the average wind velocities are low, the cavity needs to be ventilated at higher flow rates when the temperature reaches the 22 °C (71.6 F) mark as the STPV need to be cooled down. For March and April, that the average wind speed is higher, and the ambient temperature starts to get higher, the operation of the DSF-STPV changes and the basic insulation cases operate better at lower flow rates. This is happening because the cavity of the basic insulation cases reaches easier the average temperature of 22 °C (71.6 F), point at which the mechanical ventilation starts to operate resulting in a more frequent cooling down of the DSF and of the building zone. During the summer months, the need to cool down both the STPV and the building result in higher airflow

rates within the DSF for both insulation cases. For medium width cavities, the same logic applies but there is small differentiation as the preferred ventilation strategy for the advanced insulation case is mechanical ventilation when the incident solar radiation is greater than 200 W/m^2 and closed otherwise, indicating that when there is sufficient incident solar radiation the cavity can be ventilated to either use the preheated air and/or to cool down the SPTV. October is a specific case that the ventilation of the cavity is minimum for all cavity widths and all strategies preferred. October is the month with the greatest incident solar radiation, creating the need for more frequent but constant STPV cooling and less heating load for the adjacent zone as more sunlight reaches the zone.

In general, there are not significant differences in the net-energy balance between smaller or wider cavities, with a small increase in the balance as the cavities get smaller. Strategy #10 is preferred with different velocity set-points. San Francisco presents a positive energy balance for all the months with the worst months being the summer months. In addition, there are not significant differences between the basic (B1) and the advanced (B2) insulation cases, with the difference being around 3%.

4A Baltimore, Maryland (mild, humid)

For Baltimore, which has a mild and humid climate, representing 4A climate zone of ASHRAE, the behaviour of the DSF-STPV changes for cavity widths wider or lower than 0.60 m / 1.97 ft. For narrower than 0.60 m (1.97 ft) cavities, the DSF-STPV operates optimally if the cavity is ventilated. For very narrow and medium cavities (0.15 m - 0.20 m wide / 0.50 – 0.66 ft and 0.40 m to 0.50 m / 1.31 ft to 1.64 ft respectively) the DSF is closed when the average temperature of the cavity is lower than the middle of the occupants' comfort level (22 °C / 71.6 F), and mechanically ventilated otherwise (strategy #10). A slight differentiation of the previous strategy is preferred for cavities 0.25 m and 0.30 m wide (0.82 ft and 0.88 ft), where the DSF is mechanically ventilated if the temperature of the adjacent to the DSF zone is smaller than the average temperature of cavity (strategy #7). For cavity widths up to 0.50 m (1.64 ft) the cavity is ventilated with a low velocity set-point during the winter (from October to March) and with high velocity set-point for the rest of the months. As the average ambient temperature during the winter months is lower in comparison to the previously studied cases and the average wind velocity is relatively high, the need for heating the zone is increased. Low velocity set-points during the winter assists the warming-up of the air within the cavity, that is later introduced into the HVAC as preheated air. The cooling load during the summer months is low as the average ambient temperature is also low as well as the direct incident solar radiation that penetrates the zone. Thus, the high velocity set-points are preferred as the STPVs and the adjacent zones are cooled down by the mechanically ventilated DSF. For wider cavities (greater or equal to 0.60 m / 1.97 ft) during the winter months the cavity is ventilated with the lowest possible velocity as preheated air by the DSF is utilized by the HVAC system. In contrary the DSF is closed or naturally ventilated during the summer to avoid excess fan consumption.

Looking at the annual performance of such system, narrower cavity widths are preferred with strategy #10 being the more prevalent, with infrared cavity velocity set-points during the warmer and lower during the cooler months. Shoulder seasons present positive energy balance, while either

summer or winter months present negative energy balance.

4B Albuquerque, New Mexico (mild, dry)

Albuquerque, New Mexico, has very similar degree days and similar monthly average ambient temperatures with the case of Baltimore presented earlier. Though, the average monthly incident solar radiation is increased by more than 60% during the winter months. The behaviour of the DSF changes for cavities wider than 0.40 m (1.31 ft). For narrow cavities (0.15 m to 0.30 m / 0.50 ft to 0.88 ft) the strategy follows the same principal as in narrow cavities in Baltimore; low velocity set-points during the winter to introduce the preheated air to the HVAC, and increased cavity ventilation during the summer nights when the mean temperature of the cavity is lower than mean temperature of the zone, to assist in the precooling of the building. Natural ventilation is preferred for wider cavities (strategy #2), to eliminate the fan consumption. For the winter months when the incident solar radiation on the DSF-STPV is greater, mechanically assisted flow is preferred during the night and natural ventilation is preferred when the incident solar radiation is lower than 200 W/m^2 (strategy #6). Both insulation cases (basic and advanced) have similar behaviour, with some exceptions; During the winter months the mechanical ventilation is preferred for the advanced case as the heat extraction by the building would be lower in comparison to the case with the basic insulation. Albuquerque is another case where for wide cavities, during the summer months that the wind velocity is high, natural ventilation during the night is preferred to free cool the building.

In addition to previous cases, the net-balance of a DSF-STPV system in Albuquerque is greater for narrower cavities that are mechanically ventilated (Strategy #10), for both insulation cases (B1 and B2). The net-balance difference between B1 and B2 reaches 7%, with the advanced insulation case (B2) presenting higher net-balance values. Except from the summer months, the rest of the months present positive net-values, with October and November being the months with the higher energy net-balances.

4C Seattle, Washington (marine)

Seattle Washington (4C ASHRAE climate zone) has a similar climate with Baltimore and Albuquerque in regard to average monthly temperatures and degree days, but differs regarding solar radiation, presenting a quarter of the average incident solar radiation during the winter months than Albuquerque (4B ASHRAE climate zone). Except of the very narrow cavity case (0.15 m / 0.50 ft), the rest cases of the DSF-STPV are separated to narrower and wider than 0.50 m (1.64 ft) cases. DSF-STPV with narrower cavities (0.20 m to 0.40 m / 0.66 ft to 1.31 ft) operate better when the DSF is closed all year round, while the wider cavities (0.60 m to 0.80 m / 1.97 ft to 2.62 ft) are closed when the incident solar radiation is lower than 200W/m^2 and naturally ventilated otherwise. As Seattle presents low incident solar radiation on the DSF-STPV, the need to be ventilated is minimized and it is preferred to be used as a buffer zone. For the winter months and for the advanced insulation case, the DSF is naturally ventilated if the incident solar radiation is greater than 200W/m^2 and closed otherwise. As the average incident solar radiation is low during the winter months, the incident solar radiation is rarely greater than 200W/m^2 and when this is happening, the natural ventilation is enough to drive the preheated air within the DSF and introduce it into the HVAC system. For the widest cavity examined, natural ventilation is not enough, and

the minimum mechanical ventilation rate is used to assist the flow (strategy #5). A combination of these two behaviours, as a transitional width, is presented for the middle range (0.5m) with different strategy for the basic and the advanced insulation case, where the in basic insulating case (B1) the DSF-STPV performs better when the cavity is closed during the day and for the advanced insulation case when the cavity is naturally ventilated during the night.

Looking at the annual performance of DSF-STPV, it seems that narrower mechanically ventilated cavities are in general preferred, with winter months to present negative net-values. Strategy #10, with different velocity set-points throughout the year is preferred. The difference in the energy consumption between the basic and the advanced insulation case reaches 6.8% at the narrowest cavity simulated.

5A Chicago, Illinois (cold, humid)

Chicago, Illinois, which represents 5A ASHRAE climate zone, presents comparable heating and, cooling degree days with Denver, Colorado (5B ASHRAE climate zone) but the average monthly incident solar radiation is lower and the monthly average wind velocities are higher. The behaviour of the DSF-STPV alters for cavities narrower and greater than 0.40 m (1.31 ft). For cavities narrower than 0.40 m (1.31 ft) the preferred strategy implies that the cavity is ventilated if the temperature within the zone is higher than 22 °C (71.6 F) and it is closed otherwise (strategy #10) or it is ventilated if the average temperature of the cavity is greater than the zone temperature and closed otherwise (strategy #7). During the winter months, the cavity is ventilated if there is need for heating. Because the ambient temperature is very low, the preferred velocity set-points are lower (0.20 m/s, 0.66 ft/s) in order for the air to have time to heat-up. From May till August, when the average ambient temperature is increasing (from 15.3°C to 21.8°C / 59.5 F to 71.2 F) the cavity needs to be ventilated with higher flow rates to precool the building. Similarly for the month of September and October when the need for both heating and cooling is low, lower flow rates are preferred as the cavity is ventilated only if there is potential to cool down the PV or precool the building. It can be seen that the difference in the insulation has an effect on the strategy selected as for the 0.25 m (0.82 ft) wide cavity, different strategies are preferred for the different cases, implying that for the basic insulation case, the cavity needs to be closed for more time than it is ventilated. For cavities wider than 0.40 m (1.31 ft) different strategies are applied on the cavity ventilation of the DSF-STPV. During the winter months, the cavity is ventilated all the time as the need for preheated air is constant and even during the cold winter nights the air is heated through the building losses. For this reason, the cavity velocity preferred is low, as it is important not to extract too much heat from the building but increase the recuperated heat. From March till October the cavity operates better if it closed and it acts as a buffer zone, as the need for heating is lower. For the summer months the fan consumption would result in increased energy consumption in comparison the potential energy savings. Chicago, presents fluctuation on the wind velocities with lower winds during the summer months and higher wind velocities during the winter, restricting in this way the natural ventilation strategy.

Similarly, to Seattle (4C), it seems that narrower mechanically ventilated cavities are in general preferred, with different velocity set-points throughout the year (Strategy #10). It is also seen that

during the shoulder seasons, positive net-values are presented, while the difference between the advanced and the basic insulation case can be around 17%.

5B Denver, Colorado (cold, dry)

Denver, Colorado, which represents 5B ASHRAE climate zone, presents similar ambient temperatures with Chicago (5A) but with higher incident solar radiation during the winter months. This increased incident solar radiation has an impact on the preferred strategies especially for the months of March, April, September and October. The average ambient temperature is around 0^{oC} (32 F) from November to February while ambient temperatures during the summer reach up to $23^{o}C$ (73.4 F). Increased wind velocities are presented in the shoulder seasons, with April being the windiest month. The behaviour of the DSF-STPV for Denver is separated into three different cavity widths ranges, 0.15 m to 0.25 m (0.50 ft to 0.82 ft), 0.30 m to 0.60 m (0.88 to 1.97 ft) and 0.80 m to 1.00 m (2.62 ft to 3.28 ft). For the narrower cavity cases the optimal operation of the DSF-STPV is when the cavity is closed when if the average temperature of the cavity is lower than 22 °C (71.6 F) (the middle of the occupants' comfort level) and is mechanically ventilated otherwise (strategy #10). This operation has different velocity set-points for the winter and the summer months. From March to October higher velocity-set points are preferred as the higher flow within the cavity assists at the cooling of the STPV and the building. On the other hand, for the winter months, lower velocity set-points are preferred as it is limited to the volume of the preheated air that can be introduced into the HVAC system. It can be seen that March and October are the intermediate months, for which different velocity set points are preferred based on the thermal insulation of the building. For the middle range cavity widths (0.30 m to 0.60 m / 0.88 ft to 1.97 ft), a transition occurs from mechanical ventilation (strategy #1 and strategy #10) to natural ventilation all the time (strategy #2) and closed all the time (strategy #3). A similar with the previous strategy is preferred for the basic insulation case as the cavity widens from 0.30 m to 0.40 m (0.88 ft to 1.31 ft) with the cavity being mechanically ventilated if the temperature of the adjacent to the DSF zone is smaller than the average temperature of cavity (strategy #7), while full-time mechanical ventilation is preferred for the winter months, especially for the cases of advanced thermal insulation. In addition, for the summer months and for the 0.60 m (1.97 ft) wide cavity case, natural ventilation (strategy #2) or even full-6time closed cavity (strategy #3) is preferred. For the wider cavities (0.80 m to 1.00 m / 2.62 ft to 3.28 ft), natural ventilation is preferred during the summer months, as it allows for natural cooling of the building and the STPV, without consuming electricity, while for the winter months mechanical ventilation is preferred, with low velocity set points meeting in this way the increased need for introducing preheated air into the HVAC system.

In addition to previous cases, under conditions mechanically ventilated DSF-STPV system is preferred (Strategy #10), for both insulation cases (B1 and B2). The net-balance difference between B1 and B2 reaches 12.4%, with the advanced insulation case (B2) presenting higher net-balance values. It is also seen that for the advanced invultuation case (B2), there is not great difference in the net energy values for different cavity widths. For the basic insulation case (B1), this difference can be 49%.

6A Minneapolis, Minnesota (cold, humid)

Minneapolis, Minnesota, which represents 6A of ASHRAE climate zones, presents higher incident solar radiation than Helena, Montana, which represents the 6B climate zones of ASHRAE. In addition, the average wind speed in Minneapolis is greater than those in Helena. The behaviour of the DSF-STPV is separated into two regions of cavity widths, these being the narrower than 0.50 m (1.64 ft) and the wider than 0.80 m (2.62 ft) cavities, with the 0.60 m (1.97 ft) wide cavity being a transitional cavity width. For narrow cavities, for both insulation cases and for all months of the year the DSF-STPV system presents optimal operation when it is closed. In this way the heating losses during the winter are minimized, while during the summer, when the need for cooling is limited, further mechanical ventilation of the DSF would result in increased fan consumption. In addition, for narrower cavities, natural ventilation is not preferred as the friction by the cavity prevents it. For the transitional cavity width (0.60 m / 1.97 ft) the DSF is closed for most of the time, while for the advanced insulation cases and only for the winter months, the cavity is naturally ventilated when the incident solar radiation is lower than 200 W/m^2 (during the night or overcast days) and mechanically ventilated otherwise, utilizing the preheated air for the HVAC system. For wider cavities (0.80 m to 1.00 m / 2.62 ft to 3.28 ft) the cavity is naturally ventilated (strategy #2) utilizing the increased wind velocity and buoyancy, with the preheated air to be introduced into the HVAC. During the winter the DSF is naturally cooled during the summer. In general, narrower and closed cavities (strategy #3) are preferred as it presents a better energy balance through-out the year than the wider cavities. It is seen that the difference is presented mainly during the winter months where the net balance is higher in narrower cavities than wider cavities.

In general, narrower cavities, present increased energy balance with the cavity being closed year-round. The difference between B1 and B2 for the narrower cavities reaches 8.4 %, while for different cavity widths, both B1 and B2 present a difference of approximately 24%. The fact that both insulation cases present the same difference can be explained because there is no mechanical ventilation that would expose the envelope of the building to higher convective heat transfer coefficients and extract or supply heat to the adjacent building zone.

6B Helena, Montana (cold, dry)

Helena, Montana represents ASHRAE 6B climate zone, with average ambient temperatures ranging from -7.2 °C (19 F) in the winter to 20.5 °C (68.9 F) in the summer. With 8,031 heating degree days and 386 cooling degree days, a DSF-STPV system in Helena is designed for heating. Helena presents similarities with Minneapolis, the other 6th climate region of ASHRAE, but presents differences in the operation of wider cavity configurations. The DSF-STPV behaves differently depending on the cavity width and can be separated into different regions: the narrow the wide and the transitional. For narrow cavities (narrower than 0.50 m) the DSF preforms optimally when it is closed through-out the year (strategy #3), acting as a buffer zone in the winter and minimizing the energy losses due to fan consumption. It is seen that both regions representing the 6th zone of ASHRAE have high incident solar radiation during the summer and lower during the winter, but the combination of low ambient temperature and high incident solar radiation is not enough to impose the need to further mechanically cool down the STPV. For the transitional cavity

widths (0.50 m and 0.60 m / 1.64 ft and 1.97 ft), for the winter months, mechanical ventilation is preferred (strategy #1), taking advantage of the higher increased incident solar radiation and meeting the need to preheat the air introduced into the HVAC system. For these cavity widths, the balance between the increased energy production by cooling down the STPV and the consumption of energy by the fans and the building losses due to increased convection is critical and can lead to either selecting mechanical ventilation all the time (strategy #1) or closed DSF-STPV cavity (strategy #3). For wide cavity widths (0.80 m to 1.00 m / 2.62 ft to 3.28 ft), mechanical ventilation (strategy #1) with low velocity set-points is preferred, as more preheated air is introduced into the HVAC system, decreasing the energy consumption of the zone, for the winter months. During the summer months, closed cavity during the day and natural ventilation during the night (strategy #6) is preferred allowing for night precooling of the building and minimizing the electricity consumption by the fans. In general, narrower and closed cavities present better energy balance through-out the year, with most important being the decreased energy consumption during the winter months, if the cavity is closed (strategy #3).

In addition to the Minneapolis (climate zone 6A) the annual performance of DSF-STPV is lower for narrower cavity widths. For the narrowest cavities, the difference between B1 and B2 is around 13%, while the cavity is closed. For the wider cavities where mechanical ventilation is preferred, under certain conditions, this difference is increased to 16.2%. For different cavity widths, both B1 and B2 present a difference of approximately 32%, because there is minimal mechanical ventilation, which would expose the envelope of the building to higher convective heat transfer coefficients and extract or supply heat to the adjacent building zone.

7 Duluth, Minnesota (very cold)

Duluth, Minnesota that represents ASHRAE 7th climate zone presents similar behaviour with the 6th climate region. The average ambient temperature ranges from -13.1 °C to 18.7 °C (8.4 F to 65.7 F) presenting 9,818 heating degree days and 180 cooling degree days. In addition, the average incident solar radiation and the wind speeds through-out the year are high, increasing the electricity production by the STPV and the assistance to the flow within the cavity. Similarly, to the 6th ASHRAE zone locations presented earlier, the cases are separated into narrow cavity cases (narrower than 0.50 m / 1.64 ft), transitional (0.60 m / 1.97 ft) and wide cavity cases (0.80 m to 1.00 m / 2.62 ft to 3.28 ft). The similarities between the 6th and 7th ASHRAE climate zone extend beyond the discretization of the cavity widths, to the preferred strategies for the optimal operation of the DSF-STPV. The narrower cavities (narrower than 0.50 m / 1.64 ft) operate optimally when they are closed (strategy #3) though-out the year (for both insulation cases), minimizing the losses during the winter and the fan consumption during the summer. For the transitional cavity width (0.60 m / 1.97 ft), all day long mechanical ventilation with low velocity set-points (strategy #1) is preferred from November till April and only for the advanced insulation case. Utilizing in this way the preheated air that can be introduced into the HVAC system, without extracting that much heat from the building, as the building is highly insulated. For wider cavities (0.80 to 1.00 m / 2.62 ft to 3.28 ft), for the advanced insulation case, for the same winter months (November till April) that mechanical ventilation is preferred for the transitional cavity width. A similar strategy is preferred, favouring mechanically ventilated when the incident solar radiation is greater than 200 W/m² and

naturally ventilated otherwise (strategy #4). Natural ventilation is preferred thorough the year for the basic insulation case and through-out the summer months for the advanced insulation case. Natural ventilation is preferred again for wider cavities, as the high wind velocities assists the flow within the cavity. In general, narrower cavities that are closed all months of the year operate optimally.

For Duluth, as it is for most cold climate cities, narrower cavities are preferred with closed cavities. For the narrowest cavities, the difference between B1 and B2 is around 15%, while the cavity is closed. For the wider cavities where mechanical ventilation is preferred, under certain conditions, this difference is increased to 19.6%. It is seen that even for a very cold climate during the warmer months, the net balance of the DSF-STPV zone system is positive.

8 Fairbanks, Alaska (extreme cold)

Fairbanks, Alaska, represents the 8th climate zone of ASHRAE. It has only 84 cooling degree days and 13940 heating degree days, with minimal average incident solar radiation during the winter months and low average wind velocities throughout the year. The average ambient temperature ranges from -23.2 °C (-9.8 F) to 16.8 °C (62.2 F). For narrower than 0.60 m (1.97 ft) wide cavities the DSF-STPV operates optimally if it is closed most of the time. The exceptions are presented for the narrowest cavity width simulated (0.15 m / 0.50 ft) and for 0.40 m (1.31 ft). For the 0.15 m (0.50 ft) wide cavity and for the advanced insulation case, the DSF is mechanically ventilated with low velocity set-points if the temperature of the adjacent to the DSF zone is smaller than the average temperature of cavity (strategy #7), with purpose to introduce the preheated air into the HVAC system. For the basic insulation and for the cavity width of 0.40 m (1.31 ft) wide and for the months that the average ambient temperature is below zero then the DSF-STPV operates optimally if it is mechanically ventilated with low cavity velocities if the temperature of the zone is greater than 22 °C (71.6 F) and it is closed otherwise (Strategy #10). In this case, when the temperature zone is higher and the building insulation is smaller, the increased heating losses from the building to the air cavity can be captured and then introduced into the HVAC system. The 0.80 m (2.62 ft) wide cavity acts as a transitional cavity width between the 0.15 m to 0.60 m (0.50 ft to 1.97 ft) and the 1.00 m (3.28 ft) cavity widths. In this transitional cavity width, for the basic insulation cases the cavity is closed (strategy #3) and for the advanced insulation case it is naturally ventilated during the day and closed during the night (strategy #6). The last strategy is preferred for all the months for the wider cavity (1.00 m / 3.28 ft), when there is incident solar radiation, as buoyancy can be built in a wider cavity and drive the air while, in general the cavity is closed during the night, minimizing in this way the heating loses. Smaller cavities are preferred in this case, with the cavity being closed or mechanically ventilated under certain conditions.

Finally, Fairbanks, follows the same patter as the other cold climates, with narrower and closed cavities to be preferred. For the narrowest cavities, the difference between B1 and B2 is 8.1%, while the cavity remains mainly closed throughout the year

Appendix Table A 1

1A, Miami, Florida (hot, humid) HDD 200, CDD 4198

	J	F	M	A	M	J	J	A	S	O	N	D
Itotal	150.5	153.1	128.6	104.4	81.8	79.3	83.0	95.1	107.3	133.4	144.2	152.1
Idirect	102.9	99.0	65.6	36.7	10.0	1.9	4.2	16.5	42.7	74.8	94.6	105.3
Idiff	47.6	54.1	62.9	67.7	71.7	77.4	78.8	78.6	64.6	58.6	49.6	46.8
Avg. Tamb	20.0	20.8	21.6	24.5	25.8	27.3	28.0	27.9	26.9	25.1	23.2	20.6
Avg. Vwind	4.3	4.8	5.6	5.6	4.5	3.6	3.9	4.0	3.0	3.5	4.8	4.4

2A Houston, Texas (hot, humid) HDD 1599, CDD 2700

	J	F	M	A	M	J	J	A	S	O	N	D
Itotal	122.5	115.0	116.9	96.4	82.6	84.2	86.3	97.0	121.4	144.0	141.5	115.0
Idirect	81.4	67.1	61.7	30.4	14.5	7.5	11.2	26.4	60.1	92.1	97.6	76.6
Idiff	41.1	47.9	55.1	66.0	68.0	76.7	75.1	70.5	61.3	51.9	43.8	38.3
Avg. Tamb	11.9	10.9	16.2	20.5	23.9	26.5	28.0	27.3	25.3	20.9	17.1	11.4
Avg. Vwind	4.5	3.7	4.6	3.9	4.1	3.2	3.5	3.2	3.6	3.5	3.7	3.8

2B Phoenix, Arizona (hot, dry), 1350, CDD4162

	J	F	M	A	M	J	J	A	S	O	N	D
Itotal	181.9	189.3	165.2	148.4	109.4	92.0	100.0	122.9	170.7	208.8	197.8	189.5
Idirect	139.1	138.3	106.1	82.2	42.5	25.9	28.2	57.6	111.6	158.0	151.8	150.9
Idiff	42.8	51.0	59.1	66.1	66.9	66.1	71.7	65.3	59.1	50.9	45.9	38.5
Avg. Tamb	12.1	12.4	18.5	21.8	25.9	32.3	33.3	32.4	29.6	22.7	17.3	11.4
Avg. Vwind	2.4	3.0	3.1	3.2	3.2	3.4	3.6	3.4	3.1	2.8	2.5	2.2

3A Atlanta, Georgia (hot, humid) 2991, CDD1667

	J	F	M	A	M	J	J	A	S	O	N	D
Itotal	136.7	149.9	136.9	124.1	102.1	94.1	96.9	113.6	121.9	164.8	154.1	137.1
Idirect	97.9	103.5	79.1	56.4	25.9	15.1	21.5	41.1	57.2	113.9	111.3	99.7
Idiff	38.8	46.4	57.8	67.8	76.2	79.0	75.4	72.5	64.7	50.9	42.8	37.4
Avg. Tamb	4.7	6.6	11.6	16.1	21.0	24.1	25.2	24.5	22.6	16.5	10.5	6.6
Avg. Vwind	3.5	3.9	4.9	4.6	4.3	4.0	3.1	2.8	3.7	4.1	3.5	5.0

3B-CA Los Angeles, California (hot dry), 1458, CDD727

	J	F	M	A	M	J	J	A	S	O	N	D
Itotal	155.6	167.7	143.2	132.4	103.6	93.3	99.0	123.4	137.4	162.0	166.8	166.7
Idirect	115.0	119.0	85.7	63.3	30.9	20.5	27.3	56.6	78.4	111.0	122.9	128.1
Idiff	40.7	48.6	57.5	69.1	72.7	72.7	71.8	66.9	59.0	50.9	43.9	38.6
Avg. Tamb	13.4	13.3	14.6	15.5	17.0	17.6	19.8	20.1	19.9	18.1	16.0	14.4

3B-other Las Vegas, Nevada (hot, dry), HDD 2407CDD 3201

	J	F	M	A	M	J	J	A	S	O	N	D
Itotal	201.0	201.8	180.7	153.9	121.1	104.8	110.9	139.4	186.2	211.2	215.6	205.9
Idirect	159.5	151.4	119.4	86.9	51.8	35.6	43.7	75.4	126.9	159.2	170.6	167.4
Idiff	41.5	50.5	61.3	67.0	69.3	69.2	67.2	63.9	59.2	52.1	45.0	38.5

	J	F	M	A	M	J	J	A	S	O	N	D
Avg. Tamb	6.9	11.3	11.8	19.4	22.7	30.0	32.5	31.5	27.5	19.5	12.4	8.3
Avg. Vwind	3.2	3.5	3.9	5.9	4.1	5.2	4.2	4.3	3.6	4.1	3.4	3.3

3C San Francisco, California (marine), HDD 3016, CDD 727

	J	F	M	A	M	J	J	A	S	O	N	D
Itotal	127.7	143.3	143.3	132.6	111.4	101.5	110.2	129.4	167.8	169.8	135.3	125.4
Idirect	93.9	99.5	92.6	70.4	43.1	31.5	45.2	69.3	112.5	121.8	98.2	94.3
Idiff	33.8	43.8	50.8	62.2	68.3	70.0	65.0	60.0	55.3	48.0	37.0	31.1
Avg. Tamb	8.6	11.3	10.8	12.2	13.8	14.7	16.1	16.1	16.7	15.1	12.4	9.2
Avg. Vwind	2.5	3.5	5.1	4.8	6.5	5.6	5.7	5.5	4.8	3.9	2.7	3.6

4A Baltimore, Maryland (mild, humid), HDD 4707CDD 1137

	J	F	M	A	M	J	J	A	S	O	N	D
Itotal	121.3	144.5	130.4	116.1	104.6	101.5	103.8	111.9	125.8	156.9	128.1	105.0
Idirect	87.5	101.3	78.3	54.7	34.1	27.5	30.6	46.5	72.2	110.9	93.3	75.8
Idiff	33.9	43.2	52.1	61.4	70.5	74.0	73.2	65.3	53.6	46.0	34.8	29.2
Avg. Tamb	-0.7	0.9	6.8	11.2	17.0	22.5	24.5	24.4	19.7	14.1	8.6	1.7
Avg. Vwind	4.4	5.0	4.6	5.3	4.1	3.5	3.6	3.5	3.3	3.3	4.5	4.3

4B Albuquerque, New Mexico (mild, dry), HDD 4425, CDD 1244

	J	F	M	A	M	J	J	A	S	O	N	D
Itotal	204.0	199.9	174.8	150.1	119.0	100.9	107.5	133.4	167.3	213.8	214.3	206.7
Idirect	162.2	151.5	113.1	82.4	49.0	31.9	39.3	65.7	110.0	162.3	171.0	166.5
Idiff	41.9	48.4	61.7	67.7	70.0	69.0	68.2	67.7	57.2	51.4	43.2	40.2
Avg. Tamb	2.0	4.3	7.1	12.8	18.8	22.7	25.5	23.5	20.5	13.3	6.3	1.5
Avg. Vwind	4.1	3.8	5.1	4.0	4.5	4.3	4.5	4.2	3.5	3.7	2.9	3.5

4C Seattle, Washington (marine), HDD 4908, CDD 190

	J	F	M	A	M	J	J	A	S	O	N	D
Itotal	54.5	79.7	106.5	111.7	122.0	118.7	127.0	123.0	144.2	95.0	57.4	42.0
Idirect	35.7	50.0	62.5	52.2	46.6	43.8	57.9	56.0	98.2	60.6	34.2	26.6
Idiff	18.8	29.7	44.1	59.6	75.4	74.9	69.1	67.0	46.0	34.3	23.2	15.5
Avg. Tamb	4.5	6.6	7.0	9.5	13.0	15.2	17.7	18.0	15.4	11.4	7.1	4.8
Avg. Vwind	4.1	3.5	3.5	4.9	3.9	3.7	3.8	3.7	3.8	3.7	4.9	3.3

5A Chicago, Illinois (cold, humid), HDD 6536, CDD 752

	J	F	M	A	M	J	J	A	S	O	N	D
Itotal	107.3	117.2	118.8	119.9	116.5	108.1	114.9	115.9	131.5	134.5	96.7	78.2
Idirect	76.2	75.1	64.3	58.5	44.2	32.4	40.9	48.0	75.6	91.0	64.6	51.5
Idiff	31.1	42.0	54.5	61.3	72.3	75.7	74.0	67.9	55.9	43.5	32.1	26.7
Avg. Tamb	-4.7	-2.2	1.6	8.4	15.3	21.1	23.5	21.8	18.1	11.7	4.3	-2.5
Avg. Vwind	4.9	5.2	5.4	5.6	3.8	4.9	3.5	3.8	3.4	5.2	4.6	5.3

5B Denver, Colorado (cold, dry), HDD 6020, CDD 679

	J	F	M	A	M	J	J	A	S	O	N	D
Itotal	187.4	170.7	174.3	121.4	116.0	108.1	111.2	129.8	163.2	177.8	160.0	165.4
Idirect	151.7	127.9	122.6	61.3	46.0	41.1	43.9	67.6	107.0	134.5	123.0	133.8
Idiff	35.7	42.8	51.7	60.1	70.0	67.0	67.3	62.2	56.2	43.3	37.1	31.6
Avg. Tamb	0.8	-0.1	6.1	5.8	15.5	23.1	22.3	22.6	19.2	10.1	2.9	1.4
Avg. Vwind	3.8	3.5	4.4	5.3	3.8	3.4	3.0	4.5	4.1	3.8	4.2	3.2

6A Minneapolis, Minnesota (cold, humid), HDD 7981, CDD 682

	J	F	M	A	M	J	J	A	S	O	N	D
Itotal	136.9	150.7	140.5	122.4	123.8	119.7	121.2	131.4	143.7	141.1	102.4	102.4
Idirect	103.3	105.6	85.9	61.7	52.0	44.5	46.8	65.2	88.7	98.7	71.9	74.8
Idiff	33.6	45.1	54.5	60.7	71.8	75.2	74.5	66.2	55.0	42.4	30.5	27.6
Avg. Tamb	-11.8	-8.1	0.3	8.7	16.0	20.5	22.0	21.6	16.1	8.8	0.7	-8.1
Avg. Vwind	4.8	4.4	5.4	5.2	4.7	4.2	4.4	4.2	4.1	4.9	4.5	4.6

6A Minneapolis, Minnesota (cold, humid), HDD 7981, CDD 682

	J	F	M	A	M	J	J	A	S	O	N	D
Itotal	136.9	150.7	140.5	122.4	123.8	119.7	121.2	131.4	143.7	141.1	102.4	102.4
Idirect	103.3	105.6	85.9	61.7	52.0	44.5	46.8	65.2	88.7	98.7	71.9	74.8
Idiff	33.6	45.1	54.5	60.7	71.8	75.2	74.5	66.2	55.0	42.4	30.5	27.6
Avg. Tamb	-11.8	-8.1	0.3	8.7	16.0	20.5	22.0	21.6	16.1	8.8	0.7	-8.1
Avg. Vwind	4.8	4.4	5.4	5.2	4.7	4.2	4.4	4.2	4.1	4.9	4.5	4.6

6B Helena, Montana (cold, dry), HDD 8031CDD 386

	J	F	M	A	M	J	J	A	S	O	N	D
Itotal	96.7	114.3	146.3	127.6	123.6	120.1	138.9	150.1	157.2	150.0	119.5	89.7
Idirect	69.3	78.2	95.4	63.1	51.0	48.3	73.1	88.5	103.9	108.7	90.0	65.9
Idiff	27.3	36.1	50.9	64.4	72.6	71.8	65.8	61.7	53.3	41.3	29.5	23.8
Avg. Tamb	-7.2	-4.6	2.2	5.6	10.8	16.7	20.5	18.6	14.4	8.0	14.2	-5.3
Avg. Vwind	3.4	3.0	3.9	3.9	3.5	4.0	3.5	3.1	3.0	3.9	3.1	3.9

7 Duluth, Minnesota (very cold), HDD 9818, CDD 180

	J	F	M	A	M	J	J	A	S	O	N	D
Itotal	113.4	137.7	150.3	127.0	121.0	118.0	116.4	125.0	125.5	125.6	90.5	91.9
Idirect	82.6	96.0	86.5	63.9	52.3	40.2	43.8	56.8	72.3	85.0	62.5	66.3
Idiff	30.9	41.7	63.8	63.1	68.8	77.8	72.6	68.3	53.2	40.6	28.0	25.6
Avg. Tamb	-13.1	-11.0	-5.4	2.6	9.2	15.4	18.7	16.5	11.5	5.8	-2.1	-10.8
Avg. Vwind	5.1	4.9	5.7	5.2	4.0	4.5	4.0	3.2	4.8	5.4	5.2	4.4

8 Fairbanks, Alaska (extreme cold), HDD 13940, CDD 84

	J	F	M	A	M	J	J	A	S	O	N	D
Itotal	29.2	75.3	141.7	166.0	156.9	150.8	147.0	125.7	107.2	73.7	38.7	18.3
Idirect	24.1	56.5	101.2	96.4	83.4	67.3	70.2	64.5	67.8	52.0	30.8	15.8
Idiff	5.2	18.7	40.4	69.6	73.5	83.6	76.8	61.2	39.5	21.7	7.9	2.5
Avg. Tamb	-23.2	-21.9	-12.8	-2.4	9.1	15.0	16.8	13.4	6.7	-3.1	-15.7	-20.0
Avg. Vwind	1.7	1.5	2.9	3.7	3.2	3.6	2.8	2.9	2.1	2.8	1.3	1.4

Appendix Table A 2

Loc	Cavity Depth	J B1	J B2	F B1	F B2	M B1	M B2	A B1	A B2	M B1	M B2	J B1	J B2	J B1	J B2	A B1	A B2	S B1	S B2	O B1	O B2	N B1	N B2	D B1	D B2	Year B1	Year B2
Miami	0.15	0.20	0.15	1.00	0.20	1.00	0.20	1.00	0.20	0.20	1.00	-	1.00	1.00	1.00	0.60	1.00	1.00	1.00	1.00	1.00	0.20	1.00	0.20	0.20		
		9	9	9	9	9	9	9	9	9	9	2	12	9	9	9	9	9	9	9	9	9	9	9	9		
		0.89	1.47	1.25	1.45	0.99	1.03	-0.51	-0.46	-2.05	-1.90	-3.01	-2.80	-2.93	-2.92	-2.00	-1.77	-1.11	-0.80	-0.33	0.23	0.21	0.87	1.09	1.39	-0.62	-0.35
	0.20	0.20	0.20	1.00	0.20	1.00	0.20	1.00	0.20	0.20	1.00	-	1.00	1.00	1.00	-	1.00	1.00	1.00	1.00	1.00	0.20	1.00	0.20	0.20		
		9	9	9	9	9	9	9	9	9	9	6	9	9	9	6	9	9	9	9	9	9	9	9	9		
		0.79	1.22	1.20	1.42	1.00	1.03	-0.51	-0.47	-2.04	-1.89	-3.02	-2.74	-2.91	-2.94	-1.96	-1.76	-1.06	-0.71	-0.35	0.22	0.08	0.69	0.91	1.33	-0.66	-0.38
	0.25	0.20	0.25	1.00	0.20	1.00	0.20	1.00	0.20	0.20	1.00	1.00	1.00	1.00	1.00	0.60	1.00	1.00	1.00	1.00	1.00	0.20	1.00	-	0.20		
		9	9	9	9	9	9	9	9	9	9	9	9	9	9	9	9	9	9	9	9	9	9	2	9		
		0.73	1.08	1.35	1.43	1.01	1.04	-0.52	-0.48	-2.03	-1.88	-2.96	-2.77	-2.89	-2.94	-1.94	-1.75	-1.05	-0.72	0.12	0.42	0.05	0.57	0.80	1.24	-0.61	-0.40
	0.30	0.20	0.30	1.00	0.20	1.00	0.20	1.00	0.20	0.20	1.00	1.00	1.00	1.00	1.00	-	1.00	1.00	1.00	1.00	1.00	0.20	1.00	0.20	0.20		
		9	9	9	9	9	9	9	9	9	9	9	9	9	9	2	9	9	9	9	9	9	9	9	9		
		0.73	1.00	1.44	1.47	0.99	1.01	-0.51	-0.47	-2.02	-1.88	-2.94	-2.79	-2.88	-2.93	-1.94	-1.75	-1.01	-0.72	0.32	0.45	0.10	0.56	0.77	1.23	-0.58	-0.40
	0.40	0.20	0.40	1.00	0.20	1.00	0.20	1.00	0.20	0.20	1.00	1.00	1.00	1.00	1.00	0.60	1.00	1.00	1.00	1.00	1.00	0.20	1.00	0.20	0.20		
		9	9	9	9	9	9	9	9	9	9	9	9	9	9	9	9	9	9	9	9	9	9	9	9		
		1.32	1.38	1.45	1.48	0.97	0.98	-0.50	-0.46	-2.02	-1.91	-2.93	-2.78	-2.86	-2.92	-1.93	-1.74	-1.09	-0.84	0.24	0.42	0.76	0.87	1.29	1.38	-0.44	-0.34
	0.50	0.20	0.50	1.00	0.20	1.00	0.20	1.00	0.20	0.20	1.00	1.00	1.00	1.00	1.00	-	1.00	1.00	1.00	1.00	1.00	0.20	1.00	0.20	0.20		
		9	9	9	9	9	9	9	9	9	9	9	9	9	9	6	9	9	9	9	9	9	9	9	9		
		1.43	1.49	1.23	1.28	0.96	0.98	-0.49	-0.46	-2.01	-1.94	-2.92	-2.77	-2.85	-2.91	-1.92	-1.73	-1.05	-0.79	-0.04	0.04	0.85	0.89	1.45	1.46	-0.45	-0.37
	0.60	0.20	0.60	1.00	0.20	1.00	0.20	1.00	0.20	-	1.00	1.00	1.00	1.00	1.00	0.60	1.00	1.00	1.00	1.00	1.00	0.20	1.00	0.20	0.20		
		9	1	9	1	9	1	9	1	3	1	9	1	9	1	9	1	9	1	9	1	9	1	9	1		
		1.51	1.53	1.18	1.38	0.97	0.98	-0.48	-0.45	-2.02	-1.93	-2.91	-2.77	-2.85	-2.91	-1.90	-1.73	-0.94	-0.81	-0.15	0.27	0.76	0.78	1.47	1.47	-0.45	-0.35
	0.80	-	-	-	-	-	-	-	-	-	-	-	-	-	-	-	-	-	-	-	-	-	-	-	-		
		3	3	3	3	3	3	3	3	3	3	3	3	3	3	3	3	3	3	3	3	3	3	3	3		
		0.87	1.38	1.41	1.43	0.99	1.00	-0.47	-0.45	-2.01	-1.93	-2.90	-2.76	-2.84	-2.90	-1.88	-1.72	-0.93	-0.79	0.35	0.40	0.15	0.57	0.91	1.26	-0.53	-0.38
	1.00	-	-	-	-	-	-	-	-	-	-	-	-	-	-	-	-	-	-	-	-	-	-	-	-		
		3	3	3	3	3	3	3	3	3	3	3	3	3	3	3	3	3	3	3	3	3	3	3	3		
		1.28	1.47	1.44	1.48	1.00	1.01	-0.47	-0.44	-2.00	-1.93	-2.90	-2.76	-2.83	-2.89	-1.90	-1.76	-0.87	-0.77	0.37	0.42	0.60	0.88	1.16	1.35	-0.43	-0.33
Houston	0.15	1.00	0.15	1.00	0.40	1.00	0.20	1.00	0.20	1.00	1.00	0.80	1.00	0.20	1.00	0.20	0.60	1.00	1.00	1.00	1.00	0.20	0.20	1.00	0.20		
		10	10	10	10	10	10	10	10	10	10	10	10	10	10	10	10	10	10	10	10	10	10	10	10		
		0.92	0.98	0.77	0.90	1.07	1.12	-0.08	-0.06	-1.56	-1.42	-2.70	-2.36	-4.17	-3.32	-3.10	-2.03	-1.06	-0.31	0.46	0.95	1.29	1.45	0.93	1.02	-0.60	-0.26
	0.20	1.00	0.20	1.00	0.40	1.00	0.20	1.00	0.20	1.00	1.00	0.80	1.00	0.20	1.00	0.20	0.60	1.00	1.00	1.00	1.00	0.20	0.20	1.00	0.20		
		10	10	10	10	10	10	10	10	10	10	10	10	10	10	10	10	10	10	10	10	10	10	10	10		
		0.87	0.95	0.74	0.87	1.06	1.11	-0.08	-0.07	-1.55	-1.41	-2.62	-2.36	-4.08	-3.25	-2.99	-1.92	-0.57	-0.30	0.62	0.94	1.18	1.40	0.90	1.00	-0.54	-0.25
	0.25	1.00	0.25	1.00	0.40	1.00	0.20	1.00	0.20	1.00	1.00	0.80	1.00	0.20	1.00	0.20	0.60	1.00	1.00	1.00	1.00	0.20	0.20	1.00	0.20		
		10	10	10	10	10	10	10	10	10	10	10	10	10	10	10	10	10	10	10	10	10	10	10	10		
		0.84	0.93	0.71	0.86	1.07	1.13	-0.09	-0.07	-1.55	-1.41	-2.61	-2.35	-4.06	-3.17	-3.05	-1.94	-0.42	-0.13	0.70	0.96	1.16	1.35	0.87	0.99	-0.53	-0.24
	0.30	1.00	0.30	1.00	0.40	1.00	0.20	1.00	0.20	1.00	1.00	0.80	1.00	0.20	1.00	0.20	0.60	1.00	1.00	1.00	1.00	0.20	0.20	1.00	0.20		
		10	10	10	10	10	10	10	10	10	10	10	10	10	10	10	4	10	10	10	10	10	10	10	10		
		0.80	0.92	0.72	0.85	1.07	1.13	-0.09	-0.08	-1.55	-1.41	-2.61	-2.31	-3.99	-3.05	-2.92	-1.98	-0.44	-0.14	1.08	1.16	1.13	1.29	0.85	0.98	-0.49	-0.22
	0.40	1.00	0.40	1.00	0.40	1.00	0.20	1.00	0.20	1.00	1.00	0.80	1.00	0.20	1.00	0.20	0.60	1.00	1.00	1.00	1.00	0.20	0.20	1.00	0.20		
		10	4	10	10	10	10	10	10	10	10	10	10	10	10	10	10	10	10	10	10	10	10	10	10		
		0.73	0.92	0.72	0.84	1.05	1.11	-0.08	-0.08	-1.54	-1.40	-2.64	-2.26	-3.88	-3.00	-2.77	-1.78	-0.74	-0.24	1.15	1.18	1.28	1.38	0.83	0.96	-0.49	-0.20
	0.50	1.00	0.50	1.00	0.40	1.00	0.20	1.00	0.20	1.00	1.00	0.80	1.00	0.20	1.00	0.20	0.60	1.00	1.00	1.00	1.00	0.20	0.20	1.00	0.20		
		10	4	10	10	10	10	10	10	10	10	10	10	10	10	10	10	10	10	10	10	10	10	10	10		
		0.74	0.90	0.70	0.83	1.02	1.08	-0.08	-0.07	-1.54	-1.40	-2.56	-2.26	-3.75	-2.95	-2.73	-1.81	-0.66	-0.35	0.98	1.07	1.40	1.46	0.84	0.97	-0.47	-0.21
	0.60	1.00	0.60	1.00	-	1.00	-	1.00	-	1.00	-	0.80	-	0.20	-	0.20	-	1.00	-	1.00	-	0.20	-	1.00	-		
		10	4	10	2	10	2	10	2	10	2	10	2	10	2	10	2	10	2	10	2	10	2	10	2		
		0.69	0.91	0.58	0.79	1.03	1.09	-0.08	-0.07	-1.53	-1.40	-2.52	-2.25	-3.67	-2.94	-2.60	-1.73	-0.46	-0.19	0.57	0.78	1.42	1.47	0.84	0.97	-0.48	-0.22
	0.80	1.00	-	1.00	-	1.00	-	1.00	-	1.00	-	0.80	-	-	-	-	-	1.00	-	1.00	-	-	-	1.00	-		
		10	2	10	2	10	2	10	2	10	2	10	2	3	2	3	2	10	2	10	2	3	2	10	2		
		0.63	0.87	0.66	0.80	1.05	1.11	-0.07	-0.07	-1.53	-1.39	-2.51	-2.25	-3.61	-2.94	-2.56	-1.68	-0.27	-0.13	0.98	1.12	1.24	1.37	0.83	0.96	-0.43	-0.19
	1.00	1.00	1.00	1.00	-	1.00	-	1.00	-	1.00	-	0.80	-	-	-	-	-	1.00	-	1.00	-	-	-	1.00	-		
		10	4	10	3	10	3	10	3	10	3	10	3	3	3	3	3	10	3	10	3	3	3	10	3		
		0.62	0.85	0.67	0.82	1.04	1.10	-0.07	-0.06	-1.53	-1.39	-2.50	-2.24	-3.60	-2.93	-2.36	-1.67	-0.17	-0.11	1.14	1.18	1.26	1.40	0.80	0.93	-0.39	-0.18

147

Cavity		J		F		M		A		M		J		J		A		S		O		N		D		Year	
Depth		B1	B2	B1	B2	B1	B2	B1	B2	B1	B2	B1	B2	B1	B2	B1	B2	B1	B2	B1	B2	B1	B2	B1	B2	B1	B2
Phoenix	0.15	0.20 5 2.83	0.15 5 2.94	0.20 5 2.82	1.00 5 2.96	0.20 5 1.55	1.00 5 1.99	0.20 5 0.42	0.20 5 0.80	1.00 10 -1.42	1.00 5 -1.17	1.00 10 -2.36	1.00 12 -3.51	0.60 10 -3.32	0.20 5 -3.69	1.00 10 -2.03	0.20 5 -3.06	1.00 10 -0.31	0.40 5 -1.12	0.20 5 1.14	1.00 5 1.45	0.20 5 1.98	0.20 5 2.18	0.20 5 2.72	0.20 5 2.95	0.33	0.23
	0.20	0.20 5 2.72	0.20 5 2.91	0.20 5 2.78	1.00 5 2.95	0.20 5 1.61	1.00 5 1.99	0.20 5 0.63	0.20 5 0.86	1.00 10 -1.41	1.00 5 -1.17	1.00 10 -2.36	1.00 12 -3.47	0.60 10 -3.25	0.20 5 -3.57	1.00 10 -1.92	0.20 5 -3.05	1.00 10 -0.30	0.40 5 -1.04	0.20 5 1.09	1.00 5 1.42	0.20 5 1.89	0.20 5 2.13	0.20 5 2.64	0.20 5 2.88	0.34	0.24
	0.25	0.20 12 2.38	0.25 5 2.89	0.20 12 2.50	1.00 5 2.94	0.20 12 1.55	1.00 5 2.09	0.20 12 0.20	0.20 5 0.85	1.00 10 -1.41	1.00 5 -1.17	1.00 10 -2.35	1.00 5 -3.50	0.60 10 -3.17	0.20 5 -3.47	1.00 10 -1.94	0.20 5 -3.06	1.00 10 -0.13	0.40 5 -0.96	0.20 12 1.07	1.00 5 1.41	0.20 12 1.82	0.20 5 2.09	0.20 12 2.28	0.20 5 2.85	0.23	0.25
	0.30	0.20 12 2.31	0.30 5 2.88	0.20 12 2.47	1.00 5 2.94	0.20 12 1.58	1.00 5 2.11	0.20 12 0.17	0.20 5 0.83	1.00 10 -1.41	1.00 5 -1.20	1.00 10 -2.31	1.00 5 -3.52	0.60 10 -3.05	0.20 5 -3.42	1.00 4 -1.98	0.20 5 -3.06	1.00 10 -0.14	0.40 5 -0.95	0.20 12 1.16	1.00 5 1.47	0.20 12 1.77	0.20 5 2.07	0.20 12 2.21	0.20 5 2.81	0.23	0.25
	0.40	- 6 2.21	0.40 5 2.85	- 6 2.52	1.00 5 2.98	- 6 1.53	1.00 5 2.07	- 6 0.17	0.20 5 0.81	1.00 10 -1.40	1.00 5 -1.19	1.00 10 -2.26	- 6 -3.49	0.60 10 -3.00	0.20 5 -3.38	1.00 10 -1.78	0.20 5 -3.01	1.00 10 -0.24	0.40 5 -1.00	- 6 1.35	1.00 5 1.62	- 6 1.79	0.20 5 2.08	- 6 2.11	0.20 5 2.80	0.25	0.26
	0.50	- 6 2.32	0.50 5 2.90	- 6 2.53	1.00 5 2.98	- 6 1.44	1.00 5 1.83	- 6 0.23	0.20 5 0.84	1.00 10 -1.40	1.00 5 -1.22	1.00 10 -2.26	- 3 -3.51	0.60 10 -2.95	0.20 5 -3.39	1.00 10 -1.81	0.20 5 -2.84	1.00 10 -0.35	0.40 5 -1.05	- 6 1.40	1.00 5 1.64	- 6 1.97	0.20 5 2.22	- 6 2.19	0.20 5 2.83	0.28	0.27
	0.60	- 3 2.39	0.60 5 2.91	- 3 2.54	1.00 5 2.95	- 3 1.45	1.00 5 1.93	- 3 0.26	0.20 5 0.85	- 2 -1.40	1.00 5 -1.20	- 2 -2.25	- 3 -3.50	- 2 -2.94	- 3 -3.38	- 2 -1.73	0.20 5 -2.71	- 2 -0.19	0.40 5 -0.98	- 3 1.31	1.00 5 1.54	- 3 2.08	0.20 5 2.34	- 3 2.33	0.20 5 2.89	0.32	0.30
	0.80	- 3 2.49	0.80 5 2.92	- 3 2.45	1.00 5 2.92	- 3 1.60	1.00 5 2.06	- 3 0.31	0.20 5 0.86	- 2 -1.39	1.00 5 -1.19	- 2 -2.25	- 3 -3.48	- 2 -2.94	- 3 -3.36	- 2 -1.68	0.20 5 -2.37	- 2 -0.13	0.40 5 -0.90	- 3 1.26	1.00 5 1.42	- 3 2.15	0.20 5 2.28	- 3 2.43	- 3 2.91	0.36	0.34
	1.00	- 3 2.35	1.00 4 2.61	- 3 2.55	1.00 4 2.75	- 3 1.67	- 3 1.73	- 3 0.36	0.20 4 0.40	- 3 -1.39	1.00 4 -1.74	- 3 -2.24	- 3 -4.35	- 3 -2.93	- 3 -4.35	- 3 -1.67	- 3 -2.91	- 3 -0.11	0.40 4 -0.88	- 3 1.48	- 3 1.61	- 3 2.01	- 3 2.14	- 3 2.35	- 3 2.59	0.37	-0.03
Atlanta	0.15	0.20 10 0.94	0.15 10 0.94	0.20 10 1.14	0.20 10 1.14	1.00 10 1.93	0.20 10 1.93	1.00 10 1.14	1.00 10 1.14	1.00 10 -0.12	1.00 10 -0.12	1.00 10 -1.08	1.00 10 -1.08	1.00 10 -1.44	1.00 10 -1.44	1.00 10 -0.35	1.00 10 -0.35	0.20 10 0.35	1.00 10 0.35	0.20 10 2.36	0.20 10 2.36	1.00 10 2.18	0.20 10 2.18	1.00 10 1.39	1.00 10 1.39	0.70	0.70
	0.20	0.20 10 0.87	0.20 10 0.87	0.20 10 1.10	0.20 10 1.10	1.00 10 1.92	0.20 10 1.92	1.00 10 1.14	1.00 10 1.14	1.00 10 -0.12	1.00 10 -0.12	1.00 10 -1.08	1.00 10 -1.08	1.00 10 -1.39	1.00 10 -1.39	1.00 10 -0.35	1.00 10 -0.35	0.20 10 0.37	1.00 10 0.37	0.20 10 2.33	0.20 10 2.33	1.00 10 2.17	0.20 10 2.17	1.00 10 1.33	1.00 10 1.33	0.69	0.69
	0.25	0.20 10 0.85	0.25 10 0.85	0.20 10 1.06	0.20 10 1.06	1.00 10 1.93	0.20 10 1.93	1.00 10 1.12	1.00 10 1.12	1.00 10 -0.12	1.00 10 -0.12	1.00 10 -1.07	1.00 10 -1.07	1.00 10 -1.38	1.00 10 -1.38	1.00 10 -0.36	1.00 10 -0.36	0.20 10 0.45	1.00 10 0.45	0.20 10 2.28	0.20 10 2.28	1.00 10 2.15	0.20 10 2.15	1.00 10 1.29	1.00 10 1.29	0.68	0.68
	0.30	0.20 10 0.80	0.30 10 0.80	0.20 10 0.99	0.20 10 0.99	1.00 10 1.92	0.20 10 1.92	1.00 10 1.11	1.00 10 1.11	1.00 10 -0.12	1.00 10 -0.12	1.00 10 -1.07	1.00 10 -1.07	1.00 10 -1.37	1.00 10 -1.37	1.00 10 -0.37	1.00 10 -0.37	0.20 10 0.45	1.00 10 0.45	0.20 10 2.35	0.20 10 2.35	1.00 10 2.15	0.20 10 2.15	1.00 10 1.26	1.00 10 1.26	0.67	0.67
	0.40	0.20 10 0.68	0.40 10 0.68	0.20 10 0.94	0.20 10 0.94	1.00 10 1.88	0.20 10 1.88	1.00 10 1.11	1.00 10 1.11	1.00 10 -0.12	1.00 10 -0.12	1.00 10 -1.07	1.00 10 -1.07	1.00 10 -1.36	1.00 10 -1.36	1.00 10 -0.36	1.00 10 -0.36	0.20 10 0.40	1.00 10 0.40	0.20 10 2.40	0.20 10 2.40	1.00 10 2.14	0.20 10 2.14	1.00 10 1.25	1.00 10 1.25	0.66	0.66
	0.50	0.20 4 0.68	0.50 4 0.68	- 2 0.88	- 2 0.88	- 2 1.85	- 2 1.85	- 2 1.11	- 2 1.11	- 2 -0.12	- 2 -0.12	- 2 -1.06	- 2 -1.06	- 2 -1.37	- 2 -1.37	- 2 -0.35	- 2 -0.35	- 2 0.30	- 2 0.30	- 2 2.41	- 2 2.41	- 2 2.16	- 2 2.16	- 2 1.24	- 2 1.24	0.64	0.64
	0.60	0.20 4 0.64	0.60 4 0.64	- 2 0.82	- 2 0.82	- 2 1.86	- 2 1.86	- 2 1.11	- 2 1.11	- 2 -0.12	- 2 -0.12	- 2 -1.06	- 2 -1.06	- 2 -1.37	- 2 -1.37	- 2 -0.35	- 2 -0.35	- 2 0.35	- 2 0.35	- 2 2.17	- 2 2.17	- 2 2.16	- 2 2.16	- 2 1.22	- 2 1.22	0.62	0.62
	0.80	- 2 0.67	- 2 0.67	- 2 0.81	- 2 0.81	- 2 1.87	- 2 1.87	- 2 1.11	- 2 1.11	- 2 -0.12	- 2 -0.12	- 2 -1.06	- 2 -1.06	- 2 -1.36	- 2 -1.36	- 2 -0.33	- 2 -0.33	- 2 0.42	- 2 0.42	- 2 2.28	- 2 2.28	- 2 2.15	- 2 2.15	- 2 1.16	- 2 1.16	0.63	0.63
	1.00	- 2 0.71	- 2 0.71	- 2 0.92	- 2 0.92	- 2 1.86	- 2 1.86	- 2 1.12	- 2 1.12	- 2 -0.12	- 2 -0.12	- 2 -1.06	- 2 -1.06	- 2 -1.36	- 2 -1.36	- 2 -0.32	- 2 -0.32	- 2 0.40	- 2 0.40	- 2 2.37	- 2 2.37	- 2 2.11	- 2 2.11	- 2 1.16	- 2 1.16	0.65	0.65

Location	Cavity Depth	J B1	J B2	F B1	F B2	M B1	M B2	A B1	A B2	M B1	M B2	J B1	J B2	J B1	J B2	A B1	A B2	S B1	S B2	O B1	O B2	N B1	N B2	D B1	D B2	Year B1	Year B2
Los Angeles	0.15	0.20	0.15	0.20	0.20	1.00	0.20	1.00	1.00	1.00	1.00	1.00	1.00	1.00	1.00	0.20	1.00	1.00	0.20	0.20	1.00	0.20	0.20	0.20	0.20	1.47	1.47
		12	12	12	12	12	12	12	12	12	12	12	12	12	12	12	12	12	12	12	12	12	12	12	12		
		2.35	2.35	2.57	2.57	2.29	2.29	1.72	1.72	0.57	0.57	0.06	0.06	0.00	0.00	0.79	0.79	0.98	0.98	2.12	2.12	2.14	2.14	2.08	2.08		
	0.20	0.20	0.20	0.20	0.20	1.00	0.20	1.00	1.00	1.00	1.00	1.00	1.00	1.00	1.00	0.20	1.00	1.00	0.20	0.20	1.00	0.20	0.20	0.20	0.20	1.46	1.46
		12	12	12	12	12	12	12	12	12	12	12	12	12	12	12	12	12	12	12	12	12	12	12	12		
		2.28	2.28	2.56	2.56	2.29	2.29	1.73	1.73	0.57	0.57	0.07	0.07	0.00	0.00	0.78	0.78	1.00	1.00	2.06	2.06	2.10	2.10	2.06	2.06		
	0.25	0.20	0.25	0.20	0.20	1.00	0.20	1.00	1.00	1.00	1.00	1.00	1.00	1.00	1.00	0.20	1.00	1.00	0.20	0.20	1.00	0.20	0.20	0.20	0.20	1.47	1.47
		12	12	12	12	12	12	12	12	12	12	12	12	12	12	12	12	12	12	12	12	12	12	12	12		
		2.27	2.27	2.53	2.53	2.31	2.31	1.73	1.73	0.57	0.57	0.06	0.06	0.00	0.00	0.76	0.76	1.24	1.24	2.03	2.03	2.08	2.08	2.01	2.01		
	0.30	0.20	0.30	0.20	0.20	1.00	0.20	1.00	1.00	1.00	1.00	1.00	1.00	1.00	1.00	0.20	1.00	1.00	0.20	0.20	1.00	0.20	0.20	0.20	0.20	1.45	1.45
		12	12	12	12	12	12	12	12	12	12	12	12	12	12	12	12	12	12	12	12	12	12	12	12		
		2.26	2.26	2.51	2.51	2.32	2.32	1.70	1.70	0.57	0.57	0.07	0.07	0.00	0.00	0.74	0.74	1.23	1.23	2.05	2.05	1.99	1.99	2.01	2.01		
	0.40	0.20	0.40	0.20	0.20	1.00	0.20	1.00	1.00	1.00	1.00	1.00	1.00	1.00	1.00	0.20	1.00	1.00	0.20	0.20	1.00	0.20	0.20	0.20	0.20	1.46	1.46
		12	12	12	12	12	12	12	12	12	12	12	12	12	12	12	12	12	12	12	12	12	12	12	12		
		2.24	2.24	2.59	2.59	2.29	2.29	1.68	1.68	0.57	0.57	0.06	0.06	0.00	0.00	0.75	0.75	1.18	1.18	2.18	2.18	2.00	2.00	2.01	2.01		
	0.50	0.20	0.50	0.20	0.20	1.00	0.20	1.00	1.00	1.00	1.00	1.00	1.00	1.00	1.00	0.20	1.00	1.00	0.20	0.20	1.00	0.20	0.20	0.20	0.20	1.47	1.47
		12	12	12	12	12	12	12	12	12	12	12	12	12	12	12	12	12	12	12	12	12	12	12	12		
		2.34	2.34	2.65	2.65	2.27	2.27	1.70	1.70	0.57	0.57	0.06	0.06	0.00	0.00	0.75	0.75	0.88	0.88	2.19	2.19	2.26	2.26	2.02	2.02		
	0.60	0.20	0.60	0.20	0.20	1.00	0.20	1.00	1.00	1.00	1.00	1.00	1.00	1.00	1.00	0.20	1.00	1.00	0.20	0.20	1.00	0.20	0.20	0.20	0.20	1.50	1.50
		12	12	12	12	12	12	12	12	12	12	12	12	12	12	12	12	12	12	12	12	12	12	12	12		
		2.36	2.36	2.65	2.65	2.26	2.26	1.70	1.70	0.57	0.57	0.06	0.06	0.00	0.00	0.75	0.75	1.02	1.02	2.06	2.06	2.30	2.30	2.22	2.22		
	0.80	0.20	0.80	0.20	0.20	1.00	0.20	1.00	1.00	1.00	1.00	1.00	1.00	1.00	1.00	0.20	1.00	1.00	0.20	-	-	0.20	0.20	-	-	1.52	1.52
		12	12	12	12	12	12	12	12	12	12	12	12	12	12	12	12	12	12	3	3	12	12	3	3		
		2.37	2.37	2.49	2.49	2.28	2.28	1.71	1.71	0.57	0.57	0.06	0.06	0.00	0.00	0.77	0.77	1.23	1.23	2.02	2.02	2.34	2.34	2.39	2.39		
	1.00	-	-	-	-	-	-	-	-	-	-	-	-	-	-	-	-	-	-	-	-	-	-	-	-	1.51	1.51
		3	3	3	3	3	3	3	3	3	3	3	3	3	3	3	3	3	3	3	3	3	3	3	3		
		2.21	2.21	2.52	2.52	2.31	2.31	1.72	1.72	0.57	0.57	0.05	0.05	-0.01	-0.01	0.79	0.79	1.21	1.21	2.16	2.16	2.18	2.18	2.41	2.41		
Las Vegas	0.15	1.00	0.15	1.00	1.00	1.00	1.00	1.00	1.00	1.00	1.00	0.20	1.00	0.20	0.20	0.40	0.20	1.00	0.40	0.20	1.00	1.00	0.20	1.00	1.00	1.03	1.03
		5	5	5	5	5	5	5	5	5	5	5	5	5	5	5	5	5	5	5	5	5	5	5	5		
		3.35	3.35	3.38	3.38	3.25	3.25	1.58	1.58	-0.08	-0.08	-2.54	-2.54	-3.30	-3.30	-2.33	-2.33	-0.32	-0.32	2.19	2.19	3.74	3.74	3.47	3.47		
	0.20	1.00	0.20	1.00	1.00	1.00	1.00	1.00	1.00	1.00	1.00	0.20	1.00	-	-	0.40	0.20	1.00	0.40	0.20	1.00	1.00	0.20	1.00	1.00	1.03	1.03
		5	5	5	5	5	5	5	5	5	5	5	5	6	6	5	5	5	5	5	5	5	5	5	5		
		3.31	3.31	3.35	3.35	3.24	3.24	1.60	1.60	-0.05	-0.05	-2.50	-2.50	-3.35	-3.35	-2.27	-2.27	-0.26	-0.26	2.13	2.13	3.69	3.69	3.43	3.43		
	0.25	1.00	0.25	1.00	1.00	1.00	1.00	1.00	1.00	1.00	1.00	0.20	1.00	0.20	0.20	0.40	0.20	1.00	0.40	0.20	1.00	1.00	0.20	1.00	1.00	1.04	1.04
		5	5	5	5	5	5	5	5	5	5	5	5	5	5	5	5	5	5	5	5	5	5	5	5		
		3.29	3.29	3.32	3.32	3.26	3.26	1.58	1.58	-0.06	-0.06	-2.47	-2.47	-3.02	-3.02	-2.35	-2.35	-0.19	-0.19	2.09	2.09	3.66	3.66	3.40	3.40		
	0.30	1.00	0.30	1.00	1.00	1.00	1.00	1.00	1.00	1.00	1.00	0.20	1.00	0.20	0.20	0.40	0.20	1.00	0.40	0.20	1.00	1.00	0.20	1.00	1.00	1.03	1.03
		5	5	5	5	5	5	5	5	5	5	5	5	5	5	5	5	5	5	5	5	5	5	5	5		
		3.28	3.28	3.31	3.31	3.27	3.27	1.51	1.51	-0.09	-0.09	-2.46	-2.46	-2.99	-2.99	-2.45	-2.45	-0.13	-0.13	2.10	2.10	3.63	3.63	3.39	3.39		
	0.40	1.00	0.40	1.00	1.00	1.00	1.00	1.00	1.00	1.00	1.00	-	-	0.20	0.20	0.40	0.20	1.00	0.40	0.20	1.00	1.00	0.20	1.00	1.00	1.04	1.04
		5	5	5	5	5	5	5	5	5	5	6	6	5	5	5	5	5	5	5	5	5	5	5	5		
		3.26	3.26	3.34	3.34	3.25	3.25	1.51	1.51	-0.08	-0.08	-2.48	-2.48	-2.91	-2.91	-2.41	-2.41	-0.18	-0.18	2.28	2.28	3.60	3.60	3.35	3.35		
	0.50	1.00	0.50	1.00	1.00	1.00	1.00	1.00	1.00	1.00	1.00	-	-	-	-	0.40	0.20	1.00	0.40	0.20	1.00	1.00	0.20	1.00	1.00	1.08	1.08
		5	5	5	5	5	5	5	5	5	5	6	6	6	6	5	5	5	5	5	5	5	5	5	5		
		3.29	3.29	3.37	3.37	3.19	3.19	1.54	1.54	-0.08	-0.08	-2.50	-2.50	-2.88	-2.88	-2.36	-2.36	-0.24	-0.24	2.57	2.57	3.69	3.69	3.34	3.34		
	0.60	1.00	0.60	1.00	1.00	1.00	1.00	1.00	1.00	1.00	1.00	0.20	1.00	0.20	0.20	0.40	0.20	1.00	0.40	0.20	1.00	1.00	0.20	1.00	1.00	1.08	1.08
		5	5	5	5	5	5	5	5	5	5	5	5	5	5	5	5	5	5	5	5	5	5	5	5		
		3.31	3.31	3.37	3.37	3.17	3.17	1.56	1.56	-0.07	-0.07	-2.49	-2.49	-2.86	-2.86	-2.26	-2.26	-0.23	-0.23	2.26	2.26	3.76	3.76	3.42	3.42		
	0.80	1.00	0.80	1.00	1.00	1.00	1.00	1.00	1.00	1.00	1.00	-	-	-	-	-	-	1.00	0.40	-	-	1.00	0.20	1.00	1.00	0.80	0.80
		9	9	9	9	9	9	9	9	9	9	3	3	3	3	3	3	9	9	3	3	9	9	9	9		
		3.03	3.03	3.10	3.10	3.06	3.06	1.19	1.19	-0.52	-0.52	-3.12	-3.12	-3.62	-3.62	-2.30	-2.30	-0.11	-0.11	2.12	2.12	3.56	3.56	3.20	3.20		
	1.00	1.00	1.00	1.00	1.00	1.00	1.00	1.00	1.00	1.00	1.00	-	-	-	-	-	-	1.00	0.40	-	-	1.00	0.20	1.00	1.00	0.80	0.80
		9	9	9	9	9	9	9	9	9	9	3	3	3	3	3	3	9	9	3	3	9	9	9	9		
		2.94	2.94	3.07	3.07	3.05	3.05	1.24	1.24	-0.52	-0.52	-3.11	-3.11	-3.60	-3.60	-2.27	-2.27	-0.06	-0.06	2.26	2.26	3.39	3.39	3.21	3.21		

Cavity Depth	J B1	J B2	F B1	F B2	M B1	M B2	A B1	A B2	M B1	M B2	J B1	J B2	J B1	J B2	A B1	A B2	S B1	S B2	O B1	O B2	N B1	N B2	D B1	D B2	Year B1	Year B2
San Fransisco																										
0.15	1.00	0.15	1.00	0.60	0.60	1.00	0.60	1.00	1.00	1.00	1.00	1.00	1.00	1.00	1.00	1.00	1.00	1.00	0.20	1.00	1.00	0.20	0.80	1.00		
	10	10	10	10	10	10	10	10	10	10	10	10	10	10	10	10	10	10	10	10	10	10	10	10		
	1.46	1.54	1.99	2.07	2.32	2.41	1.77	1.84	1.09	1.12	0.63	0.63	0.77	0.81	1.54	1.51	2.06	2.09	2.74	2.74	1.89	1.93	1.46	1.53	1.64	1.69
0.20	1.00	0.20	1.00	0.60	0.60	1.00	0.60	1.00	1.00	1.00	1.00	1.00	1.00	1.00	1.00	1.00	1.00	1.00	0.20	1.00	1.00	0.20	0.80	-		
	10	10	10	10	10	10	10	10	10	10	10	10	10	10	10	10	10	10	10	10	10	10	10	6		
	1.43	1.51	1.98	2.06	2.31	2.39	1.77	1.83	1.08	1.11	0.62	0.62	0.75	0.79	1.54	1.51	2.06	2.10	2.69	2.70	1.87	1.91	1.42	1.51	1.63	1.67
0.25	1.00	0.25	1.00	0.60	0.60	1.00	0.60	1.00	1.00	1.00	1.00	1.00	1.00	1.00	1.00	1.00	1.00	1.00	0.20	1.00	1.00	0.20	0.80	1.00		
	10	5	10	5	10	5	10	5	10	5	10	5	10	5	10	5	10	5	10	5	10	5	10	5		
	1.41	1.50	1.96	2.05	2.29	2.38	1.76	1.82	1.07	1.11	0.62	0.63	0.78	0.79	1.52	1.49	2.08	2.08	2.66	2.68	1.85	1.89	1.40	1.49	1.62	1.66
0.30	1.00	0.30	1.00	0.60	0.60	1.00	0.60	1.00	1.00	1.00	1.00	1.00	1.00	1.00	1.00	1.00	1.00	1.00	0.20	1.00	1.00	0.20	0.80	1.00		
	10	5	10	5	10	5	10	5	10	5	10	5	10	5	10	5	10	5	10	5	10	5	10	5		
	1.39	1.49	1.95	2.04	2.26	2.36	1.75	1.82	1.07	1.11	0.62	0.62	0.78	0.79	1.49	1.47	2.24	2.24	2.62	2.67	1.84	1.88	1.38	1.48	1.62	1.67
0.40	1.00	0.40	1.00	0.60	0.60	1.00	0.60	1.00	1.00	1.00	1.00	1.00	1.00	1.00	1.00	1.00	1.00	1.00	0.20	1.00	1.00	0.20	0.80	1.00		
	10	5	10	5	10	5	10	5	10	5	10	5	10	5	10	5	10	5	10	5	10	5	10	5		
	1.37	1.47	1.94	2.04	2.25	2.36	1.73	1.80	1.06	1.10	0.61	0.62	0.80	0.79	1.48	1.46	2.22	2.23	2.68	2.73	1.83	1.87	1.37	1.47	1.61	1.66
0.50	1.00	0.50	1.00	0.60	0.60	1.00	0.60	1.00	1.00	1.00	1.00	1.00	1.00	1.00	1.00	1.00	1.00	1.00	0.20	1.00	1.00	0.20	0.80	1.00		
	10	5	10	5	10	5	10	5	10	5	10	5	10	5	10	5	10	5	10	5	10	5	10	5		
	1.35	1.46	1.94	2.03	2.24	2.36	1.72	1.80	1.05	1.10	0.61	0.62	0.82	0.79	1.50	1.48	2.19	2.24	2.77	2.78	1.85	1.89	1.35	1.46	1.62	1.67
0.60	1.00	0.60	1.00	0.60	0.60	1.00	0.60	1.00	1.00	1.00	1.00	1.00	1.00	1.00	1.00	1.00	1.00	1.00	0.20	1.00	1.00	0.20	0.80	1.00		
	10	10	10	10	10	10	10	10	10	10	10	10	10	10	10	10	10	10	10	10	10	10	10	10		
	1.34	1.45	1.93	2.02	2.24	2.35	1.72	1.80	1.05	1.10	0.61	0.62	0.82	0.79	1.51	1.48	1.98	1.98	2.77	2.77	1.87	1.92	1.34	1.45	1.60	1.65
0.80	1.00	0.80	1.00	0.60	0.60	1.00	0.60	1.00	1.00	1.00	1.00	1.00	1.00	1.00	1.00	1.00	1.00	1.00	0.20	1.00	1.00	0.20	0.80	1.00		
	10	10	10	10	10	10	10	10	10	10	10	10	10	10	10	10	10	10	10	10	10	10	10	5		
	1.31	1.42	1.91	2.01	2.22	2.33	1.71	1.79	1.05	1.10	0.61	0.62	0.82	0.80	1.52	1.49	2.10	2.23	2.68	2.68	1.87	1.94	1.31	1.43	1.59	1.65
1.00	1.00	1.00	1.00	0.60	0.60	1.00	0.60	1.00	1.00	1.00	1.00	1.00	1.00	1.00	1.00	1.00	1.00	1.00	-	-	1.00	0.20	0.80	1.00		
	10	4	10	10	10	10	10	10	10	10	10	10	10	10	10	10	10	10	3	3	10	10	10	4		
	1.28	1.41	1.90	2.00	2.21	2.33	1.70	1.79	1.04	1.10	0.61	0.62	0.82	0.80	1.54	1.51	2.31	2.42	2.61	2.68	1.84	1.91	1.29	1.42	1.60	1.67
Baltimore																										
0.15	0.20	0.15	0.20	0.20	0.20	0.20	0.40	0.20	1.00	0.60	1.00	1.00	1.00	1.00	1.00	1.00	1.00	1.00	0.20	0.20	0.20	0.20	0.20	0.20		
	10	10	10	10	10	10	10	10	10	10	10	10	10	10	10	10	10	10	10	10	10	10	10	10		
	-2.02	-1.76	0.51	0.59	1.52	1.55	1.28	1.31	0.52	0.53	-0.72	-0.73	-1.11	-0.99	-0.99	-0.74	0.48	0.47	2.13	2.14	1.39	1.43	-0.39	-0.32	0.22	0.29
0.20	0.20	0.20	0.20	0.20	0.20	0.20	0.40	0.20	1.00	0.60	1.00	1.00	1.00	1.00	1.00	1.00	1.00	1.00	0.20	0.20	0.20	0.20	0.20	0.20		
	10	10	10	10	10	10	10	10	10	10	10	10	10	10	10	10	10	10	10	10	10	10	10	10		
	-2.13	-1.95	0.46	0.53	1.47	1.52	1.26	1.30	0.52	0.52	-0.73	-0.74	-1.07	-1.04	-0.93	-0.61	0.45	0.47	2.08	2.13	1.37	1.40	-0.47	-0.39	0.19	0.26
0.25	0.20	0.25	0.20	0.20	0.20	0.20	0.40	0.20	1.00	0.60	1.00	1.00	1.00	1.00	1.00	1.00	1.00	1.00	0.20	0.20	0.20	0.20	0.20	0.20		
	7	7	7	7	7	7	7	7	7	7	7	7	7	7	7	7	7	7	7	7	7	7	7	7		
	-2.27	-2.02	0.37	0.51	1.44	1.49	1.26	1.29	0.51	0.51	-0.73	-0.73	-1.08	-1.00	-1.03	-0.67	0.81	0.89	2.03	2.08	1.35	1.39	-0.52	-0.42	0.18	0.28
0.30	0.20	0.30	0.20	0.20	0.20	0.20	0.40	0.20	1.00	0.60	1.00	1.00	1.00	1.00	1.00	1.00	1.00	1.00	0.20	0.20	0.20	0.20	0.20	0.20		
	7	7	7	7	7	7	7	7	7	7	7	7	7	7	7	7	7	7	7	7	7	7	7	7		
	-2.37	-2.08	0.37	0.53	1.39	1.45	1.24	1.28	0.50	0.51	-0.72	-0.72	-1.07	-0.99	-0.91	-0.71	0.91	0.91	2.03	2.07	1.34	1.37	-0.55	-0.44	0.18	0.27
0.40	0.20	0.40	0.20	0.20	0.20	0.20	0.40	0.20	1.00	0.60	1.00	1.00	1.00	1.00	1.00	1.00	1.00	1.00	0.20	0.20	0.20	0.20	0.20	0.20		
	10	10	10	10	10	10	10	10	10	10	10	10	10	10	10	10	10	10	10	10	10	10	10	10		
	-2.51	-2.28	0.47	0.56	1.36	1.41	1.23	1.27	0.51	0.51	-0.72	-0.73	-1.06	-0.99	-0.97	-0.78	0.89	0.89	2.14	2.18	1.32	1.36	-0.64	-0.49	0.17	0.24
0.50	0.20	0.50	0.20	0.20	0.20	0.20	0.40	0.20	1.00	0.60	1.00	1.00	1.00	1.00	1.00	1.00	1.00	1.00	0.20	0.20	0.20	0.20	0.20	0.20		
	10	1	10	1	10	10	10	10	10	10	10	10	10	10	10	10	10	10	10	10	10	10	10	1		
	-2.66	-2.37	0.33	0.54	1.34	1.39	1.22	1.26	0.50	0.51	-0.71	-0.72	-1.02	-0.98	-0.76	-0.59	0.46	0.44	2.20	2.22	1.32	1.36	-0.65	-0.51	0.13	0.21
0.60	0.20	0.60	0.20	0.20	-	0.20	-	-	-	-	-	-	-	-	-	-	-	-	0.20	0.20	0.20	0.20	0.20	0.20		
	1	1	1	1	3	1	3	3	3	3	3	3	3	3	3	3	3	3	3	3	1	1	1	10		
	-2.68	-2.46	0.29	0.52	1.34	1.40	1.21	1.25	0.51	0.51	-0.71	-0.72	-1.01	-0.94	-0.77	-0.60	0.43	0.61	2.20	2.22	1.30	1.35	-0.63	-0.51	0.12	0.22
0.80	0.20	0.80	0.20	0.20	0.20	0.20	-	-	-	-	-	-	-	-	-	-	-	-	0.20	0.20	0.20	0.20	0.20	0.20		
	1	1	1	1	1	1	3	3	3	3	3	3	3	3	3	3	3	3	1	1	1	1	1	1		
	-2.77	-2.65	0.28	0.52	1.31	1.39	1.21	1.25	0.51	0.51	-0.70	-0.71	-1.01	-0.93	-0.68	-0.55	0.88	0.87	2.04	2.06	1.28	1.34	-0.71	-0.63	0.14	0.21
1.00	0.20	1.00	0.20	0.20	0.20	0.20	-	-	-	-	-	-	-	-	-	-	-	1.00	0.20	0.20	0.20	0.20	0.20	0.20		
	1	1	1	1	1	1	6	6	6	6	6	6	6	6	6	1	1	1	1	1	1	1	1	1		
	-2.84	-2.66	0.37	0.53	1.30	1.38	1.20	1.24	0.51	0.52	-0.70	-0.71	-0.96	-0.92	-0.59	-0.50	0.89	0.89	2.06	2.08	1.24	1.29	-0.80	-0.70	0.14	0.20

Location	Cavity Depth	J B1	J B2	F B1	F B2	M B1	M B2	A B1	A B2	M B1	M B2	J B1	J B2	J B1	J B2	A B1	A B2	S B1	S B2	O B1	O B2	N B1	N B2	D B1	D B2	Year B1	Year B2
Alburquerque	0.15	0.20	0.15	0.20	0.20	0.20	0.20	1.00	0.20	1.00	1.00	1.00	1.00	1.00	1.00	1.00	1.00	0.20	1.00	1.00	0.20	1.00	1.00	0.20	1.00		
		10	10	10	10	10	10	10	10	10	10	10	10	10	10	10	10	10	10	10	10	10	10	10	10	1.68	1.75
		2.74	2.85	2.98	3.00	2.80	2.86	2.04	2.06	0.45	0.45	-0.84	-0.81	-1.69	-1.55	0.21	0.22	1.40	1.50	3.76	3.84	3.55	3.63	2.73	2.92		
	0.20	0.20	0.20	0.20	0.20	0.20	0.20	1.00	0.20	1.00	1.00	1.00	1.00	1.00	1.00	1.00	1.00	0.20	1.00	1.00	0.20	1.00	1.00	0.20	1.00		
		10	10	10	10	10	10	10	10	10	10	10	10	10	10	10	10	10	10	10	10	10	10	10	10	1.67	1.74
		2.66	2.75	2.95	2.99	2.76	2.81	2.03	2.06	0.43	0.44	-0.83	-0.81	-1.69	-1.50	0.17	0.22	1.45	1.59	3.73	3.81	3.55	3.60	2.76	2.92		
	0.25	0.20	0.25	0.20	0.20	0.20	0.20	1.00	0.20	1.00	1.00	1.00	1.00	1.00	1.00	1.00	1.00	0.20	1.00	1.00	0.20	1.00	1.00	0.20	1.00		
		10	10	10	10	10	10	10	10	10	10	10	10	10	10	10	10	10	10	10	10	10	10	10	10	1.67	1.73
		2.63	2.71	2.92	2.97	2.74	2.78	2.02	2.05	0.43	0.44	-0.82	-0.81	-1.64	-1.49	0.19	0.21	1.59	1.67	3.72	3.78	3.54	3.59	2.75	2.91		
	0.30	0.20	0.30	0.20	0.20	0.20	0.20	1.00	0.20	1.00	1.00	1.00	1.00	1.00	1.00	1.00	1.00	0.20	1.00	1.00	0.20	1.00	1.00	0.20	-		
		10	4	10	10	10	10	10	10	10	10	10	10	10	10	10	10	10	10	10	10	10	10	10	2	1.68	1.74
		2.60	2.70	2.90	2.95	2.73	2.77	1.99	2.03	0.44	0.44	-0.82	-0.80	-1.63	-1.44	0.17	0.19	1.74	1.75	3.78	3.80	3.54	3.59	2.74	2.90		
	0.40	0.20	0.40	-	-	-	-	-	-	-	-	-	-	-	-	-	-	-	-	-	-	-	-	0.20	-		
		4	4	2	2	2	2	2	2	2	2	2	2	2	2	2	2	2	2	2	2	2	2	4	2	1.67	1.74
		2.53	2.69	2.87	2.92	2.73	2.76	1.98	2.02	0.44	0.44	-0.88	-0.80	-1.62	-1.43	0.19	0.20	1.65	1.70	3.84	3.87	3.53	3.58	2.71	2.87		
	0.50	0.20	0.50	-	-	-	-	-	-	-	-	-	-	-	-	-	-	-	-	-	-	-	-	-	1.00		
		1	4	2	2	2	2	2	2	2	2	2	2	2	2	2	2	2	2	2	2	2	2	2	4	1.64	1.72
		2.57	2.68	2.80	2.85	2.69	2.73	1.99	2.03	0.44	0.45	-0.87	-0.79	-1.60	-1.42	0.21	0.22	1.34	1.51	3.84	3.87	3.52	3.59	2.72	2.93		
	0.60	0.20	0.60	-	0.20	-	-	-	-	-	-	-	-	-	-	-	-	-	-	-	-	-	-	0.20	1.00		
		4	4	2	4	2	2	2	2	2	2	2	2	2	2	2	2	2	2	2	2	2	2	4	4	1.61	1.69
		2.48	2.65	2.77	2.84	2.65	2.72	1.98	2.02	0.45	0.45	-0.87	-0.79	-1.60	-1.41	0.21	0.22	1.36	1.46	3.67	3.68	3.50	3.57	2.75	2.93		
	0.80	-	0.80	-	-	-	-	-	-	-	-	-	-	-	-	-	-	-	1.00	-	-	-	-	-	1.00		
		2	4	2	2	2	2	2	2	2	2	2	2	2	2	2	2	2	4	2	2	2	2	2	4	1.64	1.71
		2.52	2.61	2.74	2.83	2.63	2.71	1.99	2.02	0.46	0.46	-0.86	-0.79	-1.59	-1.41	0.24	0.24	1.71	1.73	3.67	3.73	3.43	3.54	2.68	2.85		
	1.00	-	1.00	-	0.20	-	0.20	-	-	-	-	-	-	-	-	-	-	-	1.00	-	-	-	-	-	1.00		
		2	4	2	4	2	4	2	2	2	2	2	2	2	2	2	2	2	4	2	2	2	2	2	4	1.64	1.72
		2.48	2.58	2.75	2.87	2.63	2.71	2.00	2.03	0.46	0.46	-0.86	-0.79	-1.58	-1.40	0.25	0.26	1.75	1.76	3.79	3.81	3.40	3.51	2.66	2.82		
Seattle	0.15	0.20	0.15	0.20	0.20	0.20	0.20	0.40	0.20	1.00	0.40	1.00	1.00	1.00	1.00	1.00	1.00	0.20	0.20	1.00	0.20	0.20	1.00	0.20	0.20		
		10	10	10	10	10	10	10	10	10	10	10	10	10	10	10	10	10	10	10	10	10	10	10	10	0.44	0.47
		-1.36	-1.31	-0.06	-0.03	0.83	0.87	1.16	1.20	1.43	1.45	1.28	1.28	1.22	1.21	1.10	1.09	1.54	1.62	0.78	0.81	-0.79	-0.75	-1.82	-1.76		
	0.20	-	-	-	-	-	-	-	-	-	-	-	-	-	-	-	-	-	-	-	-	-	-	-	-		
		3	3	3	3	3	3	3	3	3	3	3	3	3	3	3	3	3	3	3	3	3	3	3	3	0.42	0.45
		-1.40	-1.34	-0.10	-0.05	0.79	0.84	1.14	1.18	1.43	1.45	1.27	1.27	1.23	1.22	1.11	1.10	1.49	1.55	0.76	0.79	-0.82	-0.78	-1.86	-1.80		
	0.25	-	-	-	-	-	-	-	-	-	-	-	-	-	-	-	-	-	-	-	-	-	-	-	-		
		3	3	3	3	3	3	3	3	3	3	3	3	3	3	3	3	3	3	3	3	3	3	3	3	0.41	0.44
		-1.42	-1.36	-0.12	-0.07	0.77	0.81	1.13	1.17	1.43	1.45	1.27	1.27	1.22	1.21	1.13	1.12	1.50	1.57	0.75	0.78	-0.85	-0.80	-1.89	-1.83		
	0.30	-	-	-	-	-	-	-	-	-	-	-	-	-	-	-	-	-	-	-	-	-	-	-	-		
		3	3	3	3	3	3	3	3	3	3	3	3	3	3	3	3	3	3	3	3	3	3	3	3	0.40	0.44
		-1.45	-1.38	-0.14	-0.09	0.74	0.79	1.11	1.15	1.42	1.44	1.24	1.25	1.20	1.19	1.13	1.11	1.68	1.68	0.74	0.77	-0.87	-0.82	-1.95	-1.85		
	0.40	-	-	-	-	-	-	-	-	-	-	-	-	-	-	-	-	-	-	-	-	-	-	-	-		
		3	3	3	3	3	3	3	3	3	3	3	3	3	3	3	3	3	3	3	3	3	3	3	3	0.38	0.42
		-1.48	-1.41	-0.17	-0.12	0.72	0.77	1.08	1.12	1.39	1.42	1.25	1.25	1.17	1.16	1.09	1.08	1.71	1.72	0.72	0.76	-0.90	-0.85	-1.98	-1.88		
	0.50	-	0.50	-	0.20	-	-	-	-	-	-	-	-	-	-	-	-	-	-	-	-	-	-	-	0.20		
		3	5	3	5	3	6	3	6	3	6	3	6	3	6	3	6	3	6	3	6	3	6	3	5	0.37	0.41
		-1.51	-1.43	-0.19	-0.14	0.68	0.73	1.06	1.10	1.39	1.42	1.26	1.26	1.20	1.19	1.06	1.04	1.68	1.69	0.74	0.78	-0.92	-0.87	-2.01	-1.91		
	0.60	-	-	-	-	-	-	-	-	-	-	-	-	-	-	-	-	-	-	-	-	-	-	-	-		
		6	6	6	6	6	6	6	6	6	6	6	6	6	6	6	6	6	6	6	6	6	6	6	6	0.35	0.39
		-1.52	-1.44	-0.20	-0.15	0.65	0.72	1.06	1.11	1.40	1.42	1.25	1.25	1.21	1.19	1.08	1.06	1.47	1.54	0.73	0.77	-0.94	-0.88	-2.02	-1.91		
	0.80	-	-	-	-	-	-	-	-	-	-	-	-	-	-	-	-	-	-	-	-	-	-	-	-		
		6	6	6	6	6	6	6	6	6	6	6	6	6	6	6	6	6	6	6	6	6	6	6	6	0.35	0.39
		-1.54	-1.46	-0.24	-0.18	0.64	0.70	1.06	1.10	1.38	1.41	1.26	1.27	1.22	1.20	1.10	1.08	1.61	1.61	0.72	0.76	-0.96	-0.89	-2.03	-1.95		
	1.00	0.20	1.00	0.20	0.20	0.20	0.20	-	-	-	-	-	-	-	-	-	1.00	0.20	0.20	-	-	0.20	1.00	0.20	0.20		
		5	5	5	5	5	5	6	6	6	6	6	6	6	6	6	5	5	5	6	6	5	5	5	5	0.35	0.39
		-1.58	-1.49	-0.26	-0.20	0.66	0.73	1.04	1.09	1.39	1.42	1.27	1.27	1.23	1.21	1.10	1.09	1.67	1.69	0.68	0.72	-0.98	-0.91	-2.07	-1.99		

	Cavity Depth	J B1	J B2	F B1	F B2	M B1	M B2	A B1	A B2	M B1	M B2	J B1	J B2	J B1	J B2	A B1	A B2	S B1	S B2	O B1	O B2	N B1	N B2	D B1	D B2	Year B1	Year B2
Chicago	0.15	0.20 10 -5.13	0.15 10 -4.95	0.20 10 -2.07	0.20 10 -1.79	0.20 10 0.55	1.00 10 0.61	0.20 10 1.27	0.20 10 1.32	1.00 10 0.87	0.20 10 0.88	1.00 10 -0.11	1.00 10 -0.10	1.00 10 -0.37	1.00 10 -0.37	1.00 10 0.22	1.00 10 0.23	0.20 10 1.09	0.20 10 1.21	0.20 10 1.74	0.20 10 1.76	0.20 10 0.14	0.20 10 0.19	0.20 10 -4.41	0.20 10 -4.10	-0.52	-0.43
	0.20	0.20 10 -5.51	0.20 10 -5.14	0.20 10 -2.24	0.20 10 -1.98	0.20 10 0.48	1.00 10 0.55	0.20 10 1.25	0.20 10 1.30	1.00 10 0.87	0.20 10 0.88	1.00 10 -0.11	1.00 10 -0.11	1.00 10 -0.38	1.00 10 -0.37	1.00 10 0.24	1.00 10 0.25	0.20 10 1.11	0.20 10 1.19	0.20 10 1.71	0.20 10 1.74	0.20 10 0.10	0.20 10 0.15	0.20 10 -4.66	0.20 10 -4.39	-0.60	-0.49
	0.25	0.20 7 -5.70	0.25 10 -5.30	0.20 7 -2.31	0.20 10 -2.17	0.20 7 0.38	1.00 10 0.49	0.20 7 1.23	0.20 10 1.28	1.00 7 0.85	0.20 10 0.87	1.00 7 -0.12	1.00 10 -0.12	1.00 7 -0.39	1.00 10 -0.38	1.00 7 0.24	1.00 10 0.24	0.20 7 1.17	0.20 10 1.21	0.20 7 1.70	0.20 10 1.73	0.20 7 0.04	0.20 10 0.13	0.20 7 -4.74	0.20 10 -4.47	-0.64	-0.54
	0.30	0.20 7 -5.86	0.30 7 -5.52	0.20 7 -2.43	0.20 7 -2.22	0.20 7 0.31	1.00 7 0.39	0.20 7 1.22	0.20 7 1.26	1.00 7 0.84	0.20 7 0.86	1.00 7 -0.12	1.00 7 -0.12	1.00 7 -0.39	1.00 7 -0.38	1.00 7 0.22	1.00 7 0.23	0.20 7 1.18	0.20 7 1.22	0.20 7 1.69	0.20 7 1.72	0.20 7 0.02	0.20 7 0.11	0.20 7 -4.92	0.20 7 -4.57	-0.69	-0.59
	0.40	0.20 10 -6.09	0.40 10 -5.73	0.20 10 -2.67	0.20 10 -2.35	0.20 10 0.11	1.00 10 0.30	0.20 10 1.20	0.20 10 1.24	1.00 10 0.85	0.20 10 0.86	1.00 10 -0.11	1.00 10 -0.11	1.00 10 -0.38	1.00 10 -0.33	1.00 10 0.19	1.00 10 0.19	0.20 10 1.27	0.20 10 1.27	0.20 10 1.69	0.20 10 1.72	0.20 10 -0.02	0.20 10 0.04	0.20 10 -5.12	0.20 10 -4.73	-0.76	-0.63
	0.50	0.20 1 -6.17	0.50 1 -5.80	0.20 1 -2.98	0.20 1 -2.53	- 3 0.01	- 3 0.25	- 3 1.18	0.20 10 1.23	- 3 0.85	- 3 0.86	- 3 -0.11	- 3 -0.11	- 3 -0.38	- 3 -0.37	- 3 0.21	- 3 0.21	- 3 1.15	- 3 1.14	- 3 1.71	- 3 1.75	- 3 -0.05	- 3 0.01	0.20 1 -5.19	0.20 1 -4.77	-0.81	-0.68
	0.60	0.20 1 -6.09	0.60 1 -5.76	0.20 1 -3.09	0.20 1 -2.66	- 3 0.06	1.00 1 0.23	- 3 1.17	0.20 10 1.21	- 3 0.85	- 3 0.87	- 3 -0.10	- 3 -0.10	- 3 -0.34	- 3 -0.34	- 3 0.22	- 3 0.22	- 3 1.21	- 3 1.21	- 3 1.71	- 3 1.75	0.20 1 -0.09	0.20 1 -0.01	0.20 1 -5.11	0.20 1 -4.80	-0.80	-0.68
	0.80	0.20 1 -6.37	0.80 1 -6.03	0.20 1 -3.11	0.20 1 -2.64	0.20 1 0.06	1.00 1 0.24	0.20 1 1.17	0.20 1 1.21	- 3 0.85	- 3 0.87	- 3 -0.09	- 3 -0.10	- 3 -0.32	- 3 -0.32	- 3 0.22	- 3 0.22	0.20 1 1.15	0.20 1 1.19	0.20 1 1.68	- 3 1.72	0.20 1 -0.13	0.20 1 -0.05	0.20 1 -5.41	0.20 1 -4.94	-0.86	-0.72
	1.00	0.20 1 -6.56	1.00 1 -6.12	0.20 1 -2.93	- 6 -2.58	0.20 1 0.07	1.00 1 0.18	0.20 1 1.16	0.20 1 1.20	- 6 0.86	- 6 0.88	- 6 -0.09	- 6 -0.09	- 6 -0.31	- 6 -0.32	- 6 0.24	1.00 1 0.25	0.20 1 1.26	0.20 1 1.27	0.20 1 1.65	0.20 1 1.70	0.20 1 -0.15	0.20 1 -0.06	0.20 1 -5.52	0.20 1 -5.02	-0.86	-0.73
Denver	0.15	0.20 10 2.09	0.15 10 2.27	0.20 10 0.95	0.20 10 1.07	0.20 10 2.90	0.20 10 3.01	0.20 10 0.96	0.20 10 1.04	1.00 10 0.79	0.20 10 0.81	1.00 10 -0.96	1.00 10 -0.81	0.40 10 -0.69	1.00 10 -0.55	1.00 10 -0.18	1.00 10 -0.18	1.00 10 0.55	1.00 10 0.80	0.20 10 2.47	1.00 10 2.54	0.20 10 1.31	0.20 10 1.47	0.20 10 1.46	0.20 10 1.64	0.97	1.09
	0.20	0.20 10 1.98	0.20 10 2.14	0.20 10 0.85	0.20 10 1.02	0.20 10 2.85	0.20 10 2.96	0.20 10 0.92	0.20 10 0.97	1.00 10 0.76	0.20 10 0.81	1.00 10 -1.05	1.00 10 -0.82	0.40 10 -0.69	1.00 10 -0.60	1.00 10 0.09	1.00 10 0.12	1.00 10 0.55	1.00 10 0.77	0.20 10 2.26	1.00 10 2.47	0.20 10 1.09	0.20 10 1.33	0.20 10 1.41	0.20 10 1.52	0.92	1.06
	0.25	0.20 10 1.89	0.25 10 2.05	0.20 10 0.70	0.20 10 0.93	0.20 10 2.77	0.20 10 2.93	0.20 10 0.90	0.20 10 0.95	1.00 10 0.75	0.20 10 0.79	1.00 10 -1.00	1.00 10 -0.81	0.40 10 -0.83	1.00 10 -0.57	1.00 10 0.07	1.00 10 0.11	1.00 10 1.11	1.00 10 1.17	0.20 10 2.25	1.00 10 2.42	0.20 10 1.01	0.20 10 1.23	0.20 10 1.28	0.20 10 1.43	0.91	1.05
	0.30	0.20 10 1.82	0.30 10 2.00	0.20 7 0.66	0.20 10 0.90	0.20 7 2.77	0.20 10 2.91	0.20 7 0.81	0.20 10 0.93	1.00 7 0.74	0.20 10 0.77	1.00 7 -0.90	1.00 10 -0.80	0.40 7 -0.68	1.00 10 -0.52	1.00 7 -0.06	1.00 10 0.04	1.00 7 1.35	1.00 10 1.46	0.20 7 2.22	1.00 10 2.40	0.20 7 0.89	0.20 10 1.11	0.20 7 1.13	0.20 10 1.40	0.90	1.05
	0.40	0.20 7 1.68	0.40 1 1.94	0.20 7 0.43	0.20 1 0.85	0.20 7 2.72	- 2 2.88	0.20 7 0.70	- 2 0.90	1.00 7 0.75	- 2 0.79	1.00 7 -0.94	- 2 -0.80	0.40 7 -0.62	- 2 -0.51	1.00 7 -0.24	- 2 -0.22	1.00 7 1.45	- 2 1.57	0.20 7 2.43	- 2 2.48	0.20 7 0.75	- 2 1.01	0.20 7 1.01	- 2 1.37	0.84	1.02
	0.50	0.20 10 1.14	0.50 1 1.98	0.20 1 -0.10	0.20 1 0.71	0.20 10 2.59	- 2 2.80	0.20 1 0.46	- 2 0.83	1.00 10 0.74	- 2 0.77	1.00 10 -0.95	- 2 -0.79	0.40 10 -0.58	- 2 -0.47	1.00 10 -0.17	- 2 -0.09	1.00 10 0.82	- 2 0.94	0.20 10 2.50	- 2 2.54	0.20 10 0.75	0.20 1 1.03	0.20 1 0.68	- 2 1.27	0.66	0.96
	0.60	0.20 7 1.07	- 2 1.94	- 3 -0.22	- 2 0.69	- 3 2.54	- 2 2.75	- 3 0.45	- 2 0.79	1.00 7 0.74	- 2 0.76	1.00 7 -0.94	- 2 -0.79	0.40 7 -0.57	- 2 -0.46	1.00 7 0.09	- 2 0.13	1.00 7 0.68	- 2 0.97	0.20 7 2.50	- 2 2.55	0.20 3 0.76	- 2 1.04	- 3 0.64	- 2 1.16	0.65	0.96
	0.80	0.20 1 0.95	0.80 1 1.95	0.20 1 -0.25	0.20 1 0.76	0.20 1 2.58	0.20 1 2.72	0.20 1 0.46	0.20 1 0.82	- 2 0.75	- 2 0.76	- 2 -0.93	- 2 -0.77	- 2 -0.56	- 2 -0.44	- 2 0.03	- 2 0.14	- 2 1.38	1.00 1 1.45	0.20 1 2.31	1.00 1 2.42	0.20 1 0.74	0.20 1 0.99	0.20 1 0.65	0.20 1 1.18	0.68	1.00
	1.00	0.20 1 0.96	1.00 1 1.97	0.20 1 -0.30	0.20 1 0.79	0.20 1 2.58	0.20 1 2.76	0.20 1 0.47	0.20 1 0.71	- 2 0.75	- 2 0.77	- 2 -0.93	- 2 -0.77	- 2 -0.52	- 2 -0.44	- 2 0.21	- 2 0.25	- 2 1.58	- 2 1.63	0.20 1 2.36	1.00 1 2.42	0.20 1 0.71	0.20 1 1.01	0.20 1 0.61	0.20 1 1.16	0.71	1.02

152

Table columns use stacked cell values shown as "top / count / value".

Location	Cavity Depth	J B1	J B2	F B1	F B2	M B1	M B2	A B1	A B2	M B1	M B2	J B1	J B2	J B1	J B2	A B1	A B2	S B1	S B2	O B1	O B2	N B1	N B2	D B1	D B2	Year B1	Year B2
Minneapolis	0.15	- / 3 / -10.22	- / 3 / -9.70	- / 3 / -6.41	- / 3 / -6.12	- / 3 / -0.44	- / 3 / -0.31	- / 3 / 1.27	- / 3 / 1.30	- / 3 / 1.03	- / 3 / 1.05	- / 3 / 0.40	- / 3 / 0.40	- / 3 / 0.31	- / 3 / 0.32	- / 3 / 0.67	- / 3 / 0.68	- / 3 / 1.91	- / 3 / 1.92	- / 3 / 1.78	- / 3 / 1.84	- / 3 / -1.68	- / 3 / -1.55	- / 3 / -8.59	- / 3 / -8.08	-1.66	-1.52
	0.20	- / 3 / -10.77	- / 3 / -10.13	- / 3 / -6.92	- / 3 / -6.46	- / 3 / -0.65	- / 3 / -0.44	- / 3 / 1.24	- / 3 / 1.28	- / 3 / 1.03	- / 3 / 1.05	- / 3 / 0.40	- / 3 / 0.40	- / 3 / 0.31	- / 3 / 0.32	- / 3 / 0.65	- / 3 / 0.70	- / 3 / 1.89	- / 3 / 1.90	- / 3 / 1.72	- / 3 / 1.79	- / 3 / -1.85	- / 3 / -1.65	- / 3 / -8.94	- / 3 / -8.44	-1.82	-1.64
	0.25	- / 3 / -11.17	- / 3 / -10.56	- / 3 / -7.24	- / 3 / -6.77	- / 3 / -0.76	- / 3 / -0.55	- / 3 / 1.21	- / 3 / 1.26	- / 3 / 1.02	- / 3 / 1.05	- / 3 / 0.38	- / 3 / 0.38	- / 3 / 0.30	- / 3 / 0.30	- / 3 / 0.71	- / 3 / 0.72	- / 3 / 1.89	- / 3 / 1.90	- / 3 / 1.69	- / 3 / 1.78	- / 3 / -1.98	- / 3 / -1.76	- / 3 / -9.23	- / 3 / -8.84	-1.93	-1.76
	0.30	- / 3 / -11.49	- / 3 / -10.88	- / 3 / -7.46	- / 3 / -6.98	- / 3 / -0.88	- / 3 / -0.71	- / 3 / 1.20	- / 3 / 1.24	- / 3 / 1.01	- / 3 / 1.03	- / 3 / 0.37	- / 3 / 0.37	- / 3 / 0.27	- / 3 / 0.28	- / 3 / 0.70	- / 3 / 0.71	- / 3 / 1.92	- / 3 / 1.92	- / 3 / 1.68	- / 3 / 1.75	- / 3 / -2.04	- / 3 / -1.83	- / 3 / -9.50	- / 3 / -9.02	-2.02	-1.84
	0.40	- / 3 / -12.04	- / 3 / -11.25	- / 3 / -7.33	- / 3 / -6.88	- / 3 / -1.22	- / 3 / -0.87	- / 3 / 1.17	- / 3 / 1.22	- / 3 / 1.00	- / 3 / 1.02	- / 3 / 0.39	- / 3 / 0.39	- / 3 / 0.29	- / 3 / 0.29	- / 3 / 0.65	- / 3 / 0.66	- / 3 / 1.93	- / 3 / 1.94	- / 3 / 1.65	- / 3 / 1.71	- / 3 / -2.05	- / 3 / -1.84	- / 3 / -9.78	- / 3 / -8.88	-2.11	-1.87
	0.50	- / 3 / -12.44	- / 3 / -11.59	- / 3 / -7.44	- / 3 / -6.88	- / 3 / -1.16	- / 3 / -0.92	- / 3 / 1.15	- / 3 / 1.21	- / 3 / 1.01	- / 3 / 1.03	- / 3 / 0.39	- / 3 / 0.38	- / 3 / 0.30	- / 3 / 0.30	- / 3 / 0.57	- / 3 / 0.56	- / 3 / 1.92	- / 3 / 1.92	- / 3 / 1.75	- / 3 / 1.84	- / 3 / -2.09	- / 3 / -1.86	- / 3 / -9.63	- / 3 / -8.67	-2.14	-1.89
	0.60	- / 3 / -12.70	0.60 / 4 / -11.76	- / 3 / -7.63	0.20 / 4 / -7.08	- / 3 / -1.06	0.20 / 4 / -0.87	- / 3 / 1.14	- / 3 / 1.20	- / 3 / 1.01	- / 3 / 1.03	- / 3 / 0.39	- / 3 / 0.39	- / 3 / 0.29	- / 3 / 0.29	- / 3 / 0.66	- / 3 / 0.67	- / 3 / 1.77	- / 3 / 1.82	- / 3 / 1.75	- / 3 / 1.84	- / 3 / -2.07	0.20 / 4 / -1.80	- / 3 / -9.45	0.20 / 4 / -8.61	-2.16	-1.91
	0.80	- / 2 / -12.91	- / 2 / -11.87	- / 2 / -7.72	- / 2 / -7.20	- / 2 / -0.91	- / 2 / -0.70	- / 2 / 1.12	- / 2 / 1.19	- / 2 / 1.01	- / 2 / 1.04	- / 2 / 0.40	- / 2 / 0.40	- / 2 / 0.31	- / 2 / 0.31	- / 2 / 0.68	- / 2 / 0.68	- / 2 / 1.85	- / 2 / 1.85	- / 2 / 1.74	- / 2 / 1.83	- / 2 / -2.11	- / 2 / -1.87	- / 2 / -9.55	- / 2 / -8.85	-2.17	-1.93
	1.00	- / 2 / -13.13	- / 2 / -12.17	- / 2 / -7.71	- / 2 / -7.20	- / 2 / -0.79	- / 2 / -0.66	- / 2 / 1.12	- / 2 / 1.19	- / 2 / 1.02	- / 2 / 1.04	- / 2 / 0.42	- / 2 / 0.41	- / 2 / 0.32	- / 2 / 0.32	- / 2 / 0.70	- / 2 / 0.71	- / 2 / 1.91	- / 2 / 1.91	- / 2 / 1.62	- / 2 / 1.75	- / 2 / -2.09	- / 2 / -1.89	- / 2 / -9.88	- / 2 / -9.14	-2.21	-1.98
Helena	0.15	- / 3 / -8.48	- / 3 / -8.12	- / 3 / -5.29	- / 3 / -5.00	- / 3 / -0.23	- / 3 / -0.12	- / 3 / 1.32	- / 3 / 1.37	- / 3 / 1.34	- / 3 / 1.39	- / 3 / 0.55	- / 3 / 0.64	- / 3 / 0.69	- / 3 / 0.77	- / 3 / 1.55	- / 3 / 1.56	- / 3 / 2.17	- / 3 / 2.20	- / 3 / 2.08	- / 3 / 2.12	- / 3 / -0.01	- / 3 / 0.08	- / 3 / -6.48	- / 3 / -6.21	-0.90	-0.78
	0.20	- / 3 / -8.88	- / 3 / -8.41	- / 3 / -5.57	- / 3 / -5.28	- / 3 / -0.36	- / 3 / -0.21	- / 3 / 1.28	- / 3 / 1.33	- / 3 / 1.34	- / 3 / 1.38	- / 3 / 0.55	- / 3 / 0.64	- / 3 / 0.71	- / 3 / 0.75	- / 3 / 1.57	- / 3 / 1.58	- / 3 / 2.16	- / 3 / 2.18	- / 3 / 2.05	- / 3 / 2.11	- / 3 / -0.05	- / 3 / 0.02	- / 3 / -6.88	- / 3 / -6.43	-1.01	-0.86
	0.25	- / 3 / -9.17	- / 3 / -8.58	- / 3 / -5.78	- / 3 / -5.48	- / 3 / -0.39	- / 3 / -0.25	- / 3 / 1.24	- / 3 / 1.29	- / 3 / 1.32	- / 3 / 1.36	- / 3 / 0.54	- / 3 / 0.64	- / 3 / 0.70	- / 3 / 0.75	- / 3 / 1.60	- / 3 / 1.61	- / 3 / 2.15	- / 3 / 2.17	- / 3 / 2.03	- / 3 / 2.09	- / 3 / -0.08	- / 3 / 0.00	- / 3 / -7.10	- / 3 / -6.62	-1.08	-0.92
	0.30	- / 3 / -9.31	- / 3 / -8.72	- / 3 / -5.93	- / 3 / -5.60	- / 3 / -0.40	- / 3 / -0.24	- / 3 / 1.19	- / 3 / 1.25	- / 3 / 1.31	- / 3 / 1.35	- / 3 / 0.52	- / 3 / 0.57	- / 3 / 0.67	- / 3 / 0.71	- / 3 / 1.59	- / 3 / 1.60	- / 3 / 2.18	- / 3 / 2.21	- / 3 / 1.99	- / 3 / 2.08	- / 3 / -0.12	- / 3 / -0.04	- / 3 / -7.27	- / 3 / -6.77	-1.13	-0.97
	0.40	- / 3 / -9.59	- / 3 / -9.04	- / 3 / -6.18	- / 3 / -5.83	- / 3 / -0.43	- / 3 / -0.25	- / 3 / 1.14	- / 3 / 1.22	- / 3 / 1.28	- / 3 / 1.33	- / 3 / 0.61	- / 3 / 0.63	- / 3 / 0.67	- / 3 / 0.71	- / 3 / 1.54	- / 3 / 1.55	- / 3 / 2.20	- / 3 / 2.23	- / 3 / 1.98	- / 3 / 2.04	- / 3 / -0.20	- / 3 / -0.03	- / 3 / -7.47	- / 3 / -7.09	-1.21	-1.05
	0.50	0.20 / 1 / -9.82	0.50 / 1 / -9.03	- / 3 / -6.44	- / 3 / -6.06	0.20 / 1 / -0.51	0.20 / 1 / -0.29	- / 3 / 1.12	0.20 / 1 / 1.21	- / 3 / 1.28	- / 3 / 1.33	- / 3 / 0.62	- / 3 / 0.64	- / 3 / 0.71	- / 3 / 0.75	- / 3 / 1.49	- / 3 / 1.50	- / 3 / 2.19	- / 3 / 2.22	- / 3 / 2.00	- / 3 / 2.05	0.20 / 1 / -0.22	1.00 / 1 / 0.01	0.20 / 1 / -7.64	0.20 / 1 / -7.02	-1.27	-1.06
	0.60	0.20 / 1 / -9.82	0.60 / 1 / -9.14	- / 3 / -6.64	0.20 / 1 / -6.19	0.20 / 1 / -0.55	0.20 / 1 / -0.31	0.20 / 1 / 1.14	0.20 / 1 / 1.23	- / 3 / 1.28	- / 3 / 1.33	- / 3 / 0.61	- / 3 / 0.63	- / 3 / 0.70	- / 3 / 0.74	- / 3 / 1.53	- / 3 / 1.53	- / 3 / 2.04	- / 3 / 2.15	- / 3 / 1.99	- / 3 / 2.04	0.20 / 1 / -0.22	1.00 / 1 / -0.03	0.20 / 1 / -7.65	0.20 / 1 / -6.98	-1.30	-1.08
	0.80	0.20 / 1 / -10.08	0.80 / 1 / -9.29	0.20 / 1 / -6.90	0.20 / 1 / -6.29	0.20 / 1 / -0.57	0.20 / 1 / -0.34	0.20 / 1 / 1.10	0.20 / 1 / 1.20	0.20 / 1 / 1.27	- / 6 / 1.32	- / 6 / 0.66	- / 6 / 0.68	1.00 / 1 / 0.73	- / 6 / 0.77	- / 6 / 1.56	- / 6 / 1.57	- / 6 / 2.12	- / 6 / 2.15	- / 6 / 1.98	- / 6 / 2.04	0.20 / 1 / -0.36	1.00 / 1 / -0.07	0.20 / 1 / -7.64	0.20 / 1 / -7.11	-1.35	-1.12
	1.00	0.20 / 1 / -10.27	1.00 / 1 / -9.48	0.20 / 1 / -6.74	0.20 / 1 / -6.22	0.20 / 1 / -0.49	0.20 / 1 / -0.30	0.20 / 1 / 1.08	0.20 / 1 / 1.18	0.20 / 1 / 1.27	- / 6 / 1.33	- / 6 / 0.67	- / 6 / 0.69	- / 6 / 0.79	- / 6 / 0.79	0.20 / 1 / 1.58	1.00 / 1 / 1.59	0.20 / 1 / 2.17	0.20 / 1 / 2.21	- / 6 / 1.94	- / 6 / 2.00	0.20 / 1 / -0.41	1.00 / 1 / -0.14	0.20 / 1 / -7.88	0.20 / 1 / -7.32	-1.36	-1.14

		Cavity Depth	J B1	J B2	F B1	F B2	M B1	M B2	A B1	A B2	M B1	M B2	J B1	J B2	J B1	J B2	A B1	A B2	S B1	S B2	O B1	O B2	N B1	N B2	D B1	D B2	Year B1	Year B2
Duluth	0.15	- 3 -13.40	- 3 -11.87	- 3 -9.12	- 3 -8.20	- 3 -3.53	- 3 -2.92	- 3 0.77	- 3 0.98	- 3 1.25	- 3 1.34	- 3 1.14	- 3 1.15	- 3 0.76	- 3 0.73	- 3 1.19	- 3 1.19	- 3 1.59	- 3 1.65	- 3 1.26	- 3 1.37	- 3 -4.16	- 3 -3.62	- 3 -12.19	- 3 -11.03	-2.87	-2.44
	0.20	- 3 -13.79	- 3 -12.28	- 3 -9.55	- 3 -8.49	- 3 -3.82	- 3 -3.17	- 3 0.64	- 3 0.89	- 3 1.22	- 3 1.32	- 3 1.13	- 3 1.14	- 3 0.76	- 3 0.73	- 3 1.20	- 3 1.20	- 3 1.58	- 3 1.64	- 3 1.22	- 3 1.34	- 3 -4.33	- 3 -3.76	- 3 -12.62	- 3 -11.35	-3.03	-2.57
	0.25	- 3 -14.24	- 3 -12.59	- 3 -9.89	- 3 -8.72	- 3 -4.01	- 3 -3.27	- 3 0.58	- 3 0.83	- 3 1.21	- 3 1.31	- 3 1.12	- 3 1.13	- 3 0.75	- 3 0.72	- 3 1.20	- 3 1.20	- 3 1.57	- 3 1.63	- 3 1.19	- 3 1.31	- 3 -4.48	- 3 -3.88	- 3 -12.92	- 3 -11.57	-3.16	-2.66
	0.30	- 3 -14.48	- 3 -12.87	- 3 -10.17	- 3 -8.90	- 3 -4.22	- 3 -3.48	- 3 0.51	- 3 0.74	- 3 1.19	- 3 1.30	- 3 1.10	- 3 1.11	- 3 0.73	- 3 0.70	- 3 1.20	- 3 1.19	- 3 1.58	- 3 1.65	- 3 1.12	- 3 1.30	- 3 -4.60	- 3 -3.94	- 3 -13.19	- 3 -11.81	-3.27	-2.75
	0.40	- 3 -14.91	- 3 -13.27	- 3 -10.54	- 3 -9.21	- 3 -4.57	- 3 -3.64	- 3 0.45	- 3 0.68	- 3 1.17	- 3 1.29	- 3 1.11	- 3 1.12	- 3 0.73	- 3 0.70	- 3 1.15	- 3 1.16	- 3 1.56	- 3 1.63	- 3 1.06	- 3 1.29	- 3 -4.76	- 3 -4.07	- 3 -13.53	- 3 -11.92	-3.42	-2.85
	0.50	- 3 -15.21	- 3 -13.49	- 3 -10.91	- 3 -9.39	- 3 -5.06	- 3 -3.71	- 3 0.45	- 3 0.69	- 3 1.15	- 3 1.29	- 3 1.11	- 3 1.12	- 3 0.75	- 3 0.71	- 3 1.14	- 3 1.14	- 3 1.54	- 3 1.62	- 3 1.09	- 3 1.28	- 3 -4.87	- 3 -4.02	- 3 -13.63	- 3 -11.71	-3.54	-2.87
	0.60	- 3 -15.45	0.60 1 -13.58	- 3 -11.23	0.20 1 -9.52	- 3 -5.17	0.20 1 -3.63	- 3 0.46	0.20 1 0.75	- 3 1.14	- 3 1.28	- 3 1.11	- 3 1.12	- 3 0.74	- 3 0.70	- 3 1.16	- 3 1.16	- 3 1.50	- 3 1.58	- 3 1.05	- 3 1.25	- 3 -4.85	0.20 1 -4.07	- 3 -13.49	0.20 1 -11.72	-3.59	-2.89
	0.80	- 2 -15.94	0.80 4 -13.73	- 2 -11.44	0.20 4 -9.73	- 2 -4.99	0.20 4 -3.67	- 2 0.36	0.20 4 0.68	- 2 1.13	- 2 1.28	- 2 1.11	- 2 1.13	- 2 0.75	- 2 0.72	- 2 1.17	1.00 4 1.16	- 2 1.54	- 2 1.61	- 2 1.02	- 2 1.24	- 2 -5.05	0.20 4 -4.16	- 2 -13.55	0.20 4 -11.75	-3.66	-2.93
	1.00	- 2 -16.05	1.00 4 -13.88	- 2 -11.40	0.20 4 -9.74	- 2 -4.73	0.20 4 -3.47	- 2 0.36	0.20 4 0.68	- 2 1.13	- 2 1.28	- 2 1.12	- 2 1.13	- 2 0.76	- 2 0.73	- 2 1.19	1.00 4 1.19	- 2 1.54	- 2 1.62	- 2 1.00	1.00 2 1.20	- 2 -5.14	0.20 4 -4.21	- 2 -13.91	0.20 4 -12.04	-3.68	-2.96
Fairbanks	0.15	- 3 -26.91	0.15 7 -25.29	- 3 -20.70	0.20 7 -19.21	- 3 -10.91	0.20 7 -9.88	- 3 -1.74	0.20 7 -1.40	- 3 2.50	0.20 7 2.56	- 3 2.17	1.00 7 2.18	- 3 2.04	0.20 7 2.04	- 3 1.72	0.20 7 1.74	- 3 0.85	0.20 7 0.93	- 3 -6.05	0.20 7 -5.24	- 3 -19.57	0.20 7 -18.31	- 3 -25.70	0.20 7 -24.05	-8.52	-7.83
	0.20	- 3 -27.35	- 3 -25.62	- 3 -21.10	- 3 -19.54	- 3 -10.99	- 3 -10.03	- 3 -1.94	- 3 -1.58	- 3 2.48	- 3 2.55	- 3 2.15	- 3 2.16	- 3 2.02	- 3 2.02	- 3 1.71	- 3 1.73	- 3 0.83	- 3 0.89	- 3 -5.82	- 3 -5.31	- 3 -19.91	- 3 -18.57	- 3 -26.09	- 3 -24.42	-8.67	-7.97
	0.25	- 3 -27.73	- 3 -25.87	- 3 -21.52	- 3 -19.93	- 3 -11.93	- 3 -10.60	- 3 -2.32	- 3 -1.76	- 3 2.47	- 3 2.55	- 3 2.16	- 3 2.16	- 3 2.02	- 3 2.01	- 3 1.70	- 3 1.73	- 3 0.81	- 3 0.87	- 3 -6.39	- 3 -5.80	- 3 -20.34	- 3 -18.74	- 3 -26.50	- 3 -24.61	-8.96	-8.17
	0.30	- 3 -27.93	- 3 -26.05	- 3 -21.62	- 3 -20.10	- 3 -11.66	- 3 -10.96	- 3 -2.28	- 3 -1.88	- 3 2.46	- 3 2.54	- 3 2.19	- 3 2.19	- 3 2.05	- 3 2.04	- 3 1.70	- 3 1.73	- 3 0.79	- 3 0.86	- 3 -6.10	- 3 -5.78	- 3 -20.41	- 3 -18.89	- 3 -26.64	- 3 -24.76	-8.95	-8.26
	0.40	0.20 10 -28.28	- 3 -26.29	0.20 10 -21.99	- 3 -20.39	0.20 10 -12.10	- 3 -11.37	0.20 10 -2.55	- 3 -2.01	- 3 2.44	- 3 2.53	- 3 2.18	- 3 2.19	- 3 2.06	- 3 2.05	- 3 1.71	- 3 1.75	- 3 0.77	- 3 0.84	0.20 10 -6.24	- 3 -5.84	0.20 10 -20.83	- 3 -19.10	0.20 10 -26.97	- 3 -24.98	-9.15	-8.38
	0.50	- 3 -28.55	- 3 -26.44	- 3 -22.44	- 3 -20.60	- 3 -12.63	- 3 -11.40	- 3 -2.48	- 3 -2.11	- 3 2.43	- 3 2.51	- 3 2.17	- 3 2.18	- 3 2.04	- 3 2.04	- 3 1.71	- 3 1.74	- 3 0.72	- 3 0.84	- 3 -6.29	- 3 -5.83	- 3 -21.05	- 3 -19.25	- 3 -27.27	- 3 -25.13	-9.30	-8.45
	0.60	- 3 -28.75	- 3 -26.56	- 3 -22.64	- 3 -20.75	- 3 -12.79	- 3 -11.22	- 3 -2.85	- 3 -2.16	- 3 2.41	- 3 2.51	- 3 2.11	- 3 2.12	- 3 2.00	- 3 2.00	- 3 1.70	- 3 1.74	- 3 0.71	- 3 0.84	- 3 -6.60	- 3 -5.82	- 3 -21.19	- 3 -19.38	- 3 -27.42	- 3 -25.23	-9.44	-8.49
	0.80	- 3 -28.96	- 6 -26.65	- 3 -22.91	- 6 -20.79	- 3 -13.34	- 6 -11.78	- 3 -2.89	- 6 -2.15	- 3 2.41	- 6 2.51	- 3 2.14	- 6 2.15	- 3 1.99	- 6 1.99	- 3 1.64	- 6 1.69	- 3 0.71	- 6 0.83	- 3 -6.74	- 6 -5.93	- 3 -21.42	- 6 -19.43	- 3 -27.63	- 6 -25.36	-9.58	-8.58
	1.00	- 6 -29.05	- 6 -26.67	- 6 -22.93	- 6 -20.84	- 6 -13.69	- 6 -12.09	- 6 -2.82	- 6 -2.06	- 6 2.40	- 6 2.51	- 6 2.17	- 6 2.18	- 6 2.05	- 6 2.05	- 6 1.66	- 6 1.71	- 6 0.67	- 6 0.80	- 6 -6.85	- 6 -6.03	- 6 -21.45	- 6 -19.48	- 6 -27.75	- 6 -25.39	-9.63	-8.61

Appendix III: STPV Product Development

A.1. Innovative Technologies used in BIPV

ZEBRA IBC Solar Cell by ISC-Konstanz, Germany

The Zebra Interdigitated Back-Contact (IBC) solar cell could be easily adopted by the architectural community as it all the bus-bars pass by at the rear side of the Solar cells, being hidden in that way from the outside. A monocrystalline silicon solar cell with efficiency of 21% has been achieved and has the potential of exceeding 24%. It is a technology that was announced by Silfab SpA in March of 2012 and is expected to be in production in 2019 by the ISC-Konstanz in Germany (Dutch Solar Design, 2018).
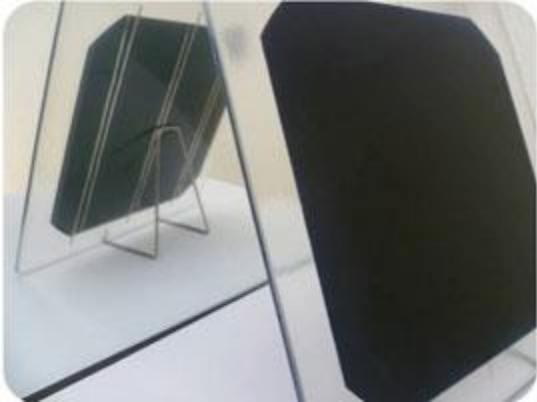
*Figure 0-1 ZEBRA IBC Solar Cell by ISC-Konstanz **(Germany)***

Dutch Solar Design Photovoltaic (DSD-PV) module, The Netherlands

A technic in which a durable print is applied on the PV, intended for a façade integrating, giving different colours and shapes to the PV panel. The same idea is broadly used to create patterns in typical glass installation in buildings and more commonly in buses and trains. An algorithm is created by which the optimal number and surface of dots is selected to cover as little as possible of the PV, maximizing in this way both the aesthetical and the electrical performance of the PV. Proposing a 25-35% cell coverage as an optimal area to achieve both. (Uyterlinde, et al., 2017)
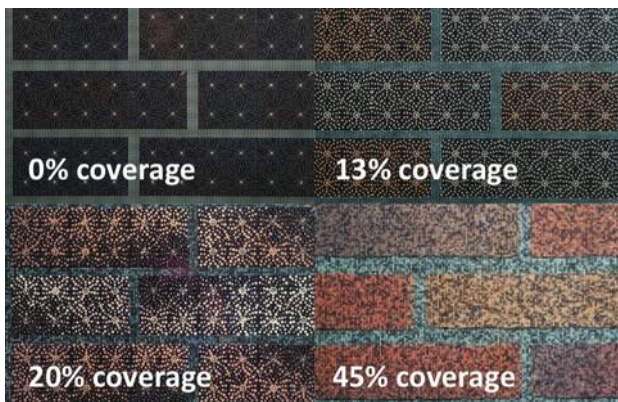
Figure 0-2 Dutch Solar Design Photovoltaic (DSD-PV) module with different dotted coverage.

Kameleon Solar ColorBlast™, The Netherlands

Monocrystaline modules using a glass on glass encapsulation and a printed ceramic pattern. The Ceramic ink is deposited and hardened on the exterior side of the glass (surface 1). The effect of the ceramic ink on the performance of the PV can vary between 75 to 90% of a typical module. (Kameleon Solar, 2018). The greater the

dots the coverage the coverage is, while by increasing the space between the dots, this coverage decreases. Darker colours require less dots, resulting in higher power generation

Figure 0-3 Kameleon Solar ColorBlast, presenting eight different colour configurations

Solaxess, Switzerland

A different approach is adopted by Solaxess, as a coloured film is applied on top of the solar cells. In this way the visible spectrum of the light is reflected while the infrared radiation is transmitted to the solar cells. In addition, the reflective coating drops the operating temperature of the PV panel increasing the efficiency of the panel. A 22% efficient monocrystalline PERC c-Si monocrystalline Solar Panel can reach approximately 220 Wp/m^2 under standard testing condition. Based on that, the coatings of Solaxess have the following results.

Table 0-1 Power production and estimated efficiencies of BIPV panels utilizing the four (4) Solaxess coloured films.

Colour	Black	Light grey	Standard White	Vivid White
Reported Wp/m²	170 Wp/m^2	121 Wp/m^2	117 Wp/m^2	106 Wp/m^2
Estimated efficiency	17%	12%	12%	10%
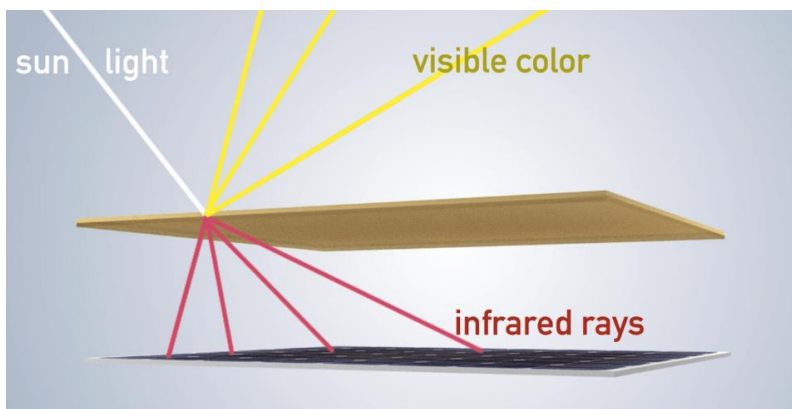
Figure 0-4 Basic principle of the coloured film by Solaxess and a Wivid White film applied on a PV.

### A.1.1. Soltech Façade by Soltech Energy, Sweeden

Soltech Energy, with a collaboration with Sapa Building systems, have developed the SolTech Façade. Having solar cells in six different colours the electricity production per area reaches between 100 Wp/m^2 to 123 Wp/m^2 for colours from yellow to grey (SolTech Energy, 2018). They are also working on the Building Integration of the PV with the use of exterior pressure plates and structural sealant glazing technique. They are also present solutions for roofing glazing applications.

Figure 0-5 Soltech façade, coloured BIPV panels and SAPA façade and roofing mounting systems

Smart Wire Connection Technology (SWCT), Meyer Burger, Germany

SWCT is a foil-wire electrode replacing the conventional ribbons. In this way, the risk of micro-cracks is reduced and at the same time the friction of the electrons traveling through the ribbons is reduced and the temperature of the PV panel is also reduced leading to a performance yield of 6% for solar cells. The cost is also reduced by having up to 80% less silver while Flux and lead are not needed for the soldering.
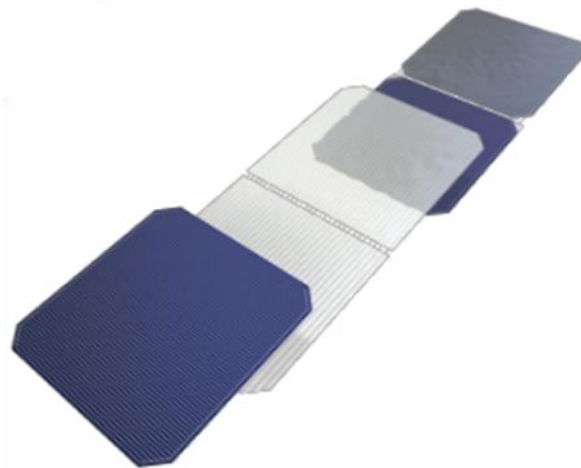
Figure 0-6 Smart Wire Connection Technology (SWCT) layer and way of application.

A.2. Review of Companies and the technologies they use for Building integrated STPV

AGC, SunEwat

One of the biggest Glass manufacturers in the world, AGC, is offering the SunEwat, an STPV that allows multiple opportunities to combine electricity generation with facades, canopies, sunshades, balustrades, louvers, spandrels and more. The company allows the designer to pick from a variety of sizes, form 400mm by 400mm to 2000mm by 4000mm. SunEwat is based on mono or polycrystalline technology with two different opacities; 44% and 88%. This result to 79Wp/m^2 to 158wp/m^2 under standard testing conditions. The thickness of the glass module is reported to be 13.6mm as it consist of 6mm, 1.6mm and 6mm thick layers.

Figure 0-7 AGC, SunEwat, integrated at IUT Michel de

ENERGYGLASS

EnergyGlass is company that has undertaken a number of big projects in Europe, regarding building integrated STPV and is based in Italy. Both crystalline silicon and thin film technologies are employed by EnergyGlass for their solar modules while they are encapsulated with the use of architectural EVA or Polyvinyl butyral (PVB). The company also allows the flexibility regarding the thickness of the module as it can be from 4mm to 15mm thick but also can produce STPV using four different glass colors (Blue, Bronze, Green or Grey).
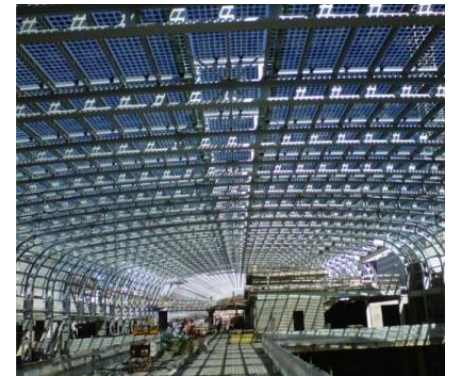
Figure 0-8 EnergyGlass, Stazione porta Susa Torino.

A.2.1. Ertex Solar, Laminated Safety glass ISO module

Ertex Solar is a company based in Austria that produces STPV modules for different kinds of applications. STPV integrated in roofs, terrace shadings, balconies and facades are developed by Ertex Solar, along with STPV that are used for car application. A unique feature of this company is that it produces curved STPV windows that are integrated into buildings. Using different c-Si cell placement, different transparencies are achieved while they report that produce the biggest STPV modules in the market that can reach the size of 2440mm x 5100mm.

Figure 0-9 Ertex Solar, Fronius Baumann Glas, Austria

Galaxy energy

Apart from the typical stand-alone roof installations and BIPV roof applications, Galaxy energy provides canopy and skylight installations. In addition to that, a residential, industrial and office building installations are completed by this company, while a series of farm building installations and carports are put through. Two different IGU models, integrating STPV are reported, presenting a visual transmittance of the second layer of 90% and 40%. The U-Value of the IGU can be as low as 0.8 for the 40%

Figure 0-10 Warehouse installation in Switzerland, by Galaxy Energy, 33.41 kW, with

transmittance IGU. An under development product is also reported, where a ventilated IGU is currently tested.

H.Glass, SFL Technologie

H.Glass is a company that installs STPV using the curtainwall technique. Except from STPV windows, ventilated facades are integrated into buildings. Dye-sensitized solar cells (DSSC), a thin film technology, are used for the STPV that can be later encapsulated onto double or triple glazing units. This based in Switzerland company also produces STPV that are used for anti-noise barriers on highways, charging stations, shelters and more.

Figure 0-11 Science Tower, Graz, Austria. Innovative glass of 3mm thickness by H. Glass

Hanergy, BIPV products

A company based in China, produces thin-film solar cells that are integrated in skylights, windows and curtainwalls. The company presents as its goals to have an architectural impact and at the same time to provide a product that is structural rigid, allowing daylighting into the building and provide shelter from wind and rain. Hanergy produces colour translucent panels based on a-Si/Ge technology having 10% to 40% visible transmittance. This result in power production per m² of 38 Wp/m² that can reach up to 82.3 Wp/m² for bifacial cells. Lastly, the panels that are developed have PVB instead of EVA.
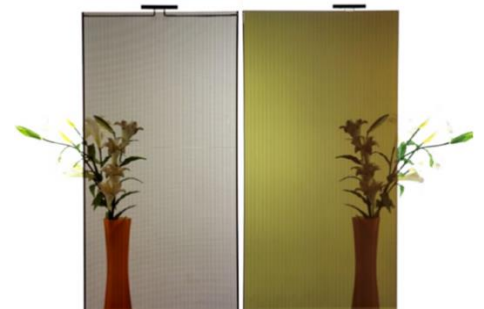

Figure 0-12 Carved translucent Panel (left) and Back electrode translucent Panel using PVB (right) by Hanerg

A.2.2. Kaneka Solar Energy

Kaneka is a company based in Japan that specializes in thin-film silicon solar panel, using a-Si and a new tandem structure that can absorb light at both ends of the visible spectrum increasing in this way their efficiency. Not many details are presented about the efficiency or the structure of these STPV panels.

Figure 0-13 Kaneka See-Through panels.

A.2.3. Megasole

Megasol is company that has its headquarters in Switzerland but is also active in China. STPV panels are developed for façade applications, roofing and balcony glazing that have protection for class 5 hail. A 20% transparency specials solar panels are integrated at the "ECO-Solar" row houses build in Uttwil (Switzerland). The thickness of the Solar Panels can range from 2mm to 12mm depending on the requirement of the application.

Figure 0-14 "ECO-Solar" row houses, Switzerland. Photo: ISELI A + P AG

A.2.4. Next Enegy Technologies

Next Energy technologies is a company based in the USA that produces STPV for window applications. More specific, STPV panels for low-e windows are produced with visible transmittances from 10% to 50%. This result from 100Wp/m² to 70Wp/m² respectively. Next Energy technologies provide panels in custom sizes, depending on architects' preferences.
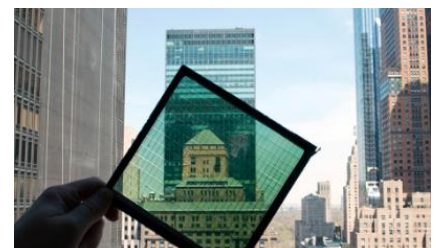

Figure 0-15 NEXT solar panel

Onyx solar is one of the biggest companies in the field of STPV meant for building integration. Both a-Si and c-Si technologies are employed by Onyx solar and the STPV panels are made by two or more safety glass that are heat treated. In addition, double or triple glazing units are created for enhanced thermal performance. The STPV of Onyx can be used for terrace floor, sidewalks, ventilated facades and other applications while the power production per sq. meter ranges from 27-164. The transparencies that Onyx provides ranges from 0% to 30%, while different colors of glasses can be employed. The based in Spain company, can create solar panels that are as small as 600mm by 600m and as large as 2000m by 4000m.

Figure 0-16 Balenciaga Store in Miami USA integrating
c-Si STPV window by Onyx solar.

Polysolar

Polysolar is a company based in UK that develop both c-Si and thin-film STPV products. The products by Polysolar are integrated in facades and curtain wall applications, skylights, canopies, roofs greenhouses and conservatories. The modules manufactured are approximately 7mm thick and have transparencies from 10% to 88%. Also, the thin-film modules are produced in a variety of dimensions, while the STPV based on c-Si have the typical 992mm by 1988mm size. Lastly, the company develops and installed IGU integrating STPV offering U values of 1.2 W/m^{2}K and SHGC values of 0.42.

Figure 0-17 Future business center in Cambridge by Polysolar.

Pilkington, Sunplus

Pilkington is one of the biggest glazing companies in the world. The new product that they manufacture is the Surplus that has a 76.4 W/m^2 and can be integrated on a double glazing. The IGU is recommended by the company to be 30mm while the STPV is laminated on an IGU of 9.5mm. The 1.5mm of these 9.5mm is the c-Si cell layer. The STPV integrated in different types of glasses can provide visual transmittance between 29% to 44%.

Figure 0-18 Pilkington, Sunplus STPV window

Romag, PowerGlaz

The PowerGlaz model from Romag is a STPV window that can be integrated to facades, atria and skylights. Based in UK, this company provides single, double or triple-glazed options with different packing factors and glass colors. The use of PVB as an interlayer guarantees a reliable architectural performance. Romag can also provide STPV for canopies, louvers, walkways and balustrades.

Figure 0-19 Romag, PowerGlaz

Sapa Building Systems

In collaboration with SolTech Energy, Sapa Building Systems move actively towards the building integration of STPV. Using both c-Si and thin film technologies and having variations in transparencies and the colors offered, the company based in Sweeden has solutions for a facade, roofs, skylights canopies etc. In addition to that, Sapa develop insulating glazing units integrating STPV while have payed attention towards modular designs, building shades. The reported dimenions of the STPV are 1200mm by 2400mm.

Figure 0-20 Partille Municipal Office.

SOLARCARPORT

Solar carport produces STPV glazing for terraces, balconies and car glasses. Solarcarport also develop STPV glasses for facades that have the flexibility to have every color, form and size. The company that is based in Germany can also print company logos suitable for façade systems. The standard transparencies provided by Solarcarpot are between 20% to 30% and can be integrated into IGU.

Figure 0-21 Solar façade by

Solaronix

Manufacturing Dye-Sensitized Solar Cells (DSSC), Solaronix can provide STPV glazing from 500mm by 1000mm up to 500mm by 2500mm. Having a variety of colors and transparencies, the Switzerland based company can provide different façade and roofing solutions, although the availability of IGU integration is not reported.

Figure 0-22 SwissTech Convention Center by Solaronix

SolTech Energy

Having a collaboration with Sapa building systems, SolTech generates STPV that can be filled with Argon and integrated on both Double and triple glazing units. Using Cadmium telluride (CdTe) technology and transparencies ranging from 10% to 90% with increments of 10%, the SolTech ST, the product manufactured by Soltech energy can generate from 9.9 Wp/m^2 to 89Wp/m^2. The sizes of the panels come in increments of 600mm up to 3000mm, and the thickness of the STPV is 14.7mm for single pane, 33.7mm for double glazing (DG) and 48.7mm for triple glazing (TG). (SolTech Energy, 2018)

Figure 0-23 CdTe of 10% (left) and 90%(right) transmittance by SolTech Enegy

Sunovation

Sunovation is a company based in Germany that produces STPV, coloured STPV, curved STPV and IGU. Using different color configurations and sizes, different transparency sizes can be achieved. In addition, Sunovation can also provide different c-Si solar cell sizes providing higher flexibility to the manufacturing of STPV. Sunovation can also provide STPV panels designed for shading.

Figure 0-24 Parking entrance by Sunovation.

Table 0-2 List of companies developing STPV for building integration and their technical characteristics

Company	Wp/m²	Technologies	Transparencies	IGU	Thicknesses (mm)	Max dimensions	Min dimensions	Location
AGC	79/158	c-Si	88%, 44%	Y	6/1.6/6	2000x4000	400x400	China
ENERGYGLASS	NR	c-Si, thin film	variations	Y	4 to 15	NR	NR	Italy
Ertex Solar	170max	c-Si	variations	Y	NR	2440x5100	NR	Austria
Galaxy Energy	NR	c-Si	11%	Y	NR	NR	NR	Germany
H. Glass	NR	DSSC	NR	DG/TG	NR	NR	NR	Switzerland
Hanergy	38.0-82.3	a-Si/Ge	10%-40%	Y	6.0/3.2/6.0	2540x1245	1245x635	China
Kaneka	NR	a-Si, tandem	NR	NR	NR	NR	NR	Japan
Megasol	NR	c-Si	20%	NR	2-12mm	NR	NR	Switzerland
Next Energy	70-100	NR	10%-50%	Y	NR	variation	NR	USA
Onyx Solar	27-164	a-Si, c-Si	0-30%	DG/TG	4-8/6-20/4-8	4000x2000	600x600	Spain
Polysolar	61.2-175	c-Si, Thin film	10% - 50%	Y	7.1	992x1988	1200x 600	UK
Pilkington	76.4	c-Si	29%-44%	Y	9.5/16/4	1540x1020	NR	UK
Romag	NR	c-Si	variations	DG/TG	NR	NR	NR	UK
Sapa	NR	c-Si, thin film	variations	Y	NR	1200x2400	NR	Sweden
Solarcarport	150max	c-Si	20%-30%	Y	NR	NR	NR	Germany
Solaronix	NR	DSSC	variations	N	NR	1000x500	2500x500	Switzerland
SolTech Energy	9.9- 113	CdTe	10%-90%	DG/TG	5 / 3.2 TCO / 5	1200x4800	600x600	Sweden
Sunovation	NR	c-Si	variations	Y	NR	variation	NR	Germany

A.3.   Literature on standards that should be followed

The PV have to meet the both the performance and structural requirements described by Standards in terms of static and safety behaviour. These are the Dynamic Loads such as wind and crowd, static loads such as body-weight, hailstorms, seismic phenomenon etc. Additionally, the BIPV should provide thermal and acoustic insulation, and meet the appearance standards.

A.3.1.   Terrestrial photovoltaic (PV) modules - Design qualification and type approval

IEC 61215-1-1:2016	Special requirements for testing of crystalline silicon photovoltaic (PV) modules
IEC 61215-1-2:2016	Special requirements for testing of thin-film Cadmium Telluride (CdTe) based photovoltaic (PV) modules
IEC 61215-1-3:2016	Special requirements for testing of thin-film amorphous silicon based photovoltaic (PV) modules
IEC 61215-1-4:2016	Special requirements for testing of thin-film Cu(In,GA)(S,Se)$_2$ based photovoltaic (PV) modules
IEC 61215-2:2016	Test procedures

IEC 61215:2016 is replacing the IEC 61646 "Thin-film terrestrial photovoltaic (PV) modules - Design qualification and type approval", that included all the Thin film technologies and is separated into two main parts; the special requirements for testing under IEC 61215-1 and the test procedures under IEC 61215-2. The first part, IEC 61215-1, has four sub-parts for crystalline silicon (c-Si), thin-film Cadmium Telluride (CdTe), thin-film amorphous silicon and thin-film Copper indium gallium selenide (CIGS) based PV. The IEC 61215-1-1 presents the test requirements for c-Si PV panels that are suitable for open-air climate applications and are tested with the procedures described under IEC 61215-2:2016.

A.3.2.   Photovoltaic (PV) module safety qualification

IEC 61730-1:2016	Requirements for construction
IEC 61730-2:2016 RLV	Requirements for testing

The IEC61730 is also separated into two parts. The requirements for construction of PV modules and are under the first part (IEC 61730-1:2016) and the requirements for testing are described under the second part (IEC 61730-

1:2016). Under this standard the specifications to prevent electric shock, fire hazards and personal injury due to stresses caused by mechanical and environmental motions are presented for both c-Si and thin film technologies.

A.3.3. Glass in building -- Laminated glass and laminated safety glass

ISO 12543-1:2011	Definitions and description of component parts
ISO 12543-2:2011	Laminated safety glass
ISO 12543-3:2011	Laminated glass
ISO 12543-4:2011	Test methods for durability
ISO 12543-5:2011	Dimensions and edge finishing
ISO 12543-6:2011	Appearance

The ISO 12543 presents the standards for glass in buildings and more specific in laminated glass and laminated safety glass. First it describes the components of the glasses that are used in the laminated glasses and then specifies the performance requirements for laminated safety glass and laminated glass.

In continuation the test methods for the resistance to high temperature, humidity and radiation are described. The dimensions, limit deviations and edge finishes are specified on the fifth part, while the sixth part presents the defects and the test methods regarding the appearance of the laminated glass at the time of supply.

A.3.4. Canadian Standards

CAN/CGSB-12.1-2017	Safety glass standard
CSA C22.61730	Photovoltaic (PV) module safety qualification

The CAN.CGSB-12.1-2017 is a Canadian National Standard for glazing and the test methods that they should be tested upon. These tests are designed to identify the minimum performance characteristics needed by glazing in order to reduce the likelihood of injuries due to all kinds of impacts or stresses. It is important to underline that this standard does not identify the strength, durability, fire rated characteristics, appearance or methods of installation of each glazing.

The CsA C22.61730 presents the PV module safety qualification requirements for construction. Has adopted the earlier version of IEC 61730-1:2016 (IEC 61730-1:2004) with Canadian deviations.

A.3.5. European Standards

EN 356:2000	Glass in building. Security glazing. Testing and classification of resistance against manual attack
EN 410:2011	Glass in building. Determination of luminous and solar characteristics of glazing
EN 12150-1:2015	Definition and description
EN 12150-2:2004	Evaluation of conformity/Product standard
EN 12600:2002	Glass in building. Pendulum test. Impact test method and classification for flat glass
EN 13501-1:2007+A1:2009	Fire classification of construction products and building elements. Classification using test data from reaction to fire tests
EN 14449:2005	Glass in building. Laminated glass and laminated safety glass. Evaluation of conformity/product standard
EN 50583-1:2016	Photovoltaics in buildings. BIPV modules
EN 50583-2:2016	Photovoltaics in buildings. BIPV systems

The European Standard 356:2000 provides definitions and test methods for security glazing products and classifies the glazing into different categories of resistance to forces.

The EN 410:2011 standard describes the method to determine the luminous and solar characteristics of glazings. All kinds of glazing, including double and triple glazing that are intended to be integrated to buildings can be characterized under to this standard.

The EN 12150:2002 is a European Standard that focuses on monolithic flat thermally toughened soda lime silicate safety glass for use in buildings. The second part of this standard defines the tests that the glazing should pass in order to be approved, defined as safety glass, along with proposed mathematical equations that should be used.

The EN 12600:2002 is maybe the most important standard for a glazing that is integrated on a building. This standard defines a testing method for glasses that are used in buildings. This standard underline that unbreakably is not the most important issue but the way that the glass breaks is of importance.

The European Standard 13501-1:2007+A1:2009 classifies the materials that are used in buildings. Each product is classified based how its materials contribute to a building fire. It is different form the resistance to fire.

The EN 14449:2005 is a standard that focuses on the production of the glass by the factory. It covers the evaluation of the conformity of the factory production control of laminated glasses that are used in buildings.

EN 50583:2016 is a European Standard about PV modules that are used as construction products. By referencing to international standards, technical reports and guidelines, this document address manufacturers, planners, system designers, installers, testing institutes and building authorities. The second part follows the same perspective about complete PV systems that are integrated into buildings.

A.3.6. Other Standards

UL 1703	Standard for Safety Flat-Plate Photovoltaic Modules and Panels
ANSI Z97.1-2015	For Safety Glazing Materials Used In Buildings - Safety Performance Specifications And Methods Of Test
ASTM E1300 - 16	Standard Practice for Determining Load Resistance of Glass in Buildings

The UL 1703 is a standard for flat-plate PV modules. These PV panels can be either integrate or applied onto buildings or can be freestanding. This standard does not include equipment that are used along with the PV panels, any tracking mechanisms, cell assemblies, optical concentrators and PV/Thermal.

The ANSI Z97.1-2015 standard, presents the specifications and methods that a glazing should meet in order to be specified as a safety glazing. It should reduce the possibilities of cutting, piercing and hurting people when they come in contact.

The ASTM E1300-16 is a practice that determines the load resistances for certain glass types and their combinations. This covers also the formation of IGU that are under described conditions and have specified probability of breakage.

A.4.   Companies and the Standards that they meet

AGC: IEC 61215, IEC 61730 classes II, EN 14449.
EnergyGlass™: CEI EN 61215, CEI EN 61730, UNI 7697, ISO 12543 1-6, UNI EN 12600, EN 356.
Kaneka: IEC, UL.
ONYX: IEC 61646, IEC 61215, IEC 61730-1, UL 1703, ISO 12543-4:2011, EN 13501:2007, EN 356:2001, EN 410:2011, EN 12150:2005, EN 12600:2003.
Polysolar: IEC 61215, IEC 61730.
Romag: IEC 61215, IEC 61730.
SOLARCARPORT: IEC61215/IEC61730-1/-2.
Sunovation: **IEC 61215/61730,** DIN EN ISO 9001, UL 1703.
Pilkington: IEC 61215:2005/IEC 61730-1/-A2:2013.